CTU

CZECH TECHNICAL
UNIVERSITY
IN PRAGUE

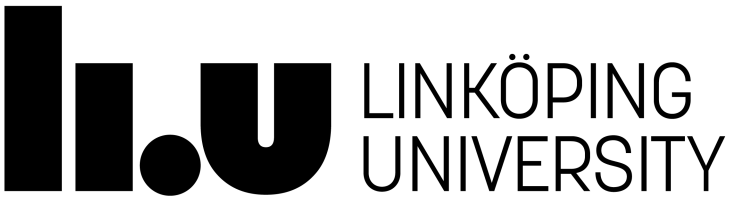

MASTER THESIS

2021

ROBERT
THEINER

CZECH
TECHNICAL UNIVERSITY
IN PRAGUE

FACULTY
OF MECHANICAL
ENGINEERING

AEROSPACE DEPARTMENT

LINKÖPING UNIVERSITY

GI LIFT AB

PRELIMINARY DESIGN OF UAV MULTICOPTER

2021

ROBERT
THEINER

MASTER'S THESIS ASSIGNMENT

I. Personal and study details

Student's name: **Theiner Robert** Personal ID number: **425288**

Faculty / Institute: **Faculty of Mechanical Engineering**

Department / Institute: **Department of Aerospace Engineering**

Study program: **Aeronautics and Astronautics**

Branch of study: **Aerospace Technology**

II. Master's thesis details

Master's thesis title in English:

Preliminary Design of UAV Multicopter

Master's thesis title in Czech:

Návrh UAV multikoptéry

Guidelines:

- Review of existing designs and technologies
- Review of certification standarts
- Definition of design requirements
- Concept studies of possible solutions
- Concept analysis and choose of the optimal solution
- Detailed design of the choosen variant

Bibliography / sources:

According to the supervisors instructions.

Name and workplace of master's thesis supervisor:

Ing. Jan Klesa, Ph.D., Department of Aerospace Engineering, FME

Name and workplace of second master's thesis supervisor or consultant:

Date of master's thesis assignment: **30.04.2021** Deadline for master's thesis submission: **06.08.2021**

Assignment valid until: _____

Ing. Jan Klesa, Ph.D.	Ing. Robert Theiner, Ph.D.	prof. Ing. Michael Valášek, DrSc.
Supervisor's signature	Head of department's signature	Dean's signature

III. Assignment receipt

The student acknowledges that the master's thesis is an individual work. The student must produce his thesis without the assistance of others, with the exception of provided consultations. Within the master's thesis, the author must state the names of consultants and include a list of references.

.	
Date of assignment receipt	Student's signature

I did this on my own.
I referred to all the sources to all the other author's content I used.

.....
Author's signature

My sincere gratitude belongs to

my parents for unrestrained support and the solid
home
they provided, allowing both me and my sister to seek education of our own choice.

Ing. Jan Klesa PhD., the Czech supervisor, for patient and spot-on
guidance
and being available to the fullest extent to share his knowledge.

David Lundström, the Swedish supervisor, for his
advice
focused on the electric propulsion in aviation.

Gunnar Dahlbäck, CEO of GI Lift AB, for the
trust
he put in me.

Stanislav Archmann, my mentor and colleague, for sharing years of
experience
in design with Siemens NX.

Thank you.

Abstract

Preliminary Design of UAV Multicopter

The overall concept is to have an autonomous unmanned aerial system composed of the multicopter, the aerostat and the spreader to perform ash spreading flight operations lasting a matter of minutes. The aim of this work is to come up with a design solution of the unmanned rotorcraft fit to lift, carry and drop payload of several hundreds kilograms of certified ash in the open forest, to analyze its power requirements and then design it in more detail. The geometry of the aerostat and the spreader have to be taken into consideration but the detailed design of these is out of the scope.

Keywords

Autonomous, Carbon/epoxy composite, Conceptual design, Drone, Multicopter, Rotorcraft, UAV, UAS, Unmanned aircraft, VTOL

Contents

Abbreviations

CAD	Computer Aided Design
CAM	Computer Aided Manufacturing
CFD	Computational Fluid Dynamics
CS	Certification Specification
EASA	European Union Aviation Safety Agency
FAA	Federal Aviation Administration
ICAO	International Civil Aviation Organization
MTOM	Maximum Take Off Mass
NACA	National Advisory Committee for Aeronautics
NASA	National Aeronautics and Space Administration
UA	Unmanned Aircraft
UAS	Unmanned Aircraft System
USAF	United States Air Force

Symbols

Fundamental Quantities

Symbol	Description	Unit
c	Chord length of rotor blade airfoil	m
D	Diameter of rotor disk	m
D_{aer}	Diameter of aerostat	m
D_{UA1}	Diameter of central mounting	mm
d_{ac}	Flight level limit	m
d_{ad}	Flight level limit	m
d_{crs}	Distance of cruise	m
d_{rtb}	Distance of return to base	m
d_{spr}	Distance of spreading	m
$\bar{D}_{\mathrm{aer}}$	Mean diameter of aerostat for $M_{\mathrm{ROOM}} = 100\mathrm{kg}$	m
h	Height of cross-section	mm
h_1	Outer height of cross-section	mm
h_2	Cavity height of cross-section	mm
h_{ef}	Effective height of cross-section	mm
L	Characteristic dimension	m
l_{gr1}	Length of outer undercarriage leg	mm
l_{gr2}	Length of inner undercarriage leg	mm
l_{UA1}	Side length of square-shaped plan form of fuselage	mm
l_{UA2}	Length of outer arm	mm
l_{UA3}	Width of arm	mm
l_{UA4}	Height of fuselage	mm
l_{UA5}	Diagonal engine axes span	mm
l_{UA6}	Outer diagonal propeller span	mm
l_{UA7}	Diagonal engine axes half span	mm
l_{UA8}	Height of undercarriage legs	mm
l_{S1}	Long dimension of hexagonal planform area of spreader	mm
l_{S2}	Short dimension of hexagonal planform area of spreader	mm

l_{S3}	Height of spreader	mm
M	Mass	kg
M_A	Aerostat structure mass	kg
M_{AH2}	Mass of aerostat hydrogen content	kg
M_{APLM}	Available payload mass of aerostat	kg
M_{ash}	Ash mass	kg
M_{bal}	Ballast mass	kg
M_{bat}	Battery mass	kg
M_O	Total overweight mass	kg
M_{OEM}	Operational empty mass	kg
M_{OOM}	Operational overweight mass	kg
M_{PLM}	Payload mass	kg
M_{ROOM}	Required operational overweight mass	kg
M_S	Empty spreader mass	kg
M_{TOM}	Take off mass	kg
M_{UA}	Mass of the unmanned aircraft structure	kg
n	Quantity amount of substance	mol
R	Radius of rotor disk	m
t	Time	s
t_{ac}	Time of axial climb	s
t_{ad}	Time of axial descent	s
t_{crs}	Time of cruise	s
t_{CC}	Thickness of compressed cap	mm
t_{CCest}	Estimated thickness of compressed cap	mm
t_{CCest}	Optimised thickness of compressed cap	mm
t_{CT}	Thickness of tensed cap	mm
t_{CTest}	Estimated thickness of tensed cap	mm
t_{CTopt}	Optimised thickness of tensed cap	mm
t_i	Time of particular phase of flight	s
t_{spr}	Time of spreading	s
t_{rtb}	Time of return to base	s
t_{tot}	Total time of any mission	s
U_{cel}	Voltage of a battery cell	V

w	Width of cross-section	mm
z_1	Distance between outer and total cross-section centres of gravity	mm
z_2	Distance between cavity and total cross-section centres of gravity	mm
z_{C}	Local z-axis coordinate of total cross-section centre of gravity	mm
z_{C1}	Local z-axis coordinate of outer cross-section centre of gravity	mm
z_{C2}	Local z-axis coordinate of cavity cross-section centre of gravity	mm
z_{Cest}	Estimated local z-axis coordinate of total cross-section centre of gravity	mm

Derived Quantities

Symbol	Description	Unit
α	Angle of attack	$^\circ$
β	Angular deflection of aerostat axis	$^\circ$
γ	Angular deflection of spreader axis	$^\circ$
δ	Angular margin in forward flight	$^\circ$
ϵ	Allowed angular deflection in final landing maneuver	$^\circ$
μ_∞	Viscosity of a fluid	$\mathrm{Pa \cdot s}$
ρ	Mass density	$\frac{\mathrm{kg}}{\mathrm{m}^3}$
ρ_{H2}	Mass density of hydrogen	$\frac{\mathrm{kg}}{\mathrm{m}^3}$
ρ_{m}	Molar density	$\frac{\mathrm{mol}}{\mathrm{m}^3}$
ρ_∞	Density of a fluid	$\frac{\mathrm{kg}}{\mathrm{m}^3}$
σ_{CCest}	Estimated stress in compressed cap	$\frac{\mathrm{N}}{\mathrm{mm}^2}$
σ_{CCopt}	Optimised stress in compressed cap	$\frac{\mathrm{N}}{\mathrm{mm}^2}$
σ_{CTest}	Estimated stress in tensed cap	$\frac{\mathrm{N}}{\mathrm{mm}^2}$
σ_{CTopt}	Optimised stress in tensed cap	$\frac{\mathrm{N}}{\mathrm{mm}^2}$
φ	Angle of aerostat wire structure	$^\circ$
Ω	Rotor angular frequency	$\frac{\mathrm{rad}}{\mathrm{s}}$
A	Area	m^2
A	Planform area of a rotor disk	m^2
A_1	Outer cross-section area	mm^2
A_2	Cavity cross-section area	mm^2
A_{aer}	Central cross-section area of aerostat	m^2
A_{b}	Planform area of a rotor blade	m^2
A_{CCest}	Estimated cross-section are of compressed cap	mm^2
A_{CTest}	Estimated cross-section are of tensed cap	mm^2
A_{UA1}	Planform-component of area of unmanned aircraft	m^2
A_{UA2}	Front-component of projected area of unmanned aircraft	m^2
A_{UA}	Projected area of unmanned aircraft, normal to relative wind	m^2
A_{SAB}	Projected area of spreader, Case A, Case B	m^2
A_{Saf}	Projected area of spreader in axial flight	m^2
A_{SC}	Projected area of spreader, Case C	m^2

A_{SD}	Projected area of spreader, Case D	m^2
A_{Sff}	Projected area of spreader in forward flight	m^2
A_{p}	Planform area	m^2
a_{spr}	Deceleration during spreading	$\frac{\mathrm{m}}{\mathrm{s}}$
a_{∞}	Speed of sound	$\frac{\mathrm{m}}{\mathrm{s}}$
$\bar{A}_{\mathrm{aer}}$	Mean Central cross-section area of aerostat for $M_{\mathrm{ROOM}} = 100\mathrm{kg}$	m^2
C	Electric capacity	Wh, Ah
C_{A1}	Third order coefficient in aerostat diameter cubic equation	1
C_{A2}	Second order coefficient in aerostat diameter cubic equation	m
C_{A3}	First order coefficient in aerostat diameter cubic equation	1
C_{A4}	Zero order coefficient in aerostat diameter cubic equation	m^3
C_{cel}	Electric capacity of a battery cell	Ah
C_{bat}	Electric capacity of a battery	Ah
D	Drag	N
D_{Aac}	Drag of aerostat in axial climb	N
D_{Aad}	Drag of aerostat in axial descent	N
D_{Aff}	Drag of aerostat in forward flight	N
D_{UAac}	Drag of unmanned aircraft in axial climb	N
D_{UAad}	Drag of unmanned aircraft in axial descent	N
D_{UAaf}	Drag of unmanned aircraft in axial flight	N
D_{UAff}	Drag of unmanned aircraft in forward flight	N
D_{UASad}	Total drag of UAS in axial descent	N
D_{Sac}	Drag of spreader in axial climb	N
D_{Sad}	Drag of spreader in axial descend	N
D_{Sff}	Drag of spreader in forward flight	N
f	Equivalent wetted area of an equivalent flat-plate	m^2
F_{ax}	Axial force in a cap	N
F_{gnd}	Ground force acting on undercarriage leg	N
F_{gndU}	Ultimate force F_{gnd}	N
$F_{\mathrm{gnd}x}$	X-component of ground force acting on undercarriage leg	N
$F_{\mathrm{gnd}z}$	Z-component of ground force acting on undercarriage leg	N
$F_{\mathrm{gnd}x\mathrm{U}}$	Ultimate force $F_{\mathrm{gnd}x}$	N
$F_{\mathrm{gnd}z\mathrm{U}}$	Ultimate force $F_{\mathrm{gnd}z}$	N

F_{O}	Total lift deficiency	N
F_{OOM}	Operational lift deficiency	N
F_{OPLM}	Payload lift deficiency	N
F_{ROOM}	Required operational lift deficiency	N
I_y	Cross-section moment of inertia	mm^4
I_{y1}	Outer cross-section moment of inertia	mm^4
I_{y2}	Cavity cross-section moment of inertia	mm^4
I_{yest}	Estimated cross-section moment of inertia	mm^4
I_{yopt}	Optimised cross-section moment of inertia	mm^4
L	Lift	N
L_{A}	Aerostat lift	N
L_{APLM}	Aerostat available lift	N
M	Molar mass	$\frac{\mathrm{kg}}{\mathrm{mol}}$
M_{Afab}	Aerostat fabric mass	$\frac{\mathrm{kg}}{\mathrm{m}^2}$
M_{B}	Bending moment	Nmm
M_{BU}	Ultimate bending moment	Nmm
M_{H2}	Molar mass of hydrogen	$\frac{\mathrm{kg}}{\mathrm{mol}}$
$\dot{M}_{\mathrm{S}}$	Spreader mass flow capability	$\frac{\mathrm{kg}}{\mathrm{s}}$
n	Engine revolutions per minute	$\frac{1}{\mathrm{min}}$
p	Pressure	Pa
P	Power	W
P_i	Required power in a particular flight phase	W
P_{I}	Input power	W
P_{O}	Output power	W
P_{Rac}	Required power in axial climb	W
P_{Raf}	Required power in axial flight	W
P_{Rcrs}	Required power in cruise	W
P_{Rff}	Required power in forward flight	W
P_{Rh}	Required power in hover	W
P_{Rrtb}	Required power in return to base	W
R	Universal gas constant	$\frac{\mathrm{J}}{\mathrm{Kmol}}$
R_{11z}	Z-component of reaction force on the outer pin of the lower arm	N
R_{11zU}	Ultimate reaction force R_{11z}	N

R_{12z}	Z-component of reaction force on the inner pin of the lower arm	N
R_{12zU}	Ultimate reaction force R_{12z}	N
R_{21z}	Z-component of reaction force on the outer pin of the upper arm	N
R_{21zU}	Ultimate reaction force R_{21z}	N
R_{22z}	Z-component of reaction force on the inner pin of the upper arm	N
R_{22zU}	Ultimate reaction force R_{22z}	N
R_{3x}	X-component of reaction force on the upper fuselage mounting	N
R_{3xU}	Ultimate reaction force R_{3xU}	N
R_{3z}	Z-component of reaction force on the fuselage mounting	N
R_{3zU}	Ultimate reaction force R_{4z}	N
R_{4x}	X-component of reaction force on the lower fuselage mounting	N
R_{4xU}	Ultimate reaction force R_{4x}	N
R_{B}	Reaction force on the outer joint of the undercarriage leg	N
R_{BU}	Ultimate reaction force R_{B}	N
R_{C}	Reaction force on he inner joint of the undercarriage leg	N
R_{CU}	Ultimate reaction force R_{C}	N
S	Surface area of control volume surrounding a rotor and its wake	m^2
S_{aer}	Surface area of aerostat	m^2
S_{C}	Compressive strength of a material	$\frac{N}{mm^2}$
S_{CUD}	Compressive strength of unidirectional carbon/epoxy composite	$\frac{N}{mm^2}$
S_{ref}	Reference area	m^2
S_{T}	Tensile strength of a material	$\frac{N}{mm^2}$
S_{TUD}	Tensile strength of unidirectional carbon/epoxy composite	$\frac{N}{mm^2}$
T	Thrust	N
T_1	Thrust of lower propulsion units in forward flight	N
T_{1x}	X-component of thrust of lower propulsion units in forward flight	N
T_{1z}	Z-component of thrust of lower propulsion units in forward flight	N
T_2	Thrust of upper propulsion units in forward flight	N
T_{2x}	X-component of thrust of upper propulsion units in forward flight	N
T_{2z}	Z-component of thrust of upper propulsion units in forward flight	N
T_{E1}	Thrust of one lower propulsion unit in forward flight	N
T_{E1U}	Ultimate thrust T_{E1}	N
T_{E2}	Thrust of one upper propulsion unit in forward flight	N

T_{E2U}	Ultimate thrust T_{E2}	N
T_{OEM}	Thrust to lift operational overweight mass	N
T_{PLM}	Thrust to lift payload mass	N
T_{Rac}	Required thrust in axial climb	N
T_{Rac}	Required thrust in axial climb	N
T_{Rad}	Required thrust in axial descent	N
T_{Rh}	Required thrust in hover	N
T_{x}	X-component of thrust	N
T_{z}	Z-component of thrust	N
U_{∞}	Velocity of relative wind	$\frac{\mathrm{m}}{\mathrm{s}}$
V	Velocity	$\frac{\mathrm{m}}{\mathrm{s}}$
V	Volume	m^3
V_{ac}	Axial climb velocity limit	$\frac{\mathrm{m}}{\mathrm{s}}$
V_{ad}	Axial descent velocity limit	$\frac{\mathrm{m}}{\mathrm{s}}$
V_{aer}	Volume of aerostat	m^3
V_{c}	Climb velocity	$\frac{\mathrm{m}}{\mathrm{s}}$
V_{crs}	Cruise velocity	$\frac{\mathrm{m}}{\mathrm{s}}$
v_{h}	Induced velocity in hover	$\frac{\mathrm{m}}{\mathrm{s}}$
v_{i}	Induced velocity	$\frac{\mathrm{m}}{\mathrm{s}}$
V_{rtb}	Return to base velocity	$\frac{\mathrm{m}}{\mathrm{s}}$
V_{spr}	Spreading velocity	$\frac{\mathrm{m}}{\mathrm{s}}$
V_{tip}	Velocity of rotor blade tip	$\frac{\mathrm{m}}{\mathrm{s}}$
V_{∞}	Velocity of relative wind	$\frac{\mathrm{m}}{\mathrm{s}}$
w	Velocity in far wake	$\frac{\mathrm{m}}{\mathrm{s}}$
W	Weight	N
W_{ash}	Ash payload weight	N
W_{A}	Aerostat structure weight	N
W_{AH2}	Aerostat hydrogen content weight	N
W_{APLM}	Available payload weight of aerostat	N
W_{bal}	Ballast weight	N
W_{bat}	Battery weight	N
W_{EM}	Empty weight	N
W_{O}	Total overweight	N

W_{OEM}	Operational empty weight	N
W_{OOM}	Operational overweight	N
W_{PLM}	Payload weight	N
W_{S}	Spreader weight	N
W_{TOM}	Take off weight	N
W_{UA}	Unmanned aircraft structure weight	N

ICAO Standard Atmosphere Constants

Symbol	Description	Unit	Value
μ_0	Primary viscosity	$\mathrm{Pa} \cdot \mathrm{s}$	0.000017894
ρ_0	Primary mass density	$\frac{\mathrm{kg}}{\mathrm{m}^3}$	1.225
g_0	Standard acceleration due to gravity	$\frac{\mathrm{m}}{\mathrm{s}^2}$	9.80665
P_0	Primary pressure	Pa	101325
R_0^*	Primary universal gas constant	$\frac{\mathrm{J}}{\mathrm{K} \cdot \mathrm{kmol}}$	8314.32
T_0	Primary temperature	K	288.15

Non-dimensional Constants

Symbol	Description	Unit	Value
ϵ	Iteration error estimator of numerical calculation	1	
η_{el}	Electric efficiency	1	
κ	Induced power correction factor	1	
λ	Inflow ratio	1	
λ_{c}	Climb velocity ratio	1	
λ_{h}	Inflow ratio in hover	1	
λ_{i}	Induced inflow ratio	1	
μ	Tip speed ratio	1	
π	Archimedes' number	1	3.14159
σ	Rotor solidity	1	
f	Safety factor	1	1.5
f_{s}	Special safety factor for composite materials	1	1.5
K	Empiric constant in blade profile power coefficient	1	
k_1	First order coefficient in induced velocity ratio approximation	1	
k_2	Second order coefficient in induced velocity ratio approximation	1	
k_3	Third order coefficient in induced velocity ratio approximation	1	
k_4	Fourth order coefficient in induced velocity ratio approximation	1	
M_∞	Mach number	1	
n	Iteration number of numerical calculation	1	
N	Number of flight phases	1	
N_{b}	Number of rotor blades	1	
n_{cel}	Required number of battery cells	1	
n_{gnd}	Ground limit load factor	1	2.8
n_{gndU}	Ground ultimate load factor	1	1.5
n_{neg}	Negative maneuvering load factor	1	-1.0
n_{pos}	Positive maneuvering load factor	1	3.5
Re	Reynolds number	1	
$Re_{\infty,\mathrm{L}}$	Reynolds number	1	
v_f	fibre volume fraction	1	

Non-dimensional Coefficients

Symbol	Description	Unit
C_d	Drag coefficient	1
C_D	Drag coefficient	1
C_{d0}	Profile (viscous) drag coefficient of a rotor blade airfoil	1
$C_{d\mathrm{A}}$	Drag coefficient of aerostat	1
$C_{d\mathrm{f}}$	Drag coefficient of fuselage	1
$C_{d\mathrm{UAaf}}$	Drag coefficient of unmanned aircraft in axial flight	1
$C_{d\mathrm{UAff}}$	Drag coefficient of unmanned aircraft in forward flight	1
$C_{d\mathrm{Sac}}$	Drag coefficient of spreader in axial climb	1
$C_{d\mathrm{Sad}}$	Drag coefficient of spreader in axial descend	1
$C_{d\mathrm{Sff}}$	Drag coefficient of spreader in forward flight	1
C_L	Lift coefficient	1
$\bar{C}_L$	Mean lift coefficient	1
C_P	Power coefficient	1
C_{P0}	Profile power coefficient	1
$C_{P\mathrm{c}}$	Climb power coefficient	1
$C_{P\mathrm{i}}$	Induced power coefficient	1
$C_{P\mathrm{p}}$	Parasitic power coefficient	1
C_Q	Total power coefficient in forward flight	1
C_T	Thrust coefficient	1
C_W	Thrust coefficient in forward flight maintaining the flight level	1

Tables

Figures

Introduction

EASA defines UAS: "'Unmanned aircraft system' ('UAS') means an unmanned aircraft and the equipment to control it remotely" [12, Page 12, Article 2, Point (1)]. The UAS aviation category has been developing swiftly in the last decade. So called "drones", commercially designed for unrestricted fun, have lately been developing into actual "adult" flying vehicles. With a growing number of drones available in the market, all the dangers connected with filling lower flight levels of the airspace all over the world with flying objects have required changes and improvements of legal regulations and restrictions. Nowadays, an operator needs a special license to operate almost any flying vehicle, with the exception of the aircraft models flown in reserved areas. By EASA: "'Unmanned aircraft system operator' ('UAS operator') means any legal or natural person operating or intending to operate one or more UAS" [12, Page 12, Article 2, Point (2)].
It is worth mentioning that this year was a milestone for unmanned aviation. On April 19, 2021, NASA's Ingenuity, a 1.8 kg autonomous unmanned helicopter, conducted the first flight in the atmosphere of Mars, thus becoming the first to perform a powered and controlled flight in a world beyond Earth.
Many concepts of larger scale civil UAS's are under development and a considerable number of them are even in the flight-capable prototype phase. Some of them are designed strictly to perform transport of inanimate objects of relatively small dimensions e.g. post or parcel delivery services, and some of them are planned to be used in personal or public transport.
Today, the category of large heavy-lifting UAS's still stands on insecure grounds and most of the operations falling into this category are still carried out by conventional helicopters. Some wood products manufacturers take part in fertilizing the forest soil by turning their wood waste into certified ash in the form of granules and spreading it in the forest using helicopters. Swedish company GI Lift AB intends to bring a new concept to this market by introducing an energy efficient, fossil fuel-free sustainable solution of the UAS - a heavy lifting unmanned rotorcraft capable of lifting a payload of several hundreds of kilograms, supported by an aerostat to carry the empty weight of the structure to maximize the lifting capacity.
To do this, firstly, a conceptual study of the design solution has to be done and the preliminary sizing is to be assumed.
Next, it is necessary to analyze and estimate the performance of such a machine in relation to the power requirements for various input parameters like propeller diameter, engine revolutions per minute, payload mass, angle of attack in forward flight, velocity in forward flight and axial flight etc.
Following that, assumptions are to be made in the flight planning to estimate the amount of energy which has to be stored in the battery packs.
Lastly, the structural strength of the proposed concept geometry has to be calculated. The structure must comply with the conventional aeronautical concept of maximizing the strength and stiffness and minimizing the mass.

1 Existing Designs and Technologies

1.1 Boeing NeXt Cargo Air Vehicle

"Boeing NeXt is laying the foundation for a next-generation mobility ecosystem in which autonomous and piloted air vehicles can safely coexist" [20]. Apparently, there are more vehicles and systems in development under NeXt.
As Figure 1.2 proves, Cargo Air Vehicle's prototype structure combines a lattice structure on a main fuselage with conventional weight-optimised beams as arms. The undercarriage is an independent four-point damped structure. It is equipped with 12 engines in 6 coaxial pairs. Figure 1.2 provides a nice view of symmetrically skewed engine axes, which are likely to provide better flight stability.

Table 1.1: Design parameters of Boeing Cargo Air Vehicle [21].

Length (m)	5.33
Width (m)	6.10
Operational empty weight (kg)	450
Payload weight (kg)	227

Figure 1.1: Boeing Cargo Air Vehicle performing a flight test [25, edited].

Figure 1.2: Boeing Cargo Air Vehicle performing a flight test, side view [31, edited].

1.2 ACC Innovation AB

ACC Innovation AB is a Swedish company founded in 2007 to develop and manufacture high-technology air and sea applications. It is a part of ACC Group located in Åtvidaberg, Sweden.

1.2.1 Thunderwasp

Thunderwasp is the flagship of the aerial product line of ACC Innovation. The propulsion unit consists of a single engine that provides power through a transmission system for four helicopter-like rotors.

Table 1.2: Design parameters of ACC Innovation AB Thunderwasp [22].

Length including rotor blades (m)	6.5
Width including rotor blades (m)	6.5
Rotor blades diameter (m)	3.0
Height (m)	1.6
Empty mass (kg)	230
Fuel mass (kg)	400
Maximum take off mass (kg)	870
Number of engines (1)	1
Engine alternatives	Piston engine
	Heavy fuel engine
	Turbo shaft
Power output (kW)	151 - 180
Number of propellers (1)	4
Cruising speed $\left(\frac{\text{km}}{\text{h}}\right)$	112
Endurance (h)	+5
Endurance 300 kg payload (h)	+3
Service ceiling (m)	4000
Service ceiling 400 kg	3000
and 300 kg payload (m)	

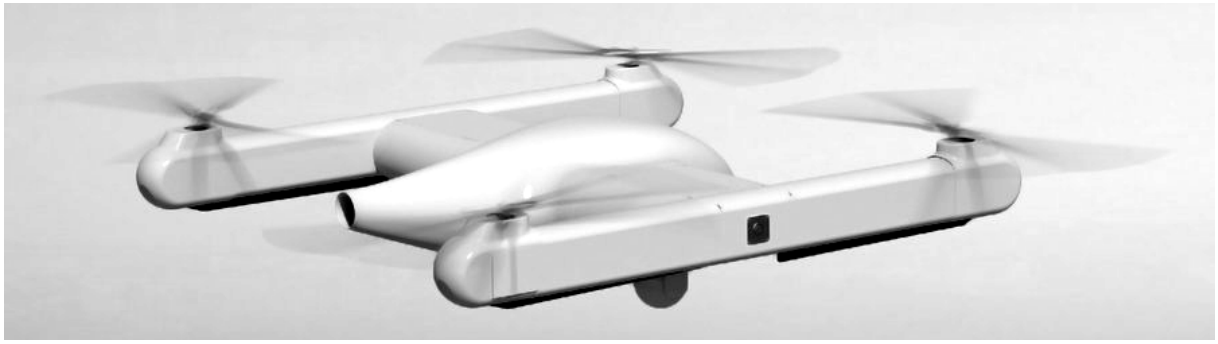

Figure 1.3: Visualization of ACC Innovation Thunderwasp [26, edited].

Figure 1.4: Prototype of ACC Innovation Thunderwasp II [27, edited].

1.2.2 Locust

Locust is intended to be a complementary product to Thunderwasp. It is a tandem-rotor unmanned helicopter.

Table 1.3: Design parameters of ACC Innovation AB Locust [22].

Rotor blades diameter (m)	2.9
Empty mass (kg)	147
Maximum take off mass (kg)	380 (Simonini 120 hp)
Number of engines (1)	1
Engine alternatives	Simonini Victor Super 2 (Automotive Gasoline)
	PBS TJ100 Turboshaft (Heavy Fuel)
	DC 12/24V (Electric)
Number of propellers (1)	2
Endurance (h)	5 (140 kg Payload)
Service ceiling (m)	4572

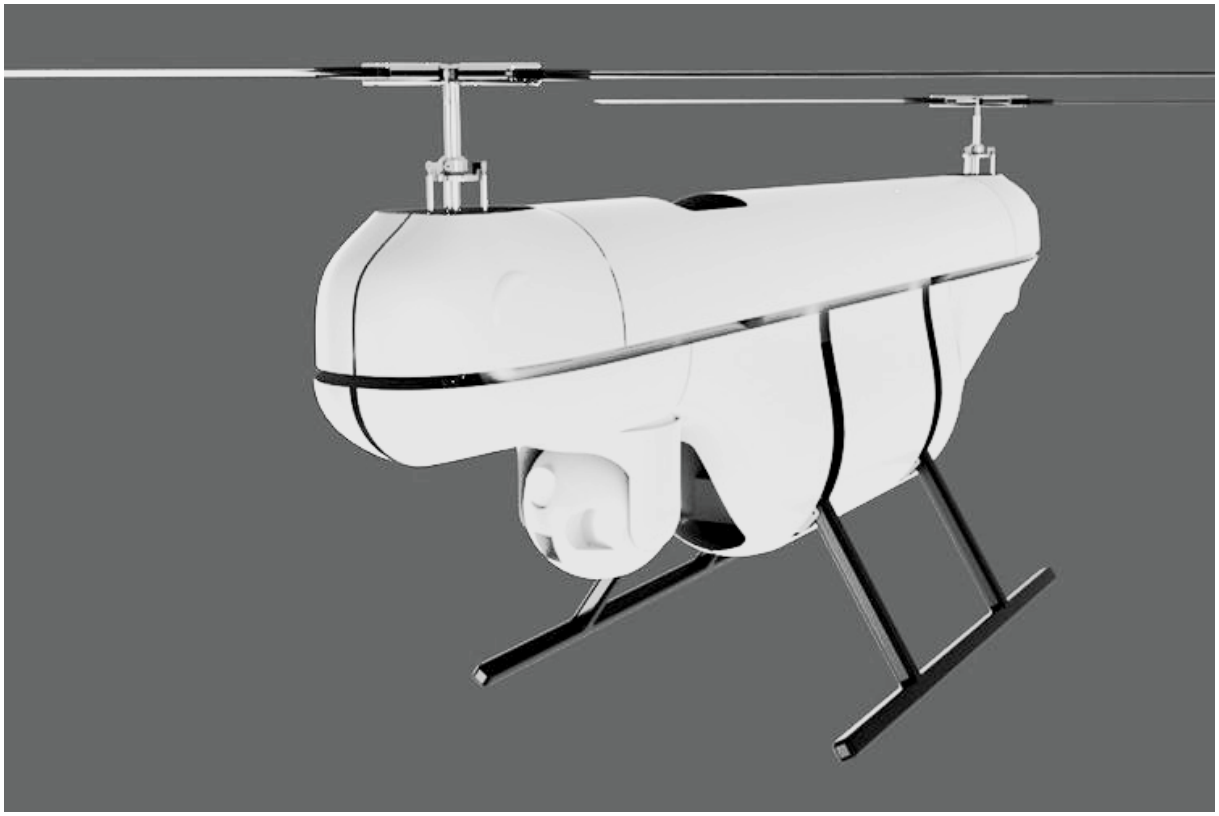

Figure 1.5: Visualization of ACC Innovation Locust [28, edited].

1.3 Volocopter VoloDrone

Volocopter GmbH is a German aircraft manufacturer based in Bruchsel and founded in 2011. The main vision of the company is to lead the way in realizing the urban air mobility phenomenon in both a manned and unmanned manner.
Based on Electric VTOL News [23], Volocopter Volodrone is built with composite-aluminium. It is controlled remotely or it can follow preplanned routes and it is capable of emergency landing even after multiple propulsion units failure.

Table 1.4: Design parameters of Volocopter VoloDrone [23].

Diameter (m)	9.2
Height (m)	2.3
Maximum take off mass (kg)	800
Payload mass (kg)	200
Number of engines (1)	18
Number of propellers (1)	18
Cruising speed $\left(\frac{\text{km}}{\text{h}}\right)$	80
Maximum speed $\left(\frac{\text{km}}{\text{h}}\right)$	110
Range (km)	40
Flight Time (h)	0.5
Batteries	Lithium-ion exchangeable batteries
Battery change out time (min)	5

Figure 1.6: Volocopter Volodrone [29, edited].

1.4 Griff Aviation 135

Griff Aviation is a Norwegian company based in Sykkylven specializing in drone design, manufacturing and service.
Griff 135 is the first of a Griff fleet. Griff Aviation claims it to be a modular design that allows battery and payload swap within seconds [24].

Table 1.5: Design parameters of Griff 135 [24].

Length folded (m)	1.44
Length unfolded (m)	2.26
Width folded (m)	0.77
Width unfolded (m)	2.41
Height (m)	0.47
Payload mass (kg)	50
Number of engines (1)	4
Number of propellers (1)	4
Flight Time (30 kg payload) (min)	25 - 30
Battery charge time (h)	1

Figure 1.7: Griff 135 [30, edited].

2 Certification Standards

To this day (1 July, 2021), there is no final certification specification for unmanned aircraft published by an official international authority. It is necessary to assemble assumed and resourceful possible certification requirements to get as close as possible to what might be the future final specification. To do so, the following documents were studied and a synthesis of their contents was used as a series of requirements for the initial conceptual design of the desired UAS.

Table 2.1: List of official documents used in certification requirements synthesis.

Authority	Document
EASA	Certification Specifications for Very Light Aeroplanes CS-VLA [13]
EASA	Certification Specifications and Acceptable Means of Compliance for Free Gas Balloons CS-31GB [14]
EASA	Certification Specifications, Acceptable Means of Compliance and Guidance Material for Small Rotorcraft CS-27 [15]
EASA	Certification Specifications, Acceptable Means of Compliance and Guidance Material for Large Rotorcraft CS-29 [16]
FAA	Advisory Circular: Certification of Normal Category Rotorcraft AC 27-1B [17]
FAA	Advisory Circular: Certification of Transport Category Rotorcraft AC 29-2C [18]

The most emphasis was put on requirements for strength with focus on the UA structure and undercarriage.

2.1 Flight Loads

Limit loads are the maximum loads expected in service [15, CS 27.301] [16, CS 29.301] [17, AC 27.301] [18, AC 29.301].

Ultimate loads are the limit loads multiplied by factor of safety [15, CS 27.301] [16, CS 29.301] [17, AC 27.301] [18, AC 29.301].

Factor of safety is $f = 1.5$ [15, CS 27.303] [16, CS 29.303] [17, AC 27.303] [18, AC 29.303].

The structure must withstand the limit loads without suffering permanent deformation [15, CS 27.305] [16, CS 29.305] [17, AC 27.305] [18, AC 29.305].

The structure must withstand the ultimate loads without failure for at least 3 seconds [15, CS 27.305] [16, CS 29.305] [17, AC 27.305] [18, AC 29.305].

Positive maneuvering load factor is $n_{\text{pos}} = 3.5$ [15, CS 27.337] [16, CS 29.337] [17, AC 27.337] [18, AC 29.337].

Negative maneuvering load factor is $n_{\text{neg}} = -1$ [15, CS 27.305] [16, CS 29.337] [17, AC 27.337] [18, AC 29.337].

Gust load is prescribed as a vertical gust of 9.1 $\frac{m}{s}$ at every critical airspeed including hover [15, CS 27.341] [16, CS 29.341] [17, AC 27.341] [18, AC 29.341].

Jettisoning all available ballast has to stop a descent of 4 $\frac{\text{m}}{\text{s}}$ [14, AMC 31GB.51].

2.2 Ground Loads

Maximum design weight is to be considered [15, CS 27.473] [16, CS 29.473] [17, AC 27.473] [18, AC 29.473].

Limit ground load factor is $n_{\text{gnd}} = 2.8$ [17, AC 27.723] [18, AC 29.723].

Ultimate ground load factor is $n_{\text{gndU}} = 1.5$ [17, AC 27.501] [18, AC 29.501].

Vertical reactions in the level landing attitude are to be considered the maximum designed weight acting evenly distributed on the undercarriage legs [15, CS 27.501] [16, CS 29.501].

Undercarriage has to withstand a limit drop test from the height of 0.33 m [15, CS 27.725].

2.3 Special Factors

Safety factor $f = 1.5$ in strength calculations of structures manufactured with composite materials must be multiplied by the special factor $f_{\text{s}} = 1.5$ [13, AMC VLA 619].

3 Design Requirements

The purpose of the designed UAS is to spread certified ash in nature. It is supposed to perform a fully autonomous flight, which is defined by EASA as: "'autonomous operation' means an operation during which an unmanned aircraft operates without the remote pilot being able to intervene" [12, Page 14, Article 2, Point (17)]. The system should be composed of the UA, the ash spreader and the aerostat. An important part of the whole system is a platform that the UAS should be transported on, take off from and land to. The platform should be equipped with an automated system for battery reload, recharge and storage.

3.1 UA Structure

The structure of the UA must withstand loading in a case of 1000 kg of ash payload. It is required to be an assembly with removable arms for easier transport and possible service. The fuselage should provide housing for all the electronic equipment including the camera system.

3.2 Propulsion

The UA should be armed with four propulsion units consisting of a pair of coaxial engines each. Battery packs are to be fitted underneath the fuselage. Engines, battery packs, appropriate controllers and additional electronic equipment will be supplied by MGM COMPRO. Propellers are expected to by supplied by HELIX.

3.3 Aerostat

The aerostat should ease the system off the battery packs weight and the weight of the structure itself, leaving the engines to provide the thrust required to handle the payload and to change the attitude during the flight. Lindstrand Technmologies are planned to supply the aerostat.

3.4 Ash Spreader

The first version of the UAS is to carry out missions with 500 kg of ash. By EASA terms: "'payload' means instrument, mechanism, equipment, part, apparatus, appurtenance, or accessory, including communications equipment, that is installed in or attached to the aircraft and is not used or intended to be used in operating or controlling an aircraft in flight, and is not part of an airframe, engine, or propeller" [12, Page 13, Article 2, Point (12)]. That means the empty ash spreader is considered a part of the UAS payload.

3.5 Desired Future Improvements

The propulsion units will be improved so as to produce enough thrust to fly with the ash payload up to 1000 kg. Also, the UAS should perform a certain type of missions without the support of the aerostat.

4 Concept Study

4.1 Overall Layout

Two possible layouts were considered. Layout B from Figure 4.2 was chosen as the one to proceed with mostly because - as plan form of layout A from Figure 4.1 reveals - propulsion thrust would introduce additional torsional loading on the unsymmetrical geometry beyond simple bending.

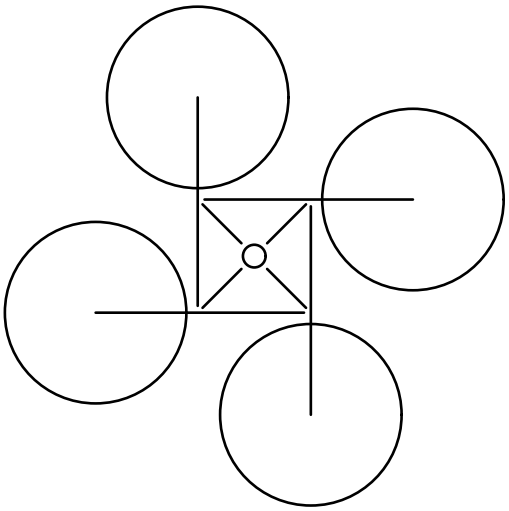

Figure 4.1: General conceptual layout A.

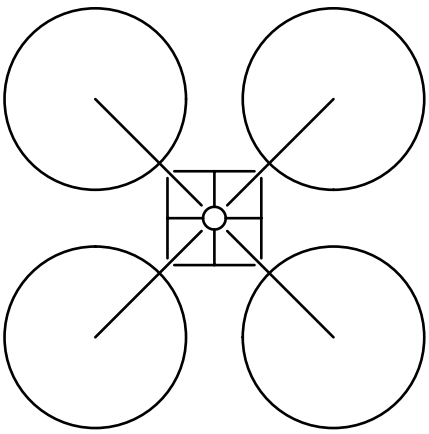

Figure 4.2: General conceptual layout B.

Open spaces within the fuselage should act as housing compartments for all the electronic equipment that is to hang firmly on a removable lid that ought to cover the whole fuselage providing roofing.

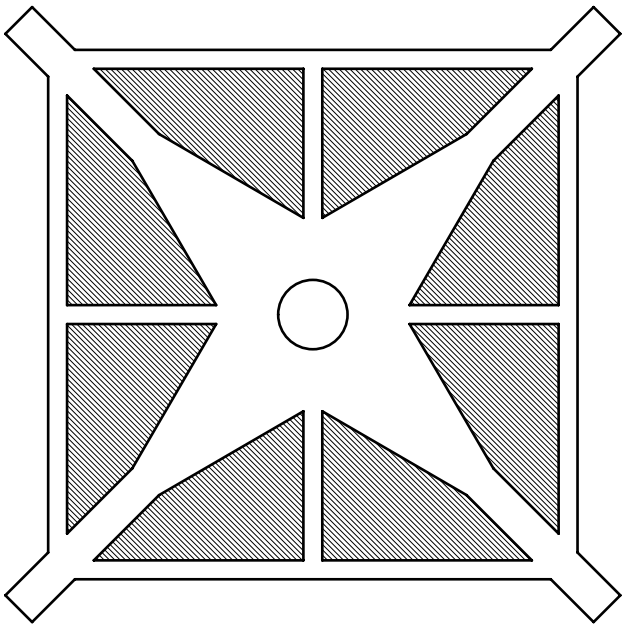

Figure 4.3: Electronic equipment compartments in plan form.

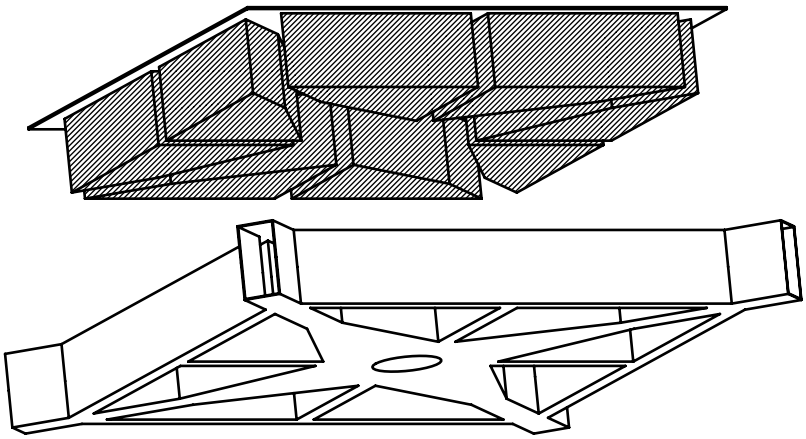

Figure 4.4: Electronic equipment geometry envelopes.

4.2 Battery Housing

Two options for battery placement are proposed. The variant A from Figure 4.5 where the battery pack would be carried on the spreader would require quite long cables to connect battery with controllers. That might cause problems considering the electronic performance. Unsymmetrical weight loading on freely hanging spreader would also be generally inconvenient. The solution of variant B from Figure 4.6 with two stiff compartments mounted symmetrically underneath the fuselage is to be carried out. It provides the exact position of the battery after programmed landing which makes it possible for the replacing system on the platform to perform automated battery replacement.

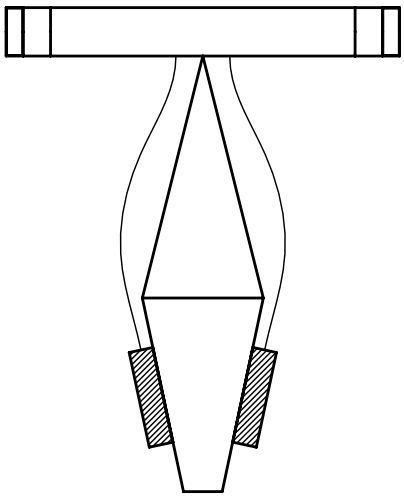

Figure 4.5: Battery placement variant A.

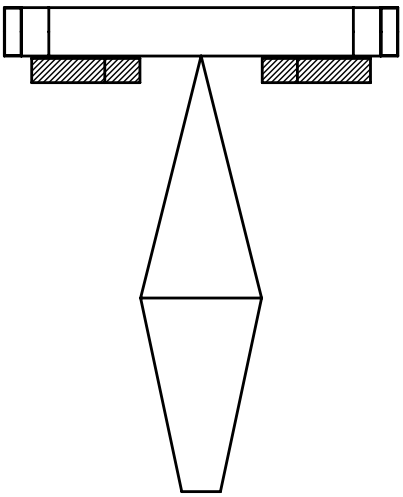

Figure 4.6: Battery placement variant B.

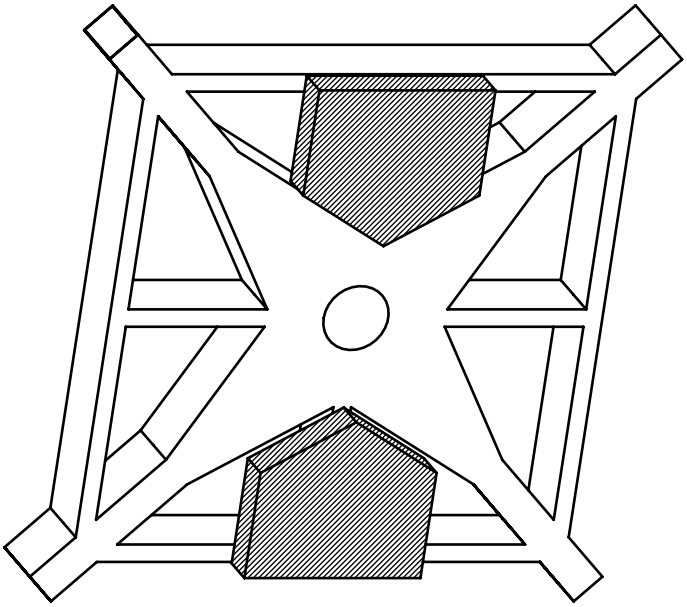

Figure 4.7: Battery compartments stiffly mounted underneath the fuselage.

4.3 Undercarriage

Two undercarriage design solutions were brought up. The solution where the bottom of the fuselage itself would act as an undercarriage, being shaped to a clipped pyramid so it would fit the landing platform exactly to provide alignment during landing, was dismissed simply because it is required for the UA to be able to take off from and to land on any available flat surface. For that reason, the conventional landing gear solution was chosen.

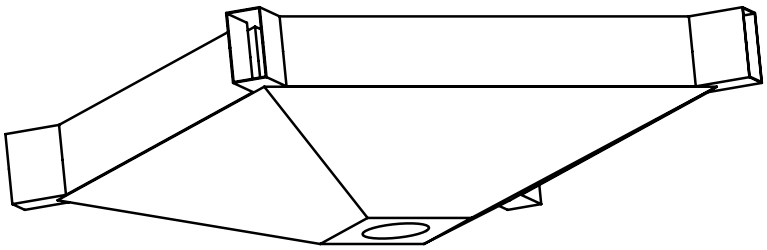

Figure 4.8: Unconventional undercarriage concept.

Conventional as it is, it still provides a variety of possible geometries. For simplicity, the legs are to be either curved or straight. Straight legs require fuselage to have angled mounting planes sticking out of the bottom outer surface. This is inconvenient but the simplicity of design and manufacturing technology far outweighs the possible advantages of curved legs.

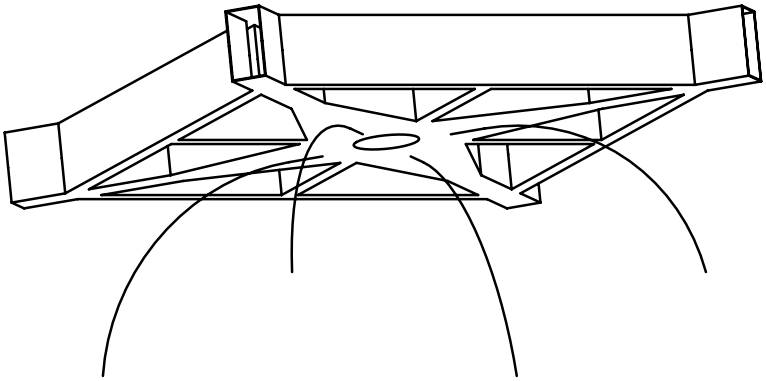

Figure 4.9: Conventional undercarriage concept; curved legs.

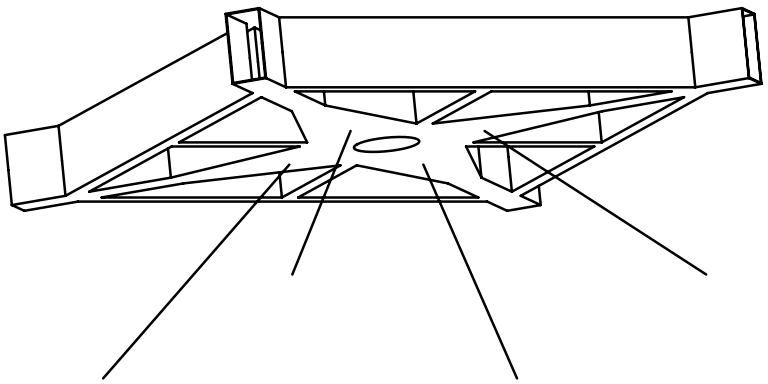

Figure 4.10: Conventional undercarriage concept; straight legs.

4.4 Preliminary Sizing

An important point in sizing is to make sure that the whole rotor disk plan form does not collide with the plan form of fuselage. There should also be enough space between the rotor disks. The fuselage itself should provide enough open space to accommodate the electronic equipment. Central mounting ought to be wide enough to provide sufficient space for manipulation during the assembly and disassembly.

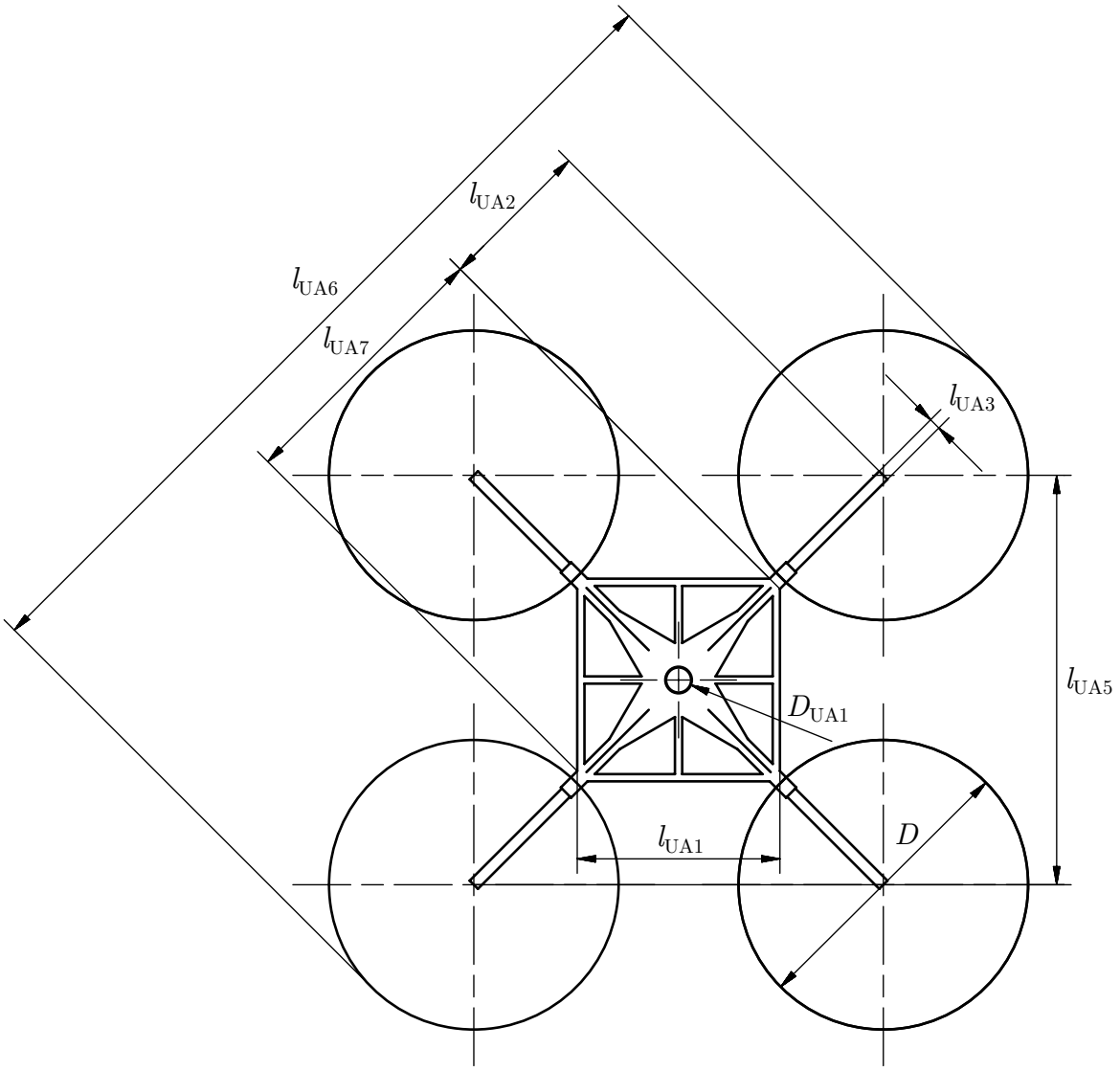

Figure 4.11: Conceptual sizing of the UA; plan form.

To design undercarriage legs, a certain angular deflection in the final landing maneuver $\epsilon\,(^\circ)$ has to be considered.

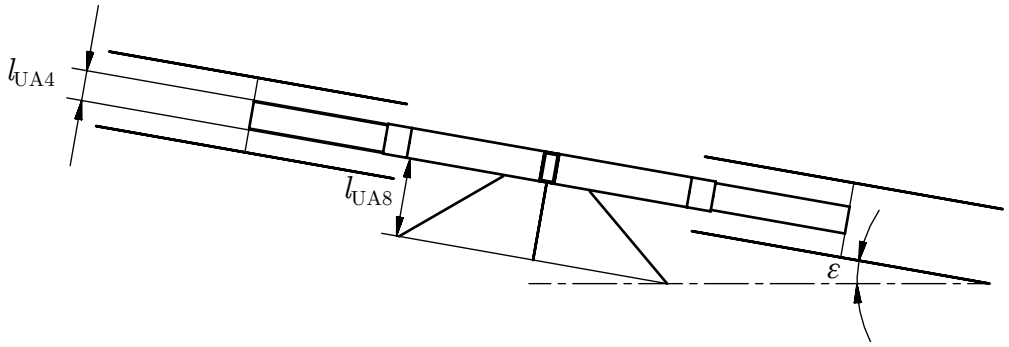

Figure 4.12: Conceptual sizing of the UA considering the undercarriage; side view.

Table 4.1: Conceptual sizing dimensions.

Symbol	Description	Unit	Value
ϵ	Allowed angular deflection in final landing maneuver	$^\circ$	10
D_{UA1}	Diameter of the central mounting	mm	200
D	Diameter of the rotor disk	mm	2000
l_{UA1}	Side length of the square-shaped plan form of the fuselage	mm	1300
l_{UA2}	Length of the outer arm	mm	1000
l_{UA3}	Width of the arm	mm	100
l_{UA4}	Height of the fuselage	mm	200
l_{UA5}	Short engine axes span	mm	4000
l_{UA6}	Outer diagonal propeller span	mm	6000
l_{UA7}	Diagonal length of the square-shaped plan form of the fuselage	mm	1900
l_{UA8}	Height of the undercarriage legs	mm	520

5 Design

5.1 Prerequisites

Calculations were done in computational software MathWorks® MATLAB 2020b. Numerical study of drag was done in CFD software ANSYS ® Fluent 2020. Structure design was done in CAD/CAM software Siemens ® NX 12.

5.1.1 International Standard Atmosphere

ICAO defines [11, Page E-vii, Table A] [11, Page E-xi, Table C] the primary characteristics of the air in atmosphere as partially provided in the Table 5.1.

Table 5.1: Several primary constants of the ICAO standard atmosphere [21] [11, Page E-xi, Table C]

Symbol	Description	Unit	Value
μ_0	Primary viscosity	$\mathrm{Pa} \cdot \mathrm{s}$	0.000017894
ρ_0	Primary mass density	$\frac{\mathrm{kg}}{\mathrm{m}^3}$	1.225
g_0	Standard acceleration due to gravity	$\frac{\mathrm{m}}{\mathrm{s}^2}$	9.80665
P_0	Primary pressure	Pa	101325
R_0^*	Primary universal gas constant	$\frac{\mathrm{J}}{\mathrm{K} \cdot \mathrm{kmol}}$	8314.32
T_0	Primary temperature	K	288.15

Since the UAS is being designed for operation in flight levels very close to sea level, the primary constants from the Table 5.1 were used in all calculations.

5.1.2 Coordinate System

Bertin's [4, Page 240, Figure 5.5] airplane coordinate system was used to reference forces and moments.

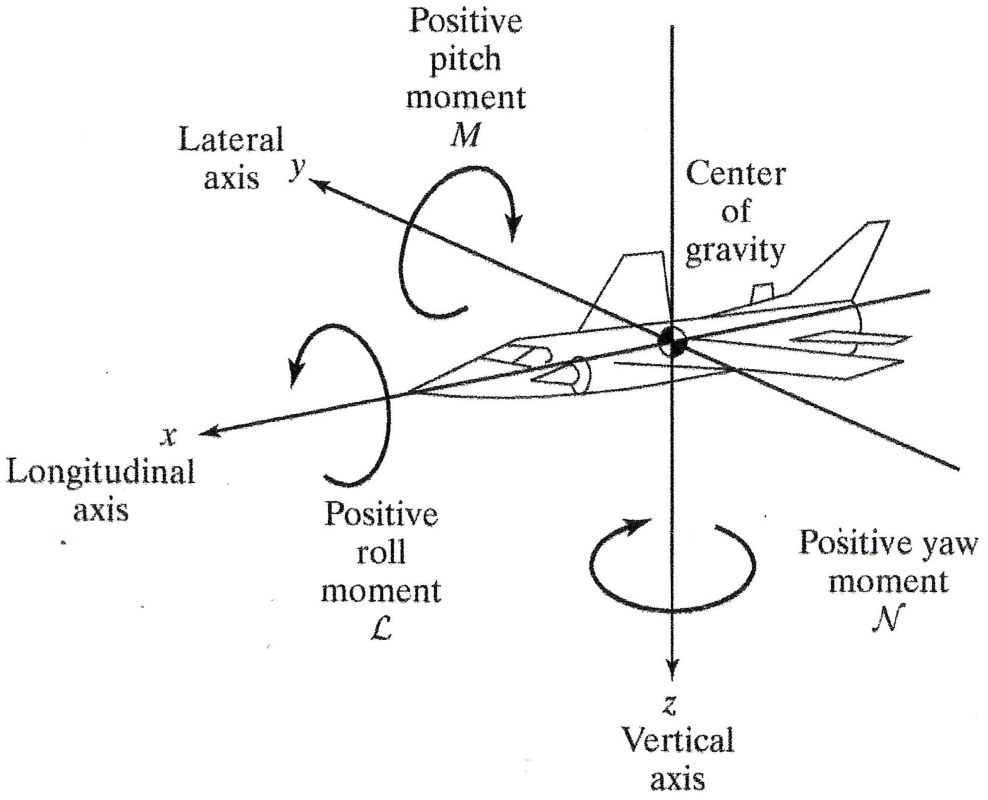

Figure 5.1: Reference axes of the airplane and the corresponding aerodynamic moments [4, Page 240, Figure 5.5]

5.1.3 Non-dimensional Coefficients

Bertin introduces [4, Page 69, Section 2.5] Mach number $M_\infty\,(1)$

$$M_\infty = \frac{V_\infty}{a_\infty} \tag{5.1}$$

where $V_\infty\,\left(\frac{\mathrm{m}}{\mathrm{s}}\right)$ is velocity of relative wind and $a_\infty\,\left(\frac{\mathrm{m}}{\mathrm{s}}\right)$ is speed of sound in fluid under the same conditions.

Bertin also introduces [4, Page 69, Equation 2.20] Reynolds number $Re_{\infty,\mathrm{L}}\,(1)$

$$Re_{\infty,\mathrm{L}} = \frac{\rho_\infty V_\infty L}{\mu_\infty} \tag{5.2}$$

where $L\,(\mathrm{m})$ is characteristic dimension of the investigated object, $\rho_\infty\,\left(\frac{\mathrm{kg}}{\mathrm{m}^3}\right)$ is density of the fluid and $\mu_\infty\,(\mathrm{Pa}\cdot\mathrm{s})$ is dynamic viscosity of the fluid.

White provides the general equation [3, Page 431, Equation 7.62] of drag coefficient $C_D\,(1)$

$$C_D = \frac{\mathrm{drag}}{\frac{1}{2}\rho V^2 A}. \tag{5.3}$$

"The area A is usually one of three types:

1. *Frontal area*, the body as seen from the stream; suitable for thick, stubby bodies, such as spheres, cylinders, cars, trucks, missiles, projectiles, and torpedoes.
2. *Planform area*, the body area as seen from above; suitable for wide, flat bodies such as wings and hydrofoils.
3. *Wetted area*, customary for surface ships and barges." [3, Page 431, Section 7.6]

where $drag\,(\mathrm{N})$ stands for air resistance force, $\rho\,\left(\frac{\mathrm{kg}}{\mathrm{m}^3}\right)$ is density of the fluid environment and $V\,\left(\frac{\mathrm{m}}{\mathrm{s}}\right)$ is velocity of relative wind.

White also provides the equation [3, Page 447, Equation 7.66b] for drag coefficient $C_D\,(1)$

$$C_D = \frac{D}{\frac{1}{2}\rho V^2 A_\mathrm{p}} \tag{5.4}$$

and the equation [3, Page 447, Equation 7.66a] for lift coefficient $C_L\,(1)$

$$C_L = \frac{L}{\frac{1}{2}\rho V^2 A_\mathrm{p}}, \tag{5.5}$$

both in a matter of wing-type geometry, where $D\,(\mathrm{N})$ is drag, $L\,(\mathrm{N})$ is lift and $A_\mathrm{p}\,(\mathrm{m}^2)$ stands for planform area.

Leishmann provides the expression [6, Page 43, Equation 2.26] for thrust coefficient $C_T\,(1)$

$$C_T = \frac{T}{\rho A V_{\text{tip}}^2} = \frac{T}{\rho A \Omega^2 R^2} \tag{5.6}$$

where $T\,(\text{N})$ is thrust, $\rho\left(\frac{\text{kg}}{\text{m}^3}\right)$ is density of air, $A\,(\text{m}^2)$ is planform area of rotor disk, $V_{\text{tip}}\left(\frac{\text{m}}{\text{s}}\right)$ is peripheral velocity of rotor blade tip, $\Omega\left(\frac{\text{rad}}{\text{s}}\right)$ is angular frequency of rotor and $R\,(\text{m})$ is radius of rotor disk.

Leishmann also provides the expression [6, Page 44, Equation 2.28] for ideal power coefficient $C_P\,(1)$ based on uniform inflow with no viscous losses

$$C_P = \frac{P}{\rho A V_{\text{tip}}^3} = \frac{P}{\rho A \Omega^3 R^3} \tag{5.7}$$

where $P\,(\text{W})$ is power.

Leishmann states: "The grouping $N_{\text{b}}cR/A$ (or $N_{\text{b}}c/\pi R$) is known as *rotor solidity*, which is the ratio of blade area to rotor disk area, and is represented by the symbol σ. Typical values of σ for a helicopter rotor range between 0.07 and 0.12" [6, Page 46, Subsection 2.2.7].

$$\sigma = \frac{\text{Blade area}}{\text{Disk area}} = \frac{A_{\text{b}}}{A} = \frac{N_{\text{b}}cR}{\pi R^2} = \frac{N_{\text{b}}c}{\pi R} \tag{5.8}$$

where $A_{\text{b}}\,(\text{m}^2)$ is planform area of rotor blade, $N_{\text{b}}\,(1)$ is number of rotor blades and $c\,(\text{m})$ is chord length of rotor blade airfoil. Also, estimation of rotor solidity can be done with the expression [6, Page 113, Equation 3.150] from Leishmann

$$\bar{C_L} = 6\left(\frac{C_T}{\sigma}\right) \tag{5.9}$$

where $\bar{C_L}\,(1)$ is mean lift coefficient. "Typically, $\bar{C_L}$ is found in the range 0.5 to 0.8 for helicopter rotors, and so the mean angles of attack for hovering flight vary from 5 to 8 degrees" [6, Page 113, Subsection 3.3.17]. After rearranging

$$\sigma = 6\left(\frac{C_T}{\bar{C_L}}\right). \tag{5.10}$$

Leishmann introduces the expression [6, Page 44, Equation 2.27] for induced inflow ratio $\lambda_{\text{i}}\,(1)$

$$\lambda_{\text{i}} = \frac{v_{\text{i}}}{\Omega R} \tag{5.11}$$

where $v_{\text{i}}\left(\frac{\text{m}}{\text{s}}\right)$ is airflow induced velocity.

Leishmann also introduces the expression [6, Page 64, Subsection 2.4.1] for tip speed ratio $\mu\,(1)$

$$\mu = \frac{V_\infty \cos(\alpha)}{\Omega R} \tag{5.12}$$

where $V_\infty\left(\frac{\text{m}}{\text{s}}\right)$ is relative wind speed and $\alpha\,(^\circ)$ is angle of attack.

5.2 Weights

5.2.1 Weights in Configuration with Aerostat, Lift Deficiency

L_{A}	Aerostat lift
F_{O}	Total lift deficiency
F_{OOM}	Operational lift deficiency
F_{OPLM}	Payload lift deficiency
W_{TOM}	Take off weight
W_{OEM}	Operational empty weight
W_{PLM}	Payload weight
W_{AH2}	Weight of the aerostat hydrogen content
W_{EM}	Empty weight
W_{S}	Spreader weight
W_{ASH}	Ash weight
W_{A}	Aerostat structure weight
W_{APLM}	Aerostat available payload weight
W_{OOM}	Operational overweight
W_{BAL}	Ballast weight
W_{UA}	Unmanned aircraft structure weight
W_{BAT}	Battery weight

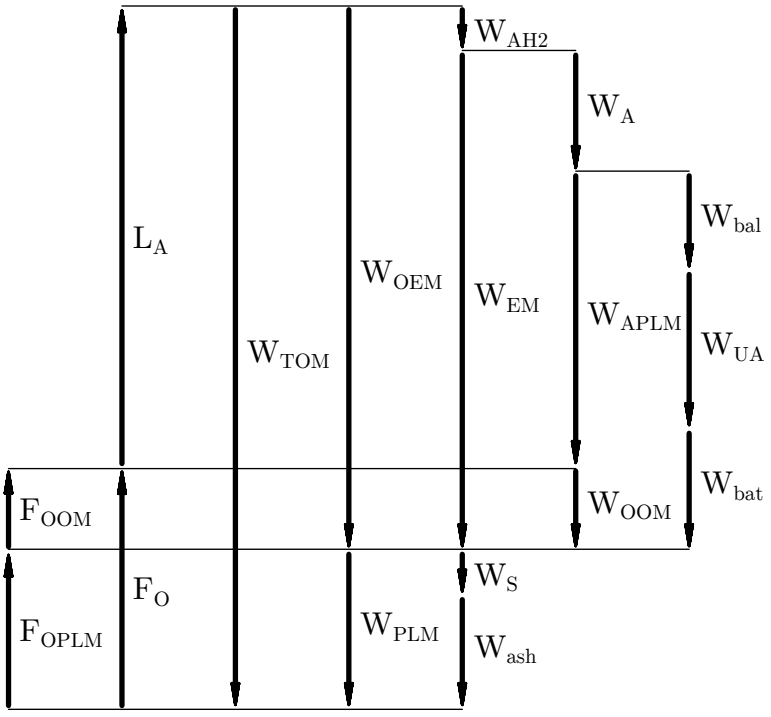

Figure 5.2: Weight breakdown of the UAS including aerostat.

It is required that take off weight $W_{\mathrm{TOM}}\,(\mathrm{N})$ of the UAS is greater than lift $L_{\mathrm{A}}\,(\mathrm{N})$ provided by aerostat, so the UAS is able to maintain a stable flight. That results in lift deficiency $F_{\mathrm{O}}\,(\mathrm{N})$. For a general payload configuration, in the case of hover, lift deficiency corresponds to required thrust in hover $T_{\mathrm{Rh}}\,(\mathrm{N})$

$$F_{\mathrm{O}} = T_{\mathrm{Rh}} \tag{5.13}$$

and in the case of axial descent without engine power, lift deficiency corresponds to total drag of the UAS $D_{\mathrm{UASad}}\,(\mathrm{N})$

$$F_{\mathrm{O}} = D_{\mathrm{UASads}}. \tag{5.14}$$

5.2.2 Operational Lift Deficiency, Operational Overweight Mass

With no payload, total lift deficiency $F_{\mathrm{O}}\,(\mathrm{N})$ is introduced only by operational overweight mass $M_{\mathrm{OOM}}\,(\mathrm{kg})$ of the UA and aerostat, and so

$$F_{\mathrm{O}} = F_{\mathrm{OOM}} \sim W_{\mathrm{O}} = W_{\mathrm{OOM}}. \tag{5.15}$$

Operational overweight $W_{\mathrm{OOM}}\,(\mathrm{N})$

$$W_{\mathrm{OOM}} = W_{\mathrm{OEM}} - L_{\mathrm{A}} = M_{\mathrm{OOM}} g_0 = M_{\mathrm{OEM}} g_0 - L_{\mathrm{A}} \tag{5.16}$$

where operational overweight mass $M_{\mathrm{OOM}}\,(\mathrm{kg})$

$$M_{\mathrm{OOM}} = M_{\mathrm{OEM}} - \frac{L_{\mathrm{A}}}{g_0}. \tag{5.17}$$

As the initial parameter for further design, required operational overweight mass $M_{\mathrm{ROOM}}\,(\mathrm{kg})$ corresponding to required operational lift deficiency $F_{\mathrm{ROOM}}\,(\mathrm{N})$ must be set.

5.2.3 Total Lift Deficiency, Total Overweight Mass

If the payload mass $M_{\mathrm{PLM}}\,(\mathrm{kg})$ is introduced, total lift deficiency $F_{\mathrm{O}}\,(\mathrm{N})$ becomes a sum of operational lift deficiency $F_{\mathrm{OOM}}\,(\mathrm{N})$ and payload lift deficiency $F_{\mathrm{OPLM}}\,(\mathrm{N})$ corresponding to payload weight $W_{\mathrm{PLM}}\,(\mathrm{N})$

$$F_{\mathrm{O}} = F_{\mathrm{OOM}} + F_{\mathrm{OPLM}} \sim W_{\mathrm{O}} = W_{\mathrm{OEM}} + W_{\mathrm{PLM}} - L_{\mathrm{A}} = W_{\mathrm{OOM}} + W_{\mathrm{PLM}}. \tag{5.18}$$

Total overweight $W_{\mathrm{O}}\,(\mathrm{N})$

$$W_{\mathrm{O}} = W_{\mathrm{OEM}} + W_{\mathrm{PLM}} - L_{\mathrm{A}} = M_{\mathrm{O}} g_0 = \left(M_{\mathrm{OEM}} + M_{\mathrm{PLM}}\right) g_0 - L_{\mathrm{A}} \tag{5.19}$$

where total overweight mass $M_{\mathrm{O}}\,(\mathrm{kg})$

$$M_{\mathrm{O}} = M_{\mathrm{OEM}} + M_{\mathrm{PLM}} - \frac{L_{\mathrm{A}}}{g_0}. \tag{5.20}$$

Alternatively, using operational overweight mass $M_{\mathrm{OOM}}\,(\mathrm{kg})$, total overweight $W_{\mathrm{O}}\,(\mathrm{N})$

$$W_{\mathrm{O}} = W_{\mathrm{OOM}} + W_{\mathrm{PLM}} = M_{\mathrm{O}} g_0 = \left(M_{\mathrm{OOM}} + M_{\mathrm{PLM}}\right) g_0, \tag{5.21}$$

where total overweight mass $M_{\mathrm{O}}\,(\mathrm{kg})$

$$M_{\mathrm{O}} = M_{\mathrm{OOM}} + M_{\mathrm{PLM}}. \tag{5.22}$$

5.2.4 Weights in Configuration Without Aerostat

If the UAS is to operate without aerostat, in the case of hover, the whole take off mass M_{TOM} (kg) has to be lifted by the required thrust in hover T_{Rh} (N) provided by engines.

T_{Rh}	Required thrust in hover
T_{OEM}	Thrust to lift operational empty mass
T_{PLM}	Thrust to lift payload mass

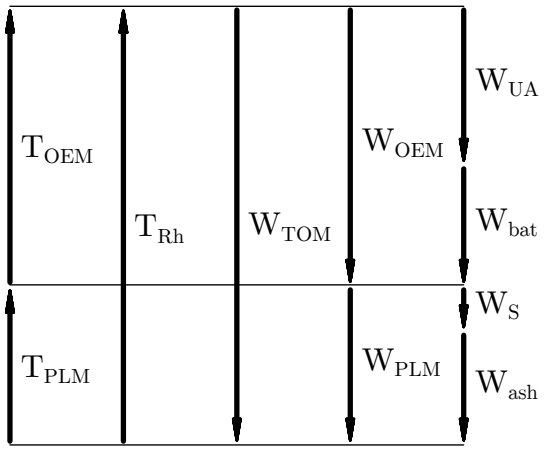

Figure 5.3: Weight breakdown of the UAS excluding aerostat.

With no payload mass M_{PLM} (kg), without the lift of aerostat L_{A} (N), thrust to lift operational empty mass T_{OEM} (N) becomes required thrust in hover T_{Rh} (N).

5.3 Drag Analysis

An estimation of the UAS drag characteristics should be done to get an idea of the flight mechanics concerning performance. The UAS structure is composed of bodies of the UA, spreader and aerostat. Drag coefficients of these bodies were investigated separately. Since the geometries of UA and spreader are fairly complex, numerical studies in ANSYS ® Fluent 2020 were performed for the cases of axial climb, axial descent and forward flight for range of relative wind velocity $V_\infty \left(\frac{\mathrm{m}}{\mathrm{s}}\right) = \{1, 5, 10\}$ in a volume 3.5 m x 3.5 m x 6 m (width x height x length).

5.3.1 Drag Analysis Model

Table 5.4: Drag coefficient calculation solver parameters.

Type	Pressure-based
Velocity Formulation	Absolute
Time	Steady
Viscosity Model	SST k-omega

Table 5.5: Drag coefficient calculation spacial discretization parameters.

Gradient	Least Squares Cell Based
Pressure	Second Order
Momentum	Second Order Upwind
Turbulent	Second Order Upwind
Specific Dissipation Rate	Second Order Upwind

Table 5.6: Drag coefficient calculation pseudo transient explicit relaxation factors.

Pressure	0.50
Momentum	0.50
Density	1.00
Body Forces	1.00
Turbulent Kinetic Energy	0.75
Specific Dissipation Rate	0.75
Turbulent Viscosity	1.00

Table 5.7: Drag coefficient calculation settings.

Time Step Method	Automatic
Time Scale Factor	1
Length Scale Method	Conservative
Verbosity	0
Number of Iterations	500

5.3.2 UA Drag Coefficient

Simplified UA geometry for the drag coefficient numerical study was set using the conceptual dimensions from Table 4.1 as displayed in Figure 5.4.

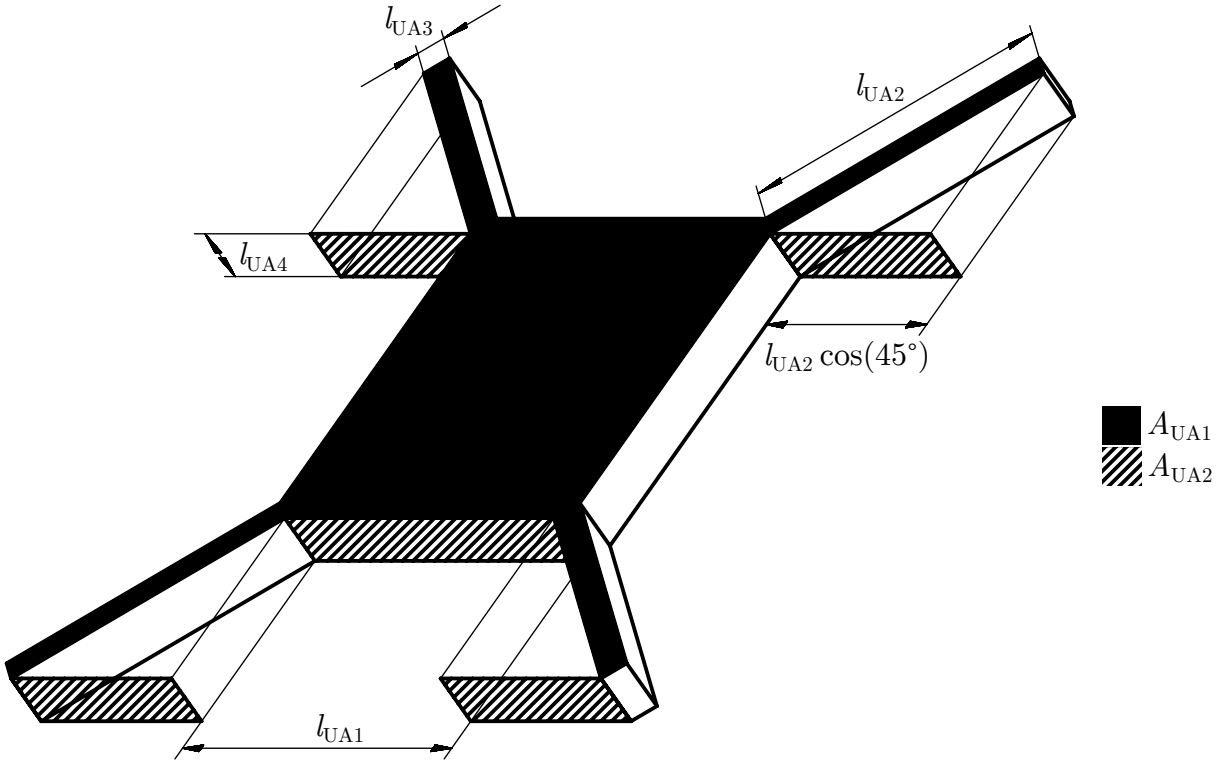

Figure 5.4: Simplified geometry of UA for drag coefficient assessment.

Introducing the flight conditions, $A_{\mathrm{UA1}}\,(\mathrm{m}^2)$ and $A_{\mathrm{UA2}}\,(\mathrm{m}^2)$ are specific areas of the simplified UA geometry from Figure 5.4 and $A_{\mathrm{UA}}(\alpha)\,(\mathrm{m}^2)$ is the total projected area of the simplified UA geometry normal to the relative wind.

$$A_{\mathrm{UA1}} = l_{\mathrm{UA1}}^2 + 4 l_{\mathrm{UA2}} l_{\mathrm{UA3}}, \tag{5.23}$$

$$A_{\mathrm{UA2}} = l_{\mathrm{UA1}} l_{\mathrm{UA4}} + 4 l_{\mathrm{UA2}} \cos(45°) l_{\mathrm{UA4}}, \tag{5.24}$$

$$A_{\mathrm{UA}} = A_{\mathrm{UA1}} \sin(\alpha) + A_{\mathrm{UA2}} \cos(\alpha). \tag{5.25}$$

Simplified UA geometry does not contain landing gear and other design features that worsen the overall drag characteristics. For that reason, the resulting drag coefficients were increased by 0.1. Finally, the UA drag coefficient in forward flight was distinguished for angles of attack smaller and greater than 22.5°.

Table 5.8: Results of the UA drag coefficient numerical study.

$\alpha\,(^\circ)$	$C_d\,(1)$			Mean	Result
	$V_\infty\left(\frac{\mathrm{m}}{\mathrm{s}}\right)$				
	1	5	10		
90	1.3128498	1.3123556	1.3122479	1.3	$C_{d\mathrm{UAaf}} = 1.4$
5	0.8075228	0.8011760	0.7999773	0.8	$C_{d\mathrm{UAff}} = 1$
22.5	0.8894248	0.8845998	0.8831973	0.9	
45	1.1064511	1.1052221	1.1051457	1.1	$C_{d\mathrm{UAff}} = 1.2$

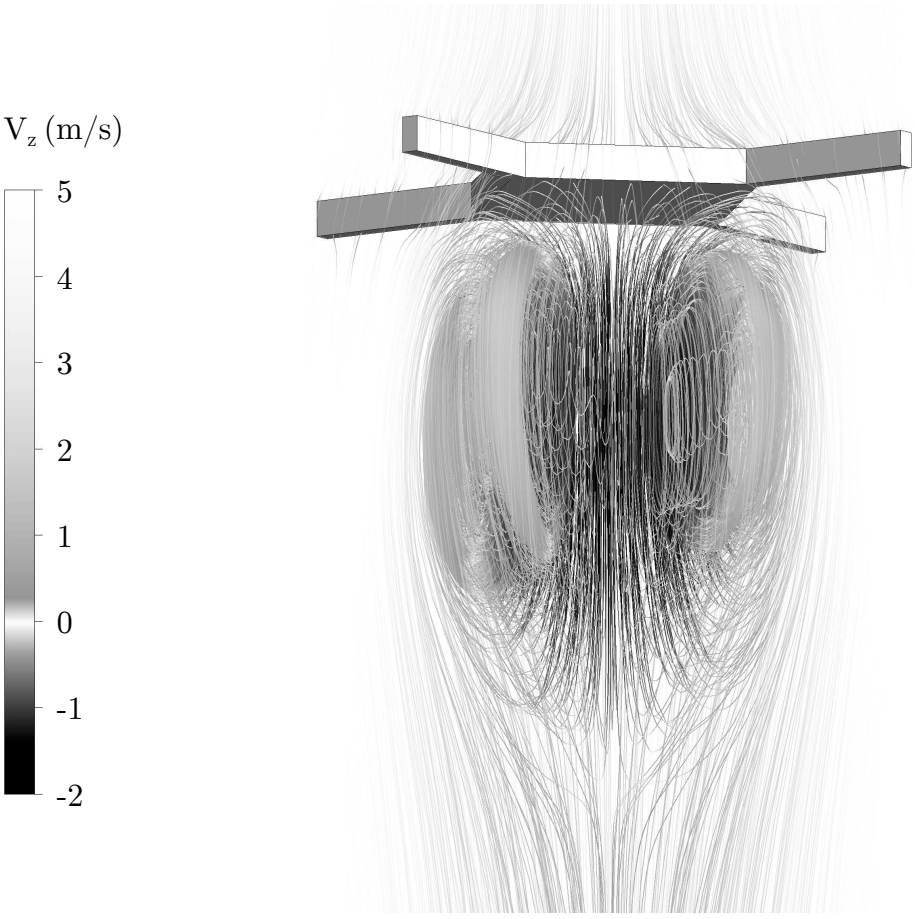

Figure 5.5: Visualization of the UA drag numerical study;
streamlines of airflow over the simplified UA geometry performing axial flight
at inflow relative wind velocity $V_\infty = 5\frac{\mathrm{m}}{\mathrm{s}}$.

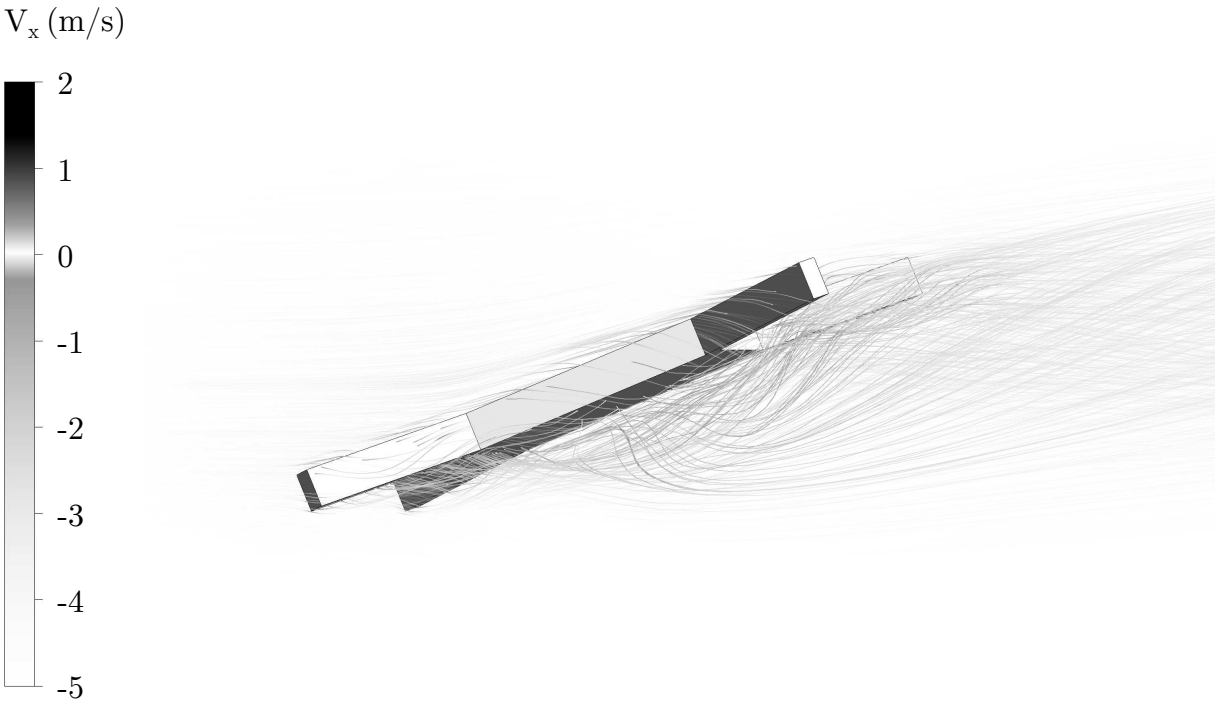

Figure 5.6: Visualization of the UA drag numerical study;
streamlines of airflow over the simplified UA geometry performing forward flight
at angle of attack $\alpha = 22.5°$ at inflow relative wind velocity $V_\infty = 5\frac{\mathrm{m}}{\mathrm{s}}$.

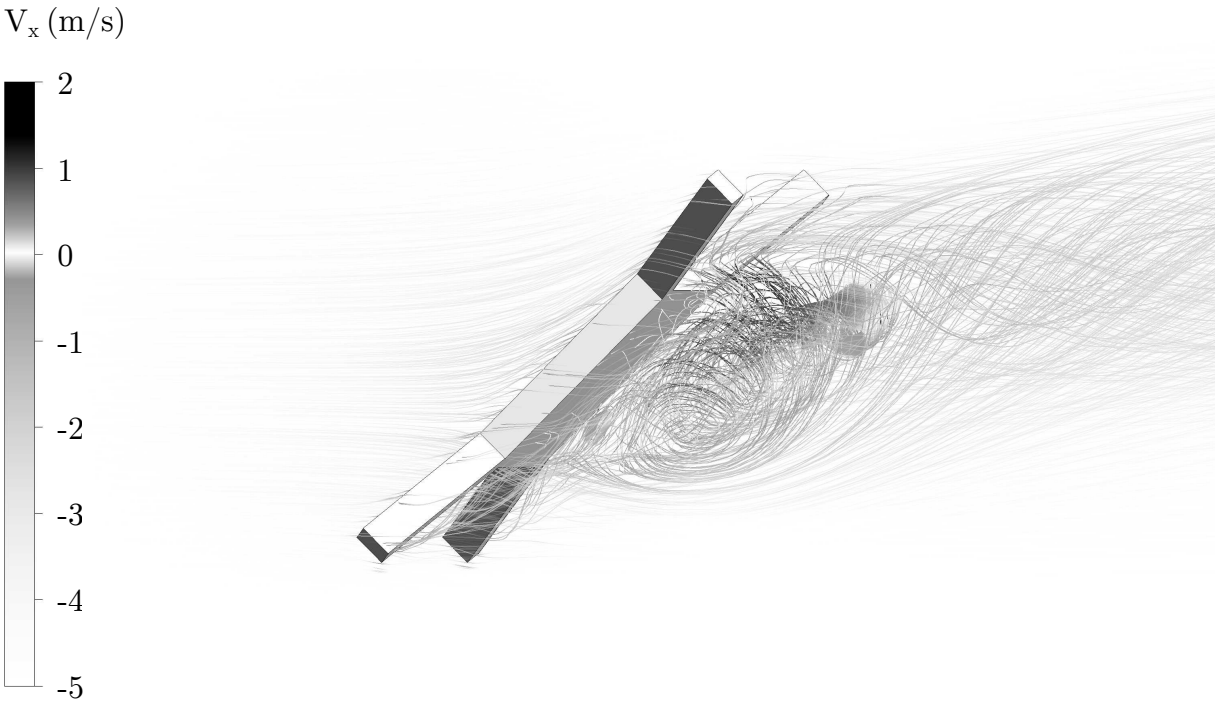

Figure 5.7: Visualization of the UA drag numerical study;
streamlines of airflow over the simplified UA geometry performing forward flight
at angle of attack $\alpha = 45°$ at inflow relative wind velocity $V_\infty = 5\frac{\mathrm{m}}{\mathrm{s}}$.

5.3.3 Spreader Drag Coefficient

The main body of the spreader is a hexagonal cone-shaped shell container reinforced with a three-beam supporting structure.

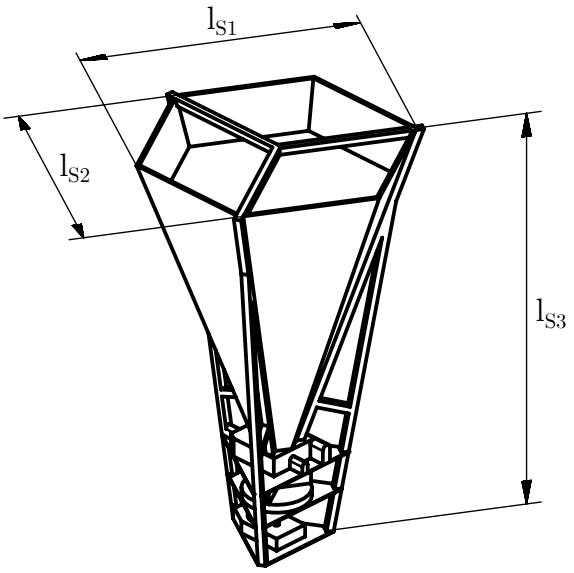

Figure 5.8: Simplified spreader geometry for drag coefficient assessment.

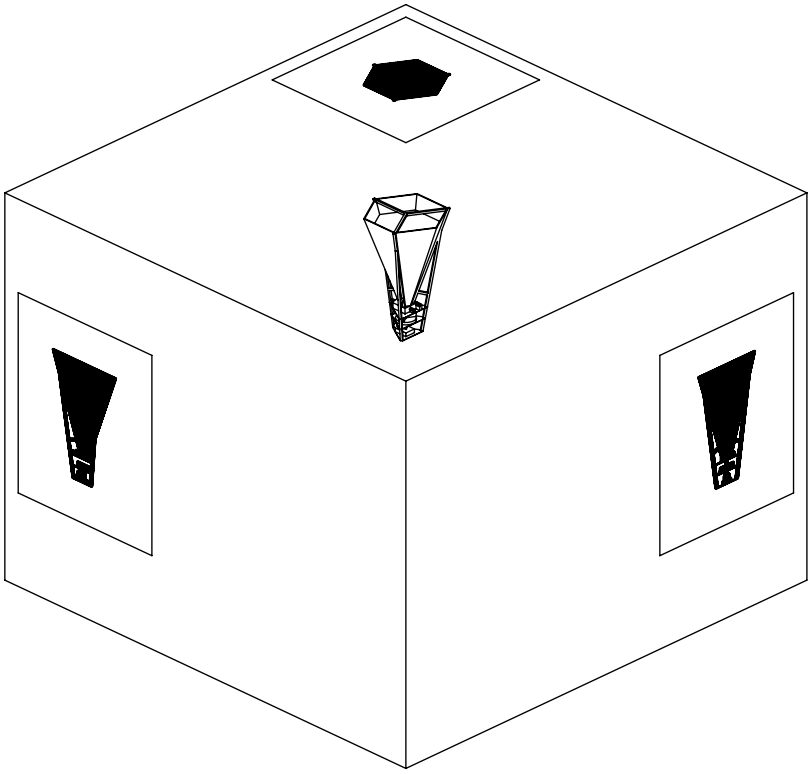

Figure 5.9: Projections of the spreader body in investigated relative wind conditions.

The same reference area should be used for both the Case A axial climb and the Case B axial descent. The drag coefficient is expected to be lower in axial descent because of the cone-shape geometry of the container.

$$A_{\mathrm{Saf}} = A_{\mathrm{SAB}} \doteq 0.87\mathrm{m}^2 \tag{5.26}$$

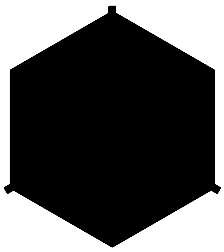

Figure 5.10: Projected area of the spreader $A_{\mathrm{SAB}}\,(\mathrm{m}^2)$, Case A and Case B.

Relative wind normal to both the Case C and the Case D projected areas was considered in drag analysis. As an estimation, a mean value of these areas was established as sufficient enough.

$$A_{\mathrm{Sff}} = \mathrm{mean}\{A_{\mathrm{SC}}; A_{\mathrm{SD}}\} \doteq 1.06\mathrm{m}^2. \tag{5.27}$$

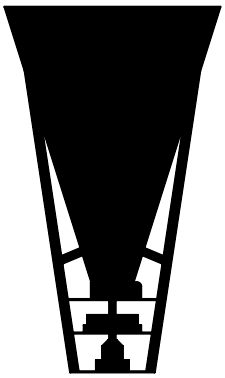

Figure 5.11: Projected area of the spreader $A_{\mathrm{SC}}\,(\mathrm{m}^2)$, Case C.

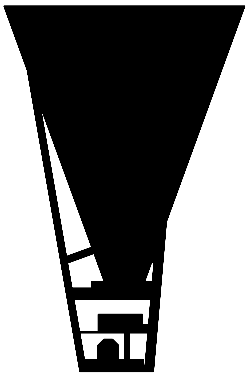

Figure 5.12: Projected area of the spreader $A_{\mathrm{SD}}\,(\mathrm{m}^2)$, Case D.

Table 5.9: Results of spreader drag coefficient numerical study.

Case	$C_d\,(1)$			
	$V_\infty\left(\frac{\mathrm{m}}{\mathrm{s}}\right)$			Mean
	1	5	10	
A	1.5263236	1.5215552	1.5242768	$C_{d\mathrm{Sac}} = 1.5$
B	0.5640351	0.5607695	0.5598601	$C_{d\mathrm{Sad}} = 0.6$
C	1.0837123	1.0845586	1.0854903	$C_{d\mathrm{Sff}} = 1.0$
D	0.9260324	0.9253882	0.9262175	

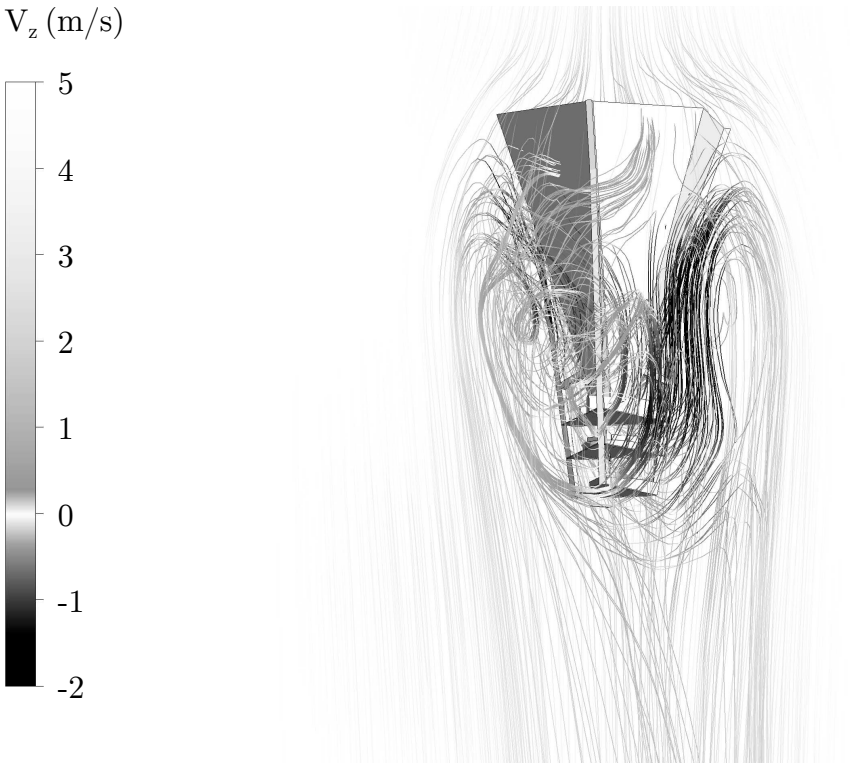

Figure 5.13: Visualization of the spreader drag numerical study;
streamlines of airflow over the simplified spreader geometry performing axial climb
at inflow relative wind velocity $V_\infty = 5\frac{\mathrm{m}}{\mathrm{s}}$, Case A.

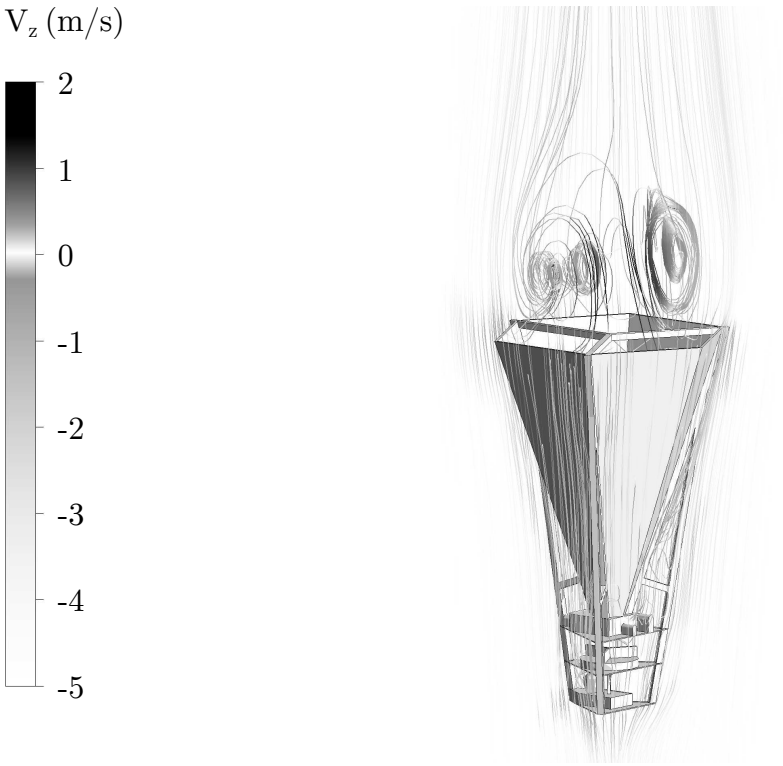

Figure 5.14: Visualization of the spreader drag numerical study;
streamlines of airflow over the simplified spreader geometry performing axial descent
at inflow relative wind velocity $V_\infty = 5\frac{\mathrm{m}}{\mathrm{s}}$, Case B.

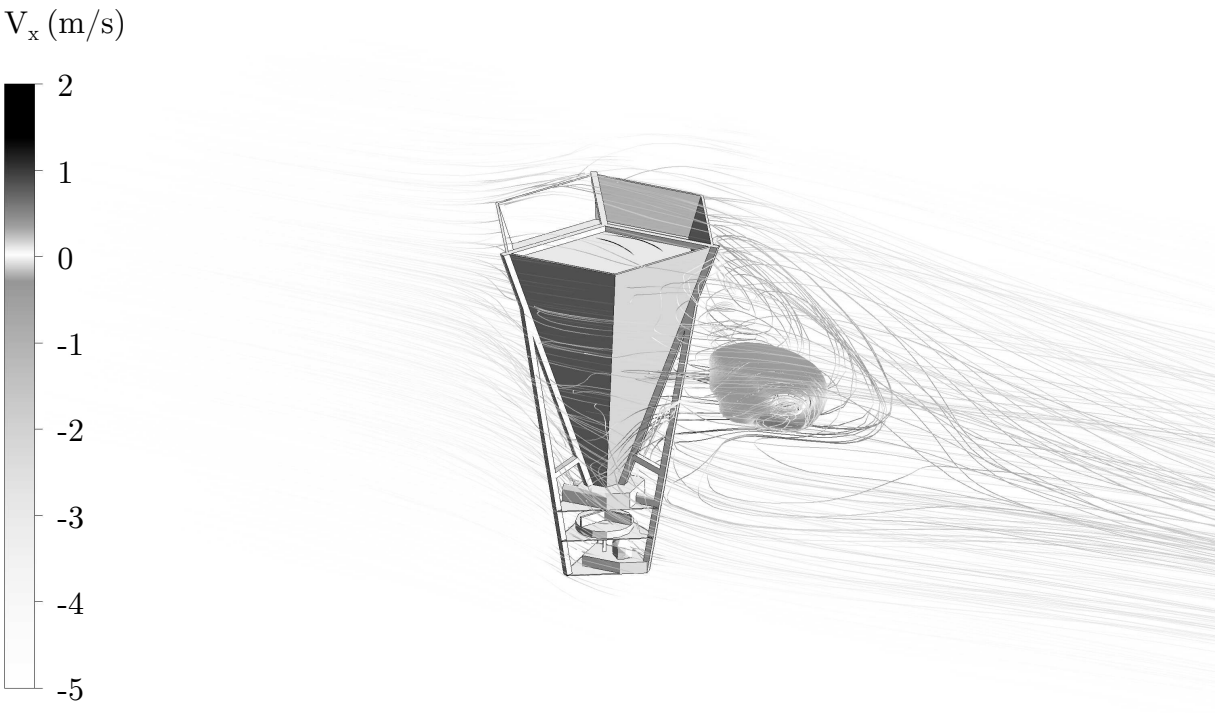

Figure 5.15: Visualization of the spreader drag numerical study;
streamlines of airflow over the simplified spreader geometry performing forward flight
at inflow relative wind velocity $V_\infty = 5\frac{\mathrm{m}}{\mathrm{s}}$, Case C.

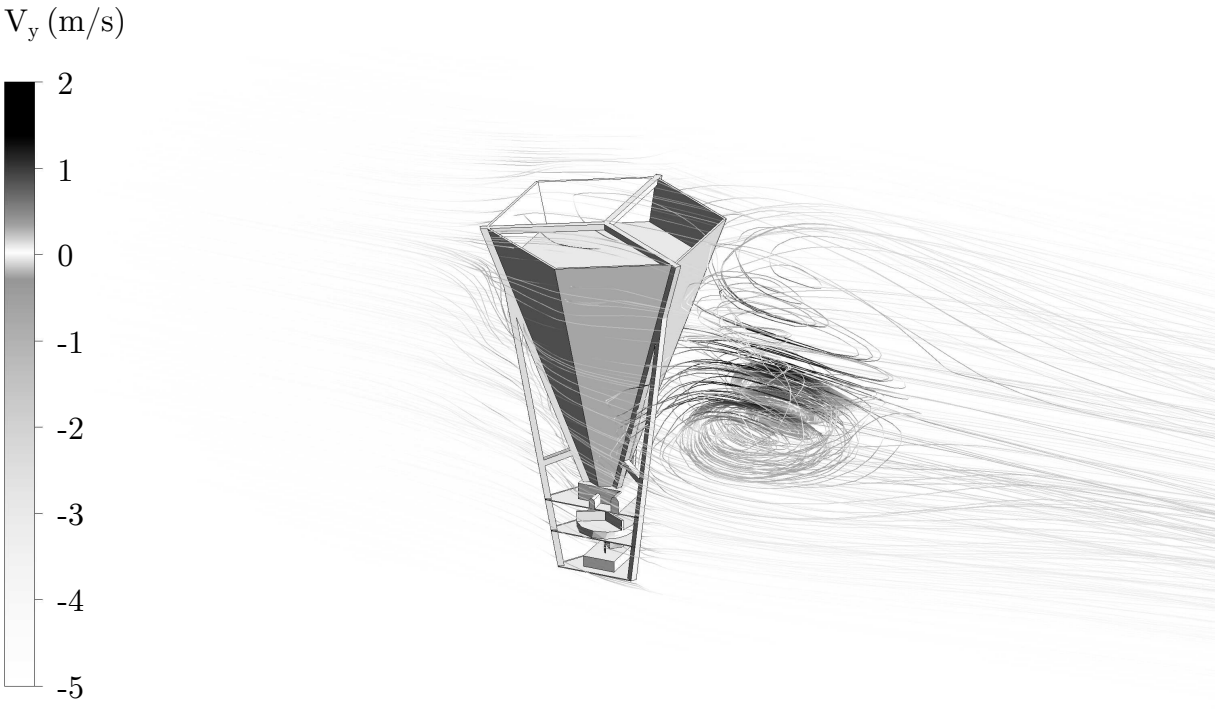

Figure 5.16: Visualization of the spreader drag numerical study;
streamlines of airflow over the simplified spreader geometry performing forward flight
at inflow relative wind velocity $V_\infty = 5\frac{\mathrm{m}}{\mathrm{s}}$, Case D.

5.3.4 Aerostat Drag Coefficient

In respect of the sphere, after the Reynolds number exceeds the order of 10^5, drag coefficient drops drastically, then slowly rises again but never reaches the initial value as displayed at Figure 5.17 [5, page 3-8, Figure 10 edited], Figure 5.18 [8, page 569, Figure 6 edited] and Figure 5.19 [2, page 587, Figure 9.25 edited].

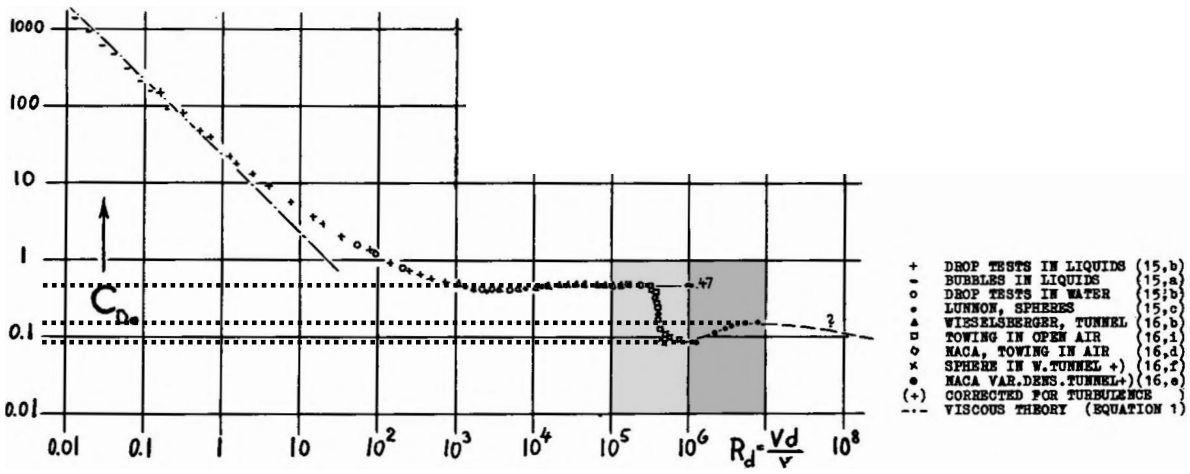

Figure 5.17: Experimental drag coefficient of the sphere
as a function of Reynolds number [5, page 3-8, Figure 10 edited]

.

"Then, quite abruptly at a Reynolds number of about $Re = 2 \times 10^5$, the turbulent shear layer reattaches to the body, resulting in a major change in the final position of separation ($\theta \cong 120°$) and in the form of the turbulent wake. This abrupt change is often referred to as the drag crisis. Associated with this change in flow pattern is a substantial change in the pressure distribution and an associated decrease in the drag coefficient, C_D, from a value of about 0.5 in the laminar separation regime to a value of about 0.2 in the turbulent separation regime" [19].

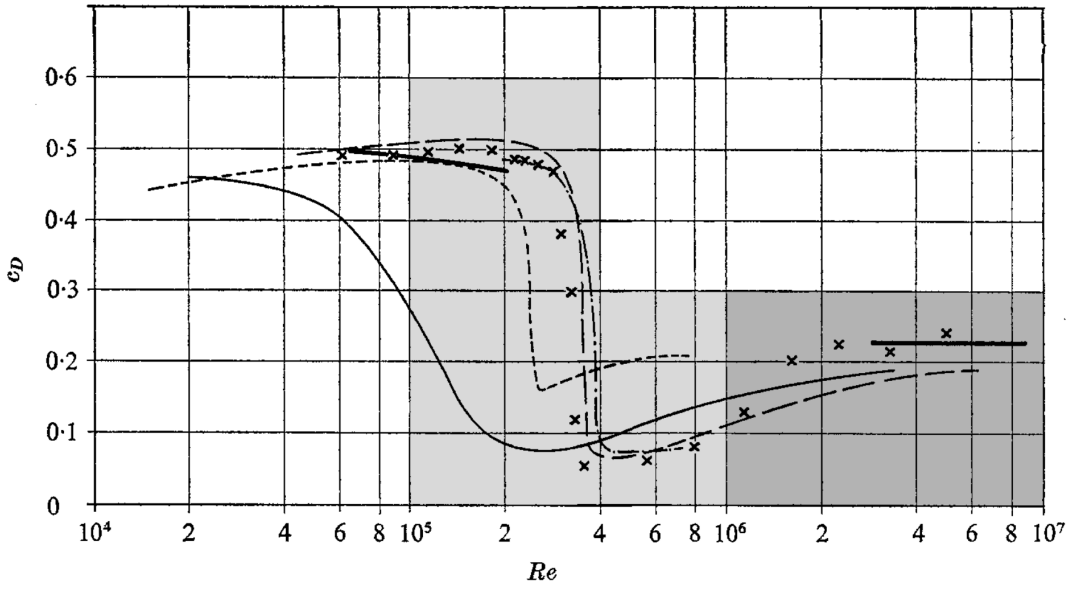

comparison with literature. ---, Wieselsberger (1922); ——, Bacon & Reid (1924); —·—, Millikan & Klein, free-flight (1933); ——, Maxworthy (1969).
Present results: ——, from strain gauges; ×, from integration.

Figure 5.18: Drag coefficient of the sphere as a function of Reynolds number [8, page 569, Figure 6 edited]

.

Surface roughness has a significant effect on the drag coefficient as well. Figure 5.19 [2, Page 587, Figure 9.25 edited] shows that drag coefficient $C_D\,(1)$ within Reynolds numbers in order of 10^6 and surface relative roughness in order of 10^{-3} reaches approximately two times higher values than in the case of a smooth surface.

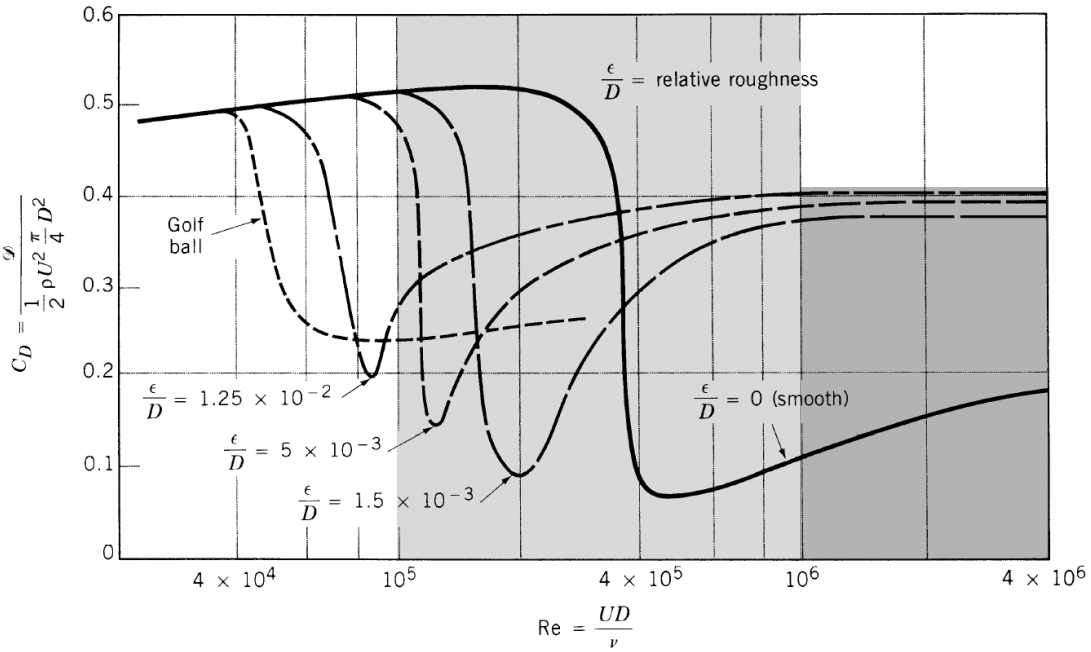

Figure 5.19: The effect of surface roughness on the drag coefficient of a sphere in the Reynolds number range for which the laminar boundary layer becomes turbulent [2, page 587, Figure 9.25 edited]

.

Various Reynolds numbers $Re\,(1)$ were computed with Equation 5.2 using the aerostat diameter $D_{\text{aer}}\,(\text{m})$ as a characteristic dimension $L\,(\text{m})$ in range $D_{\text{aer}}\,(\text{m}) \in [2, 20]$ and relative wind velocity in range $V_\infty\left(\frac{\text{m}}{\text{s}}\right) \in [1, 10]$

$$Re = \frac{\rho_0 V_\infty D_{\text{aer}}}{\mu_0} \tag{5.28}$$

Table 5.10: Reynolds numbers $Re\,(1)$ for various aerostat diameters $D_{\text{aer}}\,(\text{m})$ and relative wind velocities $V_\infty\left(\frac{\text{m}}{\text{s}}\right)$.

$D_{\text{aer}}\,(\text{m})$	$V_\infty\left(\frac{\text{m}}{\text{s}}\right)$									
	1	2	3	4	5	6	7	8	9	10
2	1.35E+05	2.70E+05	4.06E+05	5.41E+05	6.76E+05	8.11E+05	9.46E+05	1.08E+06	1.22E+06	1.35E+06
4	2.70E+05	5.41E+05	8.11E+05	1.08E+06	1.35E+06	1.62E+06	1.89E+06	2.16E+06	2.43E+06	2.70E+06
6	4.06E+05	8.11E+05	1.22E+06	1.62E+06	2.03E+06	2.43E+06	2.84E+06	3.24E+06	3.65E+06	4.06E+06
8	5.41E+05	1.08E+06	1.62E+06	2.16E+06	2.70E+06	3.24E+06	3.79E+06	4.33E+06	4.87E+06	5.41E+06
10	6.76E+05	1.35E+06	2.03E+06	2.70E+06	3.38E+06	4.06E+06	4.73E+06	5.41E+06	6.08E+06	6.76E+06
12	8.11E+05	1.62E+06	2.43E+06	3.24E+06	4.06E+06	4.87E+06	5.68E+06	6.49E+06	7.30E+06	8.11E+06
14	9.46E+05	1.89E+06	2.84E+06	3.79E+06	4.73E+06	5.68E+06	6.63E+06	7.57E+06	8.52E+06	9.46E+06
16	1.08E+06	2.16E+06	3.24E+06	4.33E+06	5.41E+06	6.49E+06	7.57E+06	8.65E+06	9.73E+06	1.08E+07
18	1.22E+06	2.43E+06	3.65E+06	4.87E+06	6.08E+06	7.30E+06	8.52E+06	9.73E+06	1.10E+07	1.22E+07
20	1.35E+06	2.70E+06	4.06E+06	5.41E+06	6.76E+06	8.11E+06	9.46E+06	1.08E+07	1.22E+07	1.35E+07

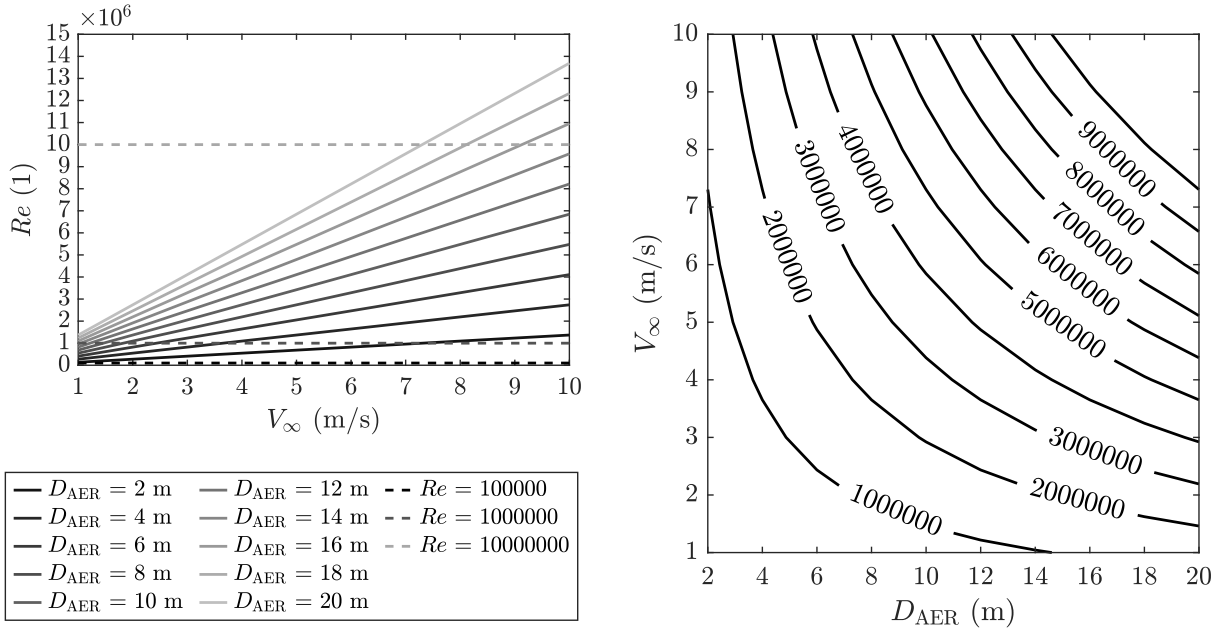

Figure 5.20: Reynolds numbers $Re\,(1)$ for various aerostat diameters $D_{\text{aer}}\,(\text{m})$ and relative wind velocities $V_\infty\left(\frac{\text{m}}{\text{s}}\right)$.

As the Table 5.10 and the Figure 5.20 prove, most of the possible combinations provide Reynolds numbers $Re\,(1)$ in the order of 10^6.

The aerostat central cross-section area $A_{\text{aer}}\,(\text{m}^2)$ for desired aerostat drag calculation is simply

$$A_{\text{aer}} = \frac{\pi D_{\text{aer}}^2}{4}. \tag{5.29}$$

5.4 Aerostat Design

5.4.1 Forces in Axial Descent Without Engine Power

The aerostat should be designed so it can support the mass of the UA including battery and possible ballast and excluding payload. Certain required operational lift deficiency F_{ROOM} (N) should be provided to maintain stability while flying with operational empty mass M_{OEM} (kg). The whole system should also descend in the case of power loss. The aerostat is expected to be filled with hydrogen.

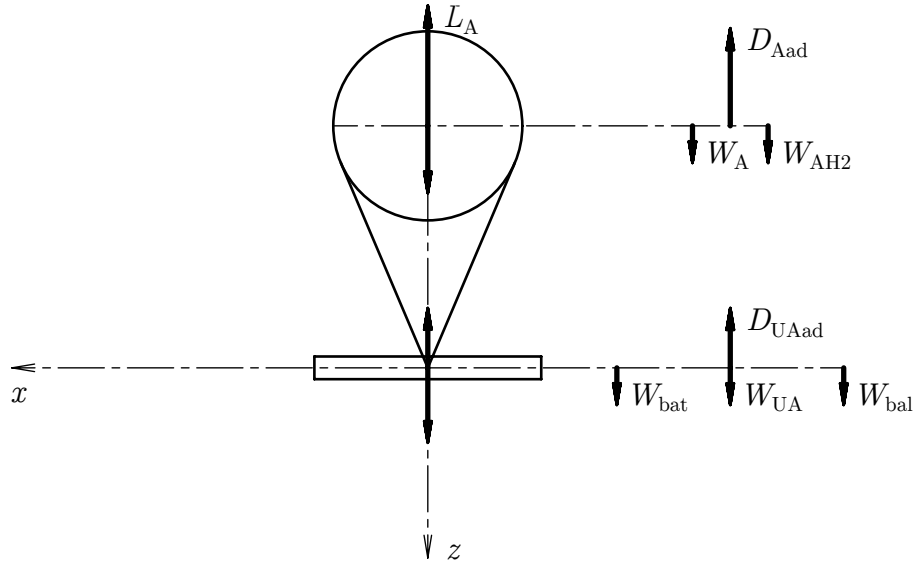

Figure 5.21: Forces acting on the UAS performing axial descent without engine power.

Equilibrium of the vertical forces in axial descent

$$\Sigma F_z : W_{\mathrm{AH2}} + W_{\mathrm{A}} + W_{\mathrm{bal}} + W_{\mathrm{UA}} + W_{\mathrm{bat}} - L_{\mathrm{A}} - D_{\mathrm{Aad}} - D_{\mathrm{UAad}} = 0. \tag{5.30}$$

Components of the Equation 5.30 are

$$W_{\mathrm{AH2}} = M_{\mathrm{AH2}} g_0 = V_{\mathrm{aer}} \rho_{\mathrm{H2}} g_0 = \frac{\pi D_{\mathrm{aer}}^3}{6} \rho_{\mathrm{H2}} g_0, \tag{5.31}$$

$$W_{\mathrm{A}} = S_{\mathrm{aer}} M_{\mathrm{Afab}} g_0 = \pi D_{\mathrm{aer}}^2 M_{\mathrm{Afab}} g_0, \tag{5.32}$$

$$W_{\mathrm{bal}} + W_{\mathrm{UA}} + W_{\mathrm{bat}} = \left(M_{\mathrm{bal}} + M_{\mathrm{UA}} + M_{\mathrm{bat}}\right) g_0, \tag{5.33}$$

$$L_{\mathrm{A}} = V_{\mathrm{aer}} \rho_0 g_0 = \frac{\pi D_{\mathrm{aer}}^3}{6} \rho_0 g_0, \tag{5.34}$$

$$D_{\mathrm{Aad}} = \frac{1}{2} \rho_0 V_{\mathrm{ad}}^2 C_{d\mathrm{A}} A_{\mathrm{aer}} = \frac{1}{2} \rho_0 V_{\mathrm{ad}}^2 C_{d\mathrm{A}} \frac{\pi D_{\mathrm{aer}}^2}{4}, \tag{5.35}$$

$$D_{\mathrm{UAad}} = \frac{1}{2} \rho_0 V_{\mathrm{ad}}^2 C_{d\mathrm{UAaf}} A_{\mathrm{UA}}(\alpha). \tag{5.36}$$

Standard acceleration due to gravity $g_0 \left(\frac{m}{s^2}\right)$ from the Table 5.1

$$g_0 = 9.80665, \tag{5.37}$$

density of air $\rho_0 \left(\frac{\text{kg}}{\text{m}^3}\right)$ in the flight levels close to the sea level from the Table 5.1

$$\rho_0 = 1.225 \tag{5.38}$$

and fabric weight $M_{\text{Afab}} \left(\frac{\text{kg}}{\text{m}^2}\right)$ used on the aerostats provided by Lindstrand Technologies Ltd.

$$M_{\text{Afab}} = 0.5. \tag{5.39}$$

ICAO [11, Page E-x, Table B] states molar mass $M_{\text{H2}} \left(\frac{\text{kg}}{\text{kmol}}\right)$ of hydrogen

$$M_{\text{H2}} = 2.01594. \tag{5.40}$$

McQuarrie [1, Page 637, Equation 16.1a] provides the equation of state for ideal gas

$$pV = nRT \tag{5.41}$$

where $p\,(\text{Pa})$ is a pressure, $V\,(\text{m}^3)$ is a volume, $n\,(\text{mol})$ is a quantity amount of substance, $R \left(\frac{\text{J}}{\text{K}\cdot\text{mol}}\right)$ is a universal gas constant and $T\,(\text{K})$ is a temperature. After plugging the values of the primary constants from the Table 5.1 into the Equation 5.41 and rearranging, for volume $V = 1\text{m}^3$

$$n = \frac{p_0 V}{\frac{R^*}{1000} T_0} = 42.29326884. \tag{5.42}$$

Molar density $\rho_m \left(\frac{\text{mol}}{\text{m}^3}\right)$ can be defined as

$$\rho_m = \frac{n}{V} \tag{5.43}$$

and mass density $\rho \left(\frac{\text{kg}}{\text{m}^3}\right)$ then

$$\rho \left(\frac{\text{kg}}{\text{m}^3}\right) = \frac{1}{1000} (1)\, M \left(\frac{\text{kg}}{\text{kmol}}\right) \rho_m \left(\frac{\text{mol}}{\text{m}^3}\right), \tag{5.44}$$

and so mass density of hydrogen $\rho_{\text{H2}} \left(\frac{\text{kg}}{\text{m}^3}\right)$

$$\rho_{\text{H2}} = \frac{1}{1000} M_{\text{H2}} n = 0.08526069239 \doteq 0.085. \tag{5.45}$$

It is to be noted that the aerostat is probably supposed to be pressurized and so the ideal gas theory simplifies the gas properties greatly. The real gas characteristics should be provided by Lindstrand Technologies Ltd.

5.4.2 Design Parameters of the Aerostat

5.4.2.1 Required Operational Lift Deficiency of the Unpowered UAS

Required operational lift deficiency $F_{\mathrm{ROOM}}\,(N)$ for known required operational overweight mass $M_{\mathrm{ROOM}}\,(N)$

$$F_{\mathrm{ROOM}} = M_{\mathrm{ROOM}} g_0 = D_{\mathrm{UASad}}, \tag{5.46}$$

where total drag of the UAS $D_{\mathrm{UASad}}\,(N)$ in axial descent with no payload

$$D_{\mathrm{UASad}} = D_{\mathrm{UAad}} + D_{\mathrm{Aad}}. \tag{5.47}$$

5.4.2.2 Aerostat Diameter

After combining Equation 5.46 with Equation 5.47 and plugging the combination into the Equation 5.30

$$\Sigma F_z : W_{\mathrm{AH2}} + W_{\mathrm{A}} + W_{\mathrm{bal}} + W_{\mathrm{UA}} + W_{\mathrm{bat}} - L_{\mathrm{A}} - F_{\mathrm{ROOM}} = 0 \tag{5.48}$$

and rearranging using the Equations 5.31 - 5.34

$$C_{\mathrm{A1}} D_{\mathrm{aer}}^3 + C_{\mathrm{A2}} D_{\mathrm{aer}}^2 + C_{\mathrm{A3}} D_{\mathrm{aer}}^1 + C_{\mathrm{A4}} = 0 \tag{5.49}$$

where

$$C_{\mathrm{A1}} = 1, \tag{5.50}$$

$$C_{\mathrm{A2}} = \frac{6 M_{\mathrm{Afab}}}{\rho_{\mathrm{H2}} - \rho_0}, \tag{5.51}$$

$$C_{\mathrm{A3}} = 0, \tag{5.52}$$

$$C_{\mathrm{A4}} = \frac{6\,(M_{\mathrm{bal}} + M_{\mathrm{UA}} + M_{\mathrm{bat}} - M_{\mathrm{ROOM}})}{\pi\,(\rho_{\mathrm{H2}} - \rho_{air})}. \tag{5.53}$$

A solution of the cubic Equation 5.49 is composed of three roots. Only a positive real root can be considered.

Table 5.11: Aerostat diameters D_{aer} (m)
for various required operational masses M_{ROOM} (kg),
sums of UA structure masses and possible ballast masses $(M_{\mathrm{UA}} + M_{\mathrm{bal}})$ (kg)
and also battery masses M_{bat} (kg).

M_{bat} (kg)	$(M_{\mathrm{UA}} + M_{\mathrm{bal}})$ (kg)	D_{aer} (m)					
		M_{ROOM} (kg)					
		25	50	75	100	125	150
50	300	9.14	8.93	8.71	8.47	8.22	7.94
	310	9.23	9.02	8.80	8.57	8.32	8.05
	320	9.31	9.10	8.89	8.66	8.42	8.16
	330	9.38	9.18	8.98	8.75	8.52	8.27
	340	9.46	9.27	9.06	8.84	8.61	8.37
	350	9.54	9.35	9.14	8.93	8.71	8.47
	360	9.61	9.42	9.23	9.02	8.80	8.57
	370	9.69	9.50	9.31	9.10	8.89	8.66
	380	9.76	9.58	9.38	9.18	8.98	8.75
	390	9.83	9.65	9.46	9.27	9.06	8.84
	400	9.90	9.72	9.54	9.35	9.14	8.93
	Mean	9.5	9.3	9.1	8.9	8.7	8.5
100	300	9.54	9.35	9.14	8.93	8.71	8.47
	310	9.61	9.42	9.23	9.02	8.80	8.57
	320	9.69	9.50	9.31	9.10	8.89	8.66
	330	9.76	9.58	9.38	9.18	8.98	8.75
	340	9.83	9.65	9.46	9.27	9.06	8.84
	350	9.90	9.72	9.54	9.35	9.14	8.93
	360	9.97	9.79	9.61	9.42	9.23	9.02
	370	10.03	9.86	9.69	9.50	9.31	9.10
	380	10.10	9.93	9.76	9.58	9.38	9.18
	390	10.17	10.00	9.83	9.65	9.46	9.27
	400	10.23	10.07	9.90	9.72	9.54	9.35
	Mean	9.9	9.7	9.5	9.3	9.1	8.9

5.4.2.3 Descent Velocity of the Unpowered UAS

Aerostat diameters $D_{\text{aer}}\,(\text{m})$ should be used to establish a range of Reynolds numbers $Re\,(1)$ for possible axial descent velocities $V_{\text{ad}}\left(\frac{\text{m}}{\text{s}}\right)$. Drag coefficient $C_{d\text{A}}\,(1)$ was estimated using Figure 5.19, expecting relative roughness of the aerostat surface smaller than 1.5×10^{-3} as

$$C_{\text{dA}} = 0.35. \tag{5.54}$$

To calculate UAS descent velocity $V_{\text{ad}}\left(\frac{\text{m}}{\text{s}}\right)$, after combining the Equations 5.35, 5.36 and 5.47, plugging into the Equation 5.46 and rearranging

$$V_{\text{ad}} = \sqrt{\frac{2M_{\text{ROOM}}g_0}{\rho_0\left(C_{d\text{A}}A_{\text{aer}} + C_{d\text{UAaf}}A_{\text{UA1}}\right)}}. \tag{5.55}$$

Table 5.12: Axial descent velocities $V_{\text{ad}}\left(\frac{\text{m}}{\text{s}}\right)$ for various required operational masses $M_{\text{ROOM}}\,(\text{kg})$, sums of UA structure masses and possible ballast masses $(M_{\text{UA}} + M_{\text{bal}})\,(\text{kg})$ and also battery masses $M_{\text{bat}}\,(\text{kg})$.

$M_{\text{bat}}\,(\text{kg})$	$(M_{\text{UA}} + M_{\text{bal}})\,(\text{kg})$	$V_{\text{ad}}\left(\frac{\text{m}}{\text{s}}\right)$					
		$M_{\text{ROOM}}\,(\text{kg})$					
		25	50	75	100	125	150
50	300	4.03	5.82	7.30	8.65	9.95	11.24
	310	4.00	5.77	7.23	8.56	9.83	11.09
	320	3.96	5.72	7.16	8.47	9.72	10.96
	330	3.93	5.67	7.10	8.39	9.62	10.83
	340	3.90	5.63	7.04	8.31	9.52	10.71
	350	3.87	5.58	6.98	8.24	9.43	10.59
	360	3.84	5.54	6.92	8.16	9.34	10.48
	370	3.82	5.50	6.86	8.09	9.25	10.38
	380	3.79	5.46	6.81	8.02	9.17	10.28
	390	3.77	5.42	6.76	7.96	9.09	10.18
	400	3.74	5.38	6.71	7.90	9.01	10.09
	Mean	3.9	5.6	7.0	8.3	9.4	10.6
100	300	3.87	5.58	6.98	8.24	9.43	10.59
	310	3.84	5.54	6.92	8.16	9.34	10.48
	320	3.82	5.50	6.86	8.09	9.25	10.38
	330	3.79	5.46	6.81	8.02	9.17	10.28
	340	3.77	5.42	6.76	7.96	9.09	10.18
	350	3.74	5.38	6.71	7.90	9.01	10.09
	360	3.72	5.34	6.66	7.83	8.93	10.00
	370	3.69	5.31	6.61	7.78	8.86	9.91
	380	3.67	5.27	6.57	7.72	8.79	9.83
	390	3.65	5.24	6.52	7.66	8.73	9.75
	400	3.63	5.21	6.48	7.61	8.66	9.67
	Mean	3.7	5.4	6.7	7.9	9.0	10.1

5.4.2.4 Required Ballast Mass of the UAS

Certification Specifications and Acceptable Means of Compliance for Free Gas Balloons CS-31GB states: "A minimum ballast quantity is considered sufficient if, when jettisoned, it stops a descent speed of 4 m/s" [14, Book 2, Section AMC 31GB.51].

For $V_{\mathrm{ad}} \leq 4$

$$M_{\mathrm{bal}} = M_{\mathrm{ROOM}} = \frac{F_{\mathrm{ROOM}}}{g_0}. \tag{5.56}$$

For $V_{\mathrm{ad}} > 4$, using combination of the Equations 5.46 and 5.47

$$F_{\mathrm{OOM}} = \frac{1}{2}\rho_0 \left(V_{\mathrm{ad}} - 4\right)^2 \left(C_{d\mathrm{A}} A_{\mathrm{aer}} + C_{d\mathrm{UAaf}} A_{\mathrm{UA1}}\right). \tag{5.57}$$

To get the final ballast mass $M_{\mathrm{bal}}\,(\mathrm{kg})$

$$M_{\mathrm{bal}} = \frac{F_{\mathrm{ROOM}} - F_{\mathrm{OOM}}}{g_0} = M_{\mathrm{ROOM}} - \frac{F_{\mathrm{OOM}}}{g_0}. \tag{5.58}$$

Table 5.13: Ballast masses M_{bal} (kg)
for various required operational masses M_{ROOM} (kg),
sums of UA structure masses and possible ballast masses $(M_{\mathrm{UA}} + M_{\mathrm{bal}})$ (kg)
and also battery masses M_{bat} (kg).

M_{bat} (kg)	$(M_{\mathrm{UA}} + M_{\mathrm{bal}})$ (kg)	M_{bal} (kg)					
		M_{ROOM} (kg)					
		25	50	75	100	125	150
50	300	25.00	45.10	59.66	71.10	80.33	87.78
	310	25.00	45.29	60.02	71.62	81.02	88.66
	320	25.00	45.47	60.37	72.13	81.69	89.51
	330	25.00	45.65	60.70	72.62	82.34	90.33
	340	25.00	45.82	61.03	73.09	82.96	91.12
	350	25.00	45.98	61.34	73.55	83.57	91.89
	360	25.00	46.14	61.64	74.00	84.16	92.63
	370	25.00	46.29	61.94	74.43	84.74	93.35
	380	25.00	46.43	62.23	74.85	85.29	94.04
	390	25.00	46.57	62.50	75.26	85.83	94.72
	400	25.00	46.71	62.78	75.66	86.36	95.38
	Mean	25.0	46.0	61.3	73.5	83.5	91.8
100	300	25.00	45.98	61.34	73.55	83.57	91.89
	310	25.00	46.14	61.64	74.00	84.16	92.63
	320	25.00	46.29	61.94	74.43	84.74	93.35
	330	25.00	46.43	62.23	74.85	85.29	94.04
	340	25.00	46.57	62.50	75.26	85.83	94.72
	350	25.00	46.71	62.78	75.66	86.36	95.38
	360	25.00	46.84	63.04	76.05	86.87	96.02
	370	25.00	46.97	63.29	76.43	87.37	96.65
	380	25.00	47.09	63.54	76.79	87.86	97.26
	390	25.00	47.21	63.79	77.16	88.34	97.85
	400	25.00	47.32	64.02	77.51	88.80	98.43
	Mean	25.0	46.7	62.7	75.6	86.3	95.3

Required ballast masses from Table 5.13 are very inconvenient. Not only would it be very insufficient to carry all the ballast mass, but the integration of the releasing system would also make the structure much more complicated. Certification Specification CS-31GB [14] expects the balloon design to be safe enough to ensure that crew or equipment are not to be harmed while descent. In the case of the desired UAS design, the aim is not to save the structure or the equipment if the engines fail to provide sufficient power, but to ensure that the system will descend, possibly get damaged or destroyed, but most importantly avoid being uncontrollably flown away. The aerostat should not be designed as a separate structure but rather as a part of either the propulsion unit or better as an emergency system for slowing down the descent in the case of power loss.

5.4.3 Aerostat Design Solutions

With no requirements for ballast mass, it is necessary to estimate the initial UA structure mass $M_{\mathrm{UA}}\,(\mathrm{kg})$, as was done in Table 5.14 for both light and heavy configurations, since the engines to provide sufficient power for heavy payload weigh approximately twice the weight of the ones for the light payload.

Table 5.14: UA structure masses $M_{\mathrm{UA}}\,(\mathrm{kg})$ estimation.

Components	Mass (kg)	
Fuselage	50	
Arms (4 pcs)	80	
Miscellaneous	10	
Controllers (8 pcs)	64	
Engines (8 pcs)	64	128
$M_{\mathrm{UA}}\,(\mathrm{kg})$	268	332

Finally, possible design parameters of the aerostat are displayed in Table 5.15.

Table 5.15: Aerostat diameters $D_{\mathrm{aer}}\,(\mathrm{m})$ and descent velocities $V_{\mathrm{ad}}\left(\frac{\mathrm{m}}{\mathrm{s}}\right)$ for various required operational masses $M_{\mathrm{ROOM}}\,(\mathrm{kg})$ and battery masses $M_{\mathrm{bat}}\,(\mathrm{kg})$ in both light and heavy configurations of UA structure mass $M_{\mathrm{UA}}\,(\mathrm{kg})$.

$M_{\mathrm{bat}}\,(\mathrm{kg})$	$M_{\mathrm{ROOM}}\,(\mathrm{kg})$	$M_{\mathrm{UA}}\,(\mathrm{kg})$			
		268		332	
		$D_{\mathrm{aer}}\,(\mathrm{m})$	$V_{\mathrm{ad}}\left(\frac{\mathrm{m}}{\mathrm{s}}\right)$	$D_{\mathrm{aer}}\,(\mathrm{m})$	$V_{\mathrm{ad}}\left(\frac{\mathrm{m}}{\mathrm{s}}\right)$
50	25	8.87	4.14	9.40	3.93
	50	8.64	6.00	9.20	5.66
	75	8.40	7.55	8.99	7.09
	100	8.14	8.97	8.77	8.37
	125	7.86	10.35	8.54	9.60
	150	7.56	11.75	8.29	10.81
100	25	9.29	3.97	9.77	3.79
	50	9.09	5.73	9.59	5.45
	75	8.87	7.18	9.40	6.80
	100	8.64	8.49	9.20	8.01
	125	8.40	9.74	8.99	9.15
	150	8.14	10.99	8.77	10.26

For further required power estimation calculations, the mean value of aerostat diameter $\bar{D}_{\mathrm{aer}}\,(\mathrm{m})$ for required overweight mass $M_{\mathrm{ROOM}} = 100\mathrm{kg}$ from Table 5.15

$$\bar{D}_{\mathrm{aer}} \doteq 8.7. \tag{5.59}$$

5.5 Performance

5.5.1 Momentum Theory

The approach known as momentum theory allows prediction of the rotor thrust and power on a non-scientific engineering level. Flow of an ideal fluid through an infinitesimally thin rotor disk is considered one-dimensional, quasi-steady, incompressible and inviscid. Figure 5.22 [6, Page 38, Figure 2.5] was described by Leishmann as: "This figure represents the helicopter rotor in an axial climb with velocity V_c, for which the hovering condition is obtained in the limit as $V_c \longrightarrow 0$. Let $\mathrm{d}\vec{S}$ be the unit normal area vector, which by convention always points out of the control volume" [6, Page 38, Subsection 2.2.2]. Also, $S\,(\mathrm{m}^2)$ denotes surface area of the control volume surrounding the rotor and its wake, $v_\mathrm{i}\,\left(\frac{\mathrm{m}}{\mathrm{s}}\right)$ denotes induced velocity and $w\,\left(\frac{\mathrm{m}}{\mathrm{s}}\right)$ denotes velocity in far wake.

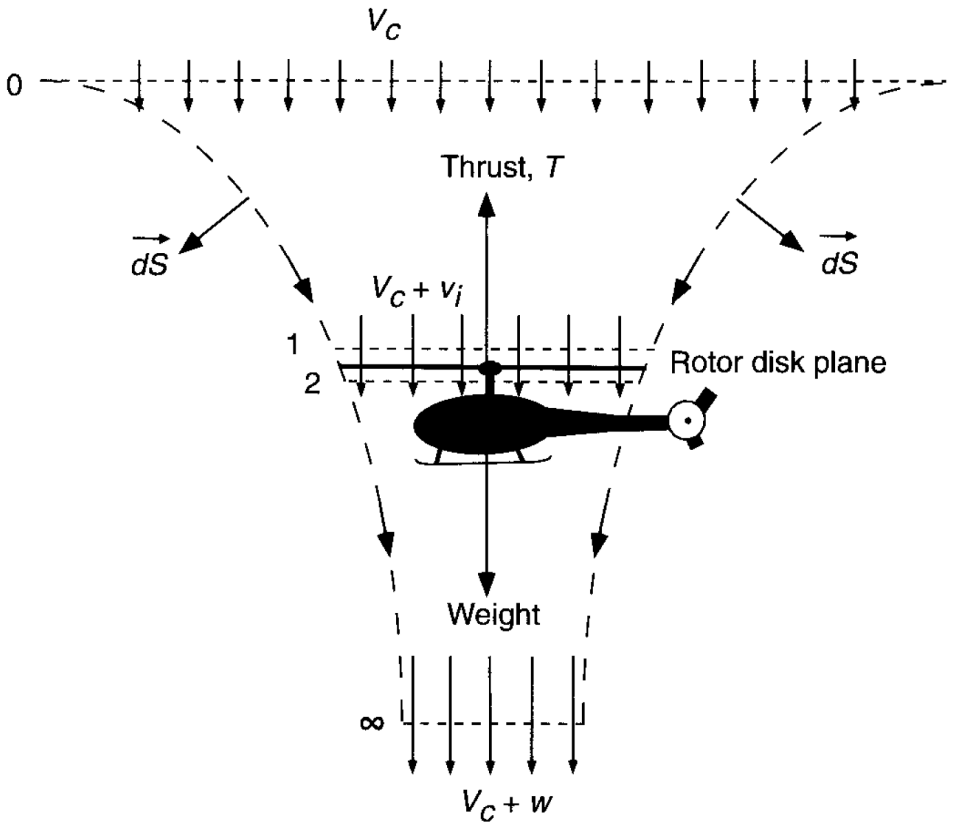

Figure 5.22: Flow model used for momentum theory analysis of a rotor in axial flight [6, Page 38, Figure 2.5].

Leishmann derives [6, Pages 38-41, Subsections 2.2.2 - 2.2.3] the expression [6, Page 40, Equation 2.10] for induced velocity $v_{\mathrm{i}}\left(\frac{\mathrm{m}}{\mathrm{s}}\right)$ based on conservation laws of mass, momentum and energy and applying them on the case of hover

$$v_{\mathrm{i}} = \frac{1}{2}w \tag{5.60}$$

and the expression [6, Page 41, Equation 2.15] for induced velocity in hover $v_{\mathrm{h}}\left(\frac{\mathrm{m}}{\mathrm{s}}\right)$

$$v_{\mathrm{h}} \equiv v_{\mathrm{i}} = \sqrt{\frac{T}{2\rho A}} = \sqrt{\left(\frac{T}{A}\right)\frac{1}{2\rho}}. \tag{5.61}$$

It is important to establish that the desired UA design layout is composed of four pairs of coaxial engines. To use the momentum theory, it is necessary to assume that the vertical distance between the two propellers is small enough in relation to the whole wake size that it is actually negligible and induced velocity is common for both propellers so they act like a single rotor disk as portrayed in Figure 5.23. This means that thrust proportionate to one rotor disk area is actually total thrust of one propulsion unit and to calculate the required power, it is to be divided by the actual number of engines.

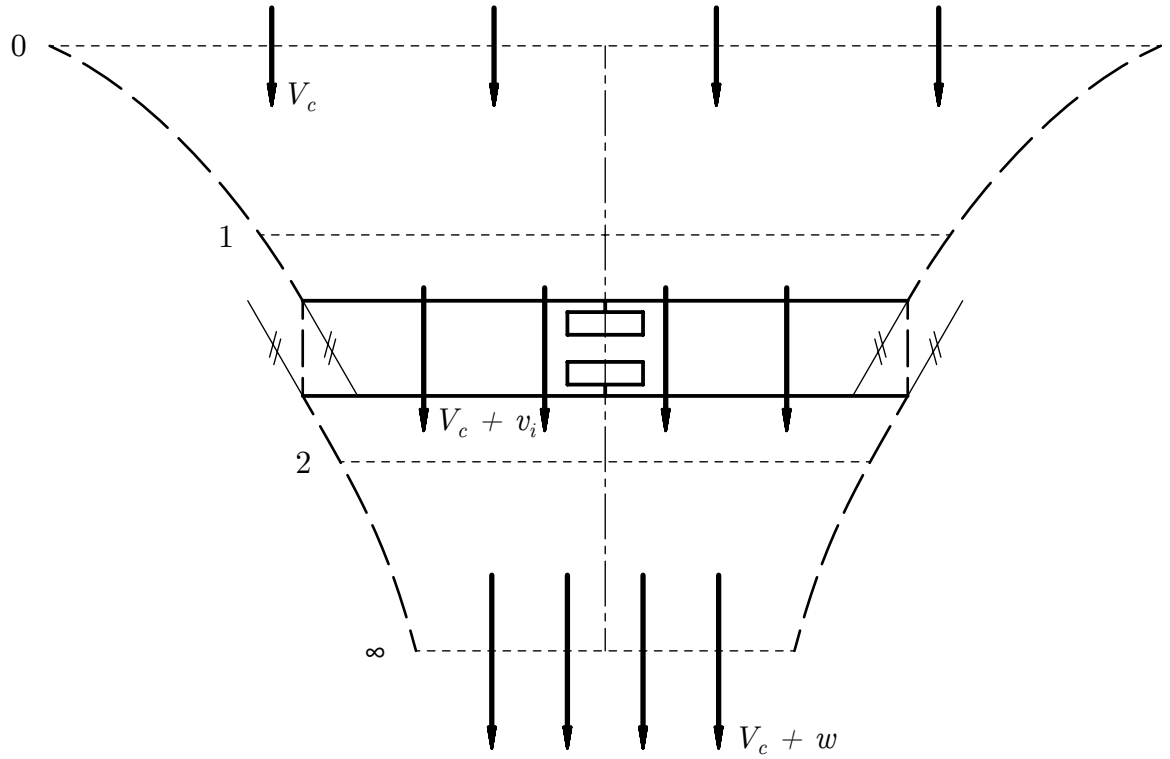

Figure 5.23: Simplified application of momentum theory from the Figure 5.22 on a pair of coaxial engines.

5.5.2 Initial Parameters of the Performance Calculation

Table 5.16: Initial parameters for performance calculation.

Symbol	Description	Unit	Value
M_{ROOM}	Required operational overweight mass	kg	100
M_{PLM}	Payload mass	kg	$[0, 1500]$
$\bar{D}_{\mathrm{aer}}$	Mean aerostat diameter	m	8.7
D	Propeller diameter	m	$[1.5, 2]$
n	Revolutions of engine per minute	$\frac{1}{\mathrm{min}}$	$[1500, 4000]$
V_{c}	Climb velocity	$\frac{\mathrm{m}}{\mathrm{s}}$	$[-8, 8]$
α	Angle of attack	$^\circ$	$[0, 90]$
δ	Angular margin in forward flight	$^\circ$	10
$\bar{C_L}$	Mean lift coefficient	1	0.5
κ	Induced power correction factor	1	1.15
K	Empiric constant in blade profile power coefficient	1	4.6
$\frac{f}{A}$	Geometry ratio	1	0.025

Required operational overweight mass $M_{\mathrm{ROOM}}\,(\mathrm{kg})$ was estimated to keep the UAS stable and controllable while flying.

Range of payload mass $M_{\mathrm{PLM}}\,(\mathrm{kg})$ was set to fulfil the possible mission requirements while the maximum actual payload mass is expected not to exceed $M_{\mathrm{PLM}} = 1000\mathrm{kg}$.

Mean aerostat diameter $\bar{D}_{\mathrm{aer}}\,(\mathrm{m})$ was given by the Equation 5.59.

Range of propeller diameter $D\,(\mathrm{m})$ was chosen based on usually used propellers.

Range of revolutions per minute $n\left(\frac{1}{min}\right)$ was based on proposal by MGM COMPRO but it is vital to check that a particular combination of a propeller diameter $D\,(\mathrm{m})$ and its RPM does not provide dangerous Mach number.

Range of angle of attack $\alpha\,(^\circ)$ was set to cover all theoretical range of motion. Collision of aerostat structure with the UA, and in the worst case its propellers, must not occur. Therefore, it needs to be checked that the combination of angle of attack $\alpha\,(^\circ)$ and angular deflection of aerostat axis $\beta\,(^\circ)$ does not exceed angular margin in forward flight $\delta\,(^\circ)$.

Angular margin in forward flight $\delta\,(^\circ)$ was estimated to provide space to maneuver while maintaining safety.

Mean lift coefficient $\bar{C_L}\,(1)$ was chosen from Leishmann [6, Page 113, Subsection 3.3.17].

Induced power correction factor $\kappa\,(1)$ was taken from Leishmann [6, Pages 44-45, Subsection 2.2.7].

Empiric constant in blade profile power coefficient $K\,(1)$ was chosen based on Leishmann [6, Page 165, Subsection 5.3.2].

Geometry ratio $\frac{f}{A}\,(1)$ was chosen based on Leishmann [6, Page 217, Table 6.1].

5.5.3 Performance in Hover

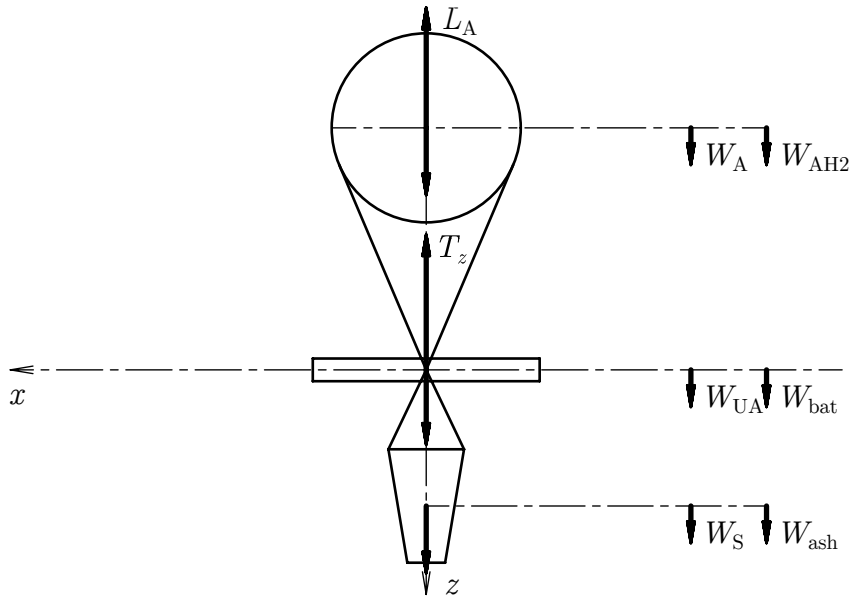

Figure 5.24: Forces acting on the UAS performing hover.

5.5.3.1 Forces in Hover

$$\Sigma F_z : W_A + W_{AH2} + W_{UA} + W_{bat} + W_S + W_{ash} - L_A - T_z = 0 \tag{5.62}$$

5.5.3.2 Required Thrust in Hover

Combining the Equation 5.62 with the Equation 5.19

$$\begin{aligned} T_z = F_O = W_{OEM} + W_{PLM} - L_A = \\ = W_A + W_{AH2} + W_{UA} + W_{bat} + W_S + W_{ash} - L_A. \end{aligned} \tag{5.63}$$

Considering required operational overweight mass $M_{ROOM}\,(\mathrm{kg})$ and the Equation 5.21, required thrust in hover $T_{Rh}\,(\mathrm{N})$

$$T_{Rh} = F_O = W_{ROOM} + W_S + W_{ash} = (M_{ROOM} + M_S + M_{ash})\, g_0 = (M_{ROOM} + M_{PLM})\, g_0. \tag{5.64}$$

Combining Equations 5.6 and 5.64, thrust coefficient $C_T\,(1)$

$$C_T = \frac{T_{Rh}}{\rho A \Omega^2 R^2} = \frac{(M_{ROOM} + M_{PLM})\, g_0}{\rho A \Omega^2 R^2}. \tag{5.65}$$

5.5.3.3 Inflow Ratio in Hover

Leishmann provides the expression [6, Page 44, Equation 2.27] for induced inflow ratio $\lambda_i\,(1)$ in relation to thrust in hover

$$\lambda_h = \lambda_i = \frac{v_i}{\Omega R} = \frac{1}{\Omega R}\sqrt{\frac{T}{2\rho A}} = \sqrt{\frac{T}{2\rho A\,(\Omega R)^2}} = \sqrt{\frac{C_T}{2}}. \tag{5.66}$$

5.5.3.4 Required Power in Hover

Leishmann provides the expression [6, Page 44, Equation 2.29] for ideal power coefficient $C_P\,(1)$ for hovering rotor

$$C_P = C_T \lambda_{\mathrm{i}} = \frac{C_T^{\frac{3}{2}}}{\sqrt{2}} \tag{5.67}$$

and expression [6, Page 44, Equation 2.32] for non-ideal induced power coefficient $C_{P\mathrm{i}}\,(1)$

$$C_{P\mathrm{i}} = \frac{\kappa C_T^{\frac{3}{2}}}{\sqrt{2}} \tag{5.68}$$

where $\kappa\,(1)$ is induced power correction factor. "This is an empirical coefficient derived from rotor measurements of flight tests, and it encompasses a number of nonideal, but physical effects, such as nonuniform inflow, tip losses, wake swirl, less than ideal wake contraction, finite number of blades, etc. For preliminary design, most helicopter manufacturers use their own measurements and experience to estimate values of κ , a typical value being about 1.15" [6, Pages 44-45, Subsection 2.2.7].

Rearranging Equation 5.9, the expression for rotor solidity $\sigma\,(1)$ becomes

$$\sigma = 6\left(\frac{C_T}{\bar{C}_L}\right) \tag{5.69}$$

and to keep the the results of calculation safe, mean lift coefficient was set $\bar{C}_L = 0.5$.

Leishmann also provides the expression [6, Page 45, Equation 2.36] for profile power coefficient $C_{P0}\,(1)$

$$C_{P0} = \frac{1}{8}\left(\frac{N_{\mathrm{b}} c R}{A}\right) C_{d0} = \frac{1}{8}\left(\frac{N_{\mathrm{b}} c R}{\pi R^2}\right) C_{d0} = \frac{1}{8}\left(\frac{N_{\mathrm{b}} c}{\pi R}\right) C_{d0} = \frac{1}{8}\sigma C_{d0} \tag{5.70}$$

where $N_{\mathrm{b}}\,(1)$ is number of rotor blades, $c\,(\mathrm{m})$ is blade airfoil chord length, $C_{d0}\,(1)$ is profile drag coefficient of the rotor blade.

Inserting Equation 5.69 into Equation 5.70

$$C_{P0} = \frac{3}{4}\left(\frac{C_T}{\bar{C}_L}\right) C_{d0}. \tag{5.71}$$

Leishmann provides the expression [6, Page 85, Equation 3.31] for power coefficient $C_P\,(1)$ by Blade Element Analysis

$$C_P = \lambda C_T + \frac{1}{8}\sigma C_{d0}. \tag{5.72}$$

Using Equation 5.68 while inserting Equation 5.71, Equation 5.72 was modified

$$C_P = C_{P\mathrm{i}} + C_{P0} = \frac{\kappa C_T^{\frac{3}{2}}}{\sqrt{2}} + \frac{3}{4}\left(\frac{C_T}{\bar{C}_L}\right) C_{d0}. \tag{5.73}$$

Using Equations 5.7 and 5.73, required power in hover $P_{\mathrm{Rh}}\,(\mathrm{W})$

$$P_{\mathrm{Rh}} = \left(\frac{\kappa C_T^{\frac{3}{2}}}{\sqrt{2}} + \frac{3}{4}\left(\frac{C_T}{\bar{C}_L}\right) C_{d0}\right) \rho A \Omega^3 R^3. \tag{5.74}$$

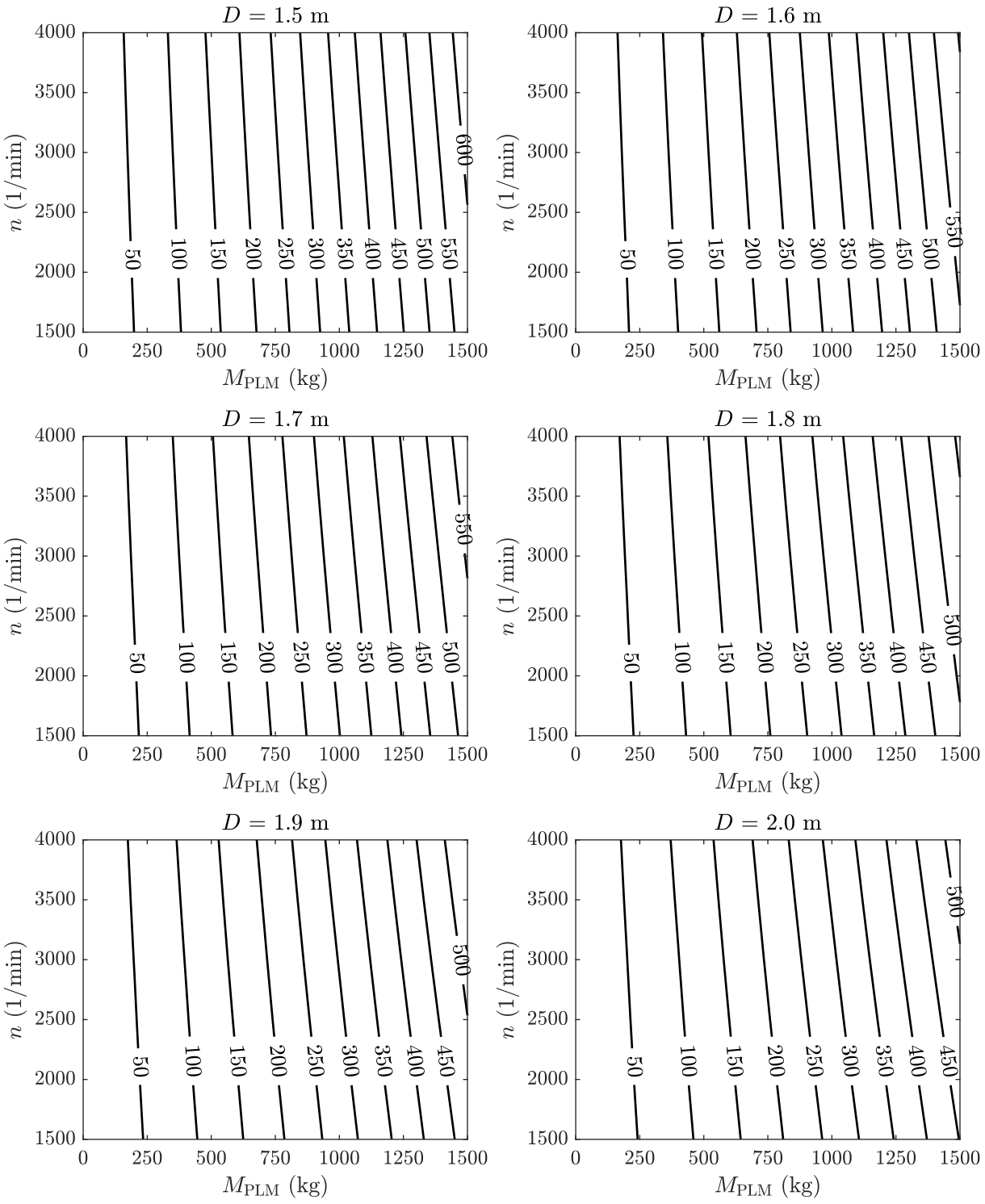

Figure 5.25: Required power in hover $P_{\mathrm{Rh}}\,(\mathrm{kW})$
as a function of payload mass $M_{\mathrm{PLM}}\,(\mathrm{kg})$
and revolutions per minute $n\left(\frac{1}{\mathrm{min}}\right)$ for various propeller diameter $D\,(\mathrm{m})$
by modified theory.

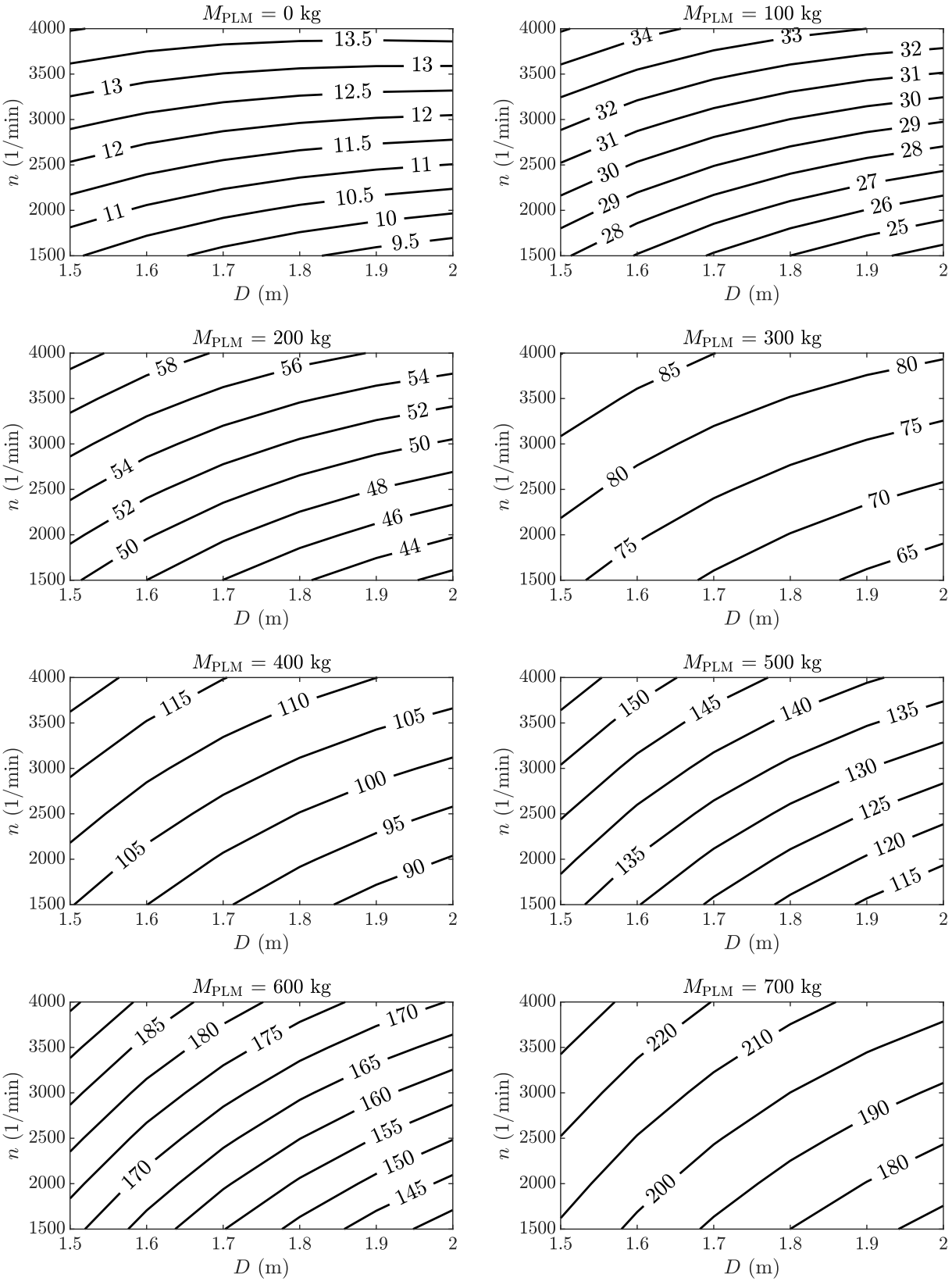

Figure 5.26: Required power in hover $P_{\mathrm{Rh}}\,(\mathrm{kW})$
as a function of propeller diameter $D\,(\mathrm{m})$
and revolutions per minute $n\left(\frac{1}{\mathrm{min}}\right)$ for various payload masses $M_{\mathrm{PLM}}\,(\mathrm{kg})$
by modified theory; light payload.

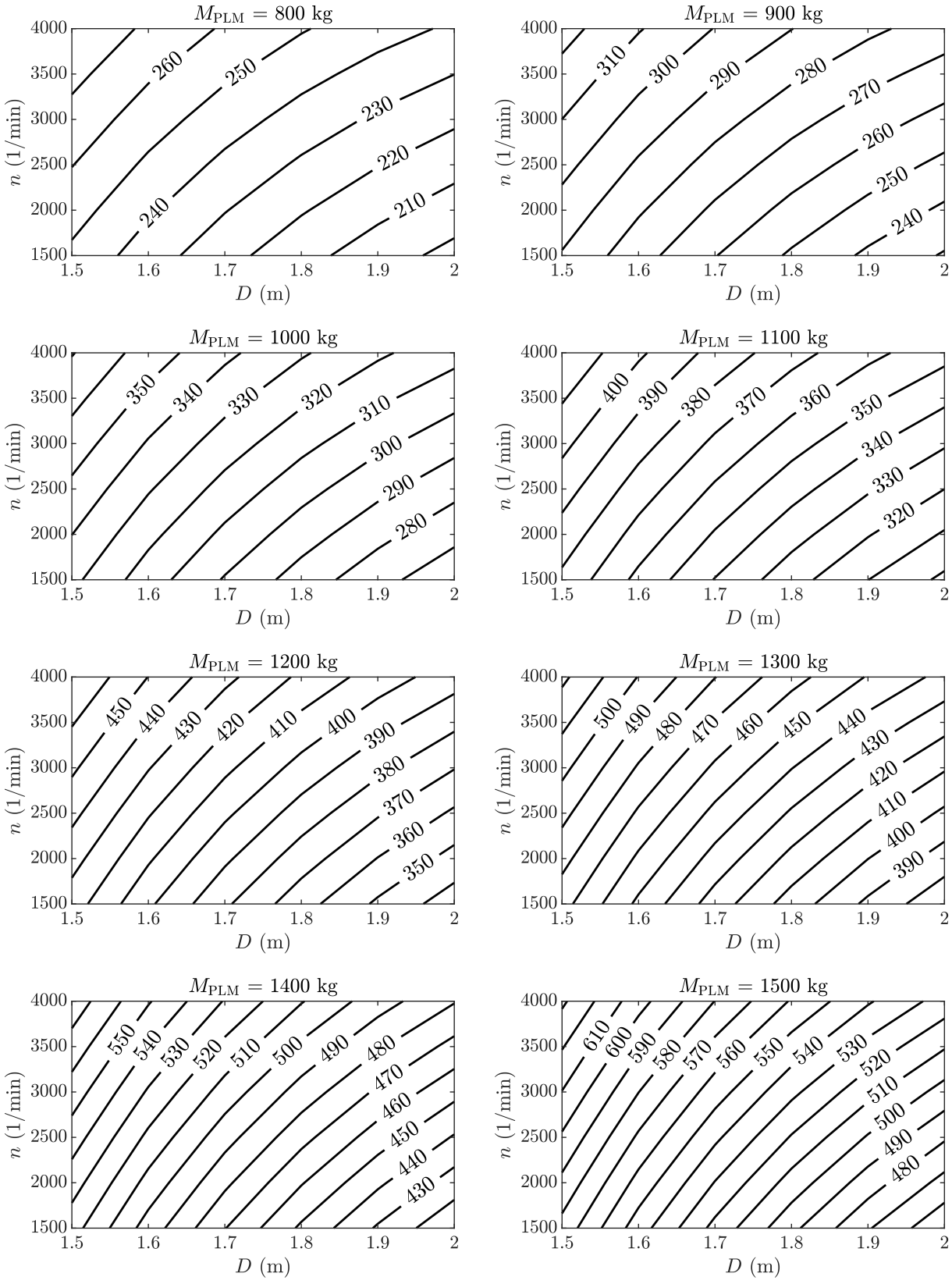

Figure 5.27: Required power in hover $P_{\mathrm{Rh}}\,(\mathrm{kW})$
as a function of propeller diameter $D\,(\mathrm{m})$
and revolutions per minute $n\left(\frac{1}{\mathrm{min}}\right)$ for various payload masses $M_{\mathrm{PLM}}\,(\mathrm{kg})$
by modified theory; heavy payload.

5.5.4 Performance in Axial Climb and Descent

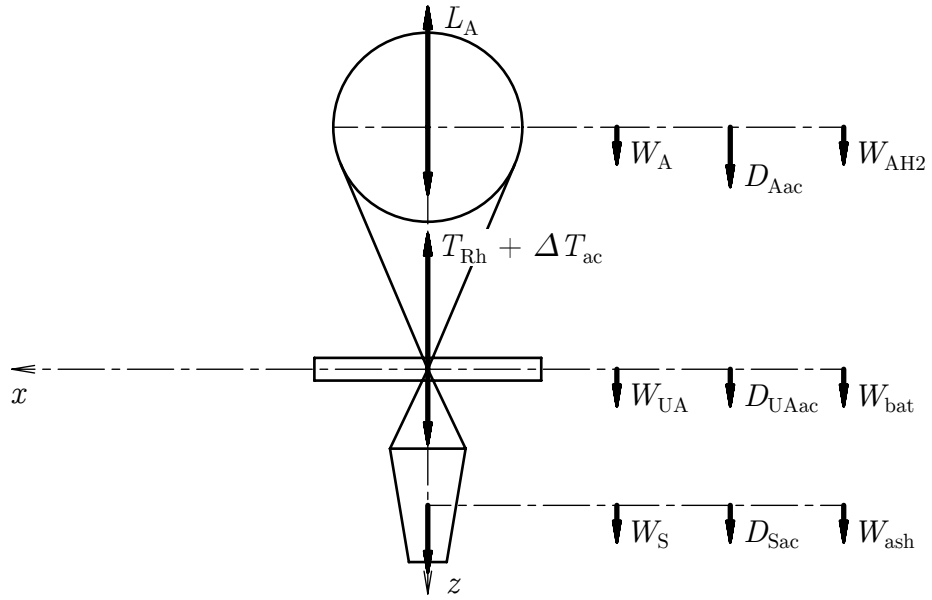

Figure 5.28: Forces acting on the UAS performing axial climb.

5.5.4.1 Thrust in Axial Climb and Descent

Axial climb demands difference in required thrust $\Delta T_\mathrm{Rac}\,(\mathrm{N})$ equal to the total drag of the UAS

$$T_\mathrm{Rac} = T_\mathrm{Rh} + \Delta T_\mathrm{Rac} = T_\mathrm{Rh} + D_\mathrm{Aac} + D_\mathrm{UAac} + D_\mathrm{Sac} \tag{5.75}$$

and in axial descent

$$T_\mathrm{Rad} = T_\mathrm{Rh} - \Delta T_\mathrm{Rad} = T_\mathrm{Rh} - D_\mathrm{Aad} - D_\mathrm{UAad} - D_\mathrm{Sad}. \tag{5.76}$$

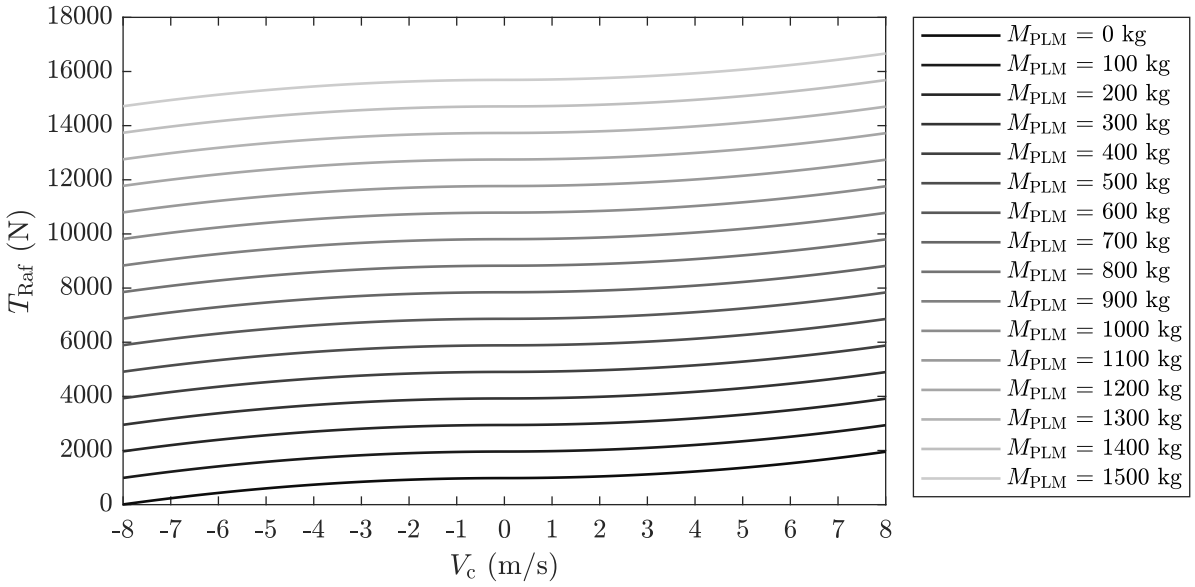

Figure 5.29: Required thrust in axial flight $T_\mathrm{Raf}\,(\mathrm{N})$
as a function of climb velocity $V_\mathrm{c}\left(\frac{\mathrm{m}}{\mathrm{s}}\right)$ and payload mass $M_\mathrm{PLM}\,(\mathrm{kg})$.

5.5.4.2 Velocity Ratios in Axial Climb and Descent

In performing axial climb, the slipstream is always under the rotor which makes the calculation straightforward. The situation is not that simple in case of axial descend. Leishmann states: "For cases where the descent velocity is in the range $-2v_\mathrm{i} < V_\mathrm{c} < 0$, the velocity at any plane through the rotor slipstream can be either upward or downward. Under these circumstances, a more complicated recirculating (and usually more turbulent) flow pattern may exist at the rotor, and momentum theory cannot be used because no definitive control volume can be established" [6, Page 55, Subsection 2.3.2].

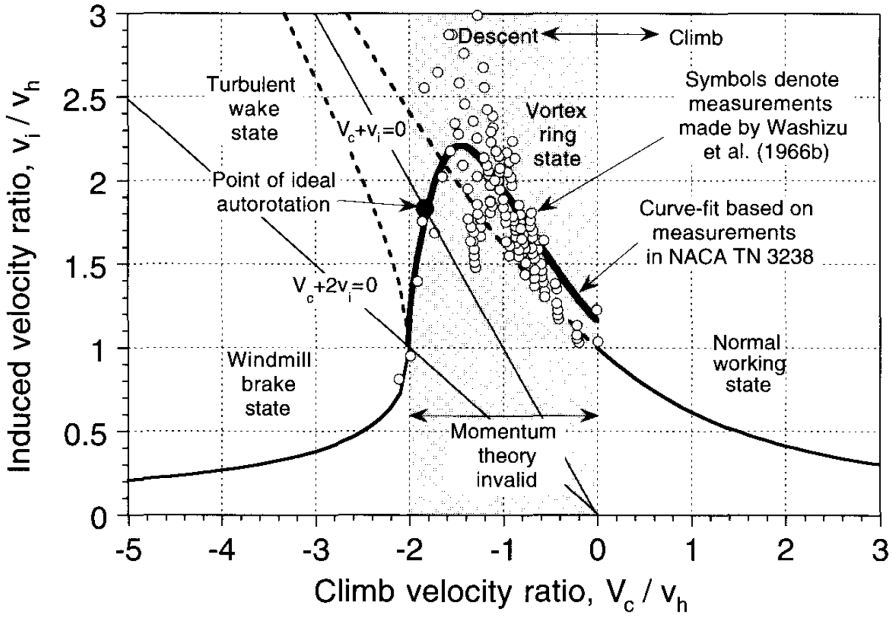

Figure 5.30: Induced velocity variation as a function of climb and descent velocity based on momentum theory (complete induced velocity curve) [6, Page 55, Figure 2.13].

Climb velocity ratio $\frac{V_\mathrm{c}}{v_\mathrm{h}}$ (1) is simply a ratio of climb velocity V_c $\left(\frac{\mathrm{m}}{\mathrm{s}}\right)$ and induced velocity in hover v_h $\left(\frac{\mathrm{m}}{\mathrm{s}}\right)$. For the purpose of conceptual design, it is necessary to establish the range of climb velocity the UAS is supposed to operate in.

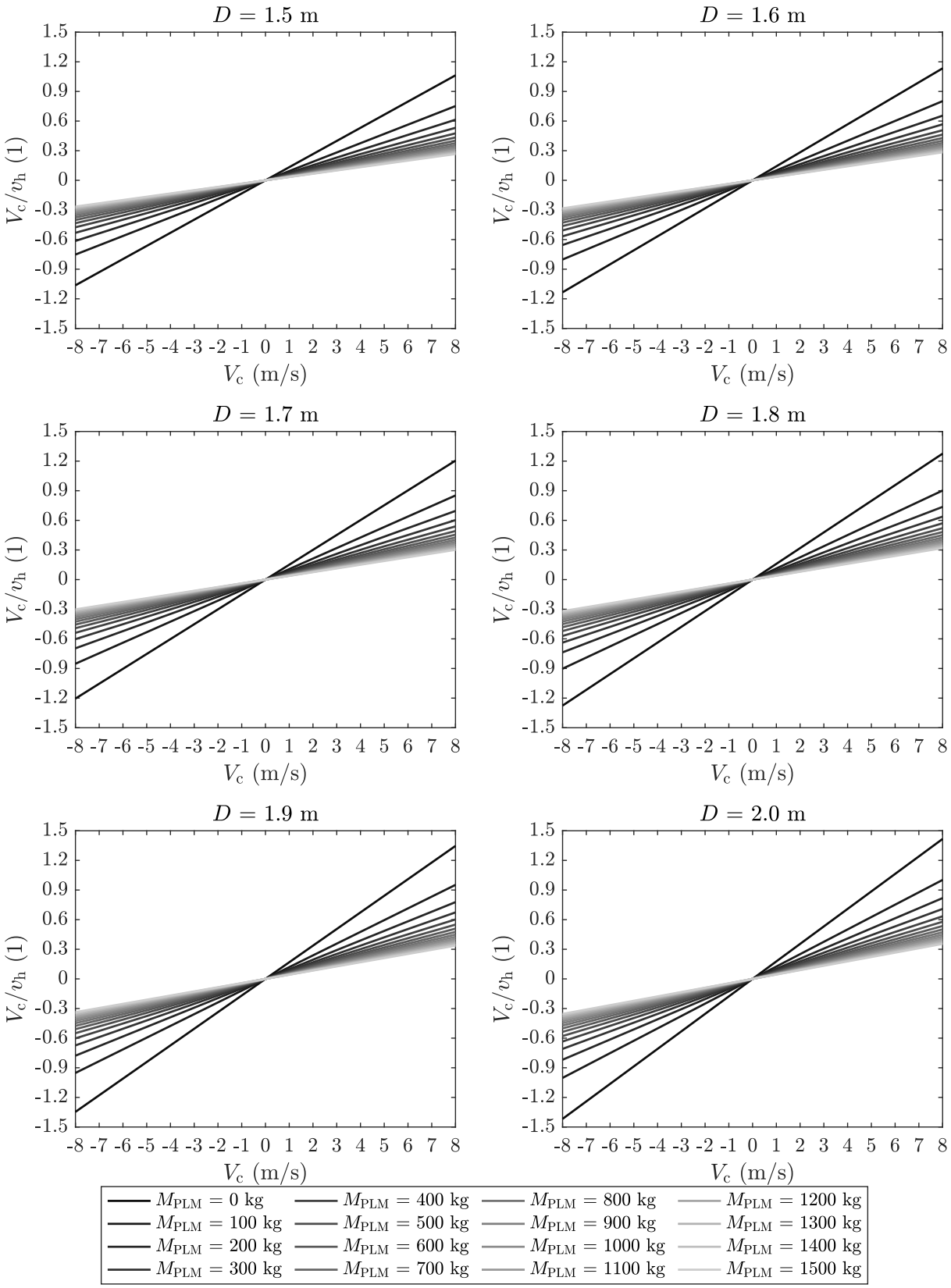

Figure 5.31: Climb velocity ratio $\frac{V_c}{v_h}$ (1) as a function of climb velocity V_c $\left(\frac{m}{s}\right)$ and payload mass M_{PLM} (kg) for various propeller diameter D (m).

For the case of axial climb where $\frac{V_\mathrm{c}}{v_\mathrm{h}} > 0$, Leishmann derives the expression [6, Page 55, Equation 2.66] for induced velocity ratio $\frac{v_\mathrm{i}}{v_\mathrm{h}}\,(1)$

$$\frac{v_\mathrm{i}}{v_\mathrm{h}} = -\left(\frac{V_\mathrm{c}}{2v_\mathrm{h}}\right) + \sqrt{\left(\frac{V_\mathrm{c}}{2v_\mathrm{h}}\right)^2 + 1} \tag{5.77}$$

and after rearrangement, induced velocity $v_\mathrm{i}\,\left(\frac{\mathrm{m}}{\mathrm{s}}\right)$

$$v_\mathrm{i} = -\left(\frac{V_\mathrm{c}}{2}\right) + \sqrt{\left(\frac{V_\mathrm{c}}{2}\right)^2 + v_\mathrm{h}}. \tag{5.78}$$

For the case of axial descent in the range $-2 \leq \frac{V_\mathrm{c}}{v_\mathrm{h}} \leq 0$, Leishmann brings the approxiamtion [6, Page 58, Equation 2.81] for induced velocity ratio $\frac{v_\mathrm{i}}{v_\mathrm{h}}\,(1)$

$$\frac{v_\mathrm{i}}{v_\mathrm{h}} = \kappa + k_1\left(\frac{V_\mathrm{c}}{v_\mathrm{h}}\right) + k_2\left(\frac{V_\mathrm{c}}{v_\mathrm{h}}\right)^2 + k_3\left(\frac{V_\mathrm{c}}{v_\mathrm{h}}\right)^3 + k_4\left(\frac{V_\mathrm{c}}{v_\mathrm{h}}\right)^4, \tag{5.79}$$

where

$$k_1 = -1.125, \tag{5.80}$$

$$k_2 = -1.372, \tag{5.81}$$

$$k_3 = -1.718, \tag{5.82}$$

$$k_4 = -0.655. \tag{5.83}$$

Because induced power correction factor $\kappa\,(1)$ was already applied in the calculation of induced velocity in hover $v_\mathrm{h}\,\left(\frac{\mathrm{m}}{\mathrm{s}}\right)$, Equation 5.79 was rearranged

$$\frac{v_\mathrm{i}}{v_\mathrm{h}} = 1 + \frac{1}{\kappa}\left[k_1\left(\frac{V_\mathrm{c}}{v_\mathrm{h}}\right) + k_2\left(\frac{V_\mathrm{c}}{v_\mathrm{h}}\right)^2 + k_3\left(\frac{V_\mathrm{c}}{v_\mathrm{h}}\right)^3 + k_4\left(\frac{V_\mathrm{c}}{v_\mathrm{h}}\right)^4\right]. \tag{5.84}$$

After further rearrangement, induced velocity $v_\mathrm{i}\,\left(\frac{\mathrm{m}}{\mathrm{s}}\right)$

$$v_\mathrm{i} = v_\mathrm{h} + \frac{v_\mathrm{h}}{\kappa}\left[k_1\left(\frac{V_\mathrm{c}}{v_\mathrm{h}}\right) + k_2\left(\frac{V_\mathrm{c}}{v_\mathrm{h}}\right)^2 + k_3\left(\frac{V_\mathrm{c}}{v_\mathrm{h}}\right)^3 + k_4\left(\frac{V_\mathrm{c}}{v_\mathrm{h}}\right)^4\right]. \tag{5.85}$$

For the case of axial descent where $\frac{V_\mathrm{c}}{v_\mathrm{h}} < -2$, Leishmann derives the expression [6, Page 57, Equation 2.76] for induced velocity ratio $\frac{v_\mathrm{i}}{v_\mathrm{h}}\,(1)$

$$\frac{v_\mathrm{i}}{v_\mathrm{h}} = -\left(\frac{V_\mathrm{c}}{2v_\mathrm{h}}\right) - \sqrt{\left(\frac{V_\mathrm{c}}{2v_\mathrm{h}}\right)^2 - 1} \tag{5.86}$$

and after rearrangement, induced velocity $v_\mathrm{i}\,\left(\frac{\mathrm{m}}{\mathrm{s}}\right)$

$$v_\mathrm{i} = -\left(\frac{V_\mathrm{c}}{2}\right) - \sqrt{\left(\frac{V_\mathrm{c}}{2}\right)^2 - v_\mathrm{h}}. \tag{5.87}$$

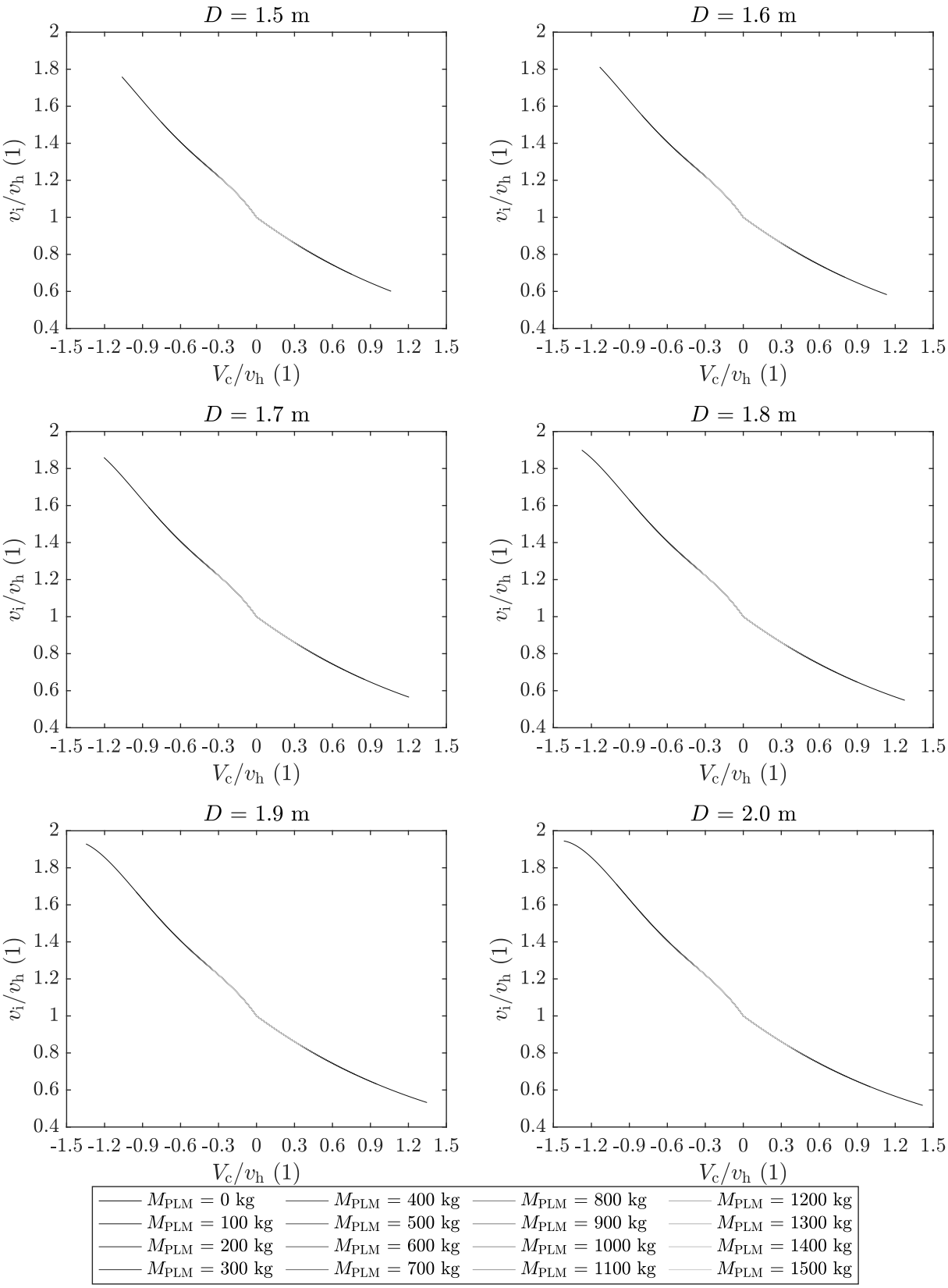

Figure 5.32: Induced velocity ratio $\frac{v_\mathrm{i}}{v_\mathrm{h}}$ (1) as a function of climb velocity ratio $\frac{V_\mathrm{c}}{v_\mathrm{h}}$ (1) and payload mass M_PLM (kg) for various propeller diameter D (m).

5.5.4.3 Required Power in Axial Climb and Descent

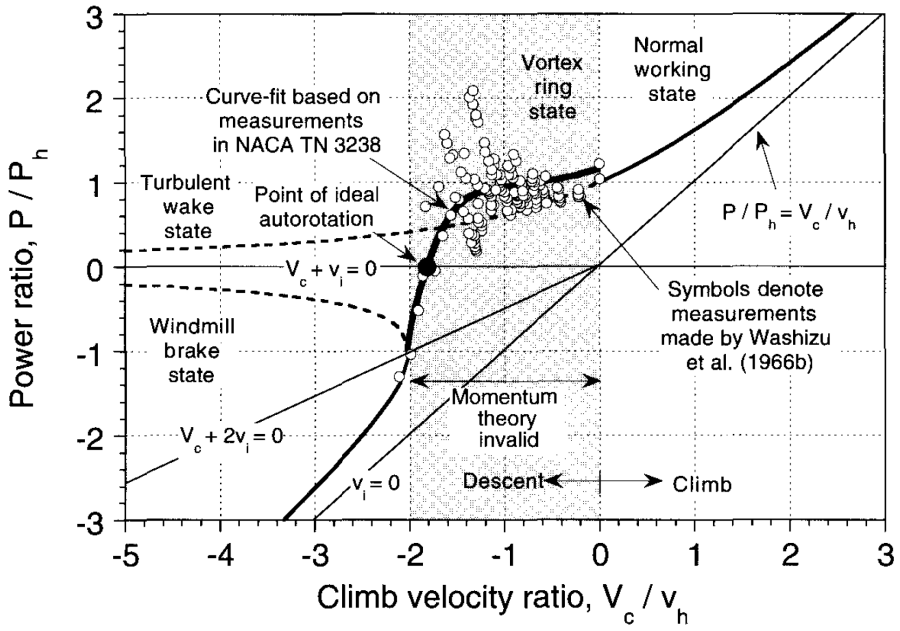

Figure 5.33: Total power required as a function of climb and descent velocity (universal power curve) [6, Page 59, Figure 2.15].

Leishmann provides the expression [6, Page 59, Equation 2.82] for power ratio $\frac{P}{P_\mathrm{h}}$ (1)

$$\frac{P}{P_\mathrm{h}} = \frac{V_\mathrm{c} + v_\mathrm{i}}{v_\mathrm{h}} = \frac{V_\mathrm{c}}{v_\mathrm{h}} + \frac{v_\mathrm{i}}{v_\mathrm{h}} \tag{5.88}$$

and after rearranging, required power in axial flight P_Raf (kW)

$$P_\mathrm{Raf} = P_\mathrm{Rh}\left(\frac{V_\mathrm{c}}{v_\mathrm{h}} + \frac{v_\mathrm{i}}{v_\mathrm{h}}\right). \tag{5.89}$$

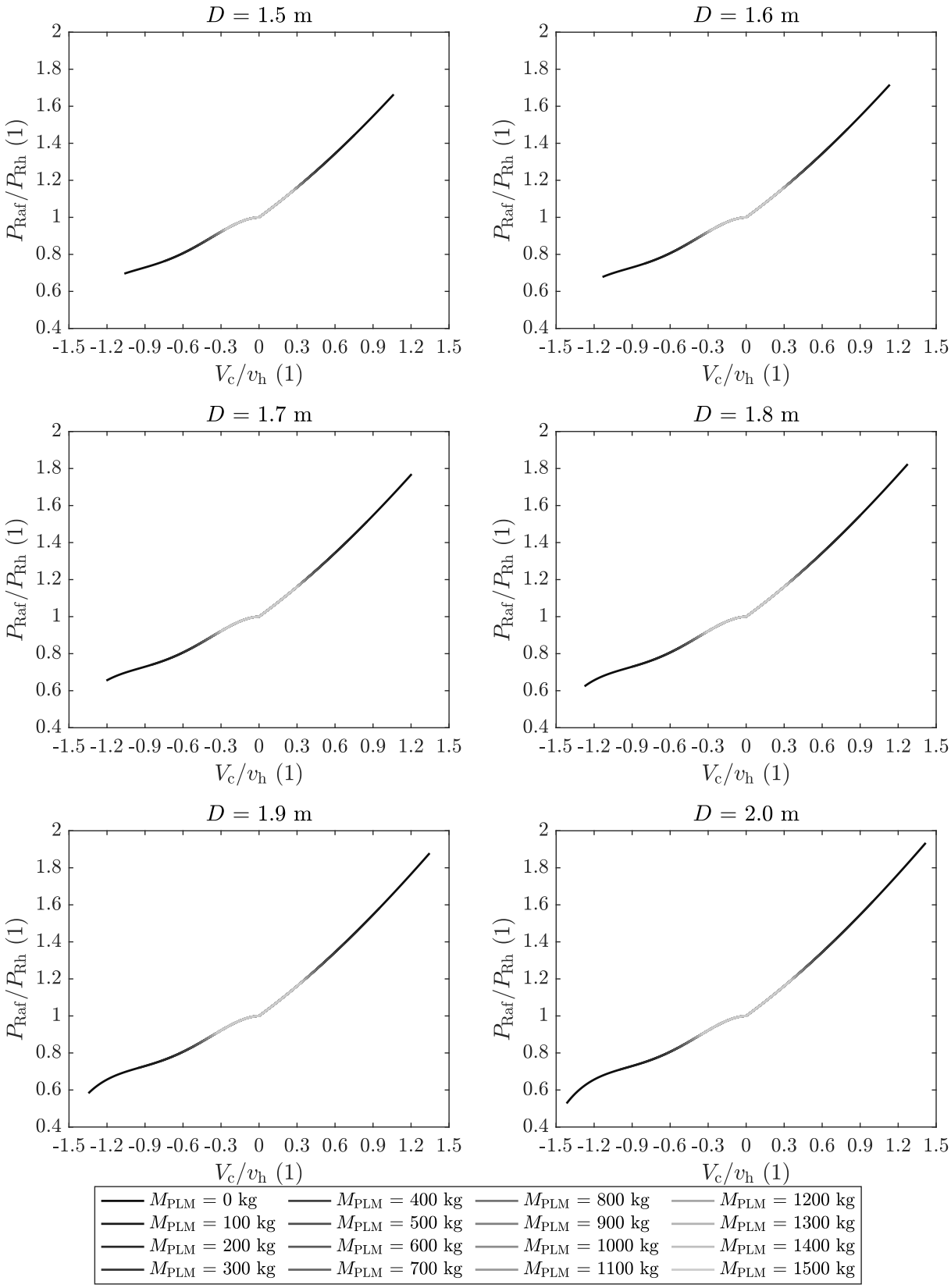

Figure 5.34: Power ratio $\frac{P_{\mathrm{Raf}}}{P_{\mathrm{Rh}}}$ (1) as a function of climb velocity ratio $\frac{V_{\mathrm{c}}}{v_{\mathrm{h}}}$ (1) and payload mass M_{PLM} (kg) for various propeller diameter D (m).

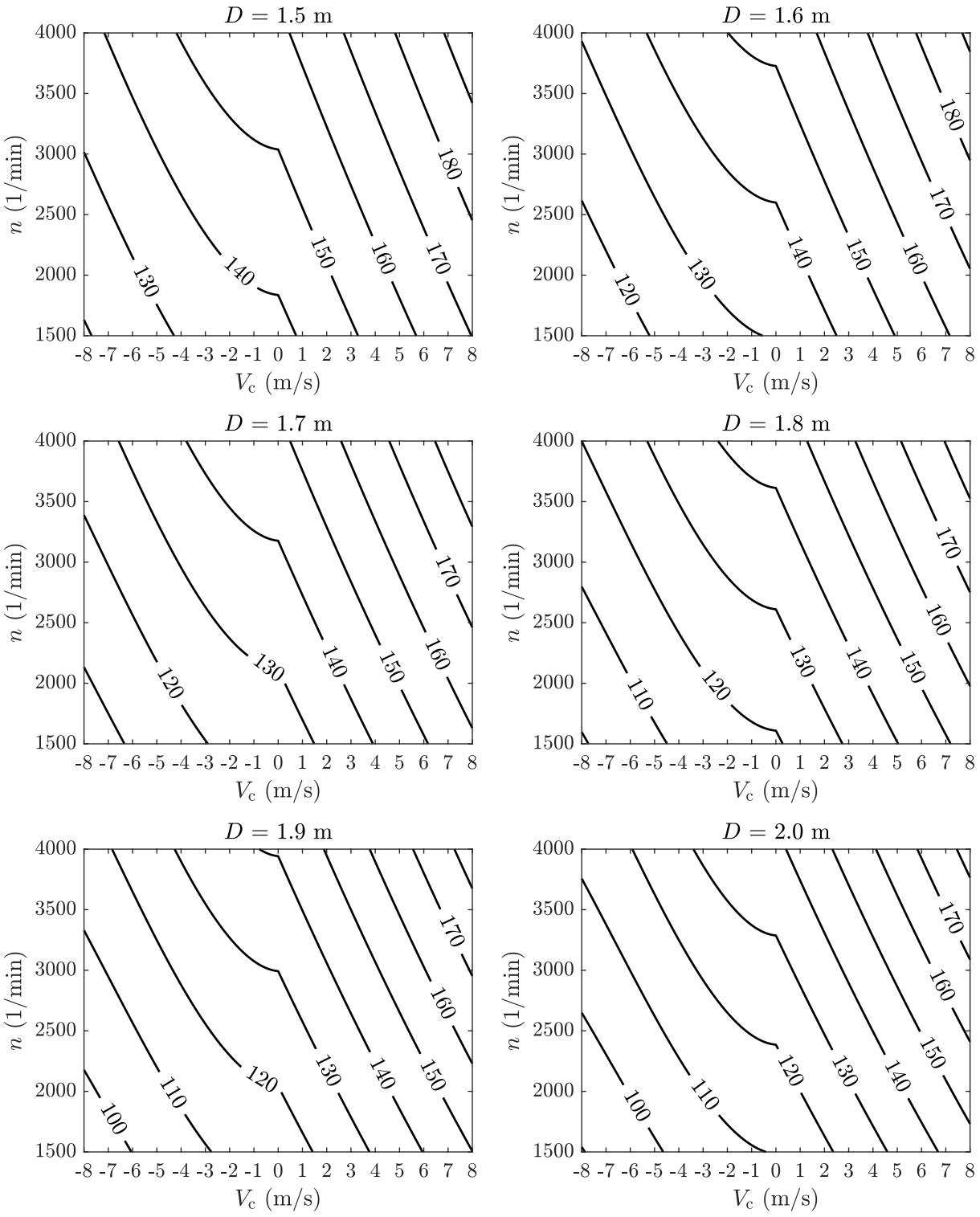

Figure 5.35: Required power in axial flight $P_{\mathrm{Raf}}\,(\mathrm{kW})$
as a function of climb velocity $V_c\left(\frac{\mathrm{m}}{\mathrm{s}}\right)$
and revolutions per minute $n\left(\frac{1}{\mathrm{min}}\right)$ for various propeller diameter $D\,(\mathrm{m})$;
payload mass $M_{\mathrm{PLM}} = 500\,(\mathrm{kg})$.

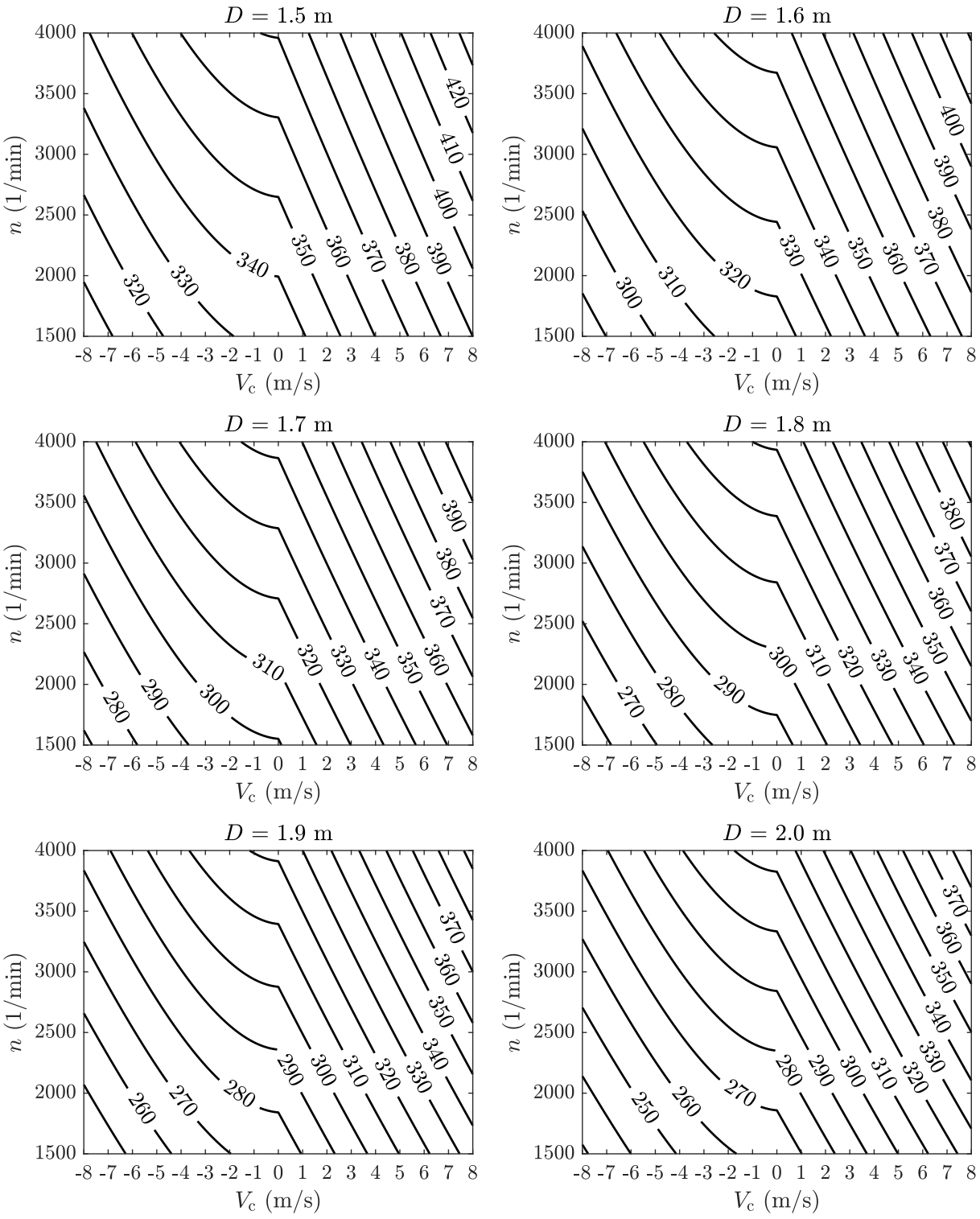

Figure 5.36: Required power in axial flight $P_{\mathrm{Raf}}\,(\mathrm{kW})$
as a function of climb velocity $V_c\,\left(\frac{\mathrm{m}}{\mathrm{s}}\right)$
and revolutions per minute $n\,\left(\frac{1}{\mathrm{min}}\right)$ for various propeller diameter $D\,(\mathrm{m})$;
payload mass $M_{\mathrm{PLM}} = 1000\,(\mathrm{kg})$.

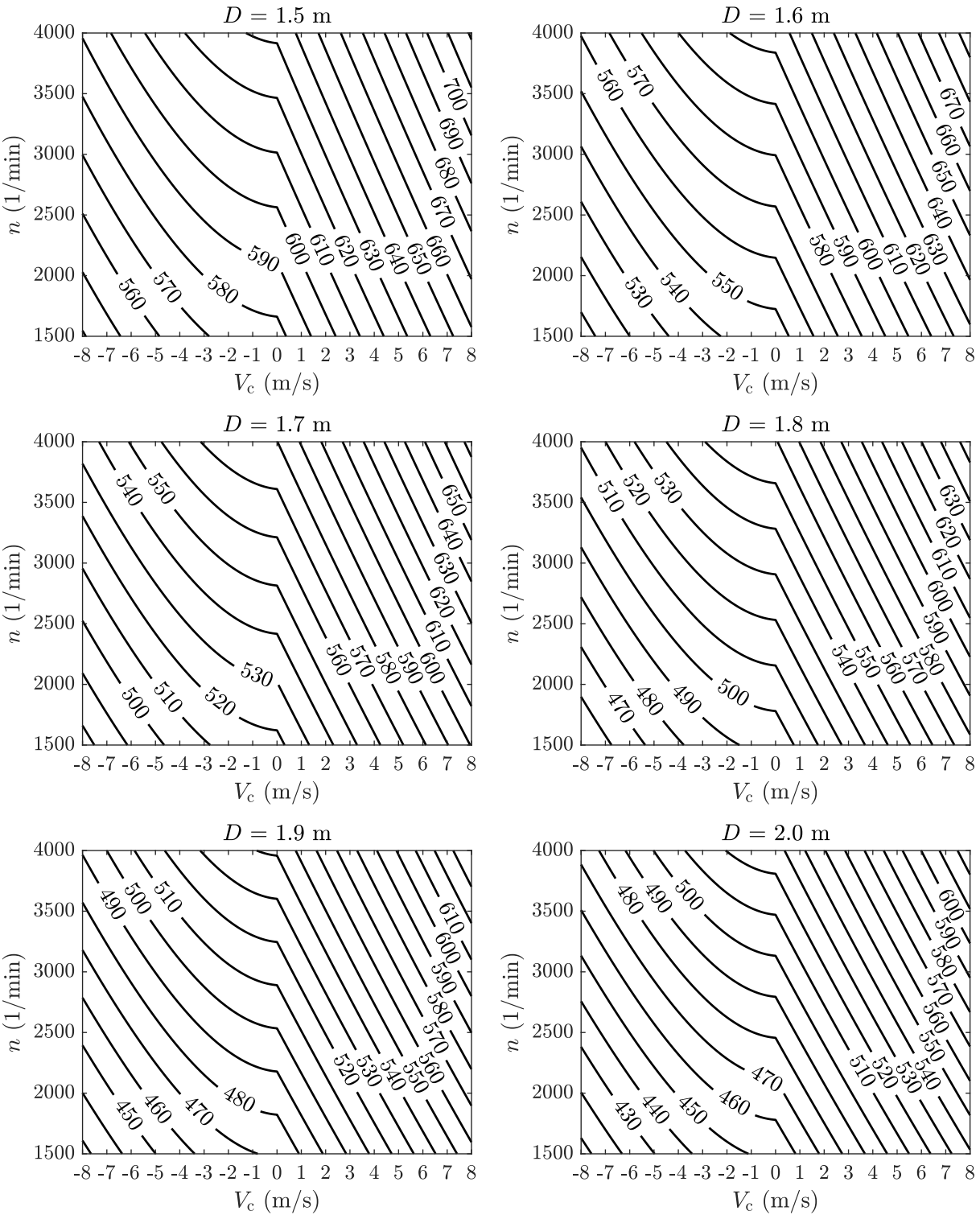

Figure 5.37: Required power in axial flight $P_{\mathrm{Raf}}\,(\mathrm{kW})$
as a function of climb velocity $V_c\left(\frac{\mathrm{m}}{\mathrm{s}}\right)$
and revolutions per minute $n\left(\frac{1}{\mathrm{min}}\right)$ for various propeller diameter $D\,(\mathrm{m})$;
payload mass $M_{\mathrm{PLM}} = 1500\,(\mathrm{kg})$.

5.5.5 Performance in Forward Flight

Performing the forward flight while sustaining the flight level requires the thrust T (N) to be split into vertical component T_z (N) and horizontal component T_x (N). T_z (N) corresponds to total lift deficiency F_{O} (N) and T_x (N) corresponds to total UAS drag in forward flight D_{UASff} (N).

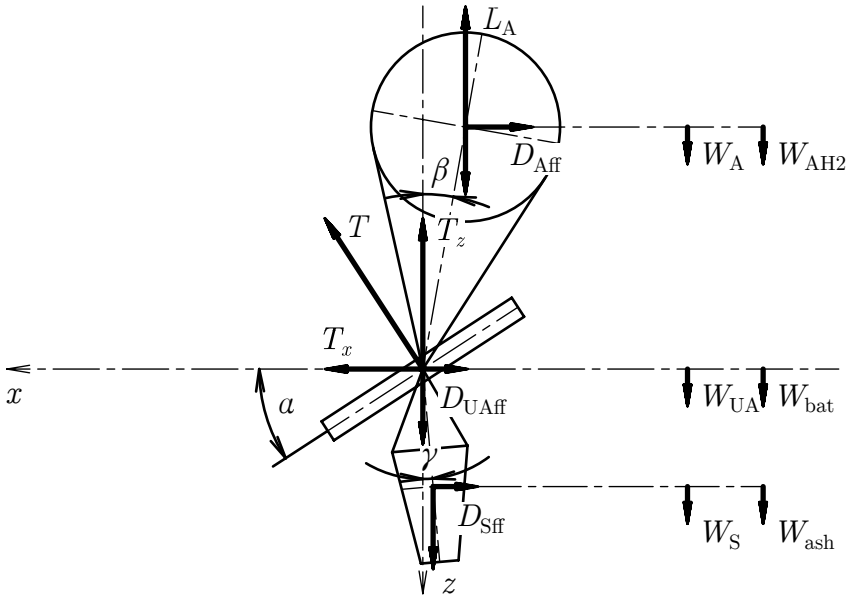

Figure 5.38: Forces acting on the UAS performing the forward horizontal flight.

5.5.5.1 Forces in Forward Flight

$$\Sigma F_x : T_x - D_{\mathrm{UAff}} - D_{\mathrm{Aff}} - D_{\mathrm{Sff}} = 0, \tag{5.90}$$

$$\Sigma F_z : W_{\mathrm{A}} + W_{\mathrm{AH2}} + W_{\mathrm{UA}} + W_{\mathrm{bat}} + W_{\mathrm{S}} + W_{\mathrm{ash}} - T_z - L_{\mathrm{A}} = 0 \tag{5.91}$$

where

$$W_{\mathrm{A}} + W_{\mathrm{AH2}} + W_{\mathrm{UA}} + W_{\mathrm{bat}} - L_{\mathrm{A}} = W_{\mathrm{ROOM}}, \tag{5.92}$$

$$\tan(\alpha) = \frac{T_x}{T_z}, \tag{5.93}$$

$$D_{\mathrm{UAff}} = \frac{1}{2}\rho V_\infty^2 C_{d\mathrm{UAff}} A_{\mathrm{UA}}(\alpha), \tag{5.94}$$

$$D_{\mathrm{Aff}} = \frac{1}{2}\rho V_\infty^2 C_{d\mathrm{A}} \bar{A}_{\mathrm{aer}} = \frac{1}{2}\rho, V_\infty^2 C_{d\mathrm{A}} \frac{\pi \bar{D}_{\mathrm{aer}}^2}{4} \tag{5.95}$$

$$D_{\mathrm{Sff}} = \frac{1}{2}\rho V_\infty^2 C_{d\mathrm{Sff}} A_{\mathrm{Sff}}. \tag{5.96}$$

5.5.5.2 Vertical Thrust in Forward Flight

Inserting Equation 5.92 into Equation 5.91 and rearranging

$$T_z = W_{\mathrm{ROOM}} + W_{\mathrm{S}} + W_{\mathrm{ash}}. \tag{5.97}$$

5.5.5.3 Horizontal Thrust in Forward Flight

Plugging Equations 5.94 - 5.96 into Equation 5.90 and rearranging

$$T_x = \frac{1}{2}\rho V_\infty^2 \left(C_{d\mathrm{UAff}} A_{\mathrm{UA}}(\alpha) + C_{d\mathrm{A}} \frac{\pi \bar{D}_{\mathrm{aer}}^2}{4} + C_{d\mathrm{Sff}} A_{\mathrm{Sff}} \right). \tag{5.98}$$

Combining Equation 5.97 with Equation 5.93 and rearranging

$$T_x = (W_{\mathrm{ROOM}} + W_{\mathrm{S}} + W_{\mathrm{ash}}) \tan(\alpha). \tag{5.99}$$

5.5.5.4 Total Thrust in Forward Flight

Trigonometric recalculation of Equation 5.97

$$T = \frac{T_z}{\cos(\alpha)} = \frac{W_{\mathrm{ROOM}} + W_{\mathrm{S}} + W_{\mathrm{ash}}}{\cos(\alpha)} \tag{5.100}$$

and inserting Equation 5.100 into the Equation 5.6

$$C_T = C_W = \frac{\frac{T_z}{\cos(\alpha)}}{\rho A \Omega^2 R^2} = \frac{W_{\mathrm{ROOM}} + W_{\mathrm{S}} + W_{\mathrm{ash}}}{\rho A \Omega^2 R^2 \cos(\alpha)} \tag{5.101}$$

where C_W (1) denotes thrust coefficient in forward flight while maintaining the flight level, meaning sustaining the vertical force equilibrium.

5.5.5.5 Velocity in Forward Flight

Inserting Equation 5.99 into Equation 5.98 and rearranging, forward flight velocity $V_\infty \left(\frac{\mathrm{m}}{\mathrm{s}}\right)$

$$V_\infty = \sqrt{\frac{2\left(W_{\mathrm{ROOM}} + W_{\mathrm{S}} + W_{\mathrm{ash}}\right)\tan(\alpha)}{\rho\left(C_{d\mathrm{UAff}} A_{\mathrm{UA}}(\alpha) + C_{d\mathrm{A}} \frac{\pi \bar{D}_{\mathrm{aer}}^2}{4} + C_{d\mathrm{Sff}} A_{\mathrm{Sff}}\right)}} \tag{5.102}$$

where obviously $V_\infty \to \infty$ for $\alpha \to 90°$.

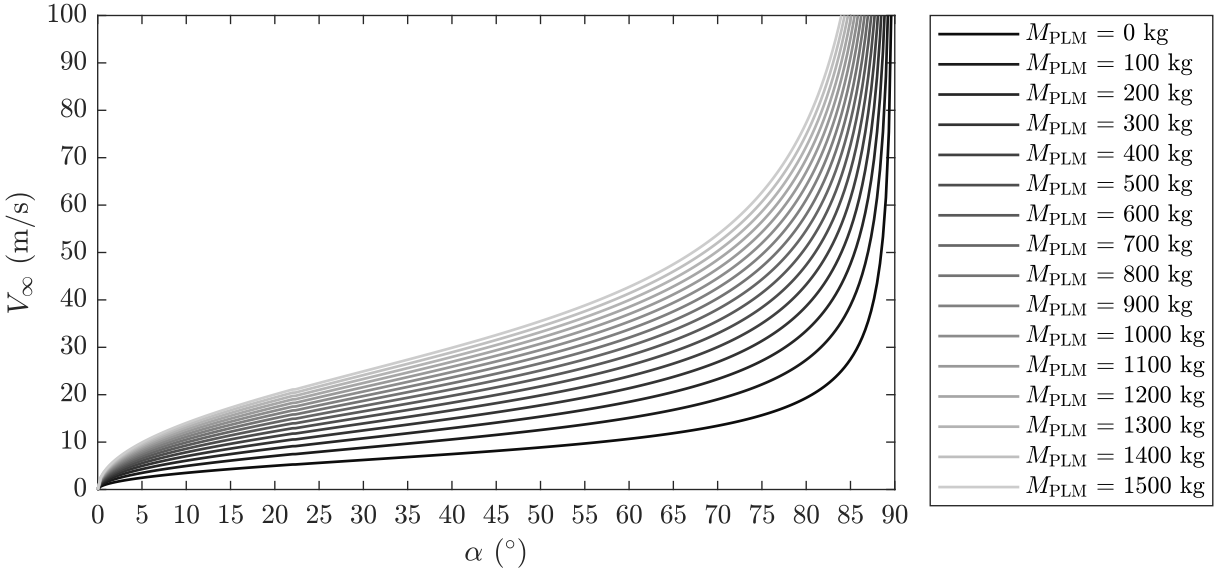

Figure 5.39: Forward flight velocity $V_\infty \left(\frac{\mathrm{m}}{\mathrm{s}}\right)$ as a function of angle of attack $\alpha\,(°)$ and payload mass $M_{\mathrm{PLM}}\,(\mathrm{kg})$.

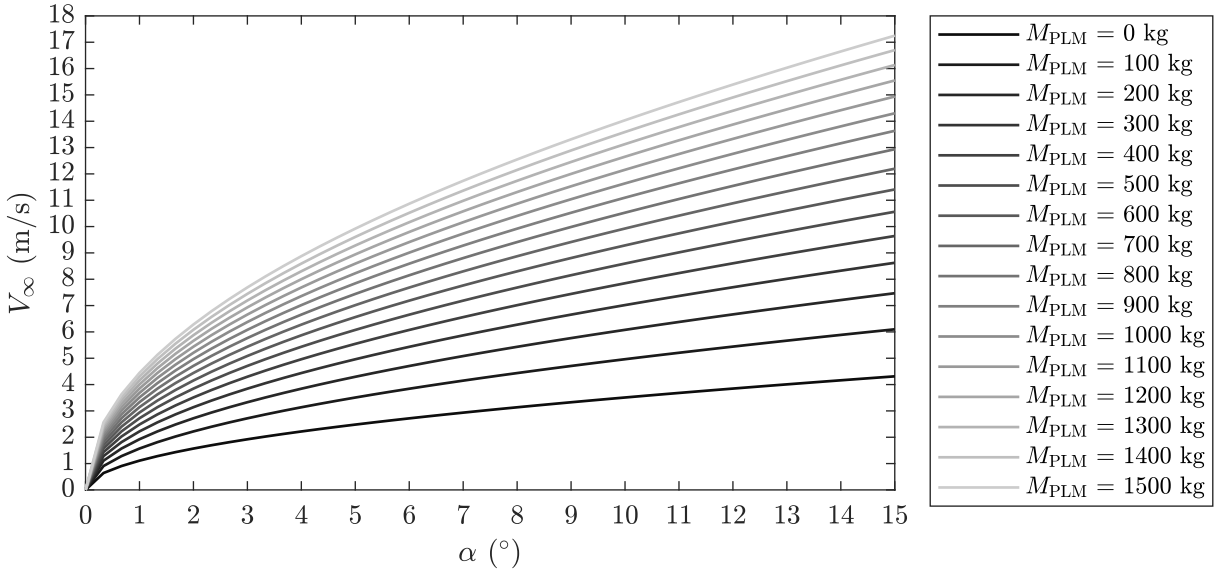

Figure 5.40: Forward flight velocity $V_\infty \left(\frac{\mathrm{m}}{\mathrm{s}}\right)$ as a function of angle of attack $\alpha\,(°)$ and payload mass $M_{\mathrm{PLM}}\,(\mathrm{kg})$; detail on the lower angles of attack.

5.5.5.6 Asymmetrical Thrust in Forward Horizontal Flight

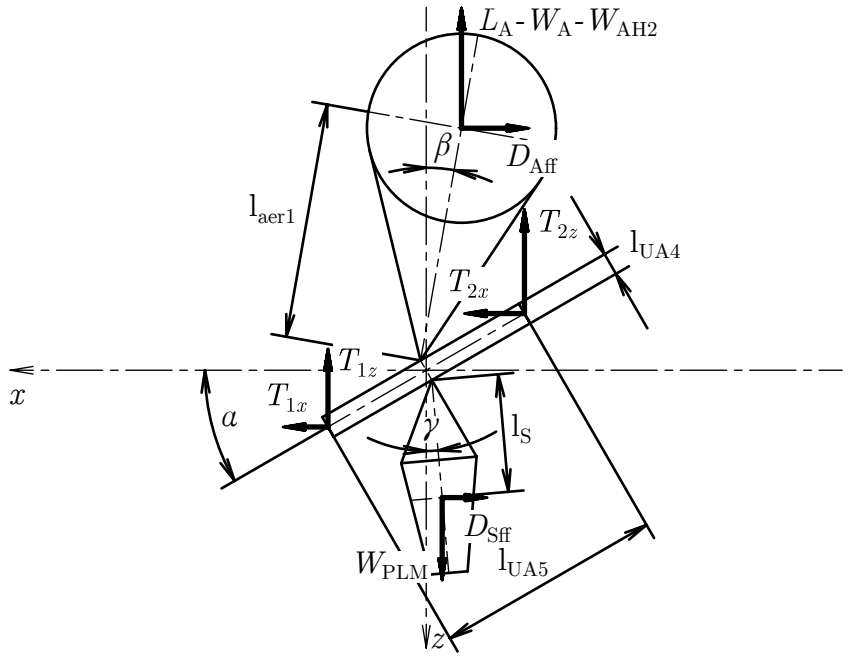

Figure 5.41: Forces acting on the UAS introducing pitch moment equilibrium about y-axis.

$$\begin{aligned}\Sigma M_y :& T_{2x}\frac{l_{\mathrm{UA5}}}{2}\sin(\alpha) + T_{2z}\frac{l_{\mathrm{UA5}}}{2}\cos(\alpha) - T_{1x}\frac{l_{\mathrm{UA5}}}{2}\sin(\alpha) - T_{1z}\frac{l_{\mathrm{UA5}}}{2}\cos(\alpha)\\ &- L_{\mathrm{APLM}}\frac{l_{\mathrm{UA4}}}{2}\sin(\alpha) - D_{\mathrm{Aff}}\frac{l_{\mathrm{UA4}}}{2}\cos(\alpha)\\ &+ D_{\mathrm{Sff}}\frac{l_{\mathrm{UA4}}}{2}\cos(\alpha) - W_{\mathrm{PLM}}\frac{l_{\mathrm{UA4}}}{2}\sin(\alpha) = 0\end{aligned} \tag{5.103}$$

where

$$L_{\mathrm{APLM}} = L_{\mathrm{A}} - W_{\mathrm{A}} - W_{\mathrm{AH2}}, \tag{5.104}$$

$$T_{1x} = T_1\sin(\alpha), \tag{5.105}$$

$$T_{1z} = T_1\cos(\alpha), \tag{5.106}$$

$$T_{2x} = T_2\sin(\alpha), \tag{5.107}$$

$$T_{2z} = T_2\cos(\alpha), \tag{5.108}$$

and so after rearranging

$$\begin{aligned}\Sigma M_y :& T_2\frac{l_{\mathrm{UA5}}}{2} - T_1\frac{l_{\mathrm{UA5}}}{2}\\ &- L_{\mathrm{APLM}}\frac{l_{\mathrm{UA4}}}{2}\sin(\alpha) - D_{\mathrm{Aff}}\frac{l_{\mathrm{UA4}}}{2}\cos(\alpha)\\ &+ D_{\mathrm{Sff}}\frac{l_{\mathrm{UA4}}}{2}\cos(\alpha) - W_{\mathrm{PLM}}\frac{l_{\mathrm{UA4}}}{2}\sin(\alpha) = 0\end{aligned} \quad . \tag{5.109}$$

Breaking down thrust in Equation 5.90 into components

$$\Sigma F_x : T_{1x} + T_{2x} - D_{\mathrm{UAff}} - D_{\mathrm{Aff}} - D_{\mathrm{Sff}} = 0 \tag{5.110}$$

and after inserting Equations 5.105 and 5.107

$$\Sigma F_x : T_1 \sin(\alpha) + T_2 \sin(\alpha) - D_{\mathrm{UAff}} - D_{\mathrm{Aff}} - D_{\mathrm{Sff}} = 0. \tag{5.111}$$

System of Equations 5.109 and 5.111 provides a solution for $T_1\,(\mathrm{N})$ and $T_2\,(\mathrm{N})$

$$\begin{bmatrix} 1 & -1 \\ 1 & 1 \end{bmatrix} \begin{pmatrix} T_1 \\ T_2 \end{pmatrix} = \begin{pmatrix} \frac{l_{\mathrm{UA4}}}{l_{\mathrm{UA5}}} \left[\sin(\alpha)\left(-L_{\mathrm{APLM}} - W_{\mathrm{PLM}}\right) + \cos(\alpha)\left(D_{\mathrm{Sff}} - D_{\mathrm{Aff}}\right)\right] \\ \frac{D_{\mathrm{UAff}} + D_{\mathrm{Aff}} + D_{\mathrm{Sff}}}{\sin(\alpha)} \end{pmatrix}. \tag{5.112}$$

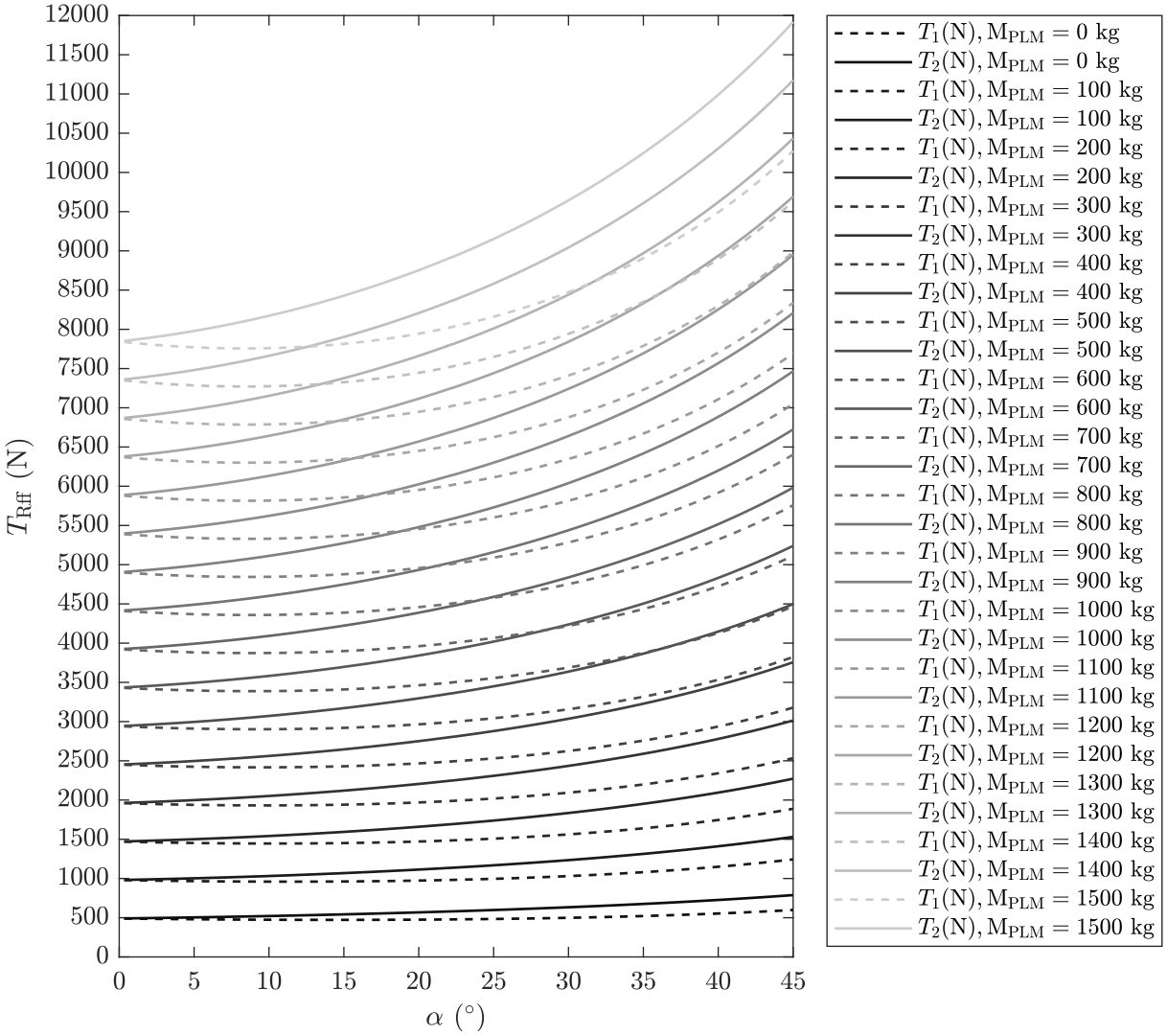

Figure 5.42: Thrust components $T_1\,(\mathrm{N})$ and $T_2\,(\mathrm{N})$ as a function of angle of attack $\alpha\,(^\circ)$ and payload mass $M_{\mathrm{PLM}}\,(\mathrm{kg})$.

5.5.5.7 Attitude Limitations in Forward Flight

Increasing the angle of attack $\alpha\,(^\circ)$ and consequently increasing the forward velocity $V_\infty\left(\frac{\mathrm{m}}{\mathrm{s}}\right)$ causes growth of aerostat drag $D_{\mathrm{Aff}}\,(\mathrm{N})$ and also the angular deflection of aerostat axis $\beta\,(^\circ)$ as shown in Figure 5.38. It is necessary to take this into consideration, so any possible collision of the aerostat wire structure with the UA or in the worst case with the propellers is avoided.

$$\tan(\beta) = \frac{D_{\mathrm{Aff}}}{L_{\mathrm{A}} - W_{\mathrm{A}} - W_{\mathrm{AH2}}} \tag{5.113}$$

and after inserting Equations 5.31, 5.32, 5.34, 5.35 and rearranging

$$\beta = \tan^{-1}\left\{\frac{\rho_0 V_\infty^2(\alpha) C_{\mathrm{dA}}}{8 g_0\left[\frac{D_{\mathrm{aer}}}{6}\left(\rho_0 - \rho_{\mathrm{H2}}\right) - M_{\mathrm{Afab}}\right]}\right\}. \tag{5.114}$$

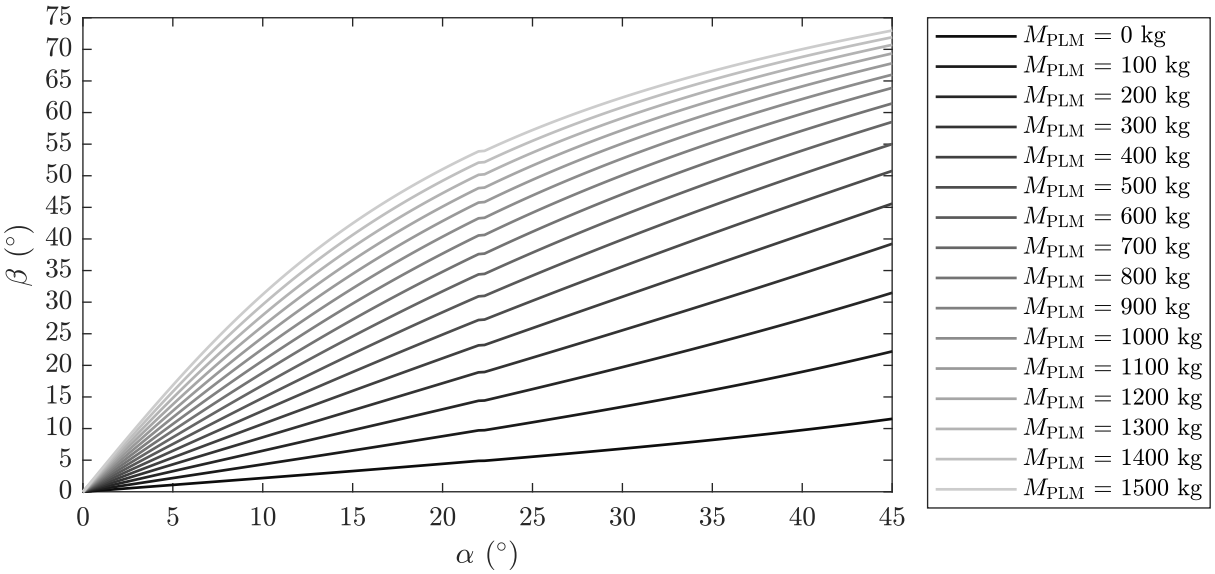

Figure 5.43: Angular deflection of aerostat axis $\beta\,(^\circ)$
as a function of angle of attack $\alpha\,(^\circ)$ and payload mass $M_{\mathrm{PLM}}\,(\mathrm{kg})$.

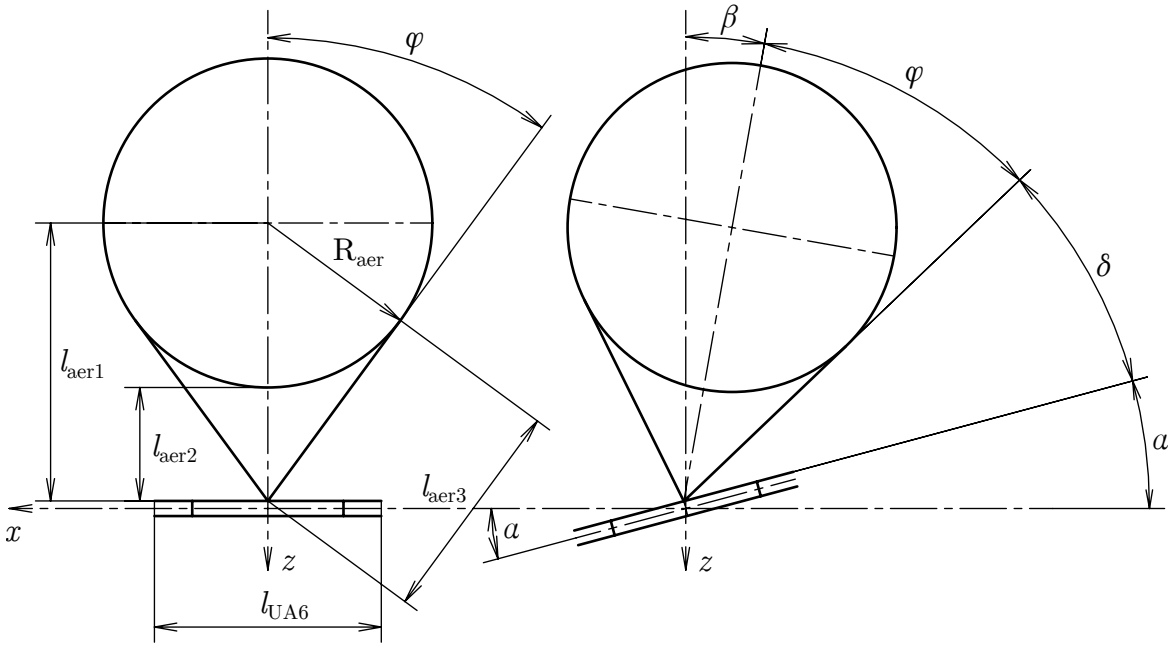

Figure 5.44: Aerostat structure geometry; angles in forward flight.

Based on the Figure 5.44

$$l_{\text{aer1}} = l_{\text{aer2}} + R_{\text{aer}}, \tag{5.115}$$

$$l_{\text{aer3}} = \sqrt{l_{\text{aer1}}^2 - R_{\text{aer}}^2} = \sqrt{\left(l_{\text{aer2}} + R_{\text{aer}}\right)^2 - R_{\text{aer}}^2}, \tag{5.116}$$

$$\tan(\varphi) = \frac{R_{\text{aer1}}}{l_{\text{aer3}}} = \frac{R_{\text{aer1}}}{\sqrt{\left(l_{\text{aer2}} + R_{\text{aer}}\right)^2 - R_{\text{aer}}^2}}, \tag{5.117}$$

$$\varphi = \tan^{-1}\left(\frac{R_{\text{aer1}}}{\sqrt{\left(l_{\text{aer2}} + R_{\text{aer}}\right)^2 - R_{\text{aer}}^2}}\right), \tag{5.118}$$

$$\delta = 90^\circ - \alpha - \beta - \varphi = 90^\circ - \alpha - \beta - \tan^{-1}\left(\frac{R_{\text{aer1}}}{\sqrt{\left(l_{\text{aer2}} + R_{\text{aer}}\right)^2 - R_{\text{aer}}^2}}\right), \tag{5.119}$$

$$\alpha + \beta \leq 90^\circ - \delta - \tan^{-1}\left(\frac{R_{\text{aer1}}}{\sqrt{\left(l_{\text{aer2}} + R_{\text{aer}}\right)^2 - R_{\text{aer}}^2}}\right), \tag{5.120}$$

where as a recommended safety measure

$$\delta = 10^\circ, \tag{5.121}$$

$$l_{\text{aer2}} \geq 1.1\frac{l_{\text{UA6}}}{2} \tag{5.122}$$

And after inserting conceptual dimensions from Table 4.1

$$\alpha + \beta \leq 43.5^\circ. \tag{5.123}$$

5.5.5.8 Estimation of Total Required Power in Forward Flight

Leishmann provides the expression [6, Page 65, Equation 2.106] for inflow ratio in forward flight $\lambda\,(1)$ considering angle of attack $\alpha\,(\mathrm{rad})$

$$\lambda = \mu\tan(\alpha) + \frac{C_T}{2\sqrt{\mu^2+\lambda^2}}. \tag{5.124}$$

Apparently, Equation 5.124 can be solved only numerically. Leishmann provides the procedure [6, Page 66, Subsection 2.4.3] for numerical simple fixed-point iteration [6, Page 66, Equation 2.112]

$$\lambda_{n+1} = \mu\tan(\alpha) + \frac{C_T}{2\sqrt{\mu^2+\lambda_n^2}} \tag{5.125}$$

where λ_0 is recommended $\lambda_0 = \lambda_\mathrm{h}$ and error estimator [6, Page 66, Equation 2.113]

$$\epsilon = \|\frac{\lambda_{n+1}-\lambda_n}{\lambda_{n+1}}\|. \tag{5.126}$$

To fulfil the condition of forward horizontal flight, Equation 5.101 was combined with the Equation 5.125

$$\lambda_{n+1} = \mu\tan(\alpha) + \frac{C_W}{2\sqrt{\mu^2+\lambda_n^2}} = \mu\tan(\alpha) + \frac{W_\mathrm{ROOM}+W_\mathrm{S}+W_\mathrm{ash}}{2\rho A\Omega^2R^2\cos(\alpha)\sqrt{\mu^2+\lambda_n^2}}. \tag{5.127}$$

Inserting Equation 5.101 into Equation 5.67, modified with induced power correction factor $\kappa\,(1)$, induced power coefficient in forward flight $C_{P\mathrm{i}}\,(1)$

$$C_{P\mathrm{i}} = \kappa C_W\lambda_\mathrm{i}. \tag{5.128}$$

Combining Equations 5.128 and 5.127

$$C_{P\mathrm{i}} = \kappa C_W\left(\mu\tan(\alpha) + \frac{C_W}{2\sqrt{\mu^2+\lambda^2}}\right) = \kappa\left(C_W\mu\tan(\alpha) + \frac{C_W^2}{2\sqrt{\mu^2+\lambda^2}}\right). \tag{5.129}$$

Leishmann provides the expression [6, Page 165, Equation 5.22] for blade profile power coefficient $C_{P0}\,(1)$

$$C_{P0} = \frac{\sigma C_{d0}}{8}\left(1+K\mu^2\right) \tag{5.130}$$

where $C_{d0}\,(1)$ is profile (viscous) drag coefficient of the rotor blade airfoil and Leishmann states: "the numerical value of K varies from 4 in hover to 5 at $\mu = 0.5$, depending on the assumptions and/or approximations that are made. In practice, usually average value of $K = 4.6$, while Stepniewski (1973) suggests $K = 4.7$. Either value will be acceptable for basic performance studies" [6, Page 165, Subsection 5.3.2].

Leishmann brings the equation [6, Page 66, Equation 5.25] for parasitic power coefficient $C_{P\mathrm{p}}\,(1)$

$$C_{P\mathrm{p}} = \frac{1}{2}\left(\frac{S_{ref}}{A}\right)\mu^3 C_{Df} = \frac{1}{2}\left(\frac{f}{A}\right)\mu^3 \tag{5.131}$$

where $S_{ref}\,(\mathrm{m}^2)$ is some reference area, $C_{Df}\,(1)$ is drag coefficient of the fuselage based on this reference area, $f\,(\mathrm{m}^2)$ is known as equivalent wetted area of equivalent flat-plate and $A\,(\mathrm{m}^2)$ is rotor disk area.

Considering the ratio $\frac{f}{A}\,(1)$, Leishmann provides the table "Typical Breakdown of Parasitic Drag Components on a Helicopter" [6, Page 217, Table 6.1] which results in $C_{P\mathrm{p}} = 0.007$. "The results show that values of f/A typically fall between 0.004 for clean helicopter designs and up to 0.025 for first-generation of heavy lift transport helicopters." [6, Page 217, Subsection 6.4.1]. To keep the calculation safe while considering not-drag-optimized UA design, $\frac{f}{A}\,(1)$ was set $\frac{f}{A} = 0.025$.

The expression for climb velocity coefficient $\lambda_{\mathrm{c}}\,(1)$

$$\lambda_{\mathrm{c}} = \frac{V_{\mathrm{c}}}{V_{\mathrm{tip}}} \tag{5.132}$$

where $V_{\mathrm{c}}\left(\frac{\mathrm{m}}{\mathrm{s}}\right)$ is climb velocity.

Leishmann brings the expression [6, Page 166, Subsection 5.3.4] for climb power coefficient $C_{P\mathrm{c}}\,(1)$

$$C_{P\mathrm{c}} = \lambda_{\mathrm{c}} C_W. \tag{5.133}$$

Total power coefficient in forward flight $C_P\,(1)$ reads

$$C_P = C_{P\mathrm{i}} + C_{P0} + C_{P\mathrm{p}} + C_{P\mathrm{c}}. \tag{5.134}$$

Leishmann breaks it down in the expression [6, Page 167, Equation 5.29]

$$C_P = C_Q = \frac{\kappa C_W^2}{2\sqrt{\lambda^2+\mu^2}} + \frac{\sigma C_{d0}}{8}\left(1+K\mu^2\right) + \frac{1}{2}\left(\frac{f}{A}\right)\mu^3 + \lambda_{\mathrm{c}} C_W. \tag{5.135}$$

Combining Equations 5.129, 5.130, 5.131 and 5.133

$$C_P = \kappa\left(C_W\mu\tan(\alpha) + \frac{C_W^2}{2\sqrt{\mu^2+\lambda^2}}\right) + \frac{\sigma C_{d0}}{8}\left(1+K\mu^2\right) + \frac{1}{2}\left(\frac{f}{A}\right)\mu^3 + \lambda_{\mathrm{c}} C_W. \tag{5.136}$$

Considering horizontal flight, where $V_{\mathrm{c}} = 0\frac{\mathrm{m}}{\mathrm{s}}$

$$C_P = \kappa\left(C_W\mu\tan(\alpha) + \frac{C_W^2}{2\sqrt{\mu^2+\lambda^2}}\right) + \frac{\sigma C_{d0}}{8}\left(1+K\mu^2\right) + \frac{1}{2}\left(\frac{f}{A}\right)\mu^3 \tag{5.137}$$

and after plugging Equation 5.137 into Equation 5.7 and rearranging, the estimated total required power in forward flight $P_{\mathrm{Rff}}\,(\mathrm{W})$

$$P_{\mathrm{Rff}} = \left[\kappa\left(C_W\mu\tan(\alpha) + \frac{C_W^2}{2\sqrt{\mu^2+\lambda^2}}\right) + \frac{\sigma C_{d0}}{8}\left(1+K\mu^2\right) + \frac{1}{2}\left(\frac{f}{A}\right)\mu^3\right]\rho A\Omega^3 R^3. \tag{5.138}$$

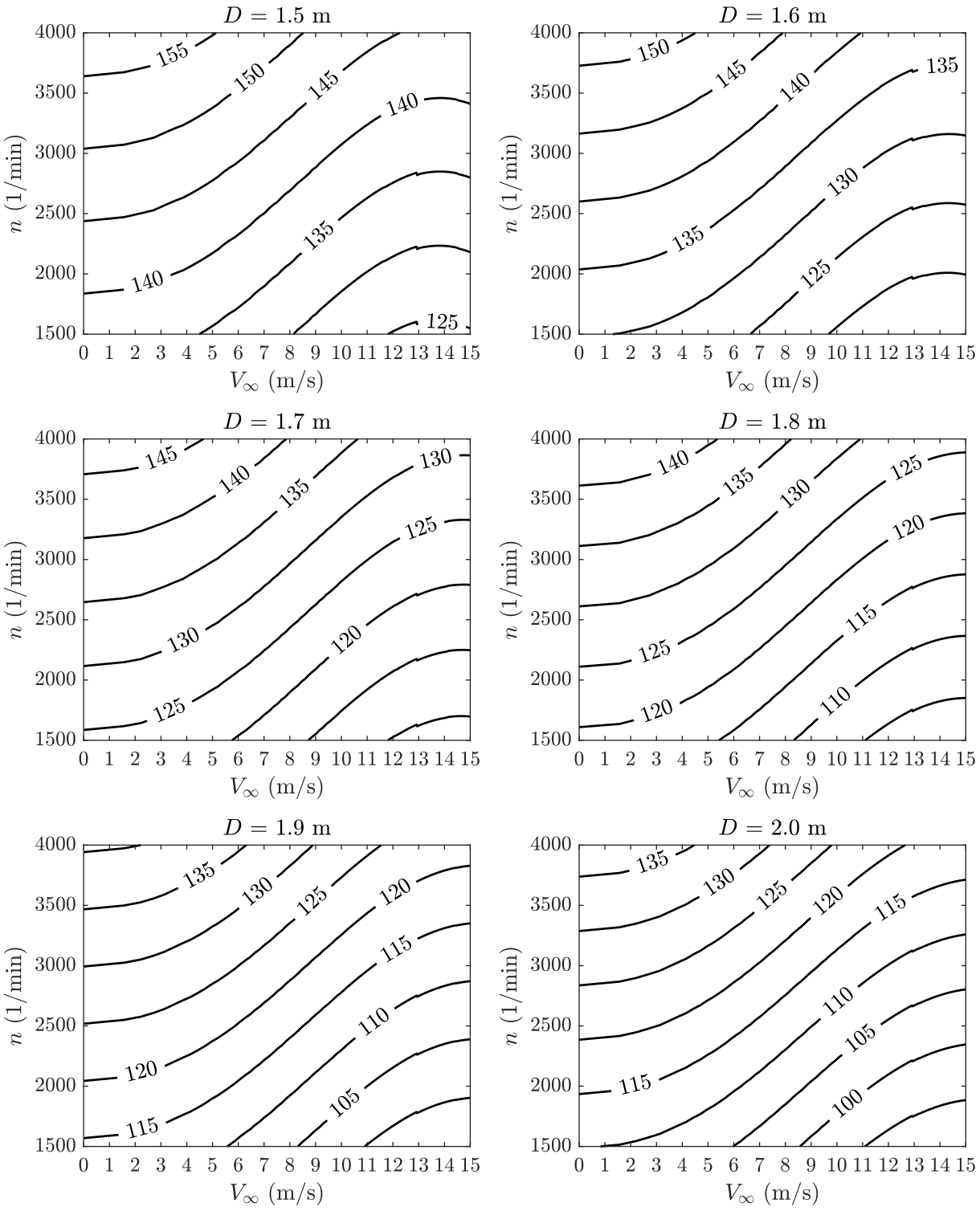

Figure 5.45: Required power in forward horizontal flight P_{Rff} (kW) as a function of forward flight velocity V_∞ $\left(\frac{\mathrm{m}}{\mathrm{s}}\right)$ and revolutions per minute n $\left(\frac{1}{\mathrm{min}}\right)$ for various propeller diameter D (m); payload mass $M_{\mathrm{PLM}} = 500$kg.

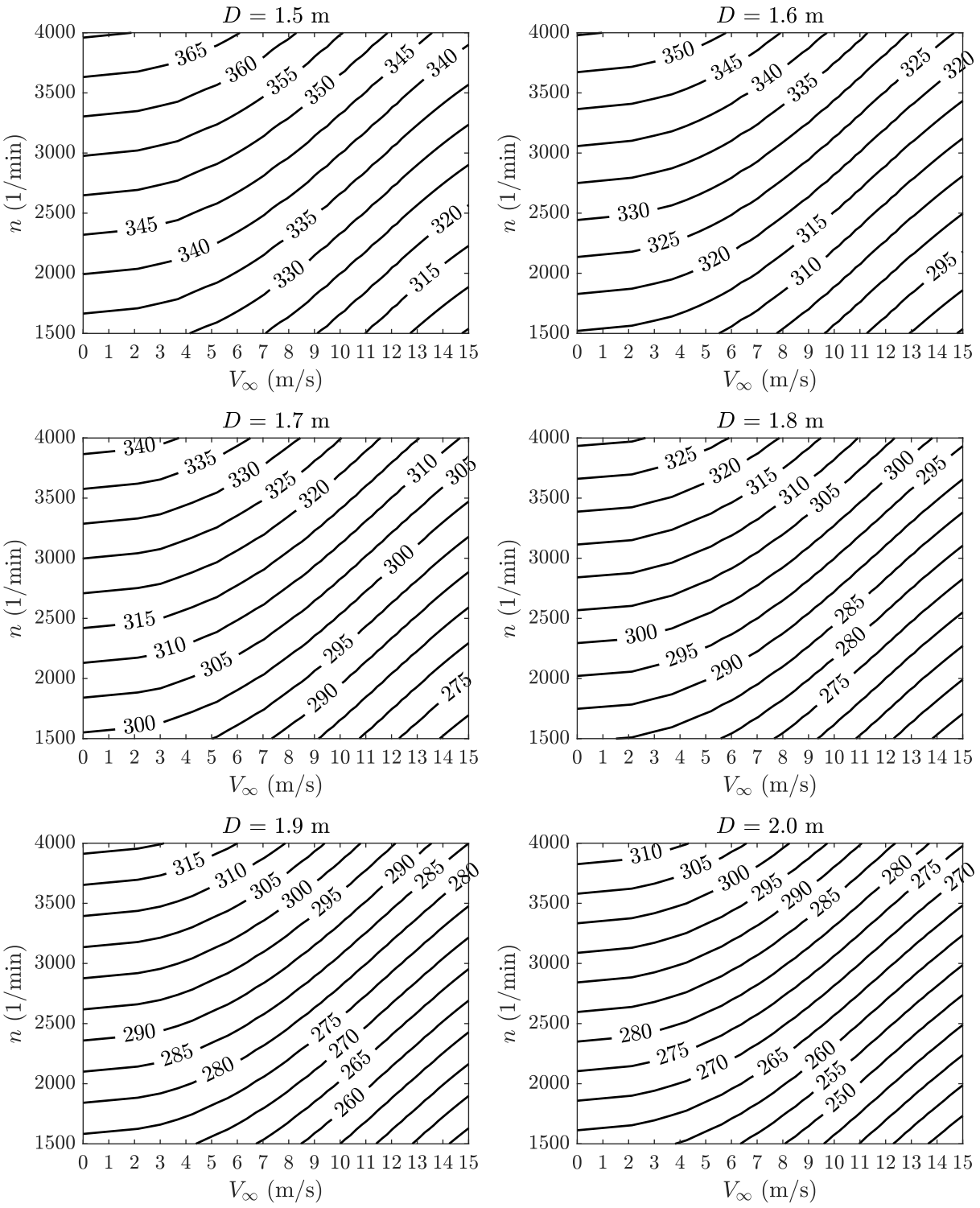

Figure 5.46: Required power in forward horizontal flight $P_{\mathrm{Rff}}\,(\mathrm{kW})$ as a function of forward flight velocity $V_\infty\left(\frac{\mathrm{m}}{\mathrm{s}}\right)$ and revolutions per minute $n\left(\frac{1}{\mathrm{min}}\right)$ for various propeller diameter $D\,(\mathrm{m})$; payload mass $M_{\mathrm{PLM}} = 1000\mathrm{kg}$.

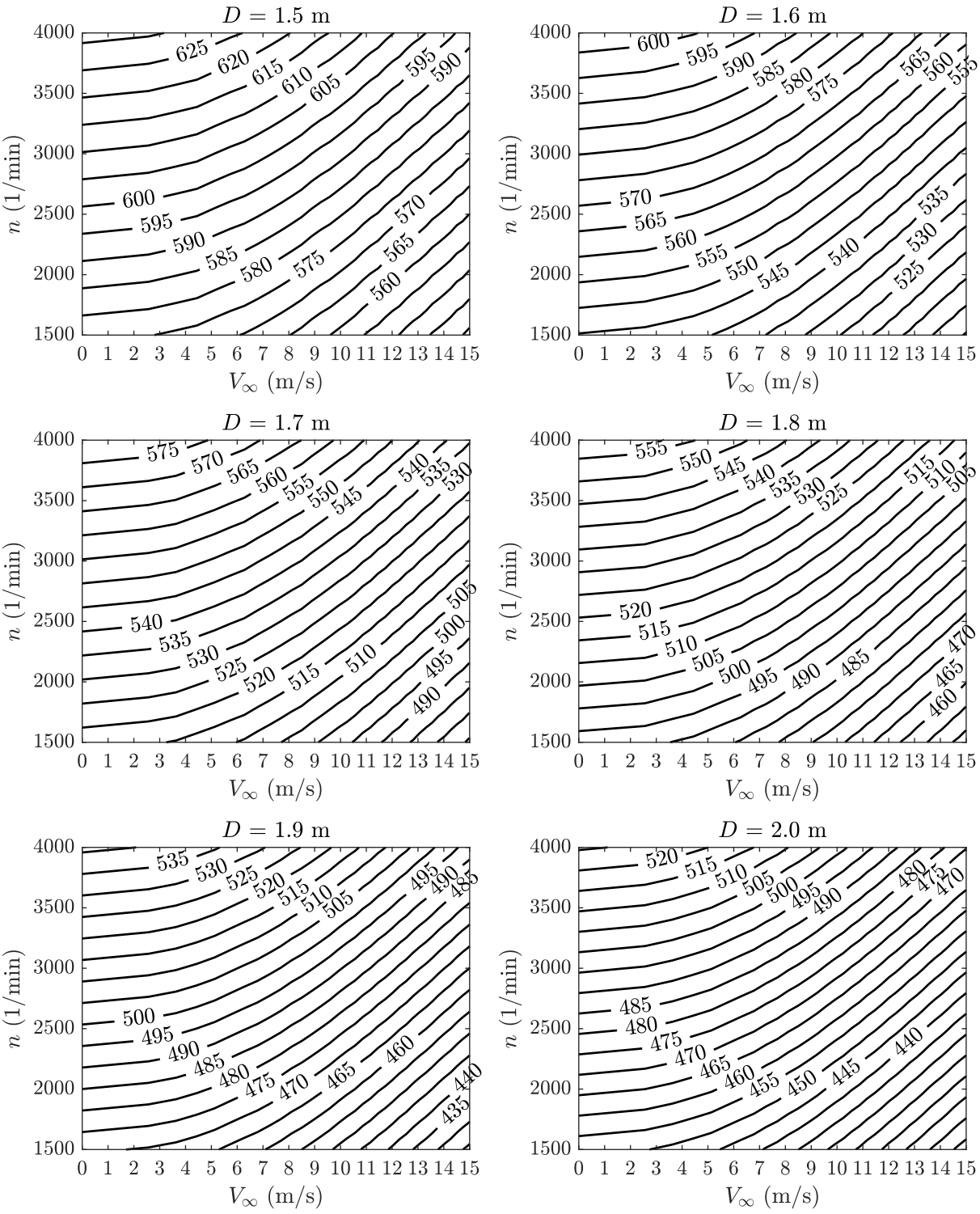

Figure 5.47: Required power in forward horizontal flight P_{Rff} (kW) as a function of forward flight velocity V_∞ $\left(\frac{\mathrm{m}}{\mathrm{s}}\right)$ and revolutions per minute n $\left(\frac{1}{\mathrm{min}}\right)$ for various propeller diameter D (m); payload mass $M_{\mathrm{PLM}} = 1500$kg.

5.5.6 Battery

5.5.6.1 Flight Planning

To be able to estimate the available energy that is to be stored in battery packs, it is necessary to set some simplification in the process of designing a universal flight plan. Figure 5.48 visualizes the extreme cases.

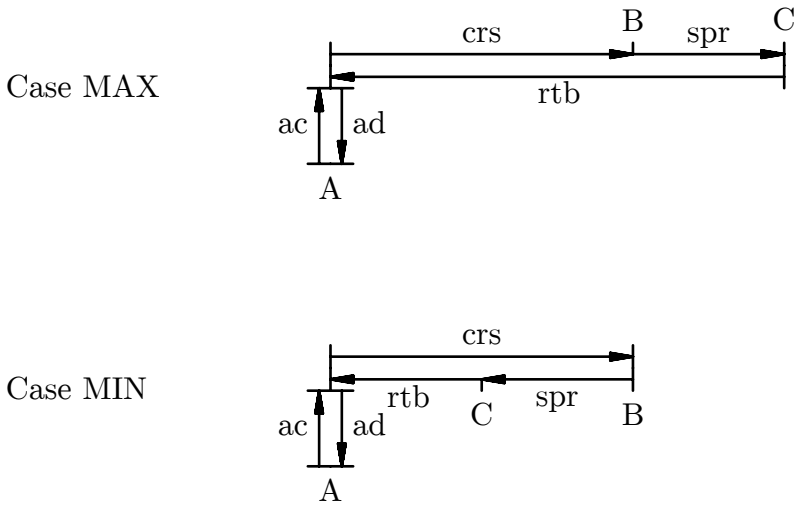

Figure 5.48: Schematic visualization of the shortest and longest possible flight plans.
A - platform
B - start spreading
C - stop spreading
ac - axial climb
crs - cruise
spr - spreading
rtb - return to base
ad - axial descend

Table 5.17: UAS parameters behaviour while performing different flight phases.

Phase	Mass	Velocity	Required Power
Axial Climb	M_{TOM}	V_{ac}	P_{Rac}
Cruise	M_{TOM}	V_{crs}	P_{Rcrs}
Spreading	$M_{\mathrm{TOM}} \longrightarrow (M_{\mathrm{OEM}} + M_{\mathrm{S}})$	$V_{\mathrm{crs}} \longrightarrow V_{\mathrm{rtb}}$	P_{Rcrs}
Return to Base	$(M_{\mathrm{OEM}} + M_{\mathrm{S}})$	V_{rtb}	P_{Rrtb}
Axial Descent	$(M_{\mathrm{OEM}} + M_{\mathrm{S}})$	V_{ad}	P_{Rh}

Total time of any mission $t_{\mathrm{tot}}\,(\mathrm{s})$

$$t_{\mathrm{tot}} = t_{\mathrm{ac}} + t_{\mathrm{crs}} + t_{\mathrm{spr}} + t_{\mathrm{rtb}} + t_{\mathrm{ad}} \tag{5.139}$$

where time of axial climb $t_{\mathrm{ac}}\,(\mathrm{s})$ and time of axial descend $t_{\mathrm{ad}}\,(\mathrm{s})$

$$t_{\mathrm{ac}} = \frac{d_{\mathrm{ac}}}{V_{\mathrm{ac}}} \tag{5.140}$$

$$t_{\mathrm{ad}} = \frac{d_{\mathrm{ad}}}{V_{\mathrm{ad}}} \tag{5.141}$$

to reach a given required flight level $d_{\mathrm{ac}} = d_{\mathrm{ad}}\,(\mathrm{m})$ at desired axial climbing velocity $V_{\mathrm{ac}}\left(\frac{\mathrm{m}}{\mathrm{s}}\right)$ and descending velocity $V_{\mathrm{ad}}\left(\frac{\mathrm{m}}{\mathrm{s}}\right)$.

Time of cruise $t_{\mathrm{crs}}\,(\mathrm{s})$

$$t_{\mathrm{crs}} = \frac{d_{\mathrm{crs}}}{V_{\mathrm{crs}}} \tag{5.142}$$

to reach a given required cruise distance $d_{\mathrm{crs}}\,(\mathrm{m})$ at desired cruise velocity $V_{\mathrm{crs}}\left(\frac{\mathrm{m}}{\mathrm{s}}\right)$.

Mass flow capability $\dot{M}_{\mathrm{S}}\left(\frac{\mathrm{kg}}{\mathrm{s}}\right)$ of the spreader should be provided to calculate the spreading time $t_{\mathrm{spr}}\,(s)$

$$t_{\mathrm{spr}} = \frac{M_{\mathrm{ash}}}{\dot{M}_{\mathrm{S}}}. \tag{5.143}$$

Spreading distance $d_{\mathrm{spr}}\,(\mathrm{m})$ of an accelerated or decelerated straight-line motion

$$d_{\mathrm{spr}} = V_{\mathrm{crs}} t_{\mathrm{spr}} + \frac{1}{2} a_{\mathrm{spr}} t_{\mathrm{spr}}^2 \tag{5.144}$$

where velocity change $a_{\mathrm{spr}}\left(\frac{\mathrm{m}}{\mathrm{s}^2}\right)$ during spreading

$$a_{\mathrm{spr}} = \frac{V_{\mathrm{rtb}} - V_{\mathrm{crs}}}{t_{\mathrm{spr}}}. \tag{5.145}$$

Time of return to base $t_{\mathrm{rtb}}\,(s)$ for both cases MAX and MIN

$$t_{\mathrm{rtb}} = \frac{d_{\mathrm{rtb}}}{V_{\mathrm{rtb}}} \tag{5.146}$$

at desired return to base velocity $V_{\mathrm{rtb}}\left(\frac{\mathrm{m}}{\mathrm{s}}\right)$ where return to base distance $d_{\mathrm{rtb}}\,(\mathrm{m})$ in Case MAX from Figure 5.48

$$d_{\mathrm{rtb}} = d_{\mathrm{crs}} + d_{\mathrm{spr}} \tag{5.147}$$

and return to base distance $d_{\mathrm{rtb}}\,(\mathrm{m})$ in Case MIN from Figure 5.48

$$d_{\mathrm{rtb}} = d_{\mathrm{crs}} - d_{\mathrm{spr}}. \tag{5.148}$$

5.5.6.2 Battery Parameters

Electric efficiency $\eta_{\mathrm{el}}\,(1)$ reads

$$\eta_{\mathrm{el}} = \frac{P_{\mathrm{O}}}{P_{\mathrm{I}}}, \tag{5.149}$$

where $P_{\mathrm{I}}\,(\mathrm{W})$ denotes input power and $P_{\mathrm{O}}\,(\mathrm{W})$ stands for output power. Capacity $C\,(\mathrm{Wh})$ is then

$$C = P_{\mathrm{I}} t \tag{5.150}$$

where $t\,(\mathrm{s})$ is time and after plugging in Equation 5.149 and rearranging

$$C_{\mathrm{bat}} = \frac{P_{\mathrm{O}}}{\eta_{\mathrm{el}}} t = \frac{\sum_{i=1}^{N} P_i t_i}{\eta_{\mathrm{el}}} \tag{5.151}$$

where $P_i\,(\mathrm{W})$ is required power and $t_i\,(\mathrm{s})$ is required time to carry out the mission phase by the desired flight profile, where $N = 5$ and

$$i \in \{\mathrm{ac}, \mathrm{crs}, \mathrm{spr}, \mathrm{rtb}, \mathrm{ad}\}\,. \tag{5.152}$$

After dividing Equation 5.151 by the battery cell voltage $U_{\mathrm{cel}}\,(\mathrm{V})$, total required battery capacity $C_{\mathrm{bat}}\,(\mathrm{Ah})$

$$C_{\mathrm{bat}} = \frac{1}{U_{\mathrm{cel}}} \frac{\sum_{i=1}^{N} P_i t_i}{\eta_{\mathrm{el}}} \tag{5.153}$$

and after plugging-in Equations 5.140 - 5.147

$$C_{\mathrm{bat}} = \frac{1}{U_{\mathrm{cel}}} \frac{P_{\mathrm{Rac}} \frac{d_{\mathrm{ac}}}{V_{\mathrm{ac}}} + P_{\mathrm{Rcrs}} \frac{d_{\mathrm{crs}}}{V_{\mathrm{crs}}} + P_{\mathrm{Rspr}} \frac{M_{\mathrm{ash}}}{\dot{M}_{\mathrm{S}}} + P_{\mathrm{Rrtb}} \frac{d_{\mathrm{crs}} + d_{\mathrm{spr}}}{V_{\mathrm{rtb}}} + P_{\mathrm{Rh}} \frac{d_{\mathrm{ad}}}{V_{\mathrm{ad}}}}{\eta_{\mathrm{el}}} \tag{5.154}$$

which, after dividing by the single battery cell capacity $C_{\mathrm{cel}}\,(\mathrm{Ah})$, provides required number of battery cells $n_{\mathrm{cel}}\,(1)$

$$n_{\mathrm{cel}} = \frac{1}{C_{\mathrm{cel}}} \frac{1}{U_{\mathrm{cel}}} \frac{\sum_{i=1}^{N} P_i t_i}{\eta_{\mathrm{el}}} \tag{5.155}$$

and so

$$n_{\mathrm{cel}} = \frac{1}{C_{\mathrm{cel}}} \frac{1}{U_{\mathrm{cel}}} \frac{P_{\mathrm{Rac}} \frac{d_{\mathrm{ac}}}{V_{\mathrm{ac}}} + P_{\mathrm{Rcrs}} \frac{d_{\mathrm{crs}}}{V_{\mathrm{crs}}} + P_{\mathrm{Rspr}} \frac{M_{\mathrm{ash}}}{\dot{M}_{\mathrm{S}}} + P_{\mathrm{Rrtb}} \frac{d_{\mathrm{crs}} + d_{\mathrm{spr}}}{V_{\mathrm{rtb}}} + P_{\mathrm{Rad}} \frac{d_{\mathrm{ad}}}{V_{\mathrm{ad}}}}{\eta_{\mathrm{el}}}. \tag{5.156}$$

5.5.7 Performance Case: $M_{\mathrm{PLM}} = 600\mathrm{kg}$

5.5.7.1 Initial Parameters of the Performance Calculation; $M_{\mathrm{PLM}} = 600\mathrm{kg}$

Table 5.18: Initial parameters for performance calculation; $M_{\mathrm{PLM}} = 600\mathrm{kg}$.

Symbol	Description	Unit	Value
M_{ROOM}	Required operational overweight mass	kg	100
M_{PLM}	Payload mass	kg	600
$\bar{D}_{\mathrm{aer}}$	Mean aerostat diameter	m	8.7
D	Propeller diameter	m	$[1.5, 2]$
n	Revolutions of engine per minute	$\frac{1}{\mathrm{min}}$	$[1500, 4000]$
α	Angle of attack	$^\circ$	$[0, 45]$
δ	Angular margin in forward flight	$^\circ$	10
$\bar{C_L}$	Mean lift coefficient	1	0.5
κ	Induced power correction factor	1	1.15
K	Empiric constant in blade profile power coefficient	1	4.6
$\frac{f}{A}$	Geometry ratio	1	0.025
V_{c}	Climb velocity	$\frac{\mathrm{m}}{\mathrm{s}}$	$[-8, 8]$
V_{ac}	Climb velocity limit	$\frac{\mathrm{m}}{\mathrm{s}}$	2
V_{ad}	Descent velocity limit	$\frac{\mathrm{m}}{\mathrm{s}}$	2
$d_{\mathrm{ac}} = d_{\mathrm{ad}}$	Flight level limit	m	100
d_{crs}	Cruise distance	m	$\{200, 400, 600\}$
$\dot{M}_{\mathrm{S}}$	Spreader mass flow	$\frac{\mathrm{kg}}{\mathrm{s}}$	10
η_{el}	Electric efficiency	1	0.9
M_{cel0}	Single battery cell mass	kg	0.047
M_{cel1}	Single battery cell mass including mountings	kg	0.055
U_{cel}	Single battery cell voltage	V	4.15
C_{cel}	Single battery cell capacity	Ah	3

Payload mass $M_{\mathrm{PLM}}\,(\mathrm{kg})$ is supposed to cover actual ash mass $M_{\mathrm{ash}} = 500\mathrm{kg}$ and the leftover 100 kg should be enough for empty spreader mass $M_{\mathrm{S}}\,(\mathrm{kg})$ and all its equipment.

Range of angle of attack $\alpha\,(^\circ)$ was limited to realistic flight conditions.

Climb velocity limit $V_{\mathrm{ac}}\left(\frac{\mathrm{m}}{\mathrm{s}}\right)$ was chosen so it brings maximum power requirement in combination with climb time to the limit flight level to provide enough margin.

Descent velocity limit $V_{\mathrm{ad}}\left(\frac{\mathrm{m}}{\mathrm{s}}\right)$ was chosen to keep safety.

Flight level limit $d_{\mathrm{ac}} = d_{\mathrm{ad}}\,(\mathrm{m})$ was estimated to provide enough height margin.

Cruise distances $d_{\mathrm{crs}}\,(\mathrm{m})$ were chosen to investigate more possible alternatives.

Spreader mass flow $\dot{M}_{\mathrm{S}}\left(\frac{\mathrm{kg}}{\mathrm{s}}\right)$ was provided by the design team of the spreader.

Electric efficiency $\eta_{\mathrm{el}}\,(1)$ was estimated to provide a certain level of accuracy.

Single battery cell parameters $M_{\mathrm{cel0}}\,(\mathrm{kg})$, $M_{\mathrm{cel1}}\,(\mathrm{kg})$, $U_{\mathrm{cel}}\,(\mathrm{V})$ and $C_{\mathrm{cel}}\,(\mathrm{Ah})$ were provided by MGM COMPRO.

5.5.7.2 Performance in Hover; $M_{\mathrm{PLM}} = 600\mathrm{kg}$

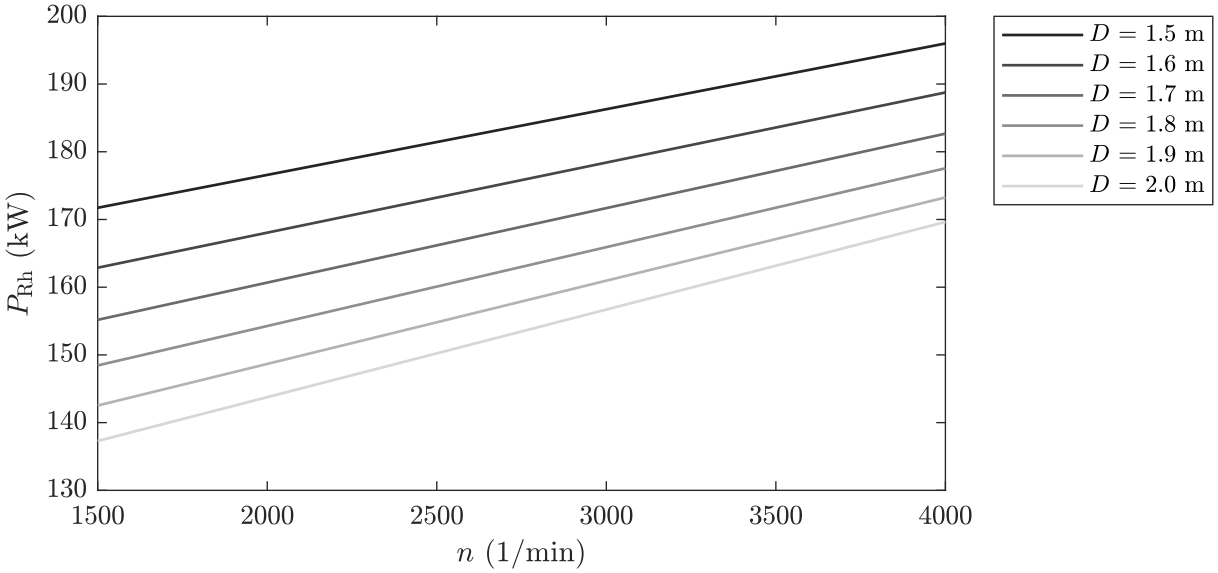

Figure 5.49: Required power in hover $P_{\mathrm{Rh}}\,(\mathrm{kW})$
as a function of revolutions per minute $n\left(\frac{1}{\mathrm{min}}\right)$
and propeller diameter $D\,(\mathrm{m})$ for payload mass $M_{\mathrm{PLM}} = 600\mathrm{kg}$.

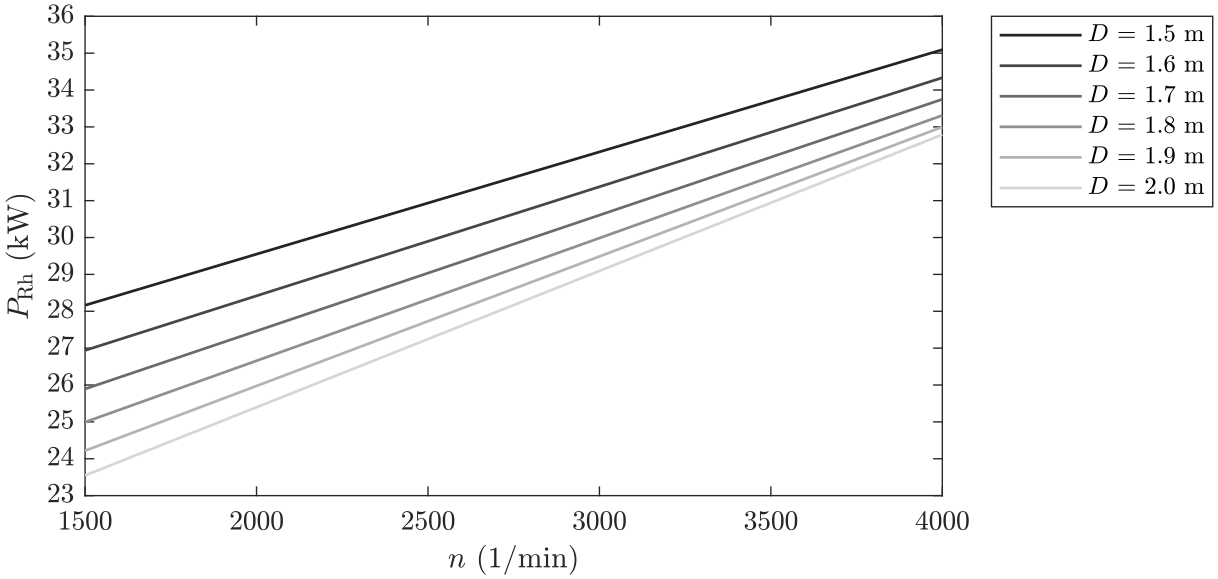

Figure 5.50: Required power in hover $P_{\mathrm{Rh}}\,(\mathrm{kW})$
as a function of revolutions per minute $n\left(\frac{1}{\mathrm{min}}\right)$
and propeller diameter $D\,(\mathrm{m})$ for payload mass $M_{\mathrm{PLM}} = 100\mathrm{kg}$.

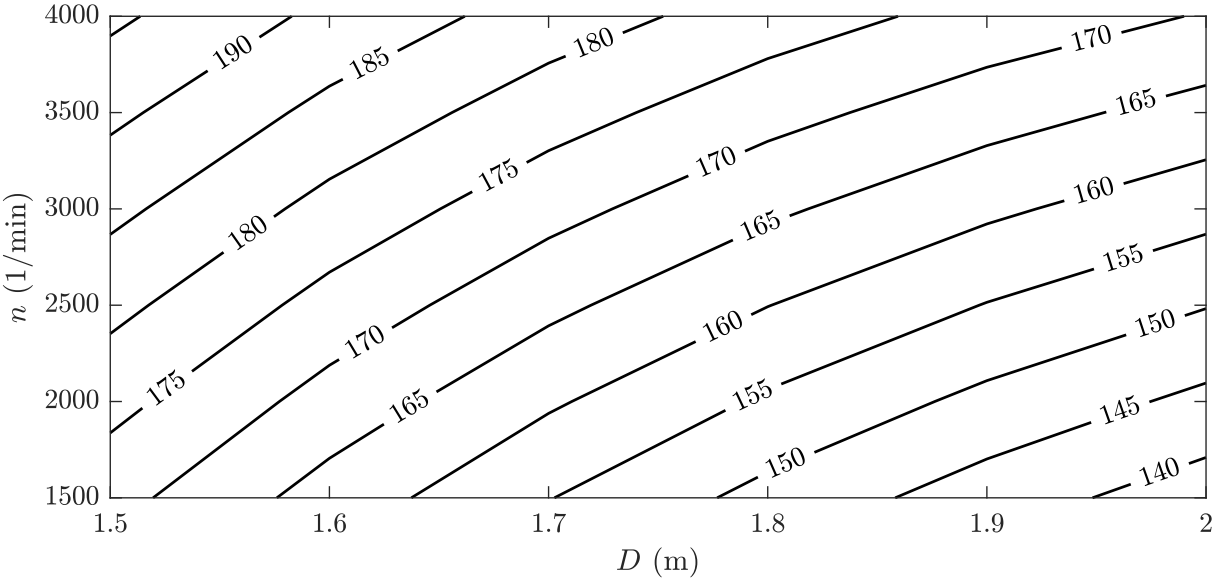

Figure 5.51: Required power in hover $P_{\mathrm{Rh}}\,(\mathrm{kW})$
as a function of propeller diameter $D\,(\mathrm{m})$
and revolutions per minute $n\left(\frac{1}{\mathrm{min}}\right)$ for payload mass $M_{\mathrm{PLM}} = 600\mathrm{kg}$.

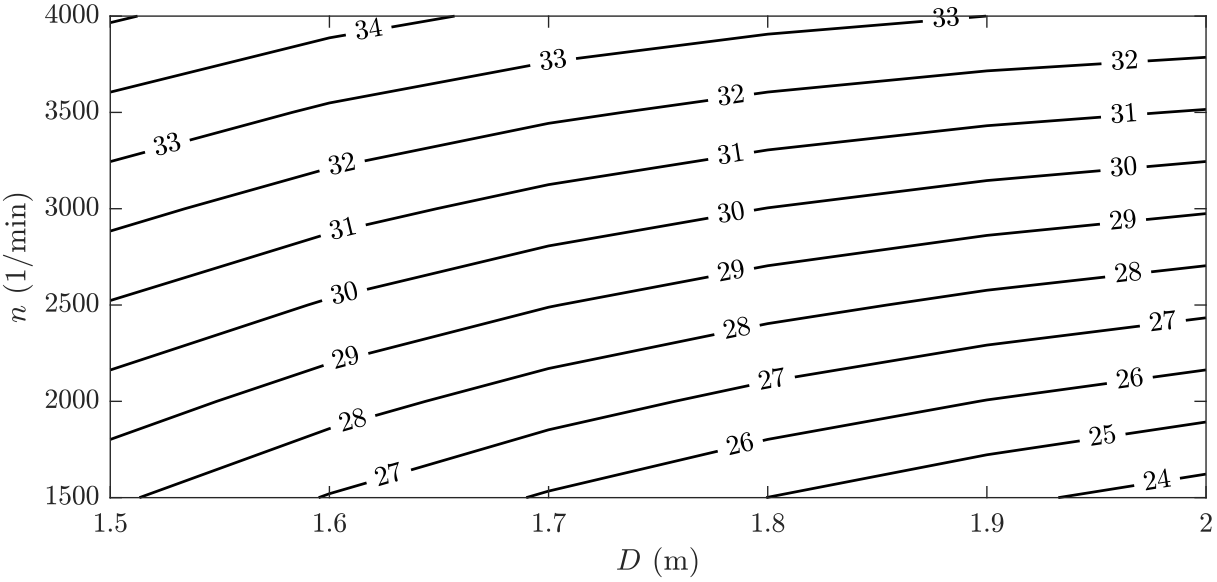

Figure 5.52: Required power in hover $P_{\mathrm{Rh}}\,(\mathrm{kW})$
as a function of propeller diameter $D\,(\mathrm{m})$
and revolutions per minute $n\left(\frac{1}{\mathrm{min}}\right)$ for payload mass $M_{\mathrm{PLM}} = 100\mathrm{kg}$.

5.5.7.3 Performance in Axial Climb and Descent; $M_{\mathrm{PLM}} = 600\mathrm{kg}$

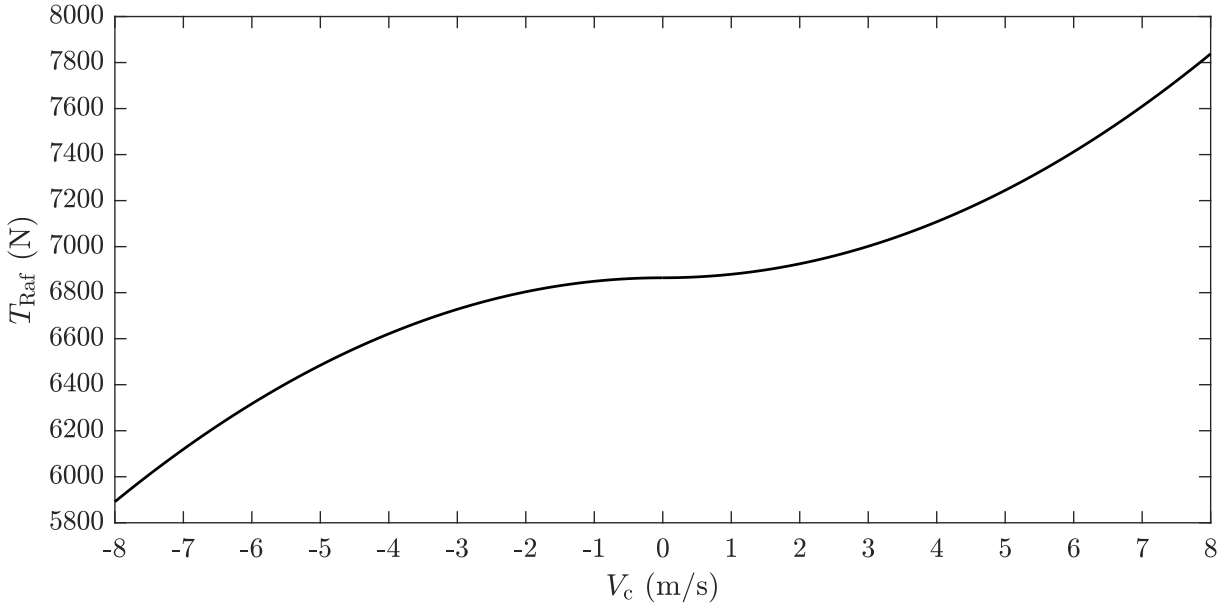

Figure 5.53: Required thrust in axial flight $T_{\mathrm{Raf}}\,(\mathrm{N})$
as a function of climb velocity $V_{\mathrm{c}}\left(\frac{\mathrm{m}}{\mathrm{s}}\right)$
for payload mass $M_{\mathrm{PLM}} = 600\mathrm{kg}$.

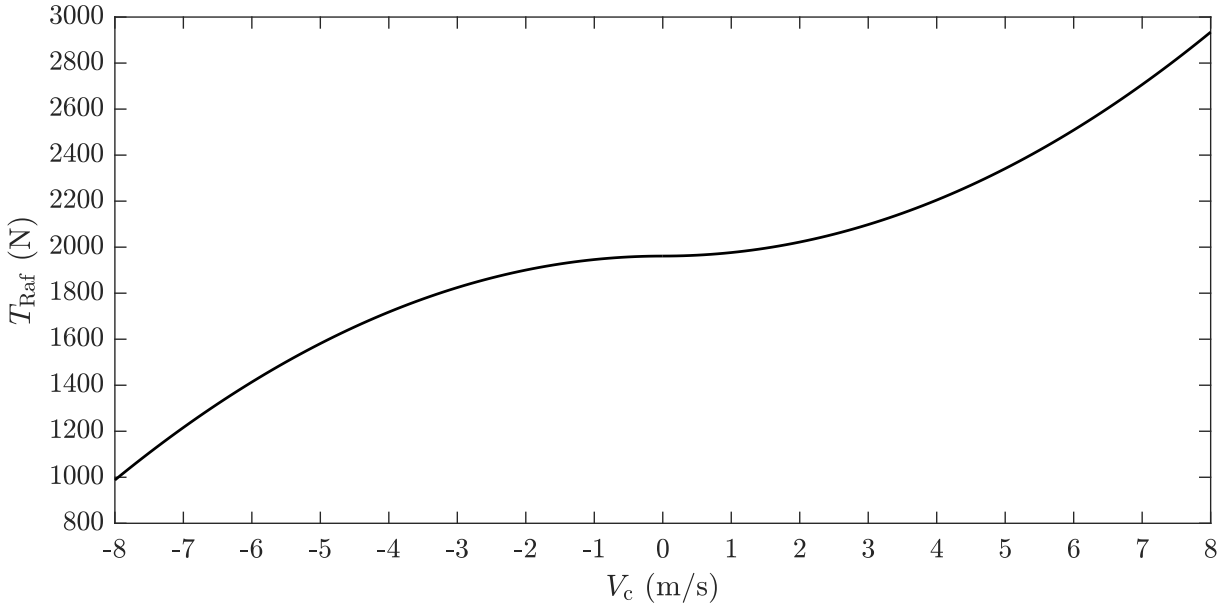

Figure 5.54: Required thrust in axial flight $T_{\mathrm{Raf}}\,(\mathrm{N})$
as a function of climb velocity $V_{\mathrm{c}}\left(\frac{\mathrm{m}}{\mathrm{s}}\right)$
for payload mass $M_{\mathrm{PLM}} = 100\mathrm{kg}$.

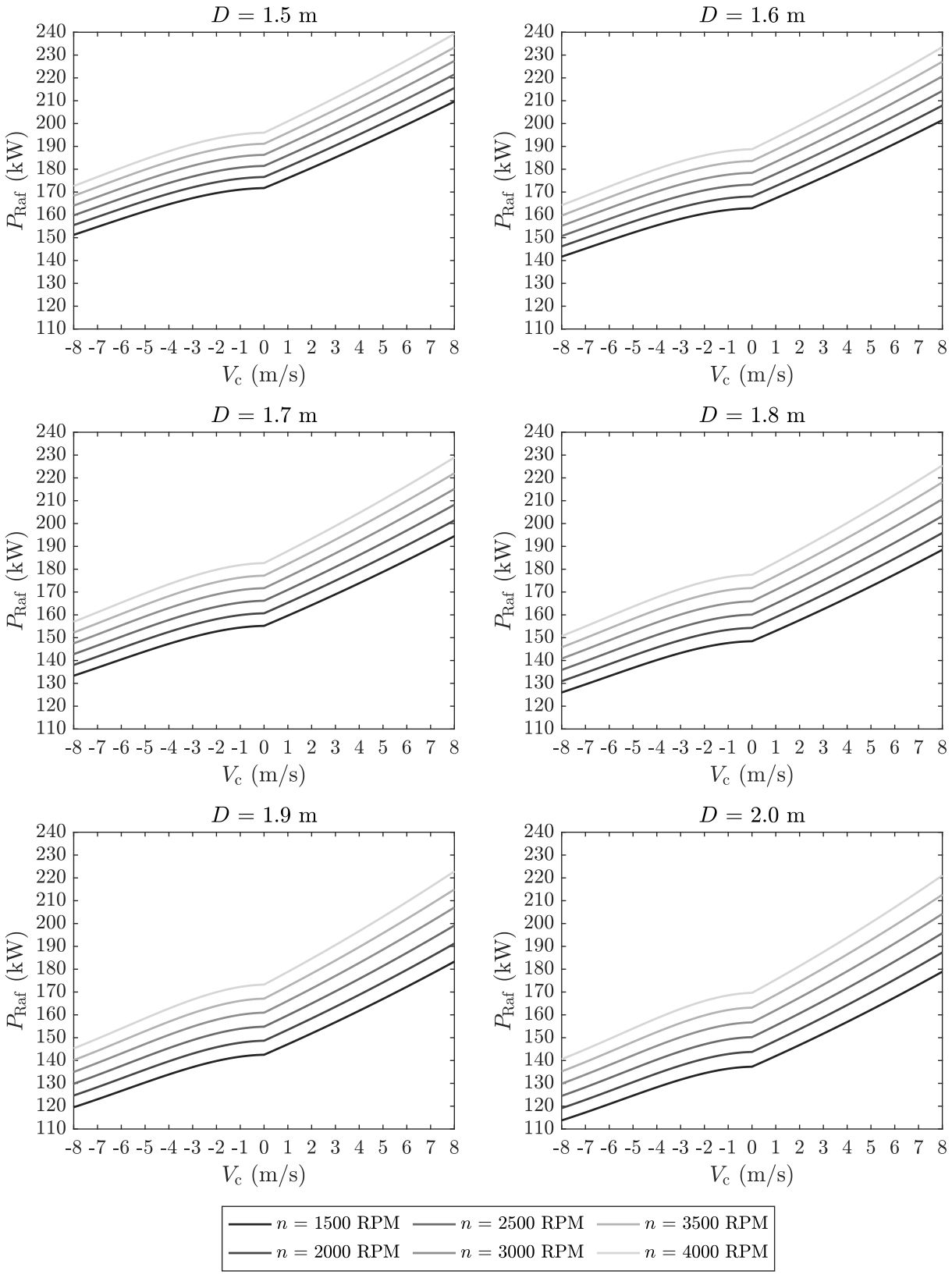

Figure 5.55: Required power in axial flight $P_{\mathrm{Raf}}\,(\mathrm{kW})$
as a function of climb velocity $V_{\mathrm{c}}\left(\frac{\mathrm{m}}{\mathrm{s}}\right)$
and revolutions per minute $n\left(\frac{1}{\mathrm{min}}\right)$ for various propeller diameter $D\,(\mathrm{m})$
and payload mass $M_{\mathrm{PLM}} = 600\mathrm{kg}$.

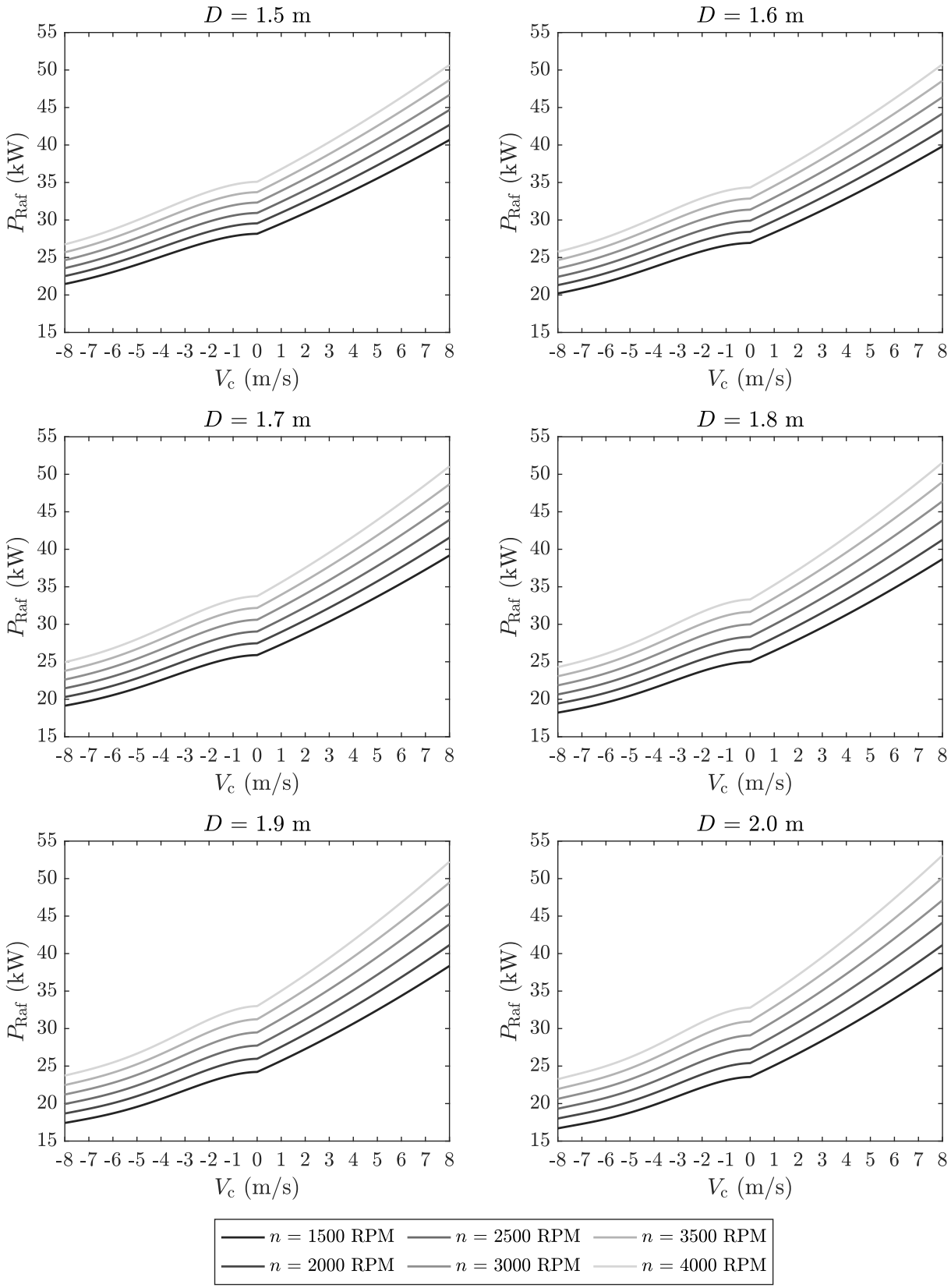

Figure 5.56: Required power in axial flight $P_{\mathrm{Raf}}\,(\mathrm{kW})$
as a function of climb velocity $V_{\mathrm{c}}\left(\frac{\mathrm{m}}{\mathrm{s}}\right)$
and revolutions per minute $n\left(\frac{1}{\mathrm{min}}\right)$ for various propeller diameter $D\,(\mathrm{m})$
and payload mass $M_{\mathrm{PLM}} = 100\mathrm{kg}$.

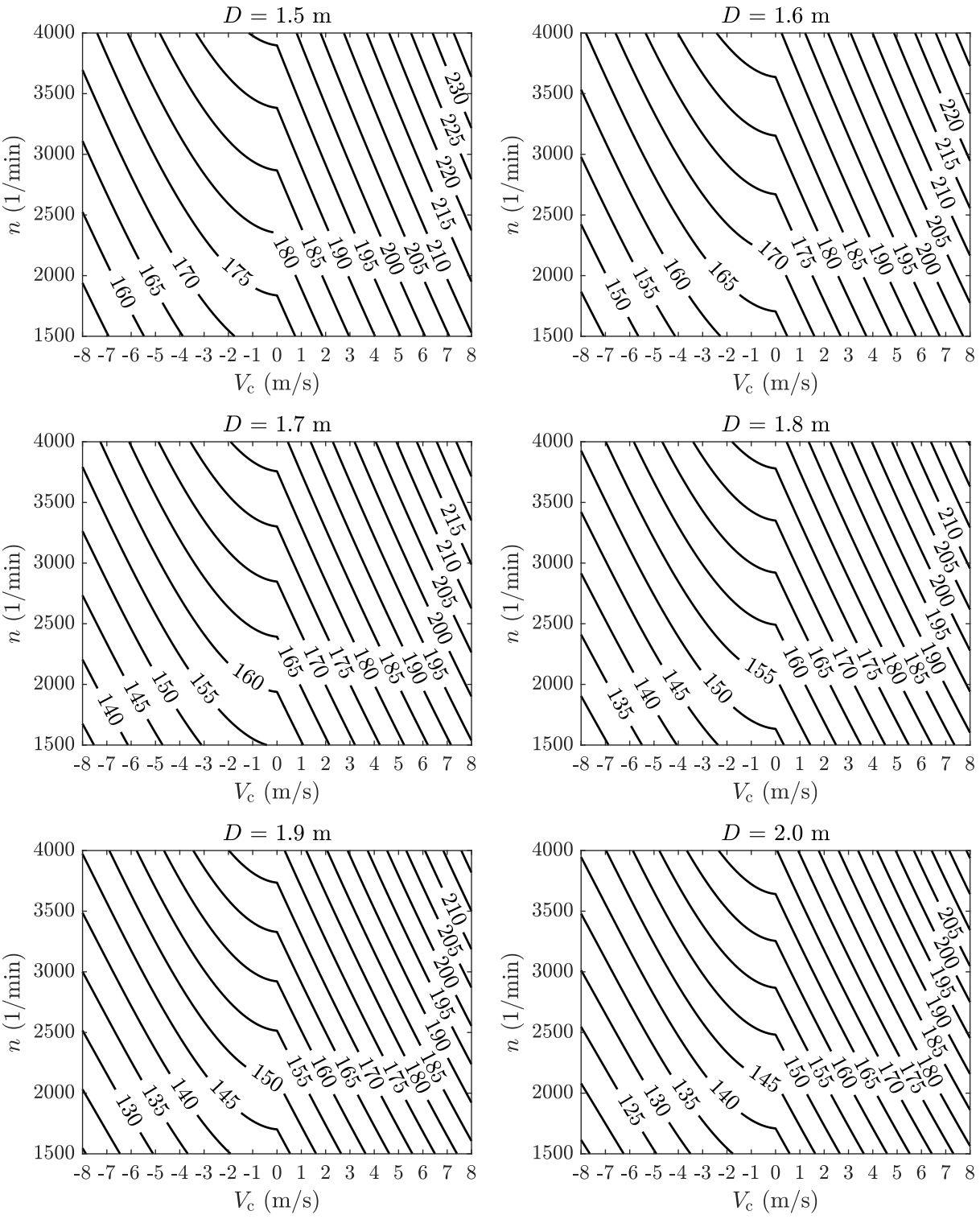

Figure 5.57: Required power in axial flight P_{Raf} (kW)
as a function of climb velocity V_c $\left(\frac{\mathrm{m}}{\mathrm{s}}\right)$
and revolutions per minute n $\left(\frac{1}{\mathrm{min}}\right)$ for various propeller diameter D (m)
and payload mass $M_{\mathrm{PLM}} = 600\mathrm{kg}$.

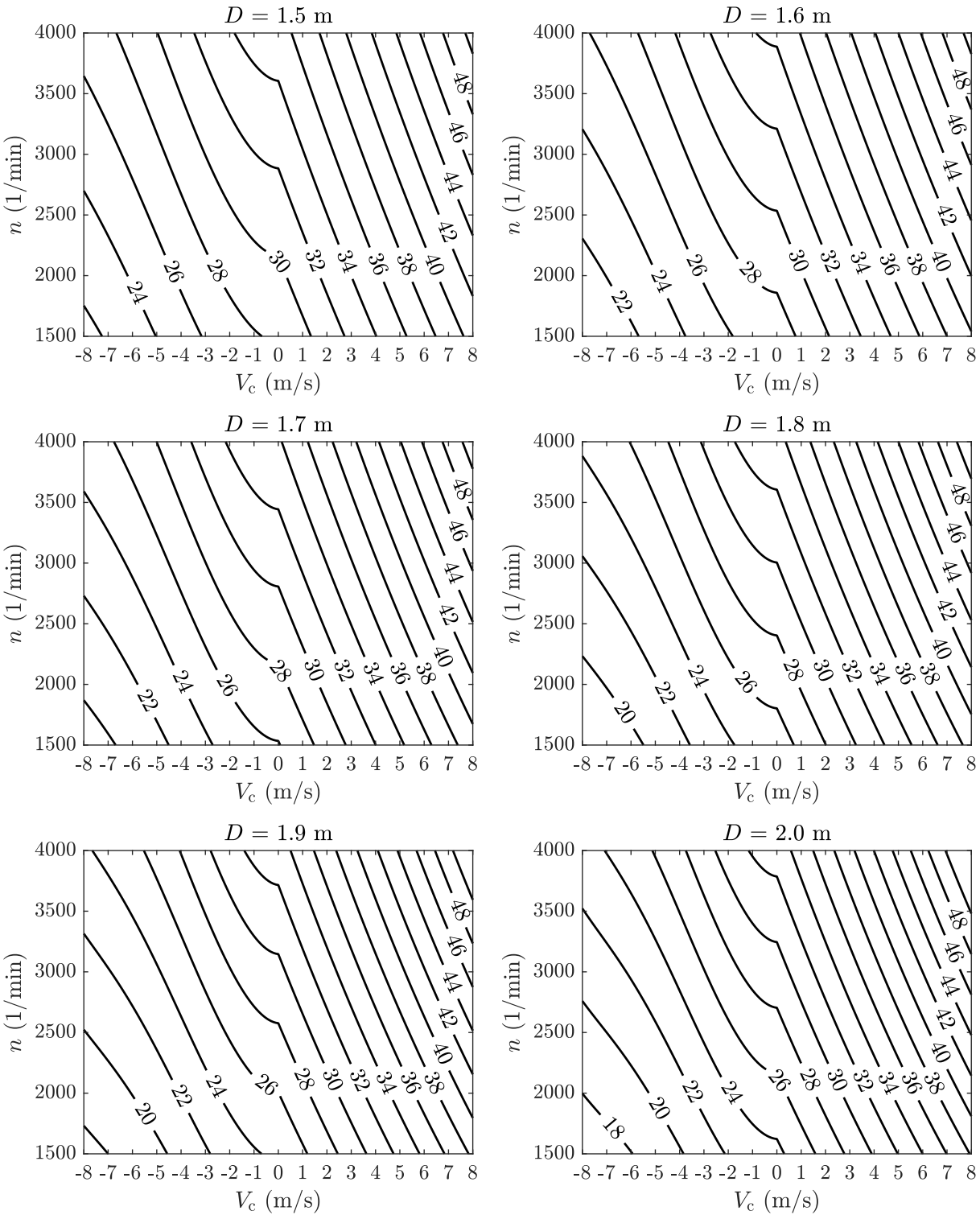

Figure 5.58: Required power in axial flight P_{Raf} (kW)
as a function of climb velocity V_c $\left(\frac{\mathrm{m}}{\mathrm{s}}\right)$
and revolutions per minute n $\left(\frac{1}{\mathrm{min}}\right)$ for various propeller diameter D (m)
and payload mass $M_{\mathrm{PLM}} = 100\mathrm{kg}$.

5.5.7.4 Performance in Forward Flight; $M_{\text{PLM}} = 600\text{kg}$

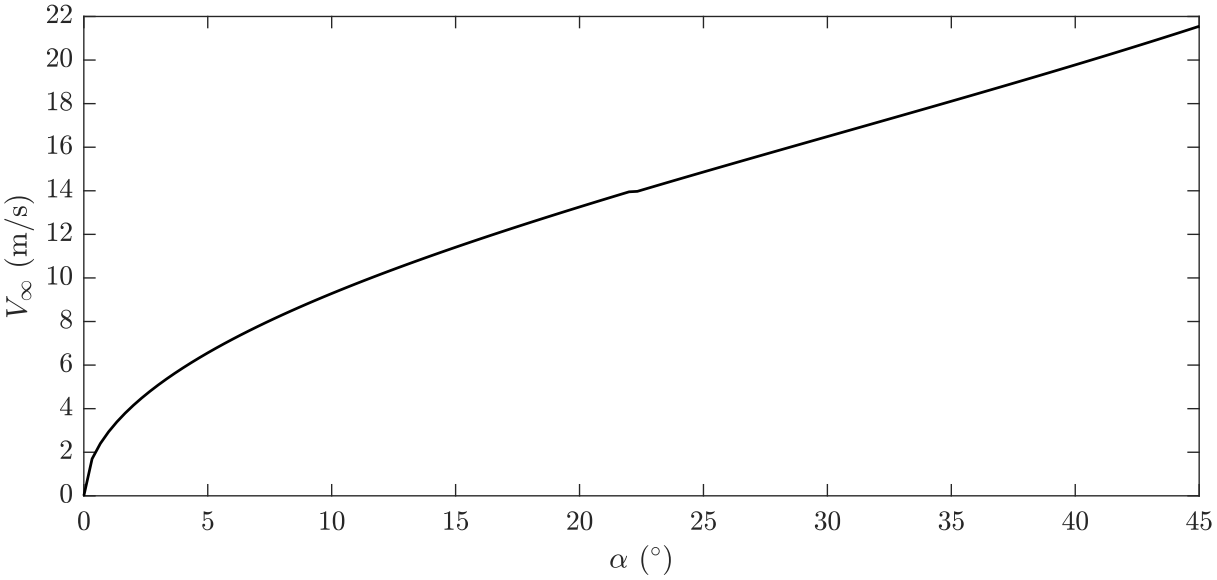

Figure 5.59: Forward flight velocity $V_\infty \left(\frac{\text{m}}{\text{s}}\right)$ as a function of angle of attack $\alpha\,(^\circ)$ for payload mass $M_{\text{PLM}} = 600\text{kg}$.

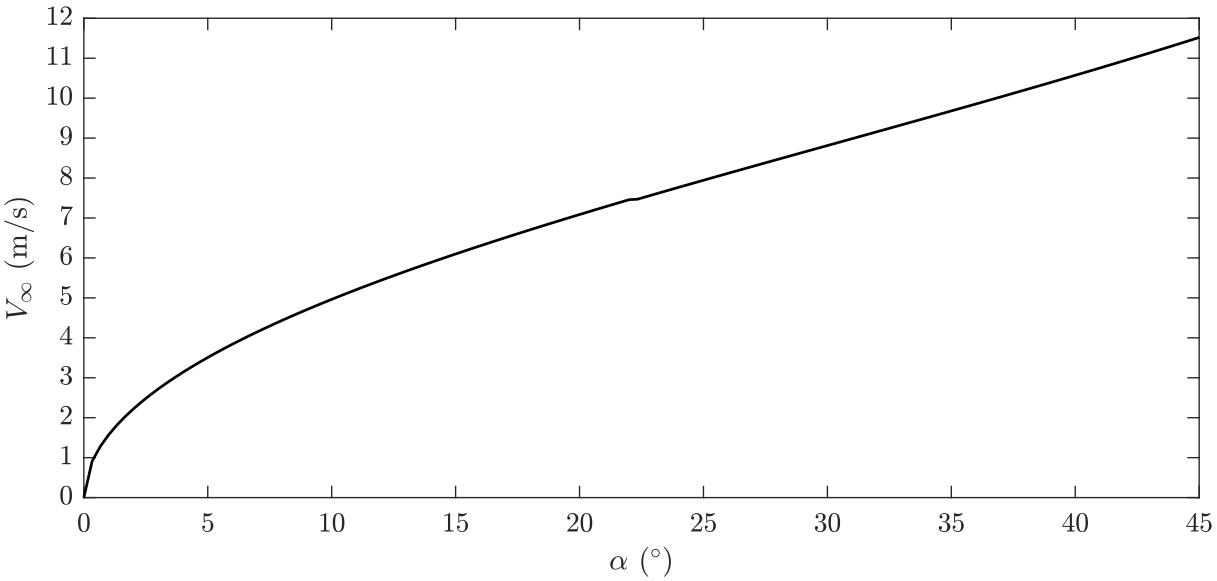

Figure 5.60: Forward flight velocity $V_\infty \left(\frac{\text{m}}{\text{s}}\right)$ as a function of angle of attack $\alpha\,(^\circ)$ for payload mass $M_{\text{PLM}} = 100\text{kg}$.

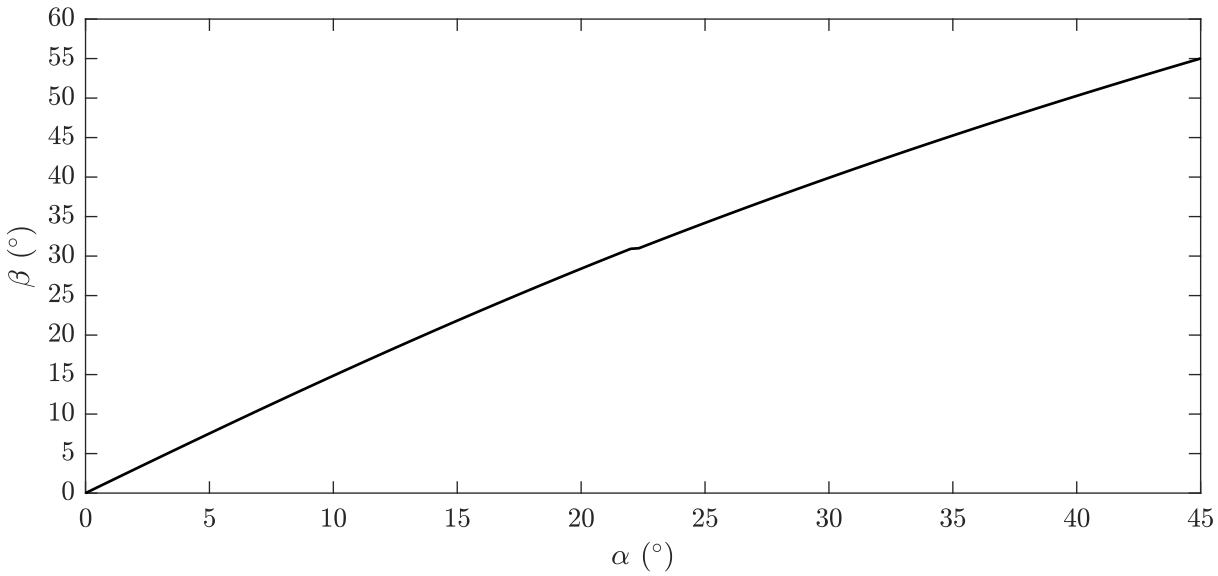

Figure 5.61: Angular deflection of aerostat axis $\beta\,(^\circ)$
as a function of angle of attack $\alpha\,(^\circ)$ for payload mass $M_{\mathrm{PLM}} = 600\mathrm{kg}$.

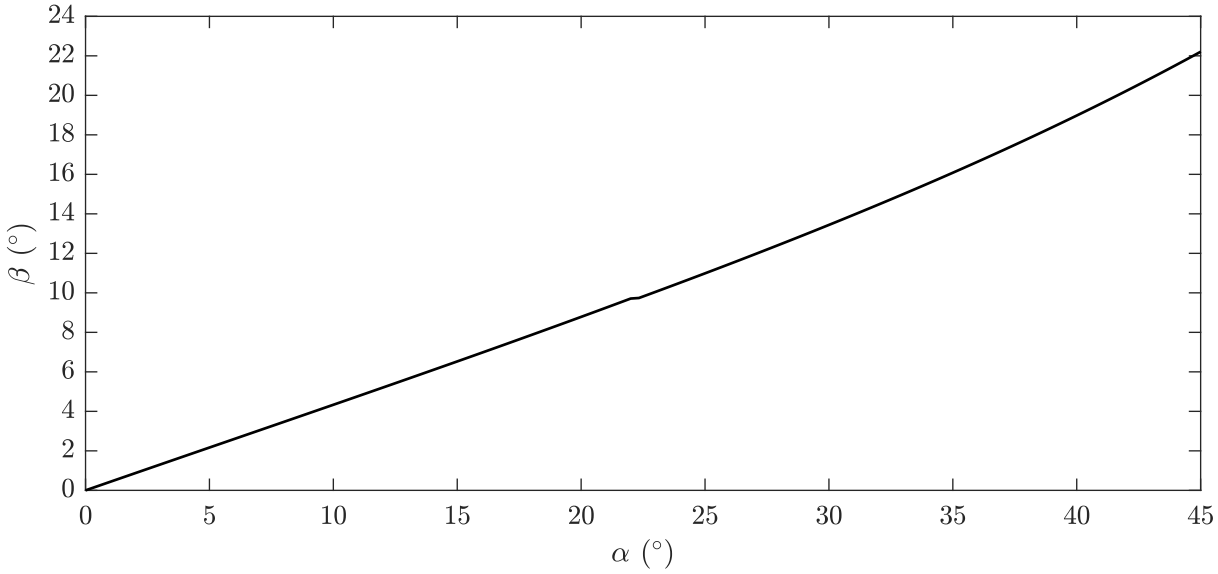

Figure 5.62: Angular deflection of aerostat axis $\beta\,(^\circ)$
as a function of angle of attack $\alpha\,(^\circ)$ for payload mass $M_{\mathrm{PLM}} = 100\mathrm{kg}$.

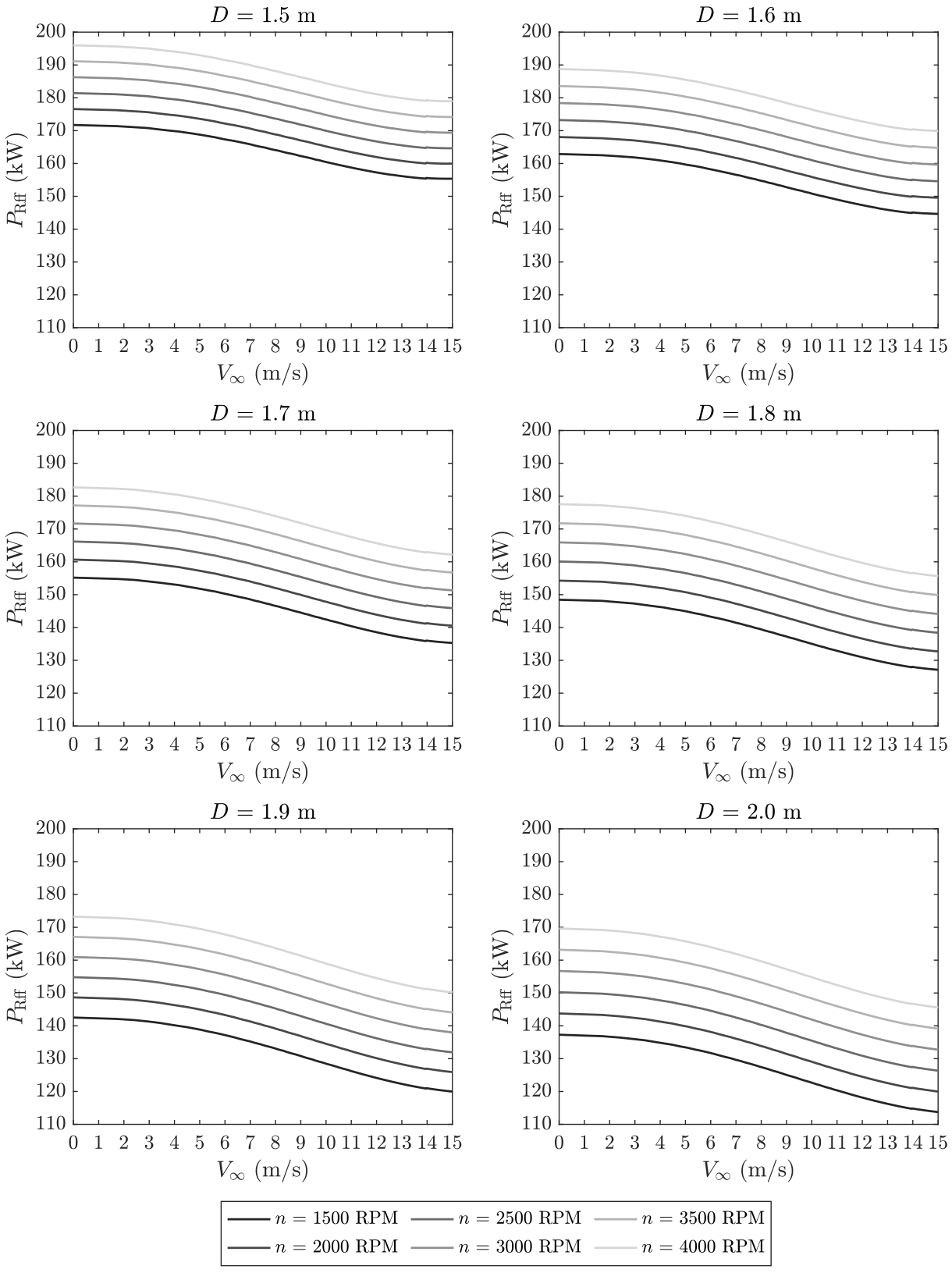

Figure 5.63: Required power in forward flight $P_{\mathrm{Rff}}\,(\mathrm{kW})$
as a function of forward flight velocity $V_\infty\left(\frac{\mathrm{m}}{\mathrm{s}}\right)$
and revolutions per minute $n\left(\frac{1}{\mathrm{min}}\right)$ for various propeller diameter $D\,(\mathrm{m})$
and payload mass $M_{\mathrm{PLM}} = 600\mathrm{kg}$.

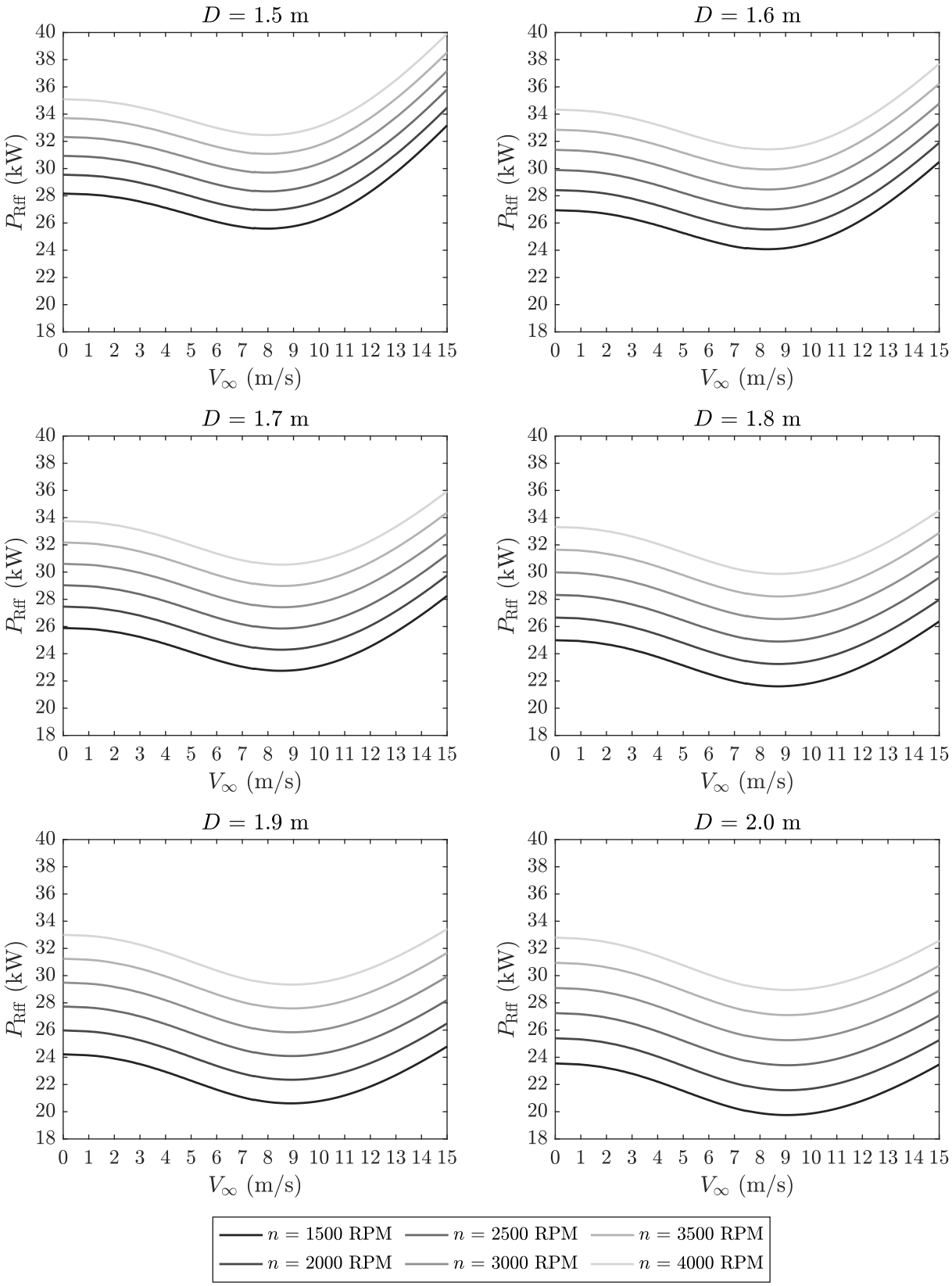

Figure 5.64: Required power in forward flight $P_{\mathrm{Rff}}\,(\mathrm{kW})$
as a function of forward flight velocity $V_\infty\left(\frac{\mathrm{m}}{\mathrm{s}}\right)$
and revolutions per minute $n\left(\frac{1}{\mathrm{min}}\right)$ for various propeller diameter $D\,(\mathrm{m})$
and payload mass $M_{\mathrm{PLM}} = 100\mathrm{kg}$.

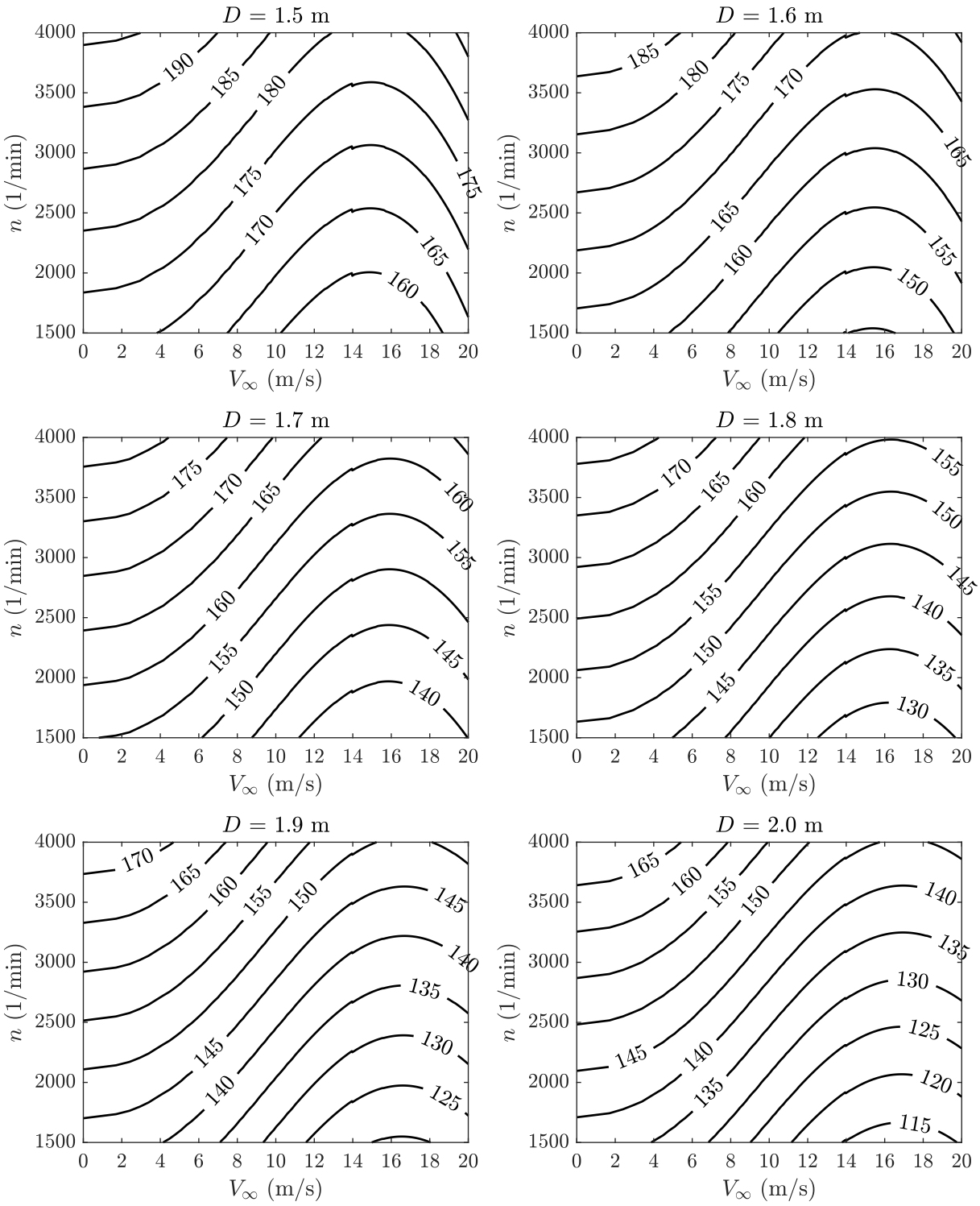

Figure 5.65: Required power in forward flight P_{Rff} (kW)
as a function of forward flight velocity V_∞ $\left(\frac{\mathrm{m}}{\mathrm{s}}\right)$
and revolutions per minute n $\left(\frac{1}{\mathrm{min}}\right)$ for various propeller diameter D (m)
and payload mass $M_{\mathrm{PLM}} = 600\mathrm{kg}$.

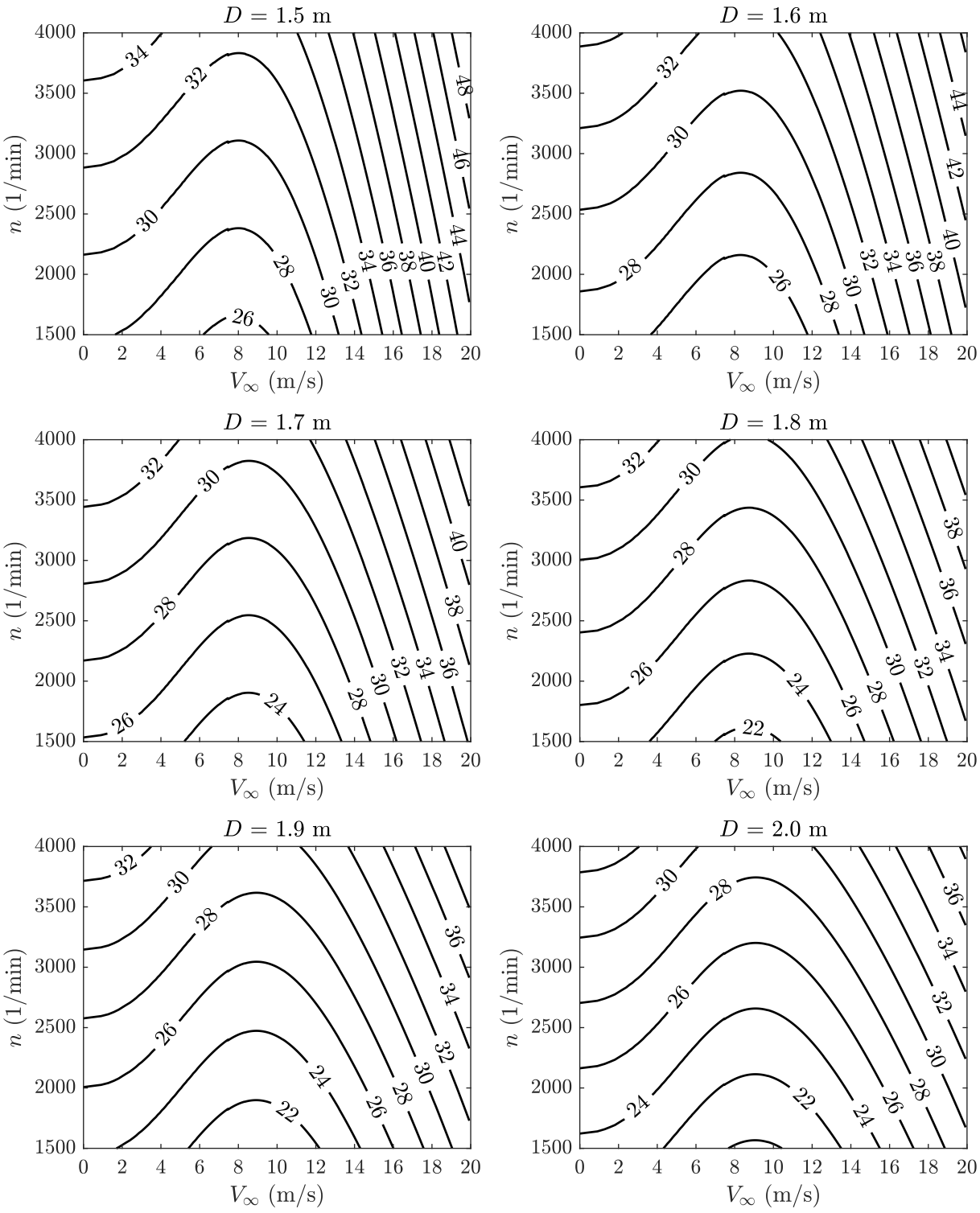

Figure 5.66: Required power in forward flight $P_{\mathrm{Rff}}\,(\mathrm{kW})$
as a function of forward flight velocity $V_\infty\left(\frac{\mathrm{m}}{\mathrm{s}}\right)$
and revolutions per minute $n\left(\frac{1}{\mathrm{min}}\right)$ for various propeller diameter $D\,(\mathrm{m})$
and payload mass $M_{\mathrm{PLM}} = 100\mathrm{kg}$.

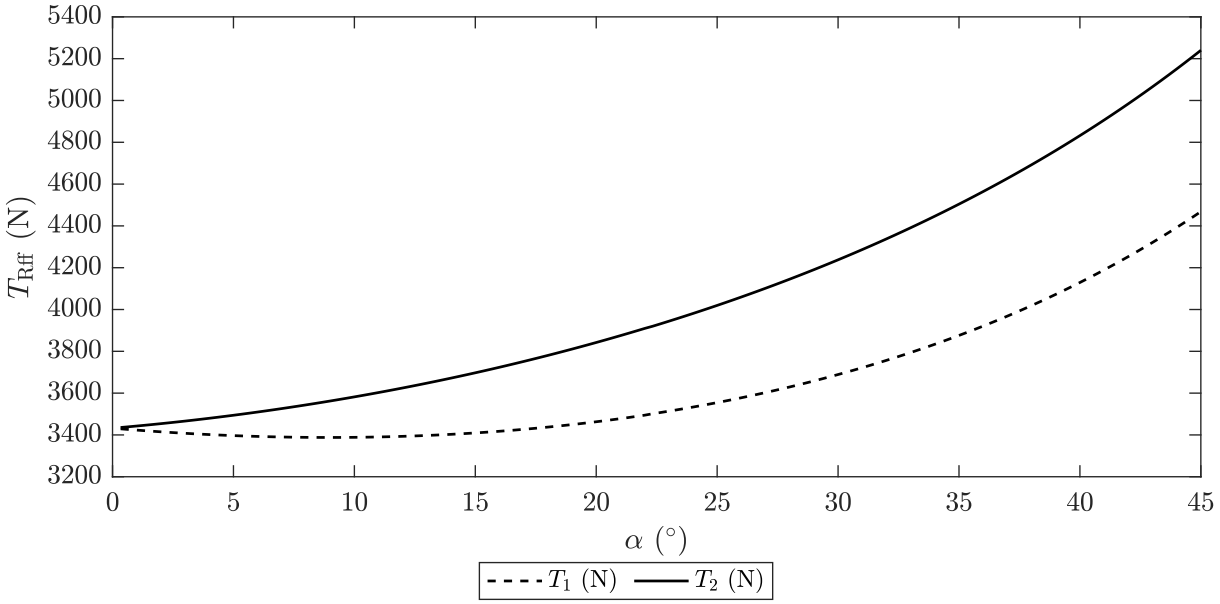

Figure 5.67: Thrust components $T_1\,(\mathrm{N})$ and $T_2\,(\mathrm{N})$ as a function of angle of attack $\alpha\,(^\circ)$ for payload mass $M_{\mathrm{PLM}} = 600\mathrm{kg}$.

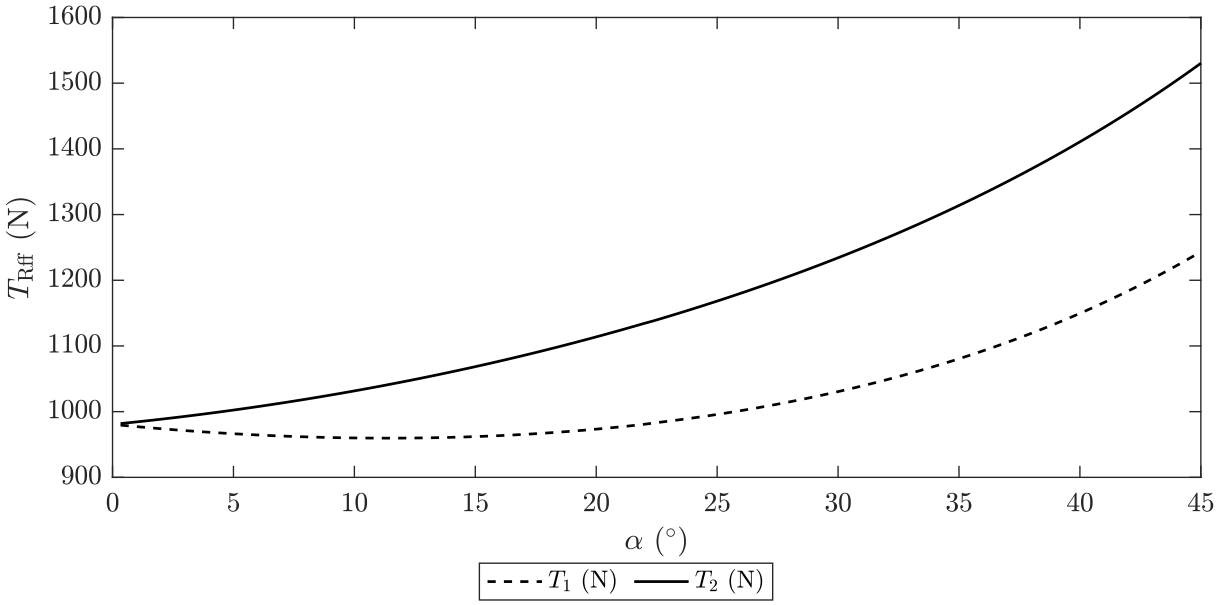

Figure 5.68: Thrust components $T_1\,(\mathrm{N})$ and $T_2\,(\mathrm{N})$ as a function of angle of attack $\alpha\,(^\circ)$ for payload mass $M_{\mathrm{PLM}} = 100\mathrm{kg}$.

5.5.7.5 Attitude Limitations in Forward Flight; $M_{\mathrm{PLM}} = 600\mathrm{kg}$

Based on findings from the Figures 5.63 and 5.65 for all the input parameters, the minimum power in forward flight with payload mass $M_{\mathrm{PLM}} = 600\mathrm{kg}$, considering approximate plot reading, is required at forward velocity that is executable only at very high angles of attack. For that reason, $V_{\mathrm{crs}} = 12\frac{\mathrm{m}}{\mathrm{s}}$ was chosen as a compromise. Checking with Figure 5.59 provides angle of attack $\alpha_{600} = 16°$, which by Figure 5.61 corresponds to the angular deflection of aerostat axis $\beta_{600} = 22°$.

Attitude Limitations check by the Equation 5.123

$$\alpha_{600} + \beta_{600} = 38° \leq 43.5° \tag{5.157}$$

proves that flight under these conditions is allowed.

Similarly, from Figures 5.64 and 5.66 for all the input parameters, the minimum power in forward flight with payload mass $M_{\mathrm{PLM}} = 100\mathrm{kg}$, considering approximate reading from plots, is required at forward velocity slightly above $V_{\mathrm{rtb}} = 8\frac{\mathrm{m}}{\mathrm{s}}$. Checking with Figure 5.59 provides angle of attack $\alpha_{100} = 25°$, which by Figure 5.61 corresponds to the angle $\beta_{100} = 11°$.

Attitude Limitations check by the Equation 5.123

$$\alpha_{100} + \beta_{100} = 36° \leq 43.5° \tag{5.158}$$

proves that flight under these conditions is allowed as well.

5.5.7.6 Battery; $M_{\mathrm{PLM}} = 600\mathrm{kg}$

Using Equations 5.140 - 5.147 for flight planning of Case MAX and Equations 5.149 - 5.156 for battery design provide, after inserting initial parameters from the Table 5.18, the final battery parameters stored in Tables 5.19, 5.20 and 5.21.

Table 5.19: Battery capacity $C_{\mathrm{bat}}\,(\mathrm{Ah})$, number of battery cells $n_{\mathrm{cel}}\,(1)$ and battery mass $M_{\mathrm{bat}}\,(\mathrm{kg})$ at various revolutions per minute $n\left(\frac{1}{min}\right)$ and propeller diameter $D\,(\mathrm{m})$ for $d_{\mathrm{crs}} = 200\mathrm{m}$.

$D\,(\mathrm{m})$	Parameter	$n\left(\frac{1}{min}\right)$					
		1500	2000	2500	3000	3500	4000
1.5	$C_{\mathrm{bat}}\,(\mathrm{Ah})$	1599.9	1649.5	1699.4	1749.5	1799.8	1850.1
	$n_{\mathrm{cel}}\,(1)$	533	550	566	583	600	617
	$M_{\mathrm{bat}}\,(\mathrm{kg})$	29.3	30.3	31.1	32.1	33.0	33.9
1.5	$C_{\mathrm{bat}}\,(\mathrm{Ah})$	1599.9	1649.5	1699.4	1749.5	1799.8	1850.1
	$n_{\mathrm{cel}}\,(1)$	533	550	566	583	600	617
	$M_{\mathrm{bat}}\,(\mathrm{kg})$	29.3	30.3	31.1	32.1	33.0	33.9
1.6	$C_{\mathrm{bat}}\,(\mathrm{Ah})$	1511.2	1564.3	1617.7	1671.3	1724.9	1778.7
	$n_{\mathrm{cel}}\,(1)$	504	521	539	557	575	593
	$M_{\mathrm{bat}}\,(\mathrm{kg})$	27.7	28.7	29.6	30.6	31.6	32.6
1.7	$C_{\mathrm{bat}}\,(\mathrm{Ah})$	1433.7	1490.2	1547.1	1604.2	1661.3	1718.5
	$n_{\mathrm{cel}}\,(1)$	478	497	516	535	554	573
	$M_{\mathrm{bat}}\,(\mathrm{kg})$	26.3	27.3	28.4	29.4	30.5	31.5
1.8	$C_{\mathrm{bat}}\,(\mathrm{Ah})$	1366.3	1426.3	1486.7	1547.2	1607.8	1668.5
	$n_{\mathrm{cel}}\,(1)$	455	475	496	516	536	556
	$M_{\mathrm{bat}}\,(\mathrm{kg})$	25.0	26.1	27.3	28.4	29.5	30.6
1.9	$C_{\mathrm{bat}}\,(\mathrm{Ah})$	1306.7	1370.3	1434.1	1498.1	1562.2	1626.3
	$n_{\mathrm{cel}}\,(1)$	436	457	478	499	521	542
	$M_{\mathrm{bat}}\,(\mathrm{kg})$	24.0	25.1	26.3	27.4	28.7	29.8
2.0	$C_{\mathrm{bat}}\,(\mathrm{Ah})$	1254.4	1321.4	1388.8	1456.3	1523.8	1591.4
	$n_{\mathrm{cel}}\,(1)$	418	440	463	485	508	530
	$M_{\mathrm{bat}}\,(\mathrm{kg})$	23.0	24.2	25.5	26.7	27.9	29.2

Table 5.20: Battery capacity C_{bat} (Ah), number of battery cells n_{cel} (1) and battery mass M_{bat} (kg) at various revolutions per minute $n\left(\frac{1}{min}\right)$ and propeller diameter D (m) for $d_{\text{crs}} = 400$m.

D (m)	Parameter	$n\left(\frac{1}{min}\right)$					
		1500	2000	2500	3000	3500	4000
1.5	C_{bat} (Ah)	1837.5	1895.2	1953.3	2011.7	2070.1	2128.7
	n_{cel} (1)	613	632	651	671	690	710
	M_{bat} (kg)	33.7	34.8	35.8	36.9	38.0	39.1
1.6	C_{bat} (Ah)	1734.0	1795.7	1857.8	1920.2	1982.7	2045.2
	n_{cel} (1)	578	599	619	640	661	682
	M_{bat} (kg)	31.8	32.9	34.0	35.2	36.4	37.5
1.7	C_{bat} (Ah)	1643.4	1709.2	1775.4	1841.8	1908.2	1974.8
	n_{cel} (1)	548	570	592	614	636	658
	M_{bat} (kg)	30.1	31.4	32.6	33.8	35.0	36.2
1.8	C_{bat} (Ah)	1564.7	1634.6	1704.8	1775.2	1845.7	1916.3
	n_{cel} (1)	522	545	568	592	615	639
	M_{bat} (kg)	28.7	30.0	31.2	32.6	33.8	35.1
1.9	C_{bat} (Ah)	1495.2	1569.1	1643.3	1717.7	1792.3	1866.9
	n_{cel} (1)	498	523	548	573	597	622
	M_{bat} (kg)	27.4	28.8	30.1	31.5	32.8	34.2
2.0	C_{bat} (Ah)	1434.0	1512.0	1590.3	1668.8	1747.3	1826.0
	n_{cel} (1)	478	504	530	556	582	609
	M_{bat} (kg)	26.3	27.7	29.2	30.6	32.0	33.5

Table 5.21: Battery capacity C_{bat} (Ah), number of battery cells n_{cel} (1) and battery mass M_{bat} (kg) at various revolutions per minute $n\left(\frac{1}{min}\right)$ and propeller diameter D (m) for $d_{\text{crs}} = 600$m.

D (m)	Parameter	$n\left(\frac{1}{min}\right)$					
		1500	2000	2500	3000	3500	4000
1.5	C_{bat} (Ah)	2075.2	2140.9	2207.2	2273.8	2340.5	2407.3
	n_{cel} (1)	692	714	736	758	780	802
	M_{bat} (kg)	38.1	39.3	40.5	41.7	42.9	44.1
1.6	C_{bat} (Ah)	1956.8	2027.1	2098.0	2169.1	2240.4	2311.7
	n_{cel} (1)	652	676	699	723	747	771
	M_{bat} (kg)	35.9	37.2	38.4	39.8	41.1	42.4
1.7	C_{bat} (Ah)	1853.2	1928.2	2003.6	2079.3	2155.2	2231.1
	n_{cel} (1)	618	643	668	693	718	744
	M_{bat} (kg)	34.0	35.4	36.7	38.1	39.5	40.9
1.8	C_{bat} (Ah)	1763.2	1842.8	1922.9	2003.1	2083.6	2164.0
	n_{cel} (1)	588	614	641	668	695	721
	M_{bat} (kg)	32.3	33.8	35.3	36.7	38.2	39.7
1.9	C_{bat} (Ah)	1683.6	1767.8	1852.5	1937.4	2022.4	2107.4
	n_{cel} (1)	561	589	617	646	674	702
	M_{bat} (kg)	30.9	32.4	33.9	35.5	37.1	38.6
2.0	C_{bat} (Ah)	1613.7	1702.6	1791.8	1881.3	1970.9	2060.5
	n_{cel} (1)	538	568	597	627	657	687
	M_{bat} (kg)	29.6	31.2	32.8	34.5	36.1	37.8

5.6 Structural Strength

5.6.1 Static Analysis of the UA

Figure 5.69 provides a simplified model of the UA for static analysis. Conceptual sizing dimensions from Table 4.1 were used for the preliminary strength calculations.

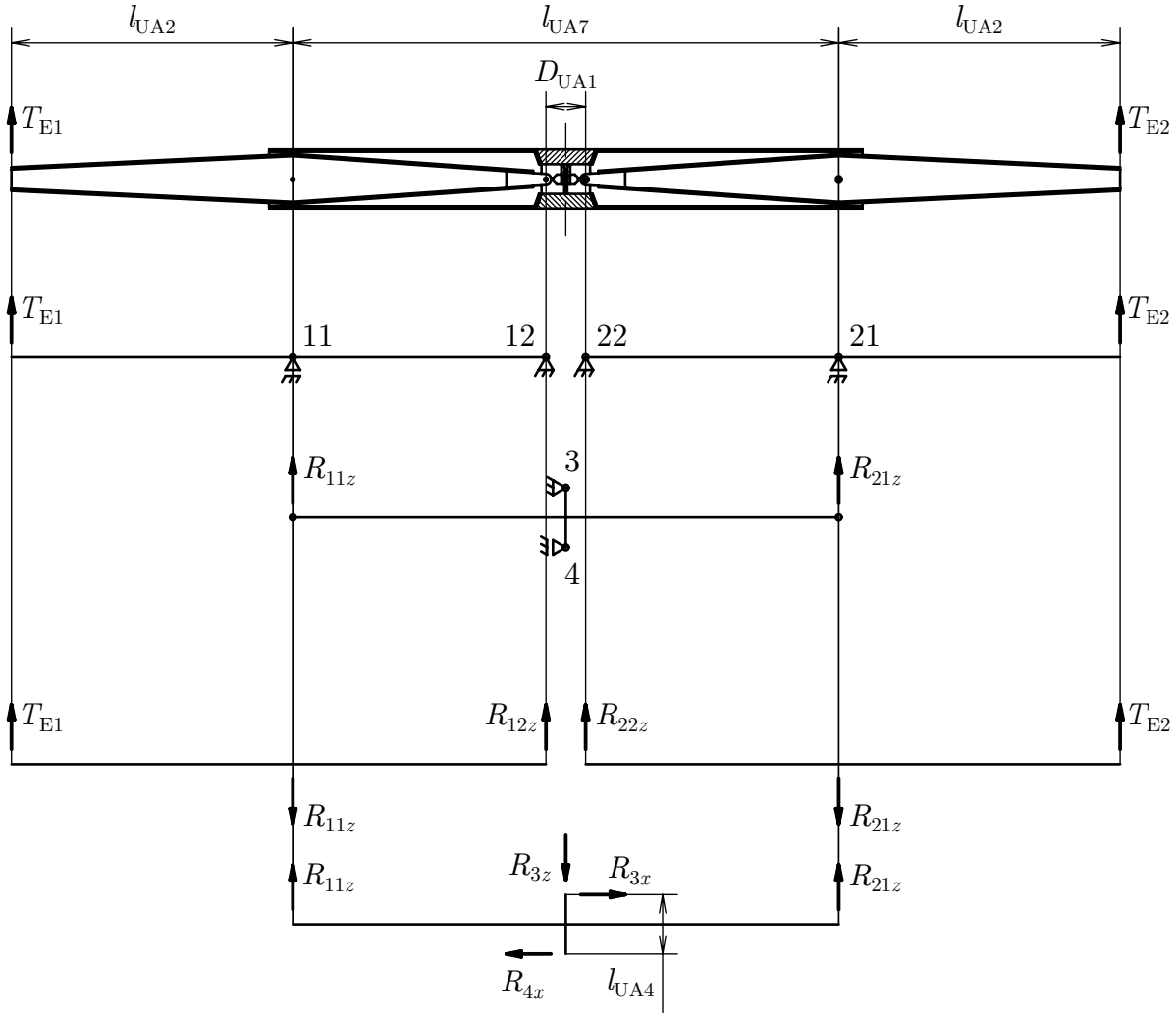

Figure 5.69: Static analysis scheme of the UA.

5.6.1.1 Static Analysis of the Arms

It is important to solve the forces in both arms from the Figure 5.69 separately. In order to investigate the limit loads, it is required to compare the final limit loads in axial climb with the limit loads in forward flight. While the final limit loads in axial climb may appear superior, the comparison is still required to find out the actual difference between the two limit loads. This is all the more necessary as the findings from Subsection 5.5.5.6 show that the thrust provided by the propulsion units in forward flight introduce asymmetrical loading.

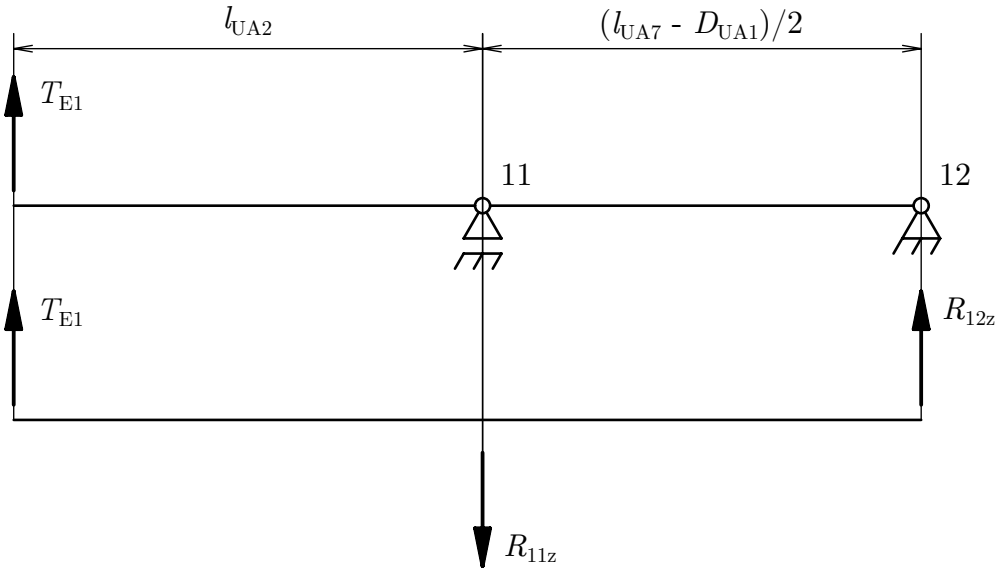

Figure 5.70: Static analysis scheme of the lower arms in forward flight.

For the lower arms in forward flight

$$\Sigma F_{\mathrm{z}} : T_{\mathrm{E1}} + R_{12z} - R_{11z} = 0, \tag{5.159}$$

$$\Sigma M_{11} : R_{12\mathrm{z}} \frac{l_{\mathrm{UA7}} - D_{\mathrm{UA1}}}{2} - T_{\mathrm{E1}} l_{\mathrm{UA2}} = 0 \tag{5.160}$$

and after rearrangement

$$R_{12z} = T_{\mathrm{E1}} \frac{2 l_{\mathrm{UA2}}}{l_{\mathrm{UA7}} - D_{\mathrm{UA1}}}, \tag{5.161}$$

$$R_{11z} = T_{\mathrm{E1}} \left(1 + \frac{2 l_{\mathrm{UA2}}}{l_{\mathrm{UA7}} - D_{\mathrm{UA1}}} \right). \tag{5.162}$$

Analogically for the upper arms

$$R_{22z} = T_{\mathrm{e2}} \frac{2 l_{\mathrm{UA2}}}{l_{\mathrm{UA7}} - D_{\mathrm{UA1}}}, \tag{5.163}$$

$$R_{21z} = T_{\mathrm{e2}} \left(1 + \frac{2 l_{\mathrm{UA2}}}{l_{\mathrm{UA7}} - D_{\mathrm{UA1}}} \right). \tag{5.164}$$

5.6.1.2 Static Analysis of the Fuselage

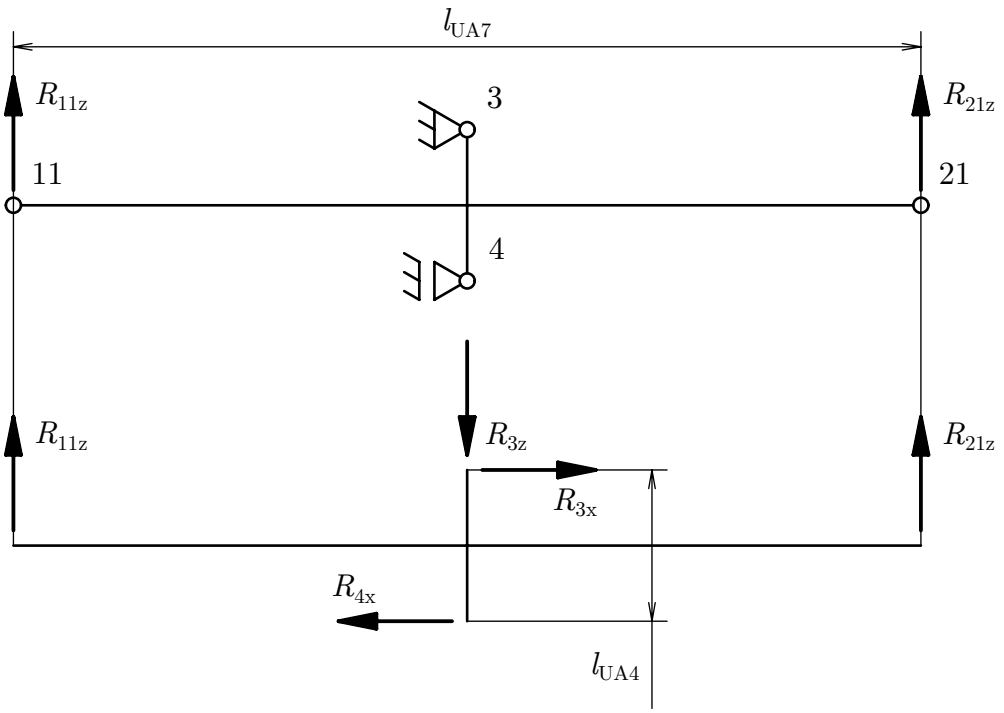

Figure 5.71: Static analysis scheme of the fuselage.

$$\Sigma F_{\mathrm{x}} : R_{3x} - R_{4x} = 0, \tag{5.165}$$

$$\Sigma F_{\mathrm{z}} : R_{11z} + R_{21z} - R_{3z} = 0, \tag{5.166}$$

$$\Sigma M_4 : R_{21z}\frac{l_{\mathrm{UA7}}}{2} - R_{11z}\frac{l_{\mathrm{UA7}}}{2} - R_{3x}l_{\mathrm{UA4}} = 0 \tag{5.167}$$

and after plugging Equations 5.162, 5.164 and rearrangement

$$R_{3z} = (T_{\mathrm{E1}} + T_{\mathrm{e2}})\left(1 + \frac{2l_{\mathrm{UA2}}}{l_{\mathrm{UA7}} - D_{\mathrm{UA1}}}\right), \tag{5.168}$$

$$R_{3x} = R_{4x} = (T_{\mathrm{e2}} - T_{\mathrm{E1}})\left(1 + \frac{2l_{\mathrm{UA2}}}{l_{\mathrm{UA7}} - D_{\mathrm{UA1}}}\right)\frac{l_{\mathrm{UA7}}}{2l_{\mathrm{UA4}}}. \tag{5.169}$$

From the Equation 5.169, it is obvious that in the case of symmetrical thrust loading

$$R_{3x} = R_{4x} = 0. \tag{5.170}$$

5.6.1.3 Static Analysis of the Undercarriage

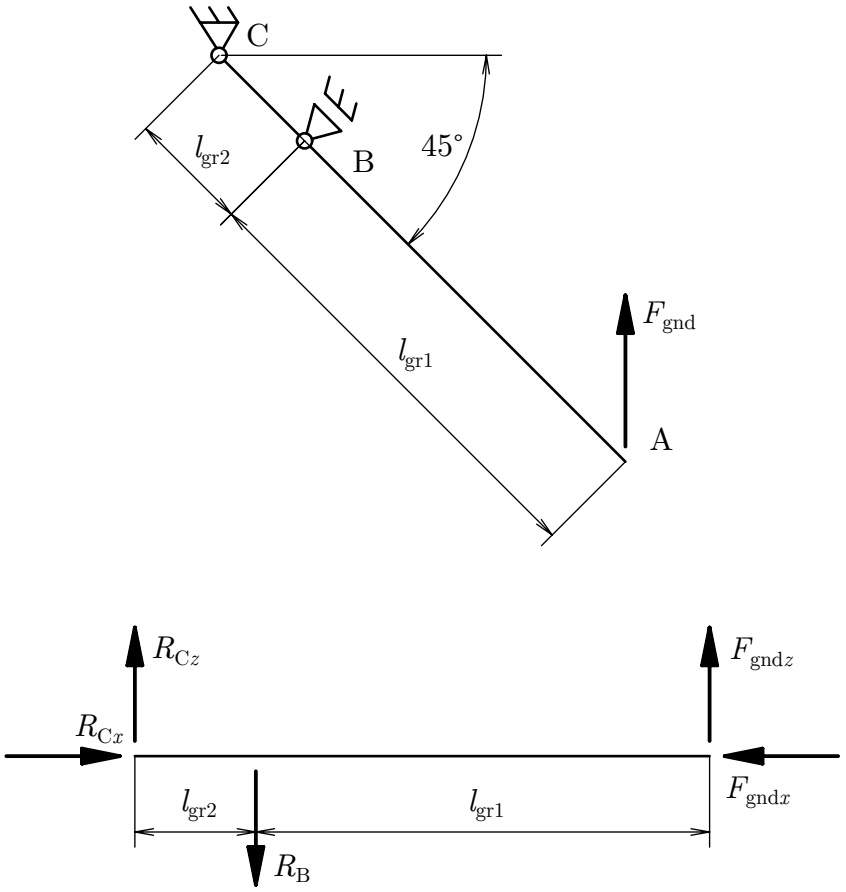

Figure 5.72: Static analysis scheme of undercarriage leg.

$$\Sigma F_{\mathrm{x}} : R_{\mathrm{C}x} - F_{\mathrm{gnd}x} = 0, \tag{5.171}$$

$$\Sigma F_{\mathrm{z}} : F_{\mathrm{gnd}z} + R_{\mathrm{C}z} - R_{\mathrm{B}} = 0, \tag{5.172}$$

$$\Sigma M_{\mathrm{B}} : F_{\mathrm{gnd}z} l_{\mathrm{gr1}} - R_{\mathrm{C}z} l_{\mathrm{gr2}} = 0 \tag{5.173}$$

where

$$F_{\mathrm{gnd}x} = F_{\mathrm{gnd}} \sin(45°), \tag{5.174}$$

$$F_{\mathrm{gnd}z} = F_{\mathrm{gnd}} \cos(45°) \tag{5.175}$$

and after inserting Equations 5.174 and 5.175 into 5.171 - 5.173 and rearrangement

$$R_{\mathrm{C}x} = F_{\mathrm{gnd}x} = F_{\mathrm{gnd}} \sin(45°), \tag{5.176}$$

$$R_{\mathrm{C}z} = F_{\mathrm{gnd}z} \frac{l_{\mathrm{gr1}}}{l_{\mathrm{gr2}}} = F_{\mathrm{gnd}} \frac{l_{\mathrm{gr1}}}{l_{\mathrm{gr2}}} \cos(45°), \tag{5.177}$$

$$R_{\mathrm{B}} = F_{\mathrm{gnd}z} \left(1 + \frac{l_{\mathrm{gr1}}}{l_{\mathrm{gr2}}}\right) = F_{\mathrm{gnd}} \left(1 + \frac{l_{\mathrm{gr1}}}{l_{\mathrm{gr2}}}\right) \cos(45°). \tag{5.178}$$

5.6.2 Limit Loads

It is necessary to investigate suspected load cases to find the limit loads. The structure is to be designed for the case of payload mass $M_{\mathrm{PLM}} = 1100\mathrm{kg}$. Positive loads are expected to be superior and so positive maneuvering load factor $n_{\mathrm{pos}} = 3.5$ was considered based on the Subsection 2.1.

In case of axial climb, maximum total required thrust in axial flight $T_{\mathrm{Raf}}\,(\mathrm{N})$ at climb velocity $V_{\mathrm{c}} = 8\frac{\mathrm{m}}{\mathrm{s}}$ from the Figure 5.73

$$T_{\mathrm{Raf}} \doteq 12750\mathrm{N}. \tag{5.179}$$

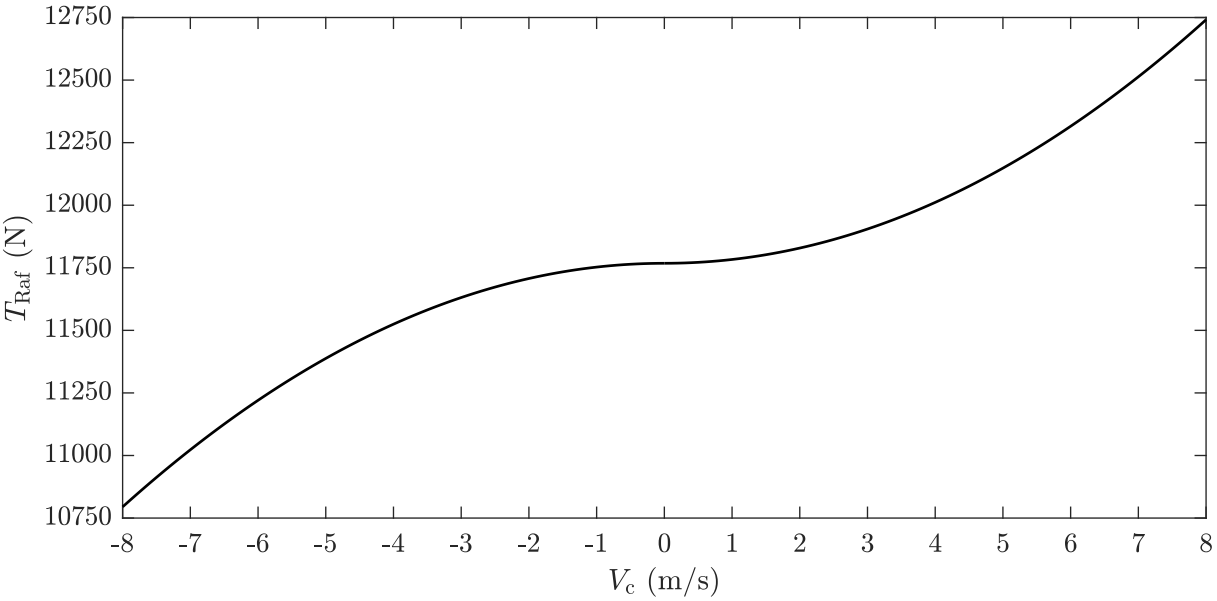

Figure 5.73: Required thrust in axial flight $T_{\mathrm{Raf}}\,(\mathrm{N})$
as a function of climb velocity $V_{\mathrm{c}}\left(\frac{\mathrm{m}}{\mathrm{s}}\right)$
for payload mass $M_{\mathrm{PLM}} = 1100\mathrm{kg}$.

For one propulsion unit

$$\frac{T_{\mathrm{Raf}}}{4} = \frac{12750}{4} \doteq 3188\mathrm{N}, \tag{5.180}$$

$$T_{\mathrm{E1}} = T_{\mathrm{e2}} = n_{\mathrm{pos}}\frac{T_{\mathrm{Raf}}}{4} = 3.5 \cdot 3188 = 11158\mathrm{N}. \tag{5.181}$$

In the case of forward flight, the maximum required thrust of the lower propulsion units $T_1\,(\mathrm{N})$ and the upper propulsion units $T_2\,(\mathrm{N})$ at the angle of attack $\alpha = 45°$ from Figure 5.74

$$T_1 \doteq 7700\mathrm{N}, \tag{5.182}$$

$$T_2 \doteq 9000\mathrm{N}. \tag{5.183}$$

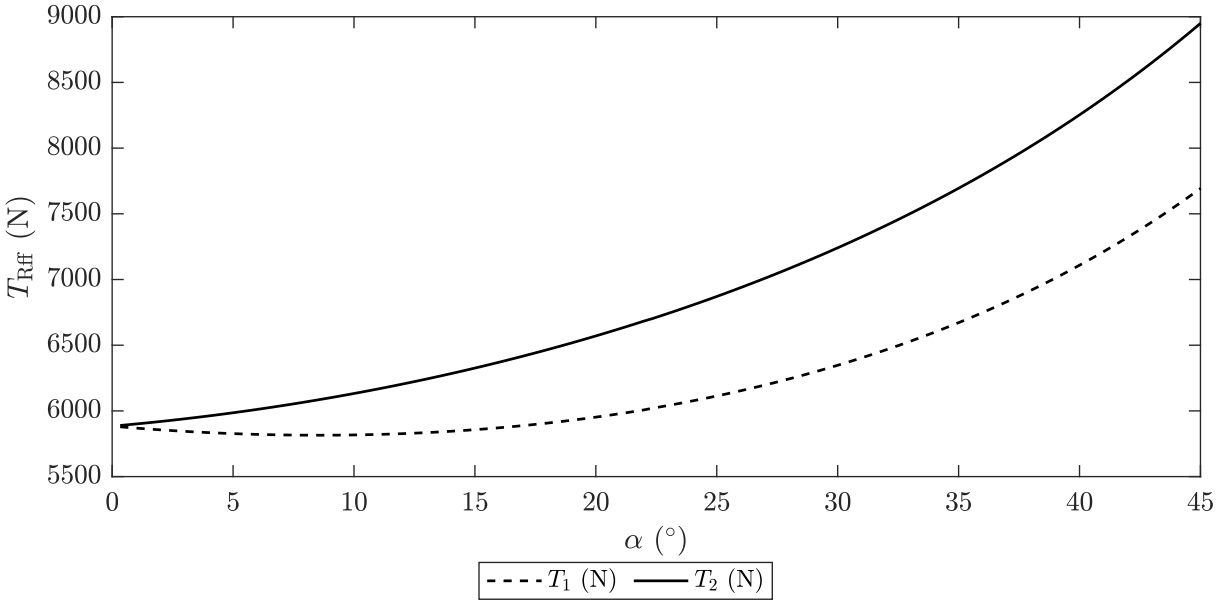

Figure 5.74: Thrust components $T_1\,(\mathrm{N})$ and $T_2\,(\mathrm{N})$ as a function of angle of attack $\alpha\,(°)$ for payload mass $M_{\mathrm{PLM}} = 1100\mathrm{kg}$.

For one propulsion unit

$$\frac{T_1}{2} = \frac{7700}{2} \doteq 3850\mathrm{N}, \tag{5.184}$$

$$\frac{T_2}{2} = \frac{9000}{2} \doteq 4500\mathrm{N}, \tag{5.185}$$

$$T_{\mathrm{E1}} = n_{\mathrm{pos}}\frac{T_1}{2} = 3.5 \cdot 3850 = 13475\mathrm{N}, \tag{5.186}$$

$$T_{\mathrm{E2}} = n_{\mathrm{pos}}\frac{T_2}{2} = 3.5 \cdot 4500 = 15750\mathrm{N}. \tag{5.187}$$

From Equations 5.181 and 5.187, it is obvious that the final limit loads occur in forward flight at angle of attack $\alpha = 45°$.

Inserting the conceptual dimensions from Table 4.1 and the thrust limit loads from Equations 5.186 and 5.187 into Equations 5.161 - 5.164 and 5.168 - 5.169

$$R_{12z} = T_{\mathrm{E1}} \frac{2l_{\mathrm{UA2}}}{l_{\mathrm{UA7}} - D_{\mathrm{UA1}}} = 13475 \cdot \frac{2 \cdot 1}{1.9 - 0.2} \doteq 15853\mathrm{N} \tag{5.188}$$

$$R_{11z} = T_{\mathrm{E1}} \left(1 + \frac{2l_{\mathrm{UA2}}}{l_{\mathrm{UA7}} - D_{\mathrm{UA1}}}\right) = 13475 \left(1 + \frac{2 \cdot 1}{1.9 - 0.2}\right) \doteq 29328\mathrm{N}, \tag{5.189}$$

$$R_{22z} = T_{\mathrm{e2}} \frac{2l_{\mathrm{UA2}}}{l_{\mathrm{UA7}} - D_{\mathrm{UA1}}} = 15750 \cdot \frac{2 \cdot 1}{1.9 - 0.2} \doteq 18529\mathrm{N} \tag{5.190}$$

$$R_{21z} = T_{\mathrm{e2}} \left(1 + \frac{2l_{\mathrm{UA2}}}{l_{\mathrm{UA7}} - D_{\mathrm{UA1}}}\right) = 15750 \left(1 + \frac{2 \cdot 1}{1.9 - 0.2}\right) \doteq 34279\mathrm{N} \tag{5.191}$$

$$\begin{aligned} R_{3z} &= (T_{\mathrm{E1}} + T_{\mathrm{e2}}) \left(1 + \frac{2l_{\mathrm{UA2}}}{l_{\mathrm{UA7}} - D_{\mathrm{UA1}}}\right) = \\ &= (13475 + 15750) \left(1 + \frac{2 \cdot 1}{1.9 - 0.2}\right) \doteq 63607\mathrm{N} \end{aligned} \tag{5.192}$$

$$\begin{aligned} R_{3x} = R_{4x} &= (T_{\mathrm{e2}} - T_{\mathrm{E1}}) \left(1 + \frac{2l_{\mathrm{UA2}}}{l_{\mathrm{UA7}} - D_{\mathrm{UA1}}}\right) = \\ &= (15750 - 13475) \left(1 + \frac{2 \cdot 1}{1.9 - 0.2}\right) \doteq 4952\mathrm{N}. \end{aligned} \tag{5.193}$$

Considering undercarriage, applying the requirements from Section 2.2 and the UA mass M_{UA} (kg) for carrying the heavy payloads from Table 5.14 to calculate ground reaction force F_{gnd} (N) and its components $F_{\mathrm{gnd}x}$ (N) and $F_{\mathrm{gnd}z}$ (N)

$$F_{\mathrm{gnd}} = \frac{M_{\mathrm{UA}}}{4} \cdot g_0 \cdot n_{\mathrm{gnd}} = \frac{332}{4} \cdot 9.80605 \cdot 2.8 \doteq 2279\mathrm{N}. \tag{5.194}$$

$$F_{\mathrm{gnd}x} = F_{\mathrm{gnd}z} = F_{\mathrm{gnd}} \cdot \cos(45°] \doteq 1612\mathrm{N}. \tag{5.195}$$

Length of the outer leg $l_{\mathrm{gr1}} = 600\mathrm{mm}$ and length of the inner leg $l_{\mathrm{gr2}} = 160\mathrm{mm}$ plugged into Equations 5.176 - 5.178 and combining with Equation 5.194

$$R_{\mathrm{C}x} = F_{\mathrm{gnd}} \sin(45°) = 2279 \cdot 0.707 \doteq 1612\mathrm{N}, \tag{5.196}$$

$$R_{\mathrm{C}z} = F_{\mathrm{gnd}} \frac{l_{\mathrm{gr1}}}{l_{\mathrm{gr2}}} \cos(45°) = 2279 \cdot \frac{600}{160} \cdot 0.707 \doteq 6043\mathrm{N}, \tag{5.197}$$

$$R_{\mathrm{B}} = F_{\mathrm{gnd}} \left(1 + \frac{l_{\mathrm{gr1}}}{l_{\mathrm{gr2}}}\right) \cos(45°) = 2279 \cdot \left(1 + \frac{600}{160}\right) \cdot 0.707 \doteq 7655\mathrm{N}. \tag{5.198}$$

5.6.3 Ultimate Loads

Limit loads calculated in Subsection 5.6.2 were multiplied by safety factor f (1) and special factor f_s (1).

$$T_\mathrm{E1U} = T_\mathrm{E1} \cdot f \cdot f_\mathrm{s} = 13475 \cdot 1.5 \cdot 1.5 \doteq 30319\mathrm{N}, \tag{5.199}$$

$$T_\mathrm{E2U} = T_\mathrm{E2} \cdot f \cdot f_\mathrm{s} = 15750 \cdot 1.5 \cdot 1.5 \doteq 35438\mathrm{N}, \tag{5.200}$$

$$R_{12z\mathrm{U}} = R_{12z} \cdot f \cdot f_\mathrm{s} = 15853 \cdot 1.5 \cdot 1.5 \doteq 35669\mathrm{N}, \tag{5.201}$$

$$R_{11z\mathrm{U}} = R_{11z} \cdot f \cdot f_\mathrm{s} = 29328 \cdot 1.5 \cdot 1.5 \doteq 65988\mathrm{N}, \tag{5.202}$$

$$R_{22z\mathrm{U}} = R_{22z} \cdot f \cdot f_\mathrm{s} = 18529 \cdot 1.5 \cdot 1.5 \doteq 41690\mathrm{N}, \tag{5.203}$$

$$R_{21z\mathrm{U}} = R_{21z} \cdot f \cdot f_\mathrm{s} = 34279 \cdot 1.5 \cdot 1.5 \doteq 77128\mathrm{N}, \tag{5.204}$$

$$R_{3z\mathrm{U}} = R_{3z} \cdot f \cdot f_\mathrm{s} = 63607 \cdot 1.5 \cdot 1.5 \doteq 143116\mathrm{N}, \tag{5.205}$$

$$R_{3x\mathrm{U}} = R_{4x\mathrm{U}} = R_{3x} \cdot f \cdot f_\mathrm{s} = R_{4x} \cdot f \cdot f_\mathrm{s} = 4952 \cdot 1.5 \cdot 1.5 \doteq 11142\mathrm{N}, \tag{5.206}$$

$$F_\mathrm{gndU} = F_\mathrm{gnd} \cdot n_\mathrm{gndU} \cdot f_\mathrm{s} = 2279 \cdot 1.5 \cdot 1.5 \doteq 5128\mathrm{N}, \tag{5.207}$$

$$F_{\mathrm{gnd}x\mathrm{U}} = F_{\mathrm{gnd}z\mathrm{U}} = F_{\mathrm{gnd}x} \cdot n_\mathrm{gndU} \cdot f_\mathrm{s} = F_{\mathrm{gnd}z} \cdot n_\mathrm{gndU} \cdot f_\mathrm{s} = 2279 \cdot 1.5 \cdot 1.5 \doteq 3626\mathrm{N}, \tag{5.208}$$

$$R_{\mathrm{C}x\mathrm{U}} = R_\mathrm{Cx} \cdot n_\mathrm{gndU} \cdot f_\mathrm{s} = 1612 \cdot 1.5 \cdot 1.5 \doteq 3626\mathrm{N}, \tag{5.209}$$

$$R_{\mathrm{C}z\mathrm{U}} = R_\mathrm{Cz} \cdot n_\mathrm{gndU} \cdot f_\mathrm{s} = 6043 \cdot 1.5 \cdot 1.5 \doteq 13597\mathrm{N}, \tag{5.210}$$

$$R_\mathrm{BU} = R_\mathrm{B} \cdot n_\mathrm{gndU} \cdot f_\mathrm{s} = 7655 \cdot 1.5 \cdot 1.5 \doteq 17223\mathrm{N}. \tag{5.211}$$

5.6.4 Dimensioning

5.6.4.1 Material Strength

The structure of the UA is heavily bended. It is necessary to design and optimise the cross-sections of bended elements to withstand the compression stress in the upper caps and tensile stress in the lower caps. Upper caps are to be designed thicker than the lower ones which is typical for wing spars where high slenderness ratio is present and so stability is an issue. This applies for both conventional homogeneous materials and composite materials.
Since the superior load comes from bending, unidirectional carbon-epoxy composite is to be used to reinforce both upper and lower caps. Tensile and compressive strength of carbon fibre composites are usually mentioned to be similar. Raymer brings the table [7, Table 14.4, Pages 368-369] of typical composite material properties where for high-strength graphite/epoxy composite in longitudinal direction both tensile and compressive strength is 180 psi which is approximately 1240 $\frac{\mathrm{N}}{\mathrm{mm}^2}$.
In the case of composite materials, stability issues of the upper cap are brought not only by the overall part geometry but also by stability of individual fibres, their orientation and quality of manufacturing process where fibres ought to be layered with special focus on sustaining the straightness. That being said, the typical value of compressive strength of unidirectional carbon fibre has to be taken with reserve, whereas tension actually straighten fibres and so the typical values of tension strength are usually valid.
Lo and Chim state: "In our search for a realistic compressive strength prediction method, we have developed a model to describe the response of unidirectional composites under axial compression. Using a combined analytical and semi-empirical approach, a simple equation was obtained to predict the compressive strength of unidirectional composites. The formulation was based on the concept of microbuckling of a representative volume element in the composite and the effect of shear deformation was included. The validity of the present equation for compressive strength predictions was established by the good correlation obtained with known experimental data for E-glass, carbon, and boron fiber composites" [9, Introduction, Page 838]. Their findings were then approved by Naik and Kumar who compared more models with the similar purpose: "Lo-Chim model gives good results as it was correlated with the same set of experimental results for obtaining experimental parameters" [10, Chapter 5, Page 307]. Their results show that the final strength is highly dependent on the fibre volume fraction v_f, a ratio of fibre to matrix volume, varying very roughly from 400 $\frac{\mathrm{N}}{\mathrm{mm}^2}$ at $v_f = 0.3$ to 1500 $\frac{\mathrm{N}}{\mathrm{mm}^2}$ at $v_f = 0.65$.

To keep the calculation safe, the compressive strength of unidirectional carbon-epoxy composite $S_{\mathrm{CUD}}\left(\frac{\mathrm{N}}{\mathrm{mm}^2}\right)$ used on the upper caps

$$S_{\mathrm{CUD}} = 500\frac{\mathrm{N}}{\mathrm{mm}^2} \tag{5.212}$$

and the tensile strength of unidirectional carbon-epoxy composite $S_{\mathrm{TUD}}\left(\frac{\mathrm{N}}{\mathrm{mm}^2}\right)$ used on the lower caps

$$S_{\mathrm{TUD}} = 1000\frac{\mathrm{N}}{\mathrm{mm}^2}. \tag{5.213}$$

5.6.4.2 Cross-Section Moment of Inertia

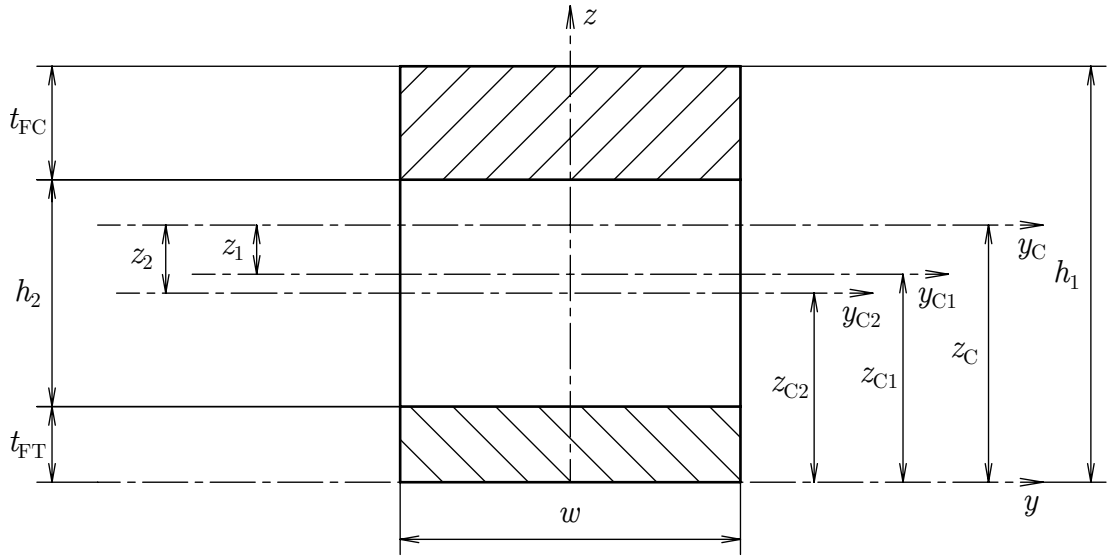

Figure 5.75: Cross-section breakdown for moment of inertia calculation.

Considering the rectangular thin wall closed profile cross-section with upper cap thicker than the lower one, neglecting webs, moment of inertia $I_y\,(\mathrm{mm}^4)$ according to Steiner's theorem

$$I_y = \left(I_{y1} + A_1 z_1^2\right) - \left(I_{y2} + A_2 z_2^2\right) \tag{5.214}$$

where

$$I_{y1} = \frac{w h_1^3}{12}, \tag{5.215}$$

$$I_{y2} = \frac{w h_2^3}{12}, \tag{5.216}$$

$$h_2 = h_1 - t_{FC} - t_{FT}, \tag{5.217}$$

$$A_1 = w h_1, \tag{5.218}$$

$$A_2 = w h_2, \tag{5.219}$$

$$z_1 = z_{C1} - z_C, \tag{5.220}$$

$$z_2 = z_{C2} - z_C, \tag{5.221}$$

$$z_C = \frac{A_1 z_{C1} - A_2 z_{C2}}{A_1 - A_2}, \tag{5.222}$$

$$z_{C1} = \frac{1}{2} h_1, \tag{5.223}$$

$$z_{C2} = t_{FT} + \frac{1}{2} h_2. \tag{5.224}$$

5.6.4.3 Dimensioning Procedure for Bended Structures

Superior load on bended structures comes from the bending moment $M_{\mathrm{B}}\,(\mathrm{Nmm})$. For both tension and compression, axial force in the analysed cap $F_{\mathrm{ax}}\,(\mathrm{N})$

$$F_{\mathrm{ax}} = \frac{M_{\mathrm{B}}}{h_{\mathrm{ef}}} \tag{5.225}$$

where effective height $h_{\mathrm{ef}}\,(\mathrm{mm})$ is in this work considered

$$h_{\mathrm{ef}} = 0.95h. \tag{5.226}$$

The estimation of cross-section area of tensed flange $A_{\mathrm{CTest}}\,(\mathrm{mm}^2)$ under the ultimate bending moment $M_{\mathrm{BU}}\,(\mathrm{Nmm})$

$$A_{\mathrm{CTest}} = \frac{1}{S_{\mathrm{T}}} F_{\mathrm{ax}} \tag{5.227}$$

and so the estimated thickness of tensed cap $t_{\mathrm{CTest}}\,(\mathrm{mm}^2)$

$$t_{\mathrm{CTest}} = \frac{A_{\mathrm{FTest}}}{w}. \tag{5.228}$$

Similarly for compressed cap

$$A_{\mathrm{CCest}} = \frac{1}{S_{\mathrm{C}}} F_{\mathrm{ax}}, \tag{5.229}$$

$$t_{\mathrm{CCest}} = \frac{A_{\mathrm{FCest}}}{w}. \tag{5.230}$$

Having estimated the geometry of tensed and compressed caps, the estimated moment of inertia $I_{y\mathrm{est}}\,(\mathrm{mm}^4)$ derived in Subsection 5.6.4.2

$$I_{y\mathrm{est}}(x) = f(h(x), t_{\mathrm{CTest}}(x), t_{\mathrm{CCest}})(x), \tag{5.231}$$

the estimated stress in tensed cap $\sigma_{\mathrm{CTest}}\left(\frac{\mathrm{N}}{\mathrm{mm}^2}\right)$

$$\sigma_{\mathrm{CTest}}(x) = \frac{M_{\mathrm{BU}}(x)}{I_{y\mathrm{est}}(x)} z_{\mathrm{Cest}}(x) \tag{5.232}$$

and the estimated stress in compressed cap $\sigma_{\mathrm{CCest}}\left(\frac{\mathrm{N}}{\mathrm{mm}^2}\right)$

$$\sigma_{\mathrm{CCest}}(x) = \frac{M_{\mathrm{BU}}(x)}{I_{y\mathrm{est}}(x)} \left(h(x) - z_{\mathrm{Cest}}(x)\right). \tag{5.233}$$

It is necessary to do a stress check. Estimated levels of stress under ultimate load must not exceed the material strength.

$$\sigma_{\mathrm{CTest}}(x) < S_{\mathrm{T}}, \tag{5.234}$$

$$\sigma_{\mathrm{CCest}}(x) < S_{\mathrm{C}}. \tag{5.235}$$

If the stress level exceeds the material strength, thickness of tensed and compressed caps are to be gradually enlarged to optimised values $t_{\mathrm{CTopt}}\,(\mathrm{mm})$ and $t_{\mathrm{CCopt}}\,(\mathrm{mm})$. These are then used to calculate $I_{y\mathrm{opt}}\,(\mathrm{mm}^4)$, $\sigma_{\mathrm{CTopt}}\left(\frac{\mathrm{N}}{\mathrm{mm}^2}\right)$ and $\sigma_{\mathrm{CCopt}}\left(\frac{\mathrm{N}}{\mathrm{mm}^2}\right)$ respectively, until the stress check complies.

5.6.4.4 Arm Dimensioning

In forward flight at the angle of attack $\alpha\,(°)$, upper arms are expected to be loaded more than the lower ones. Obviously, since all the arms are going to be manufactured identical, it is sufficient to account for the upper arms loads only.
Arm local coordinate system $(x_{\text{arm}}, y_{\text{arm}}, z_{\text{arm}})$ was set.

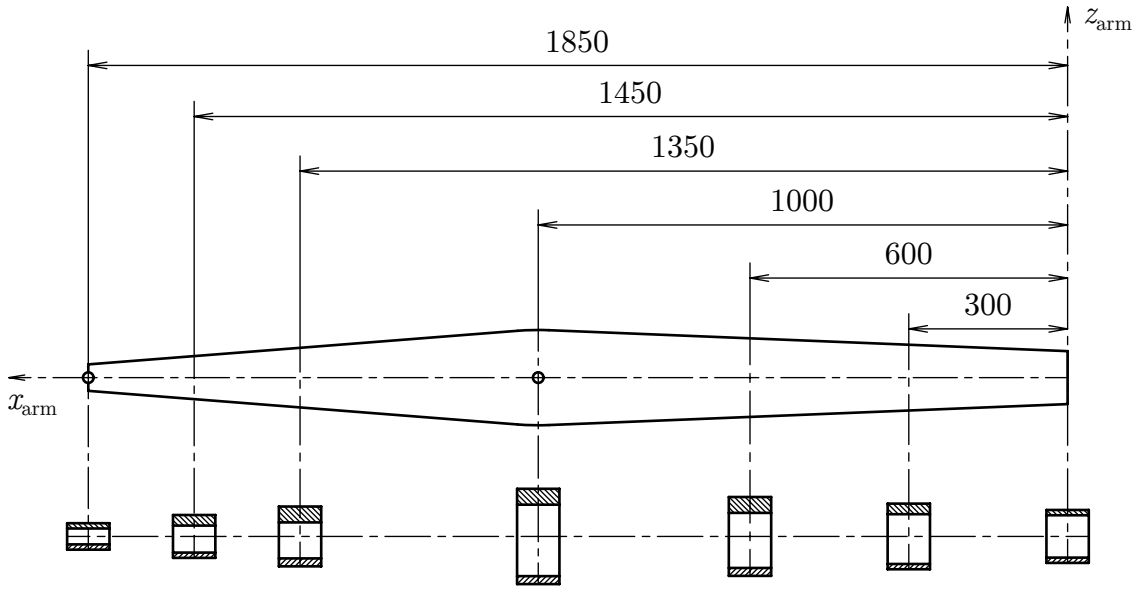

Figure 5.76: Cross-section breakdown of arm geometry.

While the width of the arm cross-sections $w = 80\text{mm}$ is constant, height $h(x_{\text{arm}})\,(\text{mm})$ varies along the x-axis and so the effective height $h_{\text{ef}}(x_{\text{arm}})\,(\text{mm})$

$$h_{\text{ef}}(x_{\text{arm}}) = 0.95h(x_{\text{arm}}). \tag{5.236}$$

The ultimate bending moment $M_{\text{BU}}(x_{\text{arm}})\,(\text{Nmm})$ acting on the outer arm $x_{\text{arm}} \in [0; l_{\text{UA2}}]$

$$M_{\text{BU}}(x_{\text{gr}}) = T_{\text{E2U}} x_{\text{arm}} \tag{5.237}$$

and the ultimate bending moment $M_{\text{BU}}(x_{\text{arm}})\,(\text{Nmm})$ acting on the inner arm $x_{\text{arm}} \in \left[l_{\text{UA2}}; l_{\text{UA2}} + \frac{l_{\text{UA7}} - D_{\text{UA1}}}{2}\right]$

$$M_{\text{BU}}(x_{\text{arm}}) = T_{\text{E2U}} x_{\text{arm}} - R_{21z\text{U}}\left(x_{\text{arm}} - l_{\text{UA2}}\right). \tag{5.238}$$

Table 5.22: Arm dimensioning parameters.

	x_{arm} (mm)						
	0	300	600	1000	1450	1650	1850
M_{BU} (Nmm)	0.00E+0	1.06E+7	2.13E+7	3.54E+7	1.67E+7	8.34E+6	0.00E+0
h (mm)	100	124	149	180	113	81	50
h_{ef} (mm)	95.00	117.80	141.55	171.00	107.35	76.95	47.50
w (mm)				80			
A_{CCest} (mm^2)	0.00	180.50	300.42	414.47	310.69	216.72	0.00
t_{CCest} (mm)	0.00	2.26	3.76	5.18	3.88	2.71	0.00
A_{CTest} (mm^2)	0.00	90.25	150.21	207.24	155.35	108.36	0.00
t_{CTest} (mm)	0.00	1.13	1.88	2.59	1.94	1.35	0.00
$I_{y\text{est}}$ (mm^4)	-	9.02E+5	2.14E+6	4.29E+6	1.25E+6	4.50E+5	-
σ_{CCest} $\left(\frac{\text{N}}{\text{mm}^2}\right)$	0	494	502	507	514	512	0
σ_{CTest} $\left(\frac{\text{N}}{\text{mm}^2}\right)$	0	968	976	982	989	990	0
t_{CCopt} (mm)	2.0	2.5	4.0	5.5	4.0	3.0	2.0
t_{CTopt} (mm)	2.0	2.0	2.0	3.0	2.0	2.0	2.0
$I_{y\text{opt}}$ (mm^4)	7.68E+5	1.32E+6	2.27E+6	4.80E+6	1.29E+6	5.92E+5	1.84E+5
σ_{CCopt} $\left(\frac{\text{N}}{\text{mm}^2}\right)$	0	447	474	478	499	464	0
σ_{CTopt} $\left(\frac{\text{N}}{\text{mm}^2}\right)$	0	554	919	851	960	678	0

5.6.4.5 Fuselage Dimensioning

The fuselage local coordinate system $(x_{\text{fus}}, y_{\text{fus}}, z_{\text{fus}})$ was set.

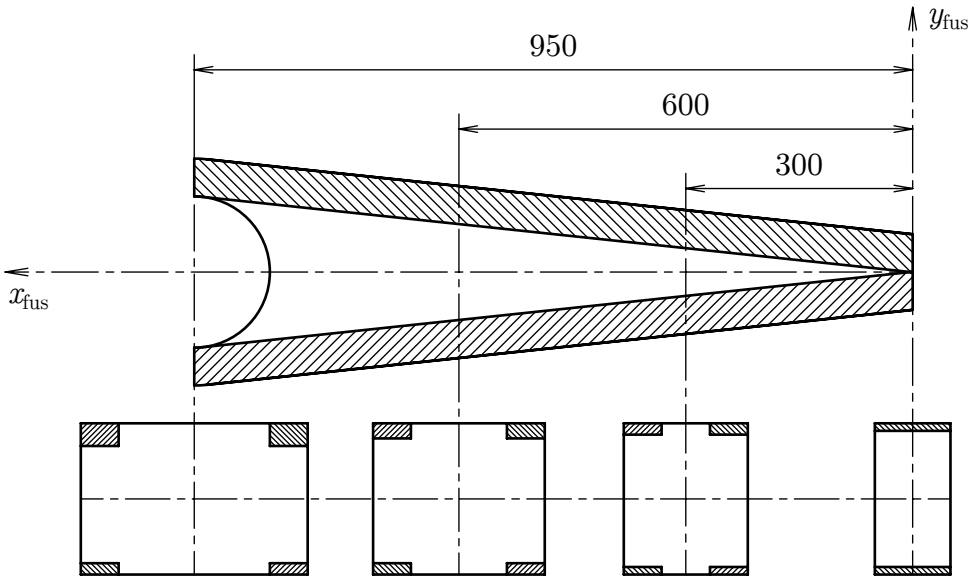

Figure 5.77: Cross-section breakdown of fuselage geometry.

The height of the fuselage $h = 200\text{mm}$ is constant and so the effective height h_{ef} (mm)

$$h_{\text{ef}} = 0.95 \cdot h = 0.95 \cdot 200 = 190\text{mm}. \tag{5.239}$$

The width of the fuselage cross-section varies along the x-axis but the caps are split into two stripes of constant width being $w = 100\text{mm}$ in total on both upper and lower cap.

The ultimate bending moment $M_{\text{BU}}(x_{\text{fus}})$ (Nmm) acting on the fuselage $x_{\text{fus}} \in \left[0; \frac{l_{\text{UA7}}}{2}\right]$

$$M_{\text{BU}}(x_{\text{gr}}) = R_{21z\text{U}} x_{\text{fus}}. \tag{5.240}$$

Since the axial reaction force $R_{3x\text{U}}$ (N) is introduced to the compressed cap, it needs to be accounted for in the estimation of the cross-section area A_{CCest} (mm^2)

$$A_{\text{CCest}} = \frac{1}{S_{\text{C}}} \left(\frac{M_{\text{BU}}(x_{\text{fus}})}{h_{\text{ef}}} + R_{3x\text{U}} \right) \tag{5.241}$$

and then in the stress calculations

$$\sigma_{\text{CCest}}(x_{\text{fus}}) = \frac{M_{\text{BU}}(x_{\text{fus}})}{I_{y\text{est}}(x_{\text{fus}})} \left(h - z_{\text{Cest}}(x_{\text{fus}})\right) + \frac{R_{3x\text{U}}}{A_{\text{CCest}}(x_{\text{fus}})}. \tag{5.242}$$

Table 5.23: Fuselage dimensioning parameters.

	x_{fus} (mm)			
	0	300	600	950
M_{BU} (Nmm)	0.00E+0	2.31E+7	4.63E+7	7.33E+7
h (mm)		200		
h_{ef} (mm)		190		
w (mm)		100		
A_{CCest} (mm^2)	22.28	253.67	485.05	755.00
t_{CCest} (mm)	0.22	2.54	4.85	7.55
A_{CTest} (mm^2)	0.00	115.69	231.39	366.36
t_{CTest} (mm)	0.00	1.16	2.31	3.66
$I_{y\text{est}}$ (mm^4)	8.87E-2	3.13E+6	6.04E+6	9.32E+6
σ_{CCest} $\left(\frac{\text{N}}{\text{mm}^2}\right)$	500	513	527	543
σ_{CTest} $\left(\frac{\text{N}}{\text{mm}^2}\right)$	0	1011	1029	1044
t_{CCopt} (mm)	2.0	3.0	5.5	8.5
t_{CTopt} (mm)	2.0	2.0	2.5	4.0
$I_{y\text{opt}}$ (mm^4)	3.92E+6	4.68E+6	6.60E+6	1.02E+7
σ_{CCopt} $\left(\frac{\text{N}}{\text{mm}^2}\right)$	56	435	469	488
σ_{CTopt} $\left(\frac{\text{N}}{\text{mm}^2}\right)$	0	591	953	959

5.6.4.6 Undercarriage Dimensioning

The undercarriage legs are planned to be built with glass fibre with unidirectional carbon fibre reinforced caps.
The arm local coordinate system $(x_{\mathrm{gr}}, y_{\mathrm{gr}}, z_{\mathrm{gr}})$ was set.

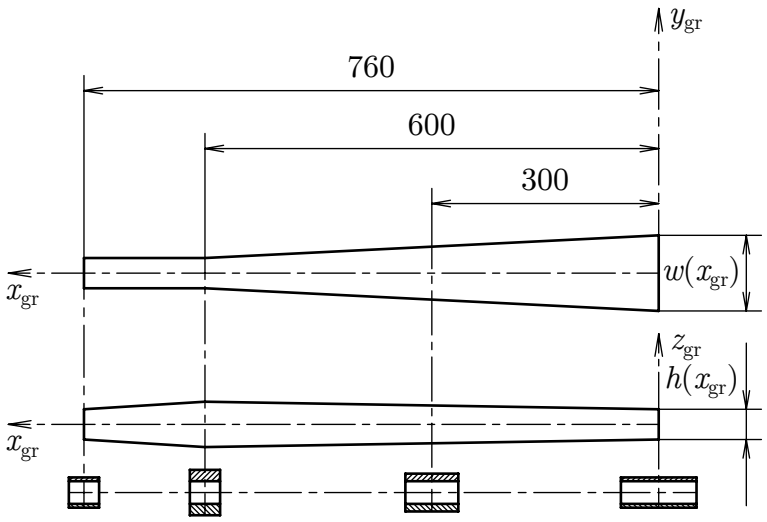

Figure 5.78: Cross-section breakdown of undercarriage leg geometry.

Both width $w(x_{\mathrm{gr}})\,(\mathrm{mm})$ and height $h(x_{\mathrm{gr}})\,(\mathrm{mm})$ vary along the x-axis.

The ultimate bending moment $M_{\mathrm{BU}}(x_{\mathrm{gr}})\,(\mathrm{Nmm})$ acting on the outer undercarriage leg $x_{\mathrm{gr}} \in [0; l_{\mathrm{gr1}}]$

$$M_{\mathrm{BU}}(x_{\mathrm{gr}}) = F_{\mathrm{gnd}z\mathrm{U}} x_{\mathrm{gr}} \tag{5.243}$$

and the ultimate bending moment $M_{\mathrm{BU}}(x_{\mathrm{gr}})\,(\mathrm{Nmm})$ acting on the inner undercarriage leg $x_{\mathrm{gr}} \in [l_{\mathrm{gr1}}; l_{\mathrm{gr1}} + l_{\mathrm{gr2}}]$

$$M_{\mathrm{BU}}(x_{\mathrm{gr}}) = F_{\mathrm{gnd}z\mathrm{U}} x_{\mathrm{gr}} - R_{\mathrm{BU}}\left(x_{\mathrm{gr}} - l_{\mathrm{gr1}}\right). \tag{5.244}$$

Since the axial force $F_{\mathrm{gnd}x\mathrm{U}}\,(\mathrm{N})$ is introduced to the compressed cap, it needs to be accounted for in the estimation of cross-section area $A_{\mathrm{CCest}}\,(\mathrm{mm}^2)$

$$A_{\mathrm{CCest}}(x_{\mathrm{gr}}) = \frac{1}{S_{\mathrm{C}}}\left(\frac{M_{\mathrm{BU}}(x_{\mathrm{gr}})}{h_{\mathrm{ef}}(x_{\mathrm{gr}})} + F_{\mathrm{gnd}x\mathrm{U}}\right) \tag{5.245}$$

and then in the stress calculations

$$\sigma_{\mathrm{CCest}}(x_{\mathrm{gr}}) = \frac{M_{\mathrm{BU}}(x_{\mathrm{gr}})}{I_{y\mathrm{est}}(x_{\mathrm{gr}})}\left(h(x_{\mathrm{gr}}) - z_{\mathrm{Cest}}(x_{\mathrm{gr}})\right) + \frac{F_{\mathrm{gnd}x\mathrm{U}}}{A_{\mathrm{CCest}}(x_{\mathrm{gr}})}. \tag{5.246}$$

Table 5.24: Undercarriage leg dimensioning parameters.

	x_{gr} (mm)			
	0	300	600	760
M_{BU} (Nmm)	0.00E+0	1.09E+6	2.18E+6	0.00E+0
h (mm)	40	50	60	40
h_{ef} (mm)	38	48	57	38
w (mm)	100	70	40	40
A_{CCest} (mm^2)	7.25	53.05	83.59	7.25
t_{CCest} (mm)	0.07	0.76	2.09	0.18
$I_{y\mathrm{est}}$ (mm^4)	5.82E+3	6.43E+4	1.40E+5	5.74E+3
σ_{CCest} $\left(\frac{\mathrm{N}}{\mathrm{mm}^2}\right)$	500	491	509	500
t_{CCopt} (mm)	1.0	2.0	2.2	1.0
$I_{y\mathrm{opt}}$ (mm^4)	7.61E+4	1.61E+5	1.35E+5	3.04E+4
σ_{CCopt} $\left(\frac{\mathrm{N}}{\mathrm{mm}^2}\right)$	36	194	485	91

Conclusion

In the initial phase, a conceptual study was done. Input parameters such as propeller diameter, angular deflection in landing, required space for the equipment housing or position of battery packs were taken into consideration for preliminary sizing.
In order to put together a performance study, the drag characteristics of the UAS had to be established. Obviously, the size of the aerostat has the largest impact on the overall drag. To assess the final aerostat diameter, the weight loading was estimated.
Required power was studied for the cases of hover, axial climb and descent and forward flight. Considering the power and simplified flight plan requirements, the required battery capacity and mass were calculated. The general performance study was then narrowed and presented for a case of 600 kg payload.
Based on the performance study, the loads acting on the structure in the case of 1100 kg payload were used for the strength analysis. As a reference for the initial calculations, the EASA and NAA Certification Specifications for helicopters were used.

The designed concept is realistic. Calculated power requirements are achievable by contemporary available technologies for an affordable price.
The flight mechanics of the UAS is to be tested and many issues associated with the dimensions and behavior of the aerostat are expected to arise.
The required strength to withstand both flight and ground loads does not require the structure to be inappropriately large or heavy for aerial application.
The stiffness of the UA might be a challenging issue. The requirement for the UA to be an easy to compile assembly introduces quite a number of critical design features. These have to be designed to provide stiff enough joints with as little tolerances as possible.

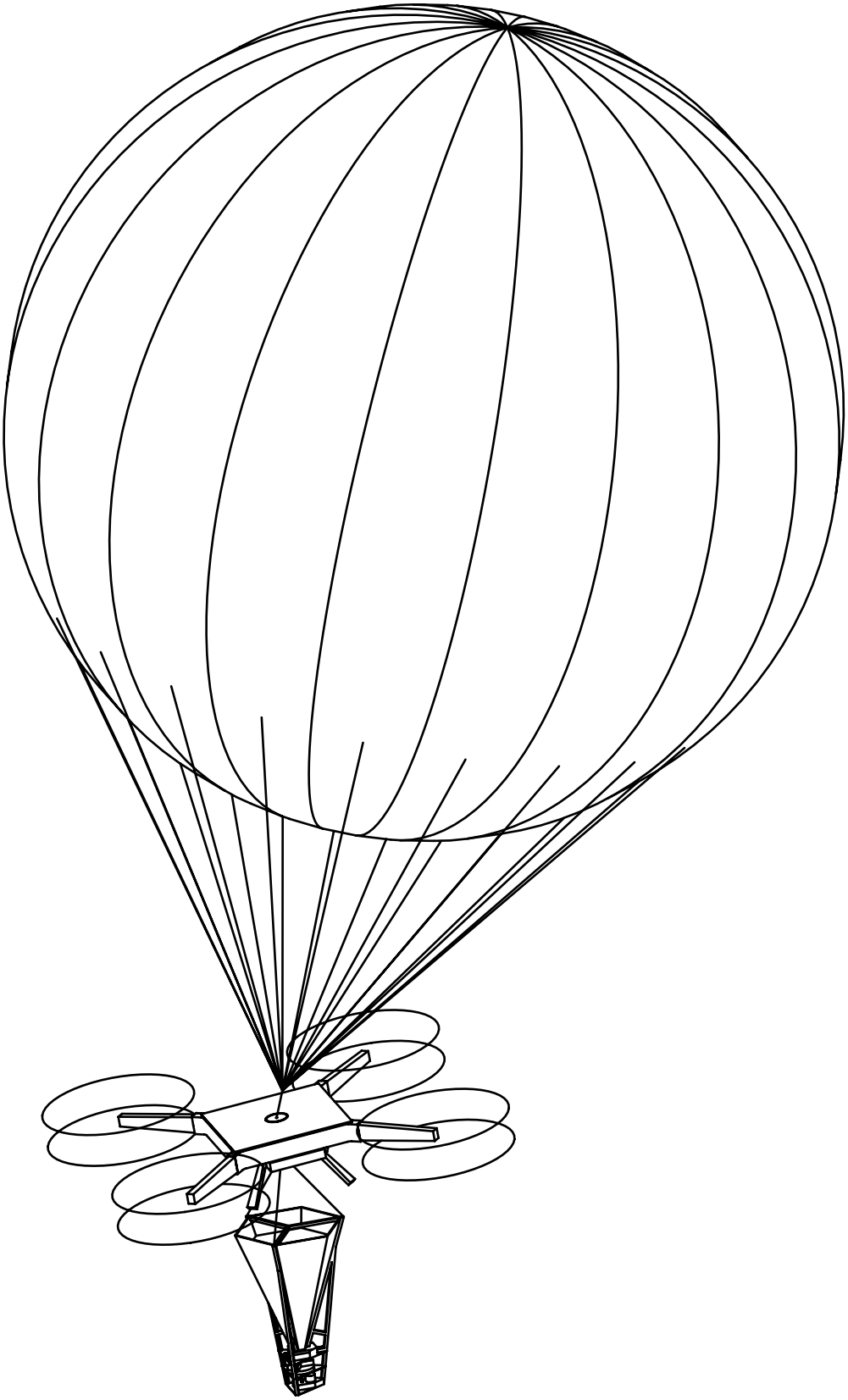

Figure 5.79: Visualization of the UAS.

Bibliography

[1] McQuarrie DA, Simon JD. *Physical Chemistry a molecular approach*. University Science Books. USA. 1997.

[2] Munson BR, Young DF, Okiishi TH. *Fundamentals of Fluid Mechanics*. 4 ed. John Wiley & Sons, Inc.. USA. 2002.

[3] White FM, Chul RY. *Fluid Mechanics*. McGraw-Hill Education. 2016.

[4] Bertin J, Cummings R. *Aerodynamics for Engineers*. 6 ed. Pearson. 2014.

[5] Dr.-Ing. Hoerner, SF. *Fluid-dynamic drag; theoretical, experimental and statistical information*. Published by the Author. USA. 1965.

[6] Leishman, JG. *Principles of Helicopter Aerodynamics*. Cambridge University Press. 2002.

[7] Raymer DP. *Aircraft Design: A Conceptual Approach*. American Institute of Aeronautics and Astronautics. 1992.

[8] Achenbach E. *Experiments on the flow past spheres at very high Reynolds numbers*. Kernforschungsanlage Julich GmbH, Julich, Germany. In: *J. Fluid Mech., Volume 54, Part 3*. Printed in Great Britain. 1972. Pages 565-575

[9] Lo KH, Chim ES-M. *Compressive Strength of Unidirectional Composites*. Shell Development Company Westhollow Research Center, Houston, Texas, USA. In: *Journal of Reinforced Plastics and Composites, Volume 2*. 1992. Pages 838-896

[10] Naik NK, Kumar RS. *Compressive Strength of Unidirectional Composites: Evaluation and Comparison of Prediction Models*. Department of Aerospace Engineering, Indian Institute of Technology, Powai, Mumbai 400 076, India. In: *Composite Structures, Volume 46, Issue 3*. November 1999. Pages 299-308

[11] International Civil Aviation Organization: *Doc 7488/3 Manual of the ICAO Standard Atmosphere extended to 80 kilometres (262 500 feet)*. 3 ed. International Civil Aviation Organization. 1993.

[12] European Aviation Safety Agency: *Easy Access Rules for Unmanned Aircraft Systems*. European Aviation Safety Agency. April 2021. [Accessed April 10, 2021]. URL <https://www.easa.europa.eu/sites/default/files/dfu/Easy%20Access%20Rules%20for%20Unmanned%20Aircraft%20Systems_0.pdf>

[13] European Aviation Safety Agency: *Certification Specifications for Very Light Aeroplanes CS-VLA*. Amendment 1. European Aviation Safety Agency, 5 March 2009. [Accessed July 19, 2021]. URL <https://www.easa.europa.eu/sites/default/files/dfu/CS-VLA%20%20Amdt%201%20combined.pdf>

[14] European Aviation Safety Agency: *Certification Specifications and Acceptable Means of Compliance for Free Gas Balloons CS-31GB*. Initial Issue. European Aviation Safety Agency, 5 December 2011. [Accessed April 28, 2021]. URL <https://www.easa.europa.eu/sites/default/files/dfu/CS-31GB%20Initial%20Issue.pdf>

[15] European Aviation Safety Agency: *Certification Specifications, Acceptable Means of Compliance and Guidance Material for Small Rotorcraft CS-27*. Amendment 8. European Aviation Safety Agency, 14 June 2021. [Accessed June 30, 2021]. URL <https://www.easa.europa.eu/sites/default/files/dfu/cs-27_amendment_8.pdf>

[16] European Aviation Safety Agency: *Certification Specifications, Acceptable Means of Compliance and Guidance Material for Large Rotorcraft CS-29*. Amendment 9. European Aviation Safety Agency, 14 June 2021. [Accessed June 30, 2021]. URL <https://www.easa.europa.eu/sites/default/files/dfu/cs-29_amendment_9.pdf>

[17] Federal Aviation Administration: *Advisory Circular: Certification of Normal Category Rotorcraft AC 27-1B*. Change 8. Federal Aviation Administration, 29 June 2018. [Accessed June 30, 2021]. URL <https://www.faa.gov/documentLibrary/media/Advisory_Circular/AC_27-1B_with_changes_1-8.pdf>

[18] Federal Aviation Administration: *Advisory Circular: Certification of Transport Category Rotorcraft AC 29-2C*. Change 8. Federal Aviation Administration, 2 July 2018. [Accessed June 30, 2021]. URL <https://www.faa.gov/documentLibrary/media/Advisory_Circular/AC_29-2C_with_changes_1-8.pdf>

[19] Christopher Earls Brennen. *Drag on a Sphere and Cylinder*. [online]. ©2006. [Accessed March 28, 2021]. URL <http://brennen.caltech.edu/fluidbook/externalflows/drag/dragonasphere.pdf>

[20] First Flights to the Future. *Learn more about Boeing NeXt*. [online]. [Accessed August 15, 2021]. URL <https://www.boeing.com/features/frontiers/2019/autonomous-flying-vehicles/index.page>

[21] Boeing Future of Flight. *Cargo Air Vehicle (CAV)*. [online]. [Accessed August 20, 2021]. URL <https://www.boeingfutureofflight.com/cav>

[22] ACC Group. *Air Drone Range*. [online]. [Accessed August 15, 2021]. URL <https://acc-group.se/products-air-drones>

[23] Electric VTOL News. *Volocopter VoloDrone*. [online]. [Accessed August 15, 2021]. URL <https://evtol.news/volocopter-volodrone/>

[24] Griff Aviation. *The Griff Fleet*. [online]. [Accessed August 15, 2021]. URL <https://griffaviation.com/the-griff-fleet/>

[25] Boeing Future of Flight. *Cargo Air Vehicle Flight Testing*. [picture]. [Accessed August 20, 2021]. URL <https://www.boeingfutureofflight.com/cav>

[26] ACC Group. *Air Drones*. [picture]. [Accessed August 15, 2021]. URL <https://acc-group.se/>

[27] ACC Group. *Air and Sea Drone Thunder Wasp II*. [picture]. [Accessed August 15, 2021]. URL <https://acc-group.se/news/2019-6-24/thunder-wasp-ii-test-flights>

[28] ACC Group. *ACC Innovation Locust.* [picture]. [Accessed August 15, 2021]. URL <https://acc-group.se/products-air-drones>

[29] Volocopter. *VoloDrone.* [picture]. [Accessed August 15, 2021]. URL <https://www.volocopter.com/solutions/volodrone/>

[30] Griff Aviation. *Griff 135.* [picture]. [Accessed August 15, 2021]. URL <https://griffaviation.com/the-griff-fleet/>

[31] Boeing. *Cargo Air Vehicle advances through flight testing* [video]. [Accessed August 20, 2021]. URL <https://www.boeing.com/features/highlights/2020/cargo-air-vehicle>

Appendix 1:
Required Power in Hover

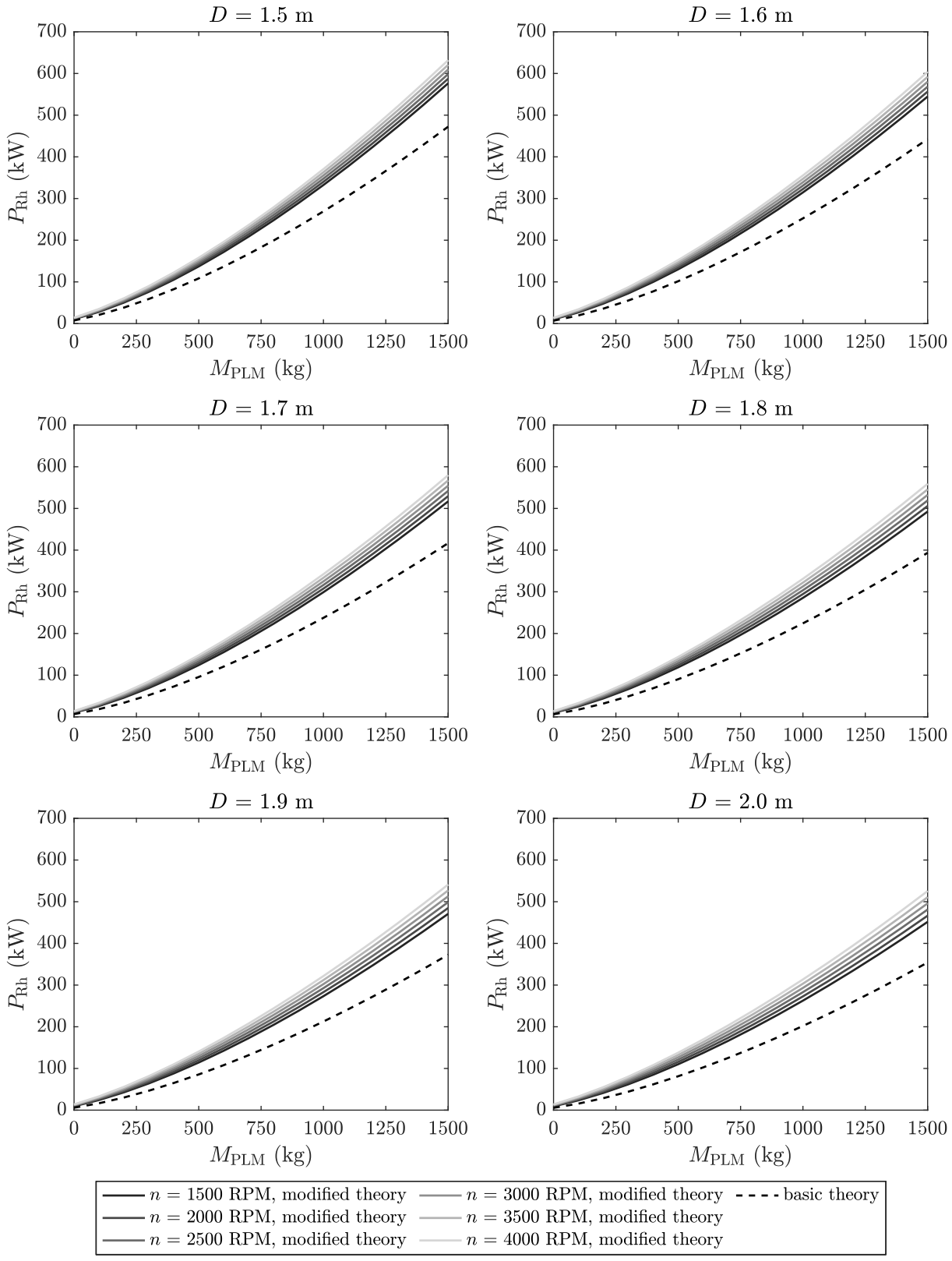

Figure 5.80: Required power in hover $P_{\mathrm{Rh}}\,(\mathrm{kW})$ as a function of payload mass $M_{\mathrm{PLM}}\,(\mathrm{kg})$
and propeller diameter $D\,(\mathrm{m})$ at various revolutions per minute $n\left(\frac{1}{\mathrm{min}}\right)$
by basic and modified theory.

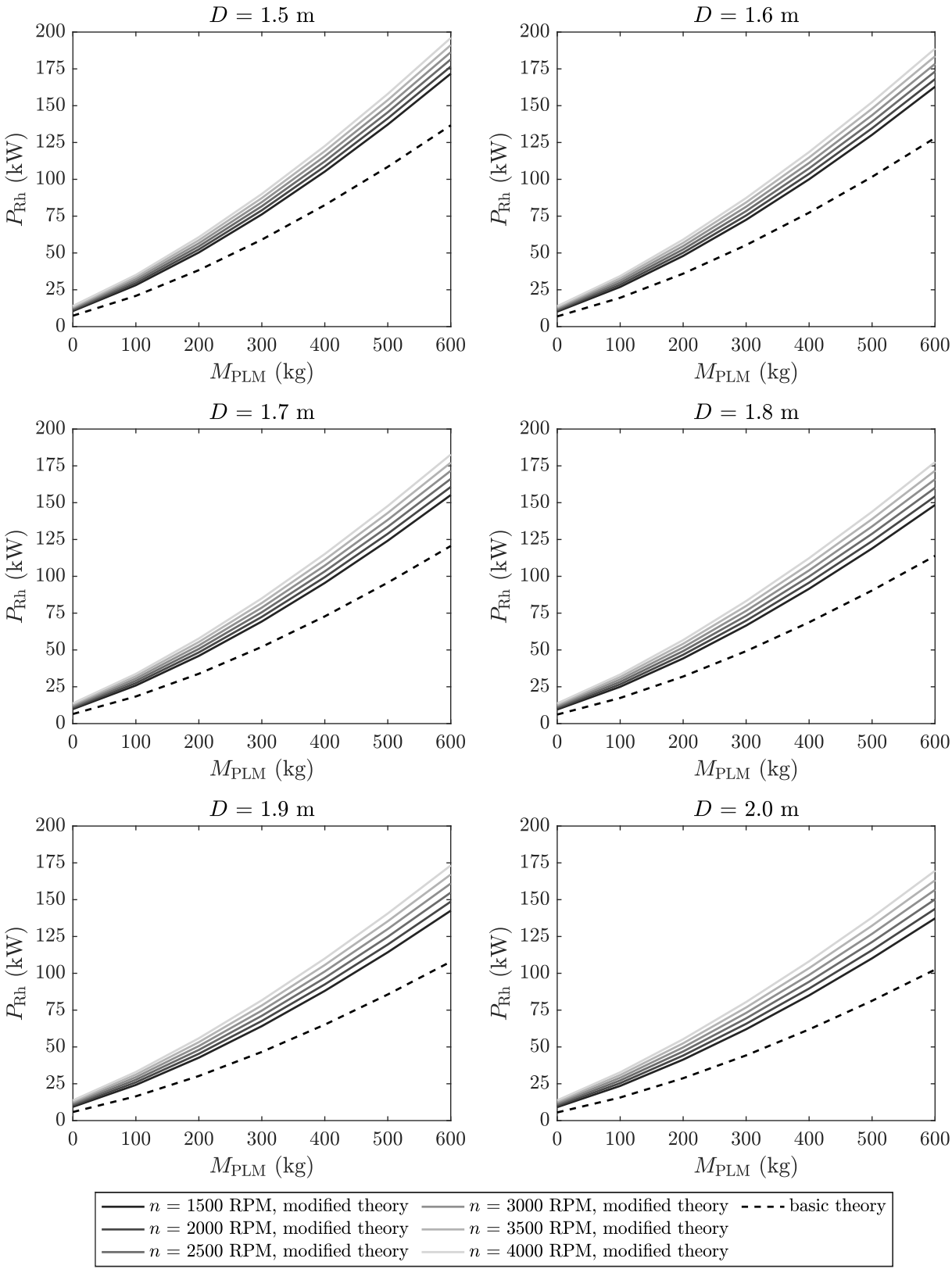

Figure 5.81: Required power in hover $P_{\mathrm{Rh}}\,(\mathrm{kW})$ as a function of payload mass $M_{\mathrm{PLM}}\,(\mathrm{kg})$
and propeller diameter $D\,(\mathrm{m})$ at various revolutions per minute $n\,\left(\frac{1}{\mathrm{min}}\right)$
by basic and modified theory; detail on light payload.

Appendix 2:
Required Power
in Axial Climb and Descend

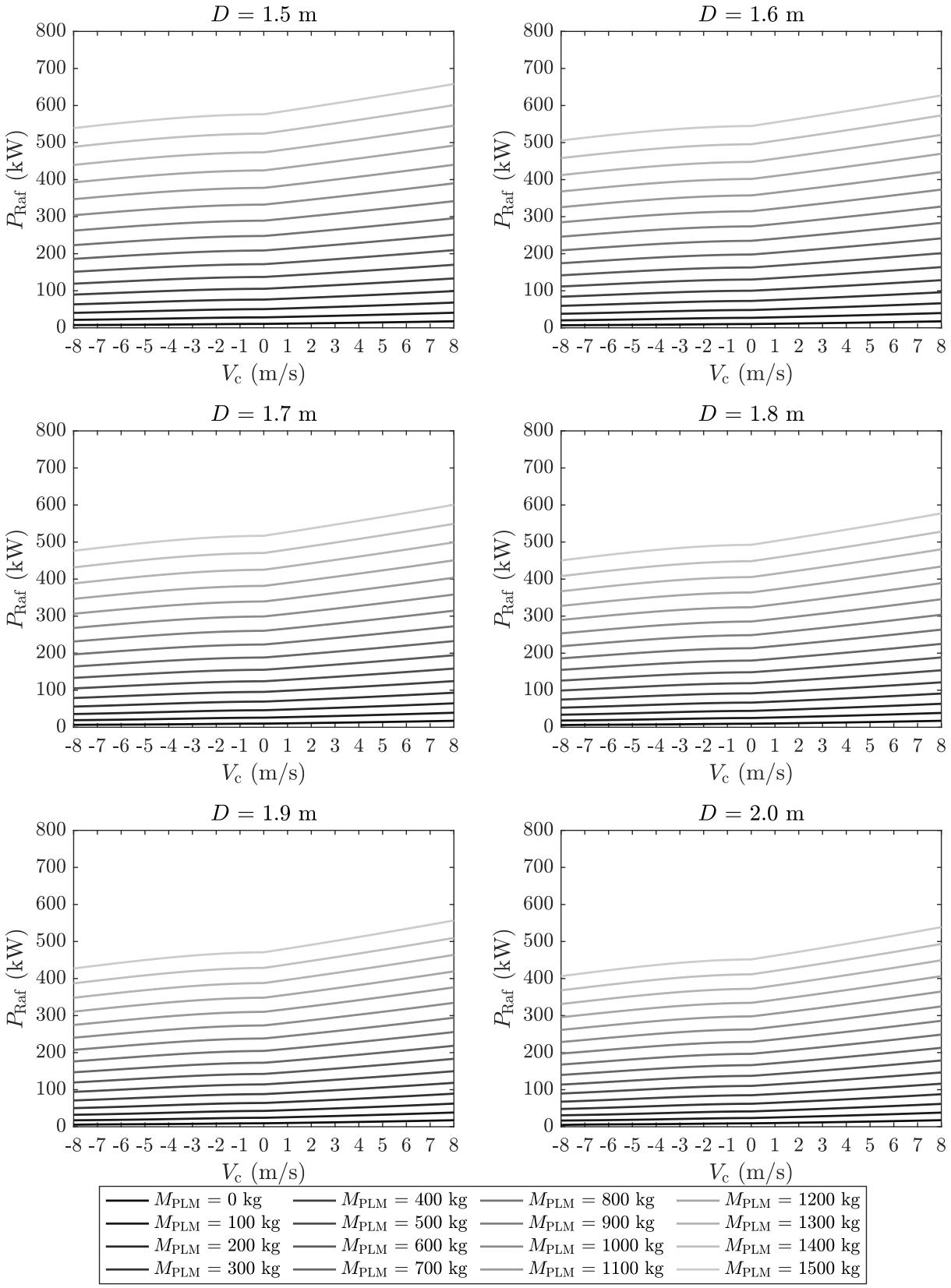

Figure 5.82: Required power in axial flight $P_{\mathrm{Raf}}\,(\mathrm{kW})$ as a function of climb velocity $V_{\mathrm{c}}\left(\frac{\mathrm{m}}{\mathrm{s}}\right)$
and payload mass $M_{\mathrm{PLM}}\,(\mathrm{kg})$ for various propeller diameter $D\,(\mathrm{m})$
at 1500 revolutions per minute $n\left(\frac{1}{\mathrm{min}}\right)$ in hover.

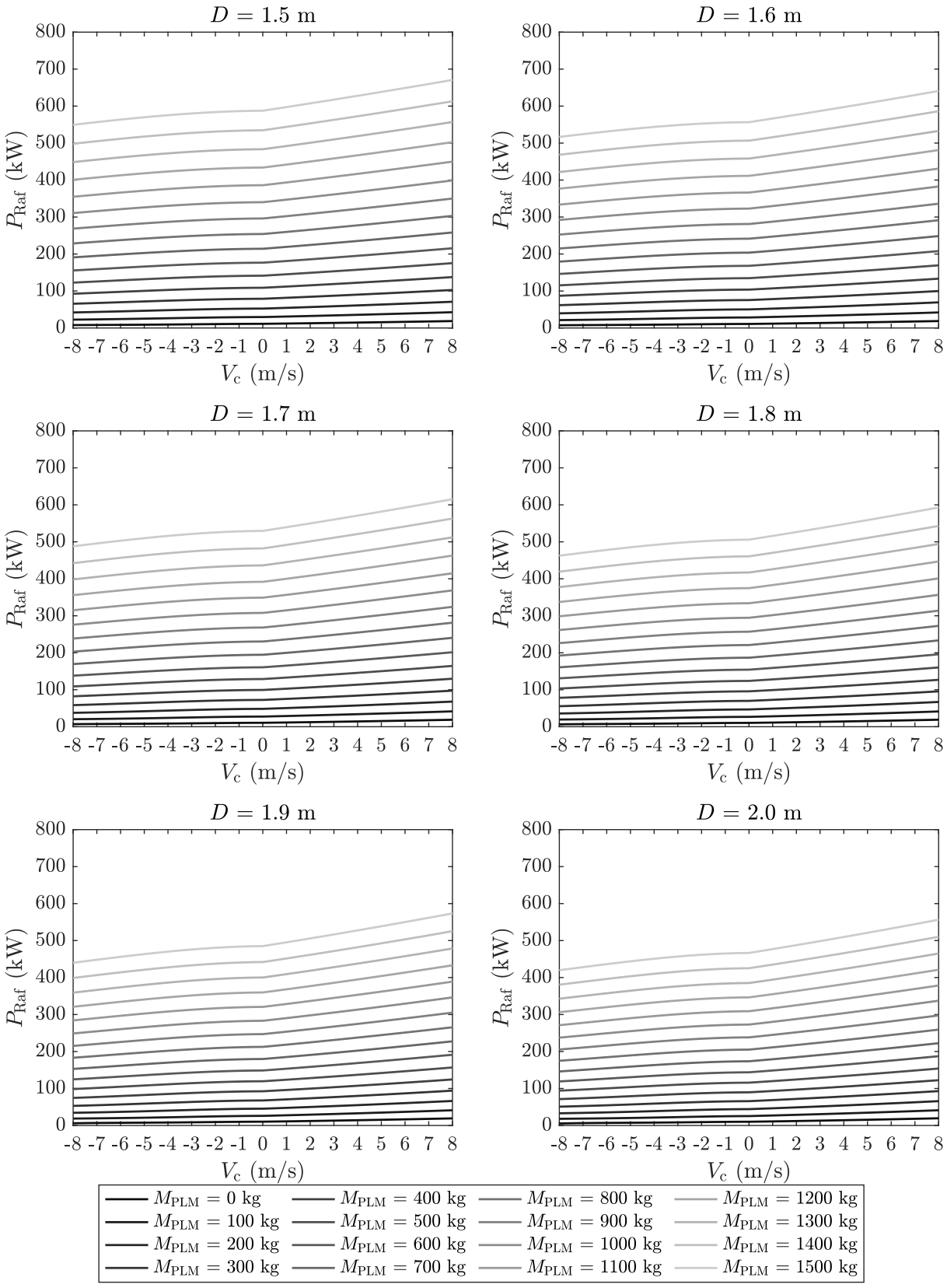

Figure 5.83: Required power in axial flight $P_{\mathrm{Raf}}\,(\mathrm{kW})$ as a function of climb velocity $V_{\mathrm{c}}\left(\frac{\mathrm{m}}{\mathrm{s}}\right)$
and payload mass $M_{\mathrm{PLM}}\,(\mathrm{kg})$ for various propeller diameter $D\,(\mathrm{m})$
at 2000 revolutions per minute $n\left(\frac{1}{\mathrm{min}}\right)$ in hover.

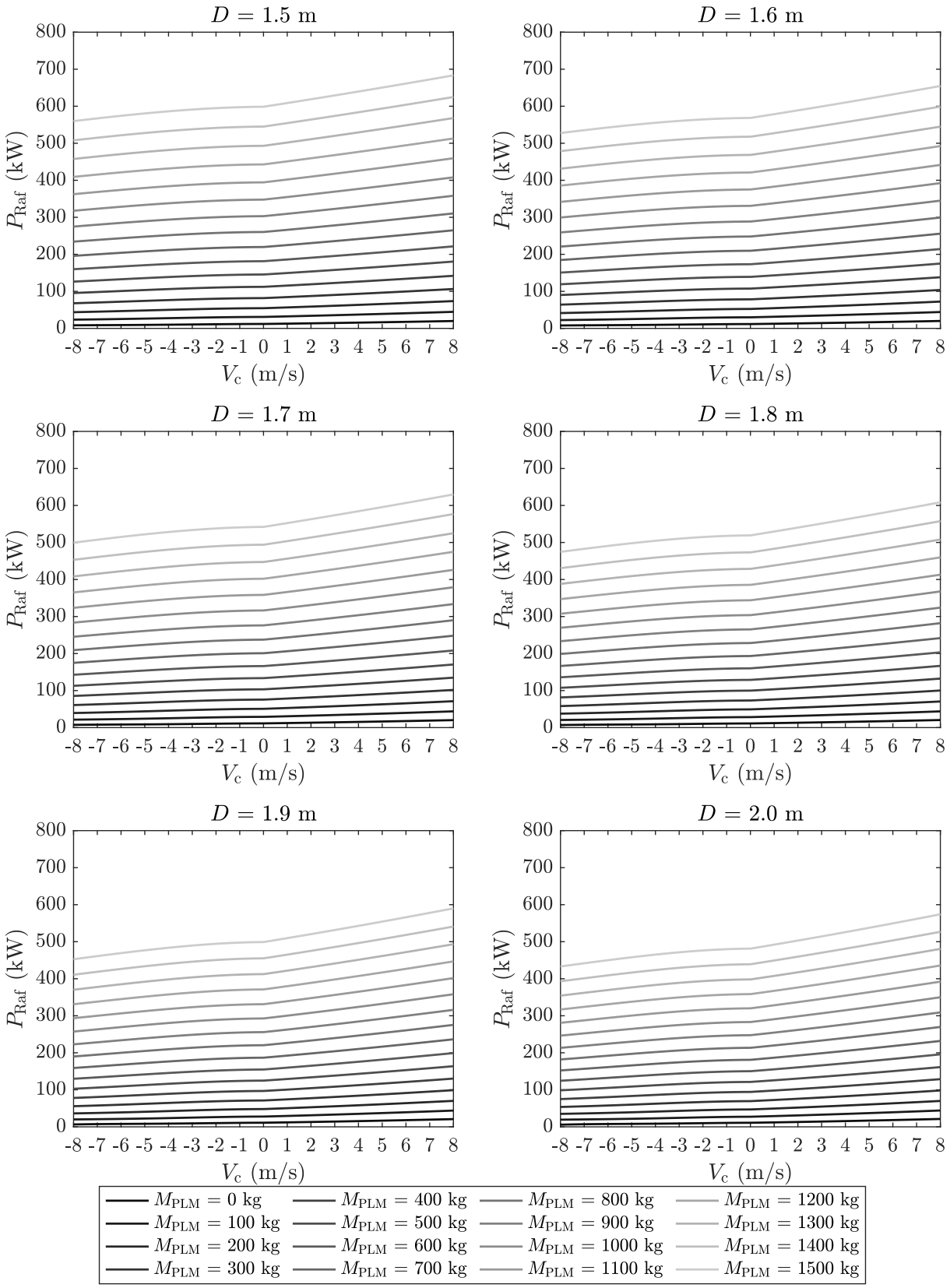

Figure 5.84: Required power in axial flight $P_{\mathrm{Raf}}\,(\mathrm{kW})$ as a function of climb velocity $V_{\mathrm{c}}\left(\frac{\mathrm{m}}{\mathrm{s}}\right)$
and payload mass $M_{\mathrm{PLM}}\,(\mathrm{kg})$ for various propeller diameter $D\,(\mathrm{m})$
at 2500 revolutions per minute $n\left(\frac{1}{\mathrm{min}}\right)$ in hover.

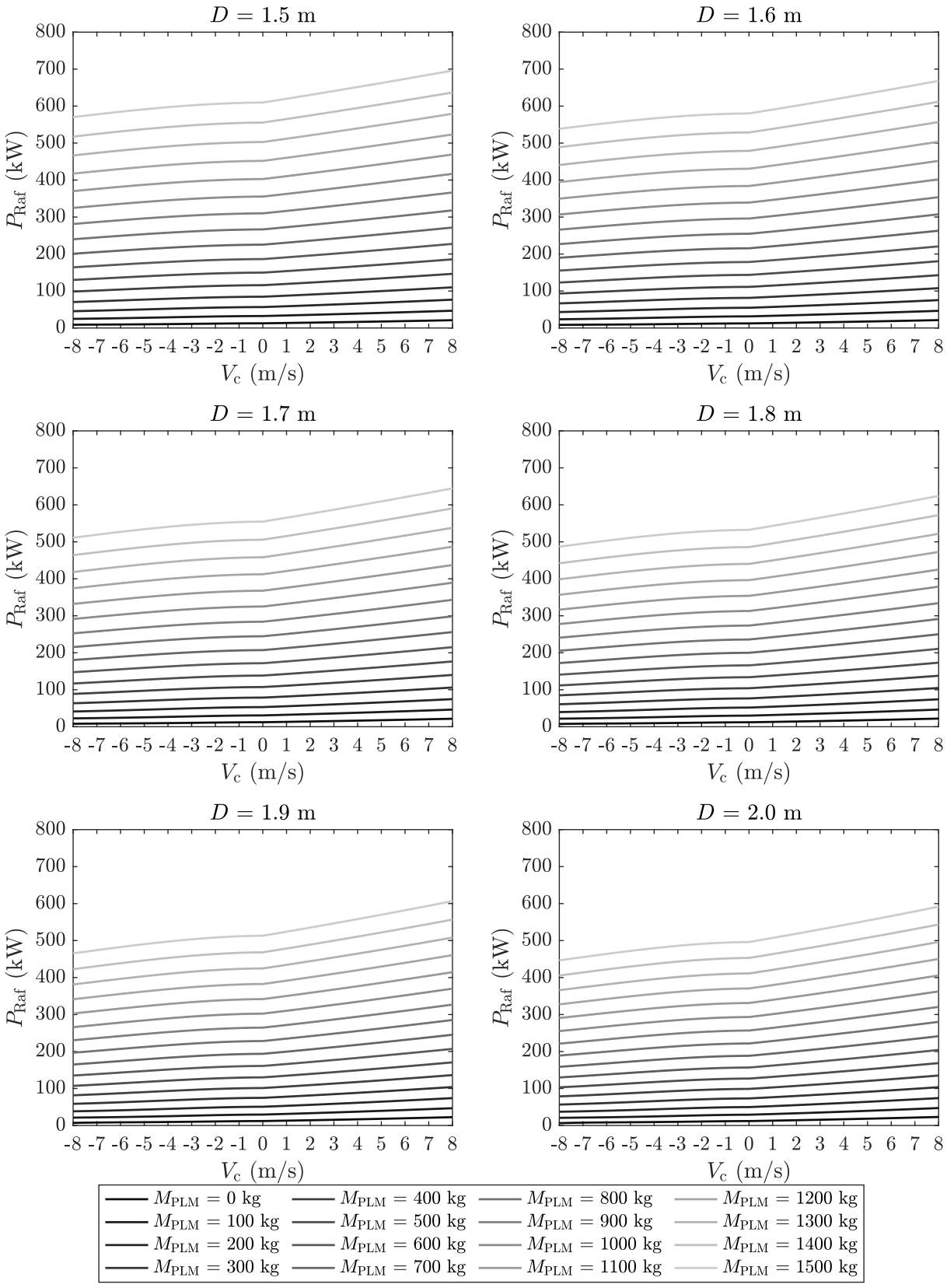

Figure 5.85: Required power in axial flight $P_{\mathrm{Raf}}\,(\mathrm{kW})$ as a function of climb velocity $V_{\mathrm{c}}\left(\frac{\mathrm{m}}{\mathrm{s}}\right)$
and payload mass $M_{\mathrm{PLM}}\,(\mathrm{kg})$ for various propeller diameter $D\,(\mathrm{m})$
at 3000 revolutions per minute $n\left(\frac{1}{\mathrm{min}}\right)$ in hover.

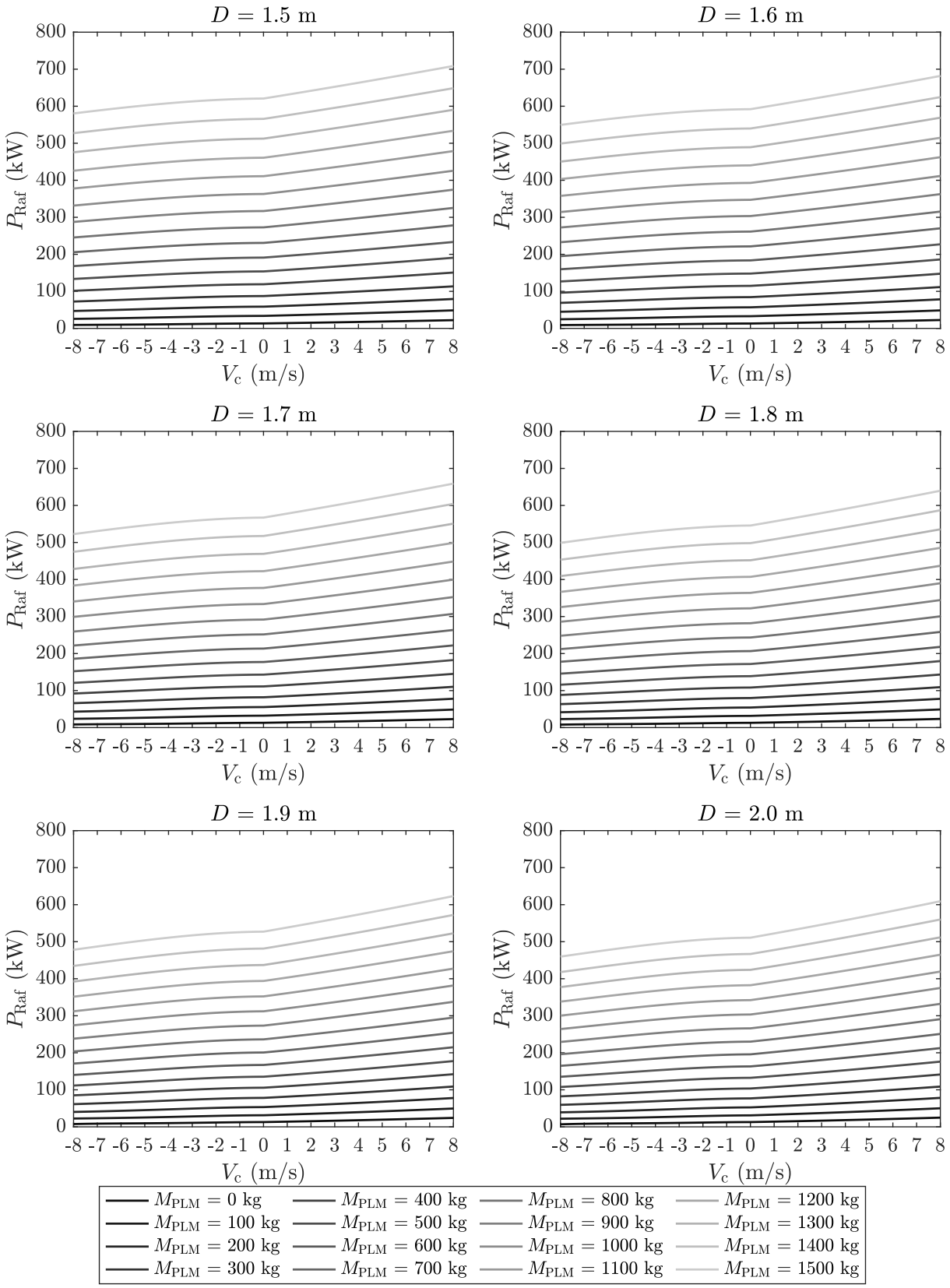

Figure 5.86: Required power in axial flight $P_{\mathrm{Raf}}\,(\mathrm{kW})$ as a function of climb velocity $V_{\mathrm{c}}\left(\frac{\mathrm{m}}{\mathrm{s}}\right)$
and payload mass $M_{\mathrm{PLM}}\,(\mathrm{kg})$ for various propeller diameter $D\,(\mathrm{m})$
at 3500 revolutions per minute $n\left(\frac{1}{\mathrm{min}}\right)$ in hover.

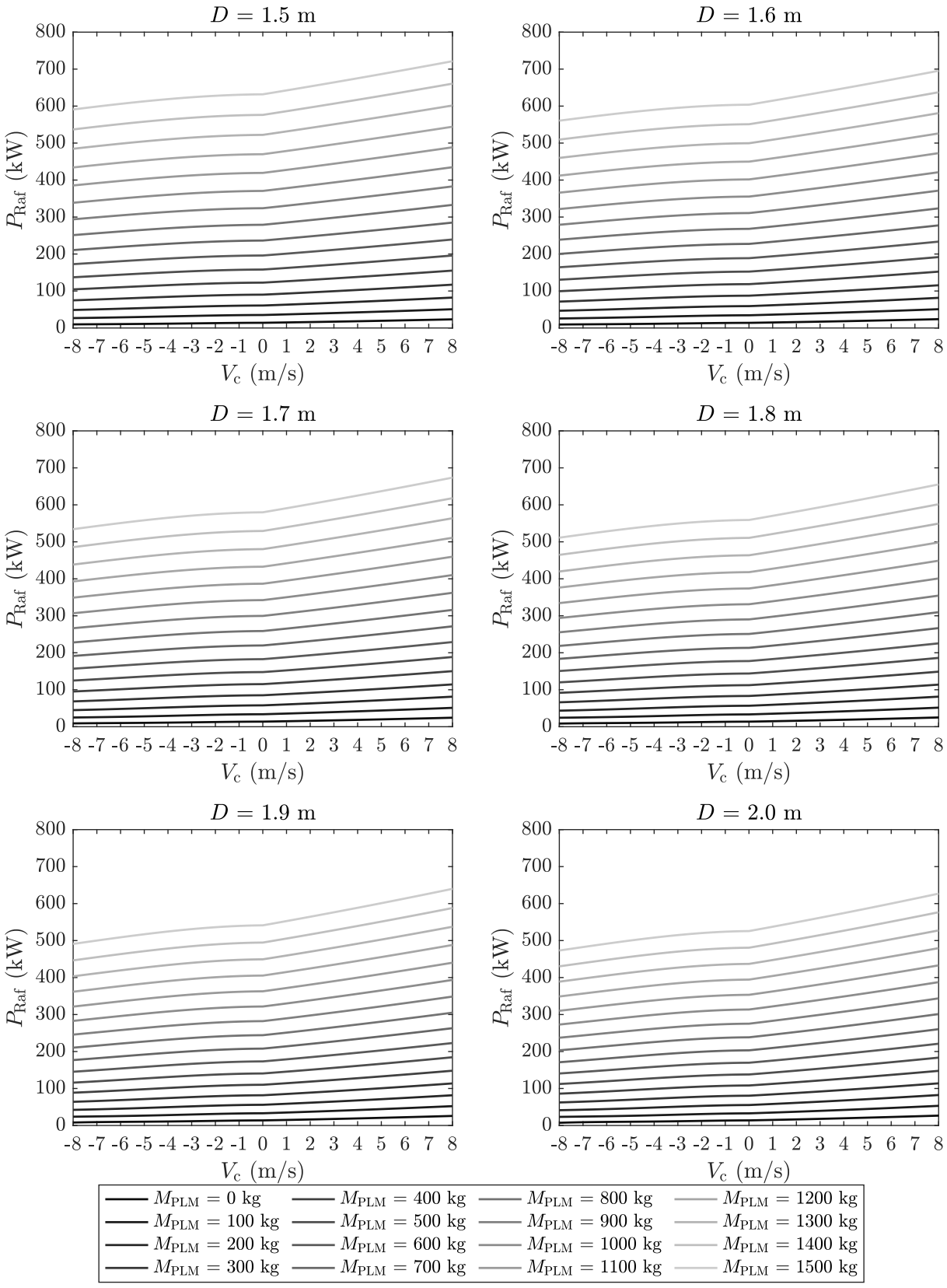

Figure 5.87: Required power in axial flight $P_{\mathrm{Raf}}\,(\mathrm{kW})$ as a function of climb velocity $V_{\mathrm{c}}\left(\frac{\mathrm{m}}{\mathrm{s}}\right)$
and payload mass $M_{\mathrm{PLM}}\,(\mathrm{kg})$ for various propeller diameter $D\,(\mathrm{m})$
at 4000 revolutions per minute $n\left(\frac{1}{\mathrm{min}}\right)$ in hover.

Appendix 3:
Required Power in Forward Flight

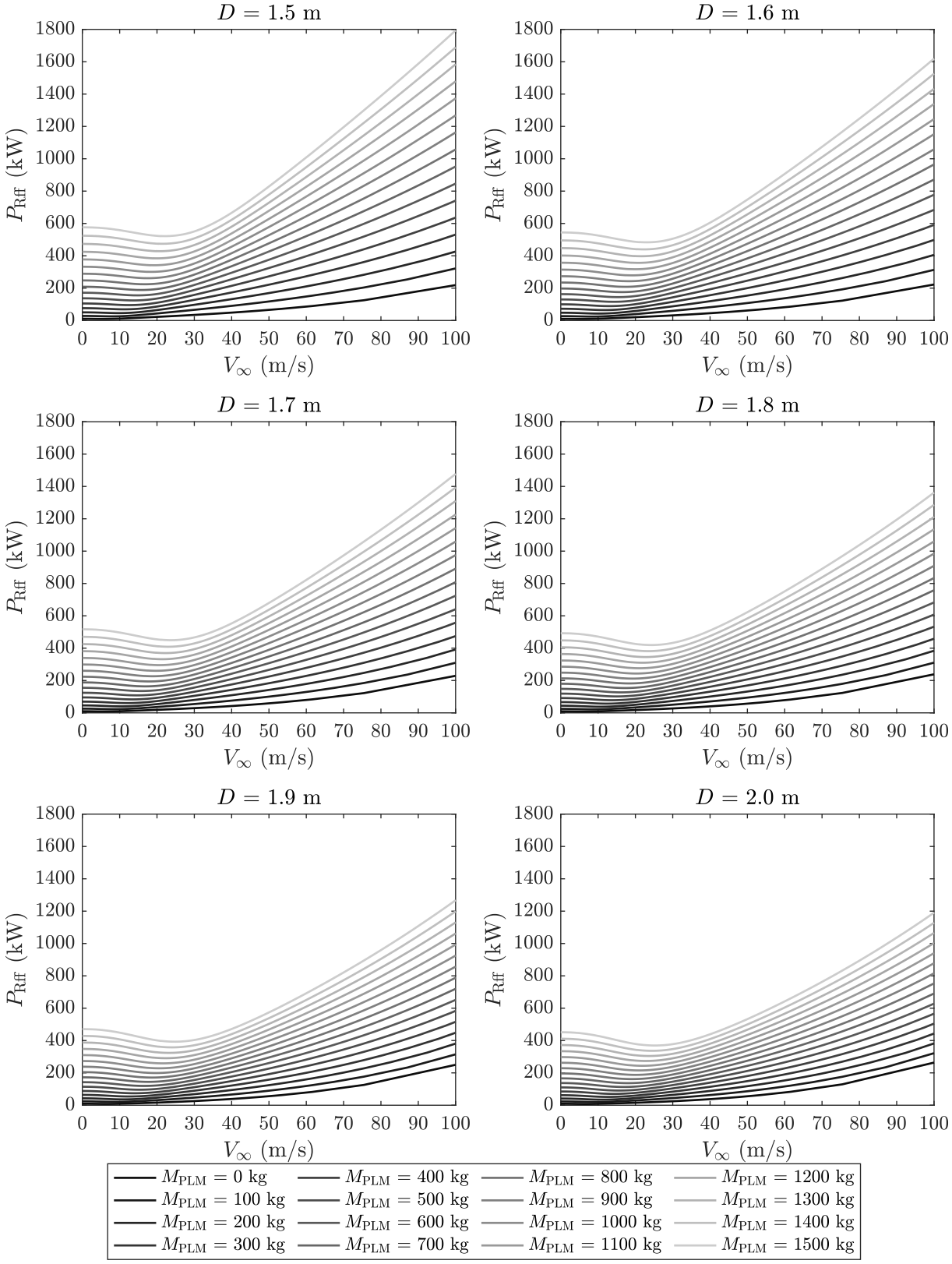

Figure 5.88: Required power in forward horizontal flight $P_{\mathrm{Rff}}\,(\mathrm{kW})$ as a function of forward flight velocity $V_\infty\left(\frac{\mathrm{m}}{\mathrm{s}}\right)$ and payload mass $M_{\mathrm{PLM}}\,(\mathrm{kg})$ for various propeller diameter $D\,(\mathrm{m})$ at 1500 revolutions per minute $n\left(\frac{1}{\mathrm{min}}\right)$.

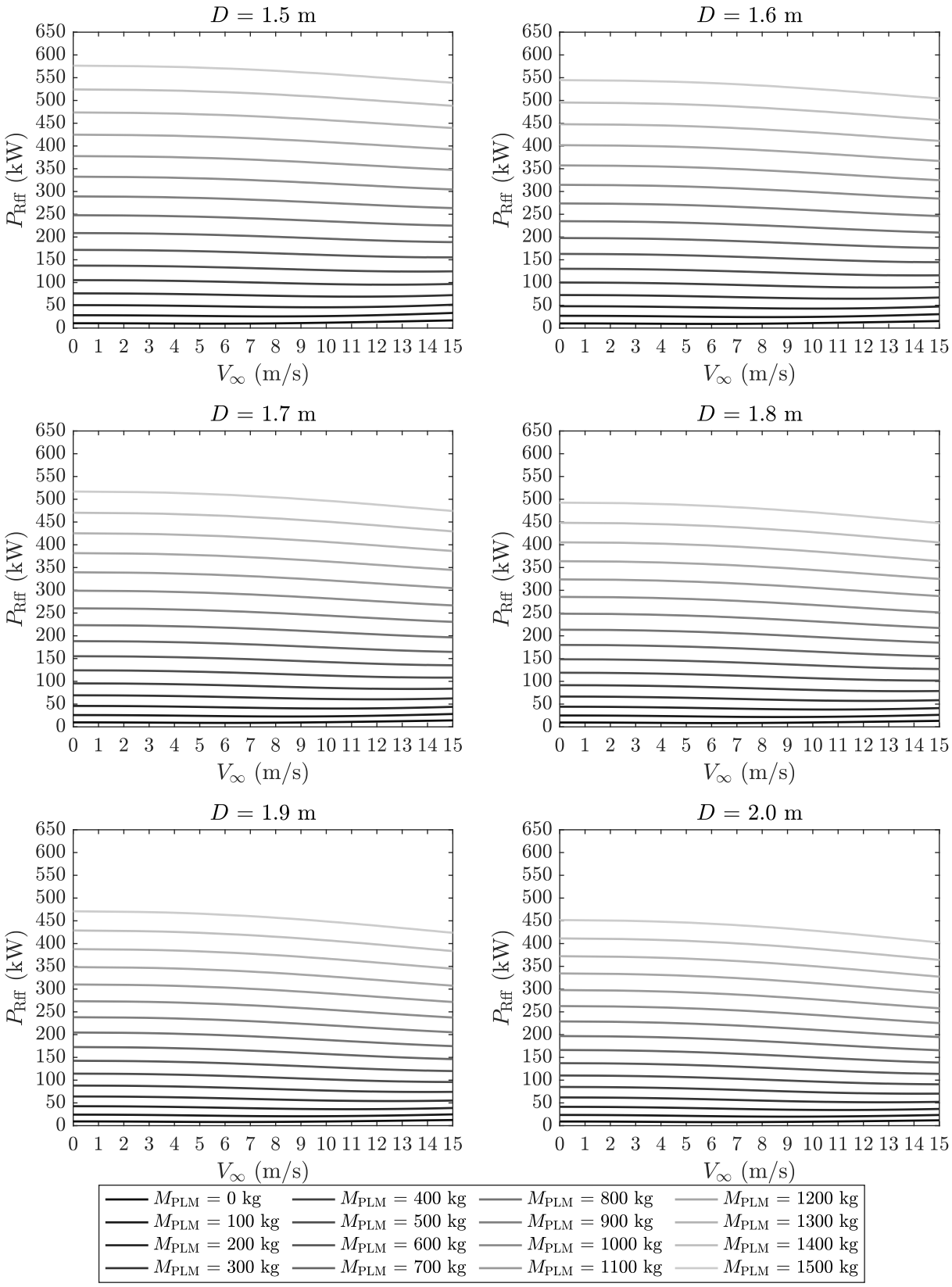

Figure 5.89: Required power in forward horizontal flight $P_{\mathrm{Rff}}\,(\mathrm{kW})$ as a function of forward flight velocity $V_\infty\left(\frac{\mathrm{m}}{\mathrm{s}}\right)$ and payload mass $M_{\mathrm{PLM}}\,(\mathrm{kg})$ for various propeller diameter $D\,(\mathrm{m})$ at 1500 revolutions per minute $n\left(\frac{1}{\mathrm{min}}\right)$; detail on low velocities.

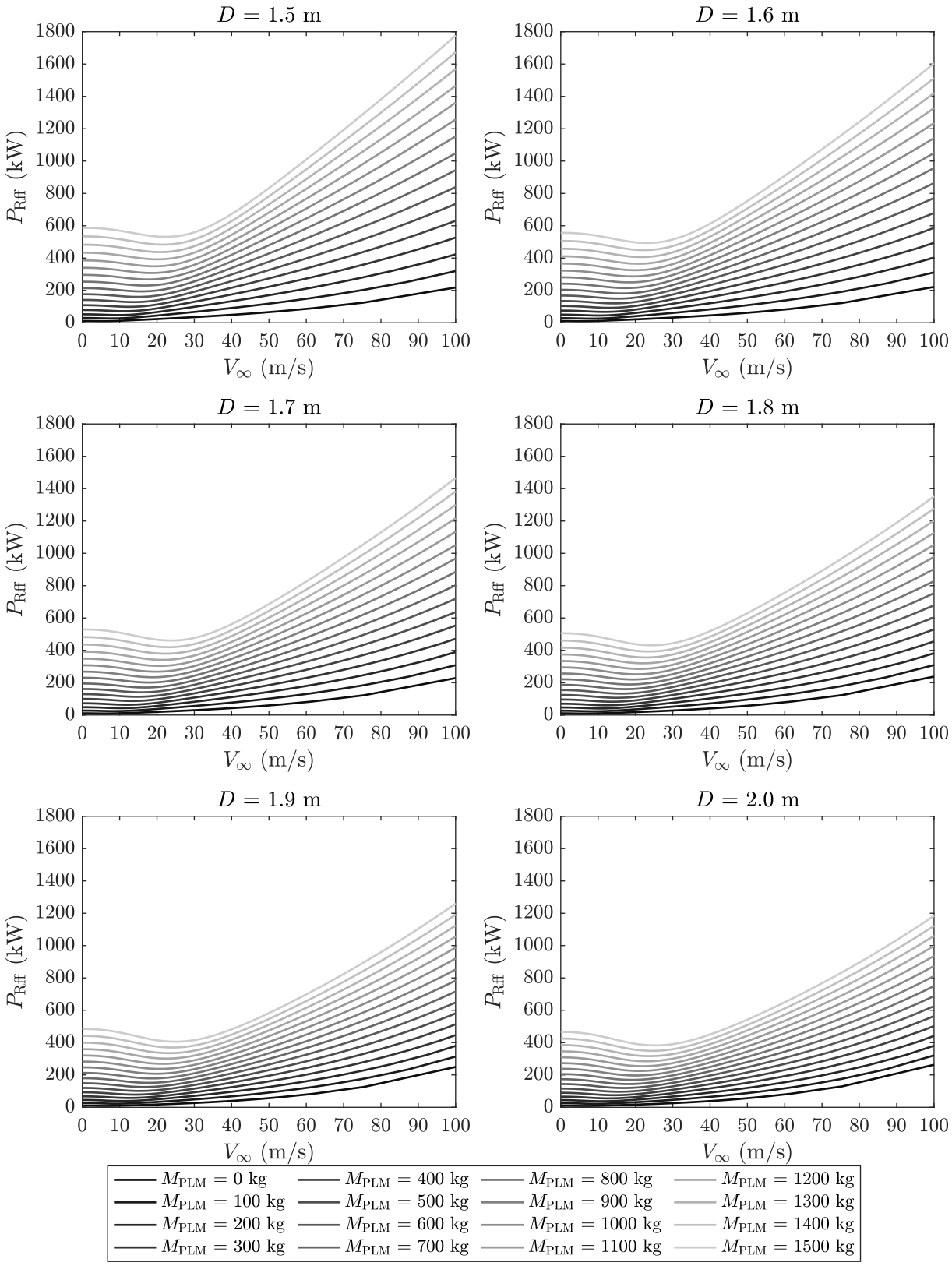

Figure 5.90: Required power in forward horizontal flight $P_{\mathrm{Rff}}\,(\mathrm{kW})$ as a function of forward flight velocity $V_\infty\left(\frac{\mathrm{m}}{\mathrm{s}}\right)$ and payload mass $M_{\mathrm{PLM}}\,(\mathrm{kg})$ for various propeller diameter $D\,(\mathrm{m})$ at 2000 revolutions per minute $n\left(\frac{1}{\mathrm{min}}\right)$.

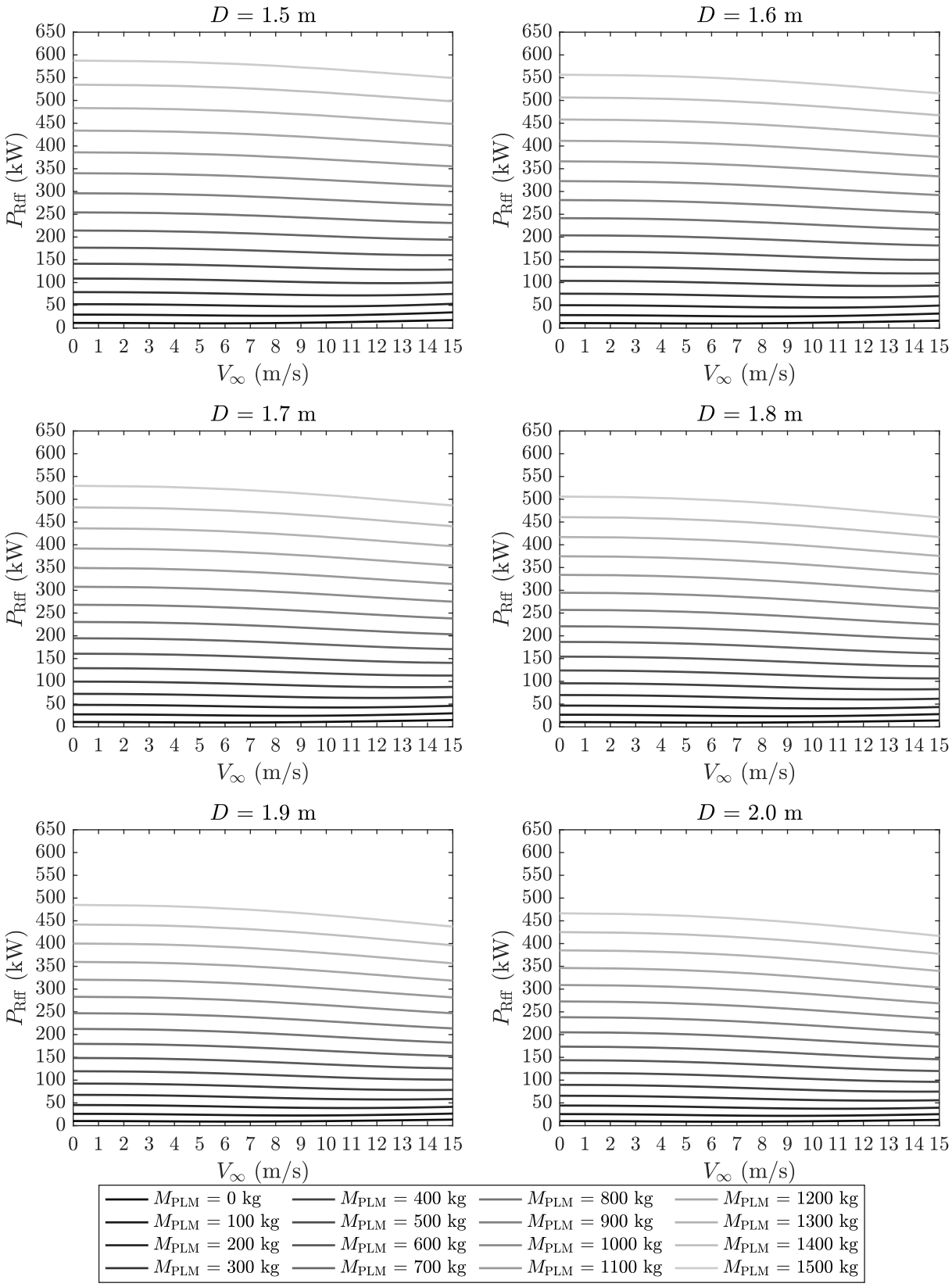

Figure 5.91: Required power in forward horizontal flight $P_{\mathrm{Rff}}\,(\mathrm{kW})$ as a function of forward flight velocity $V_\infty\left(\frac{\mathrm{m}}{\mathrm{s}}\right)$ and payload mass $M_{\mathrm{PLM}}\,(\mathrm{kg})$ for various propeller diameter $D\,(\mathrm{m})$ at 2000 revolutions per minute $n\left(\frac{1}{\mathrm{min}}\right)$; detail on low velocities.

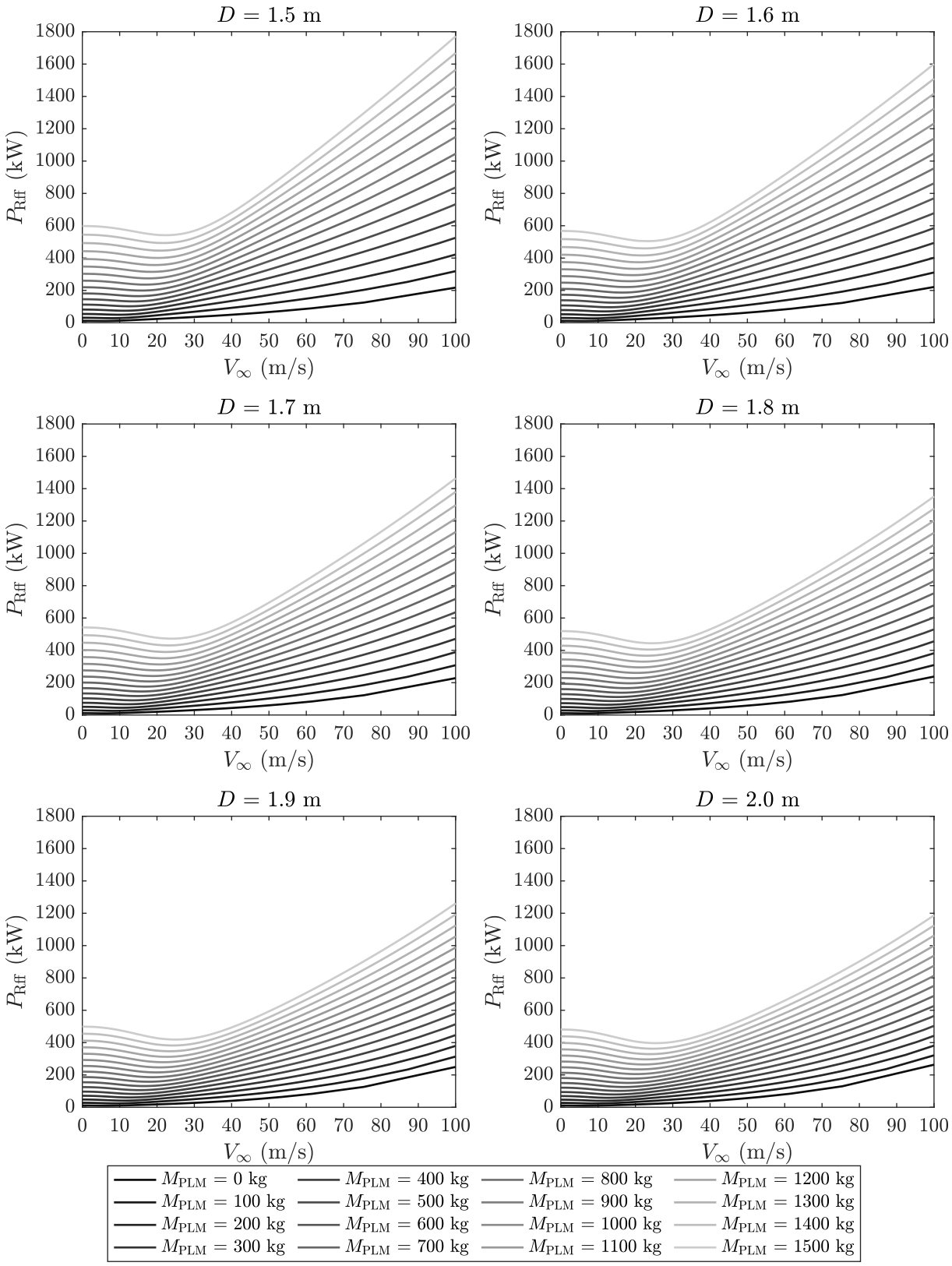

Figure 5.92: Required power in forward horizontal flight $P_{\mathrm{Rff}}\,(\mathrm{kW})$ as a function of forward flight velocity $V_\infty\left(\frac{\mathrm{m}}{\mathrm{s}}\right)$ and payload mass $M_{\mathrm{PLM}}\,(\mathrm{kg})$ for various propeller diameter $D\,(\mathrm{m})$ at 2500 revolutions per minute $n\left(\frac{1}{\mathrm{min}}\right)$.

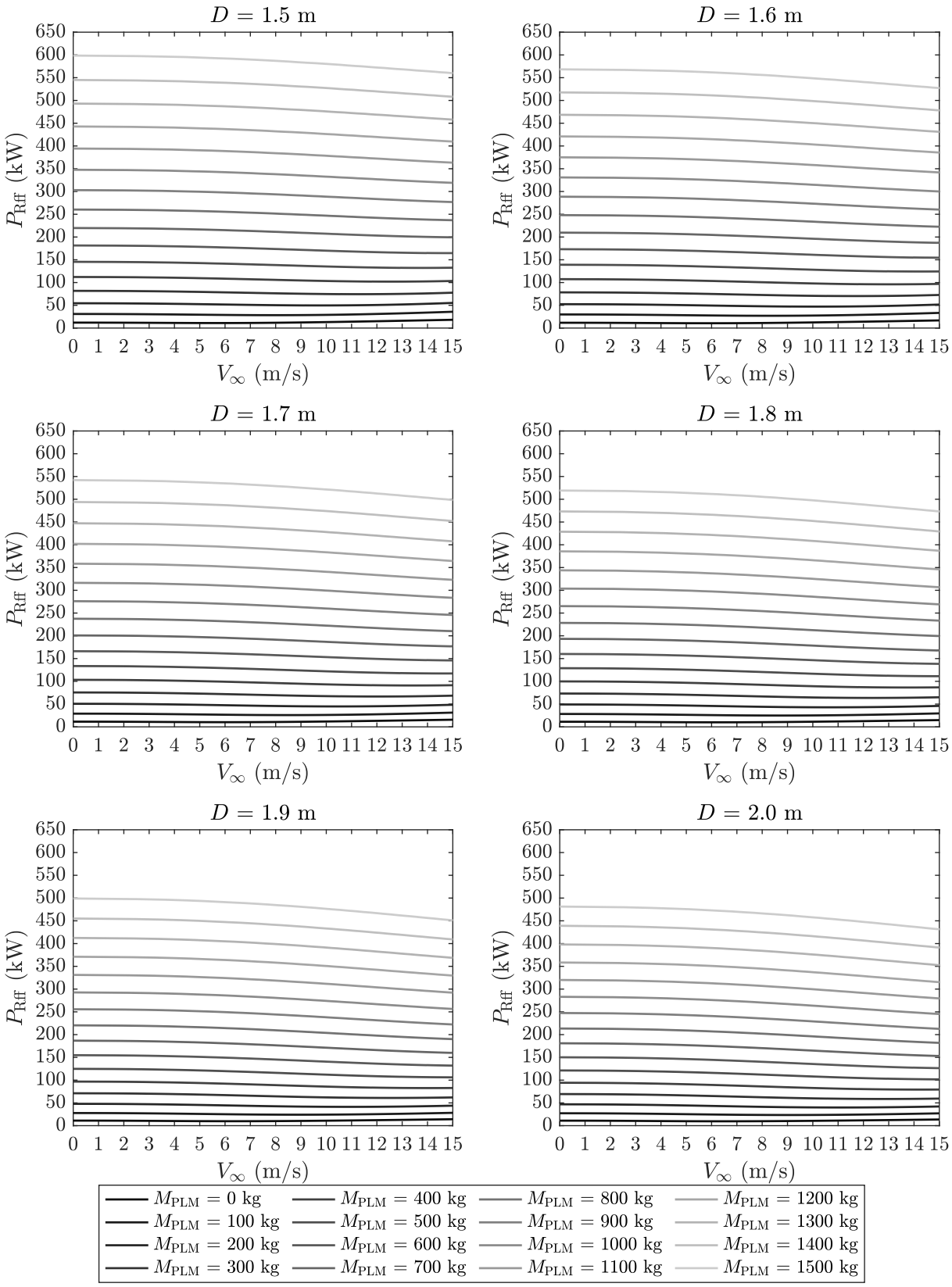

Figure 5.93: Required power in forward horizontal flight $P_{\mathrm{Rff}}\,(\mathrm{kW})$ as a function of forward flight velocity $V_\infty\left(\frac{\mathrm{m}}{\mathrm{s}}\right)$ and payload mass $M_{\mathrm{PLM}}\,(\mathrm{kg})$ for various propeller diameter $D\,(\mathrm{m})$ at 2500 revolutions per minute $n\left(\frac{1}{\mathrm{min}}\right)$; detail on low velocities.

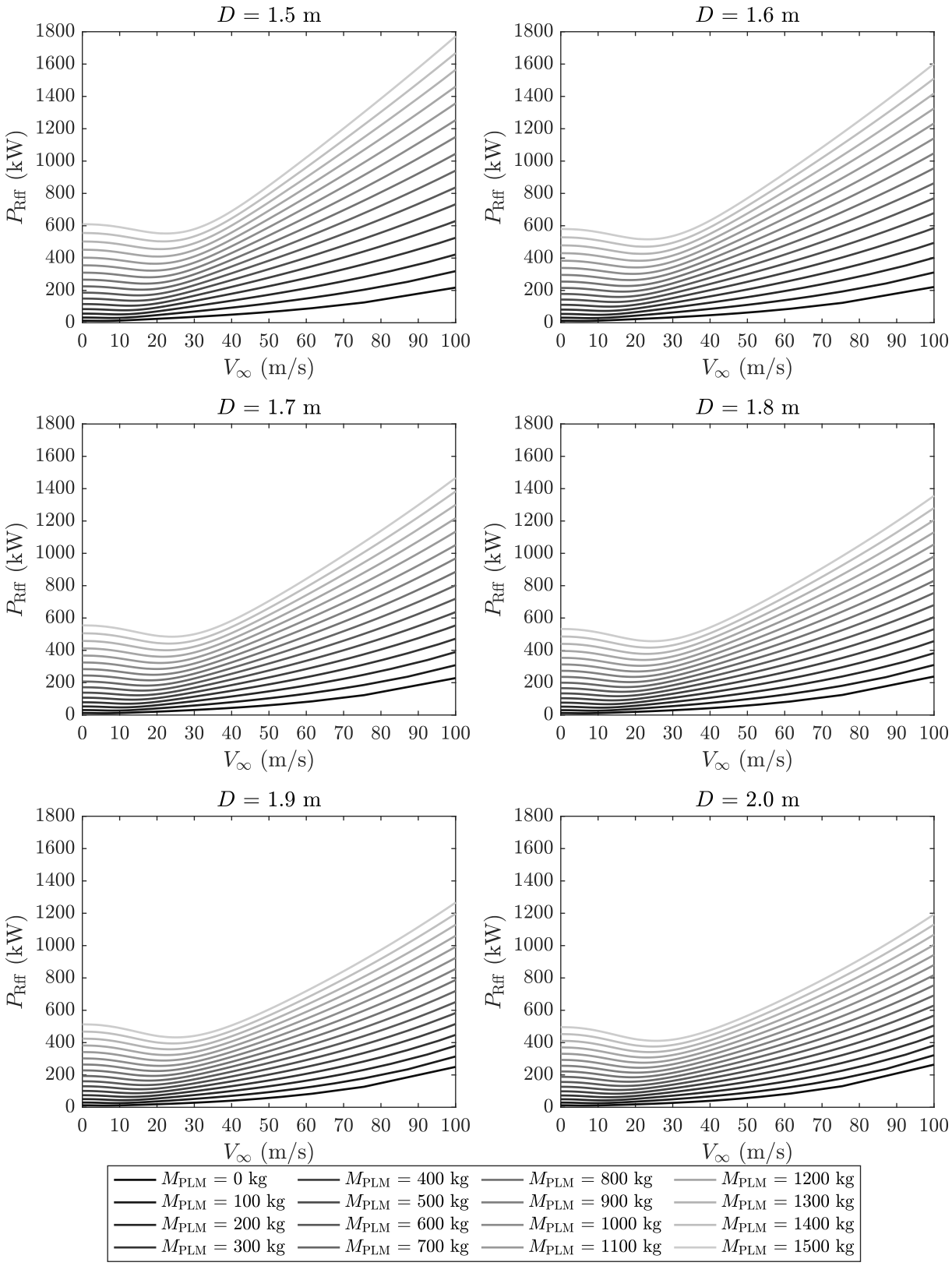

Figure 5.94: Required power in forward horizontal flight $P_{\mathrm{Rff}}\,(\mathrm{kW})$ as a function of forward flight velocity $V_\infty\left(\frac{\mathrm{m}}{\mathrm{s}}\right)$ and payload mass $M_{\mathrm{PLM}}\,(\mathrm{kg})$ for various propeller diameter $D\,(\mathrm{m})$ at 3000 revolutions per minute $n\left(\frac{1}{\mathrm{min}}\right)$.

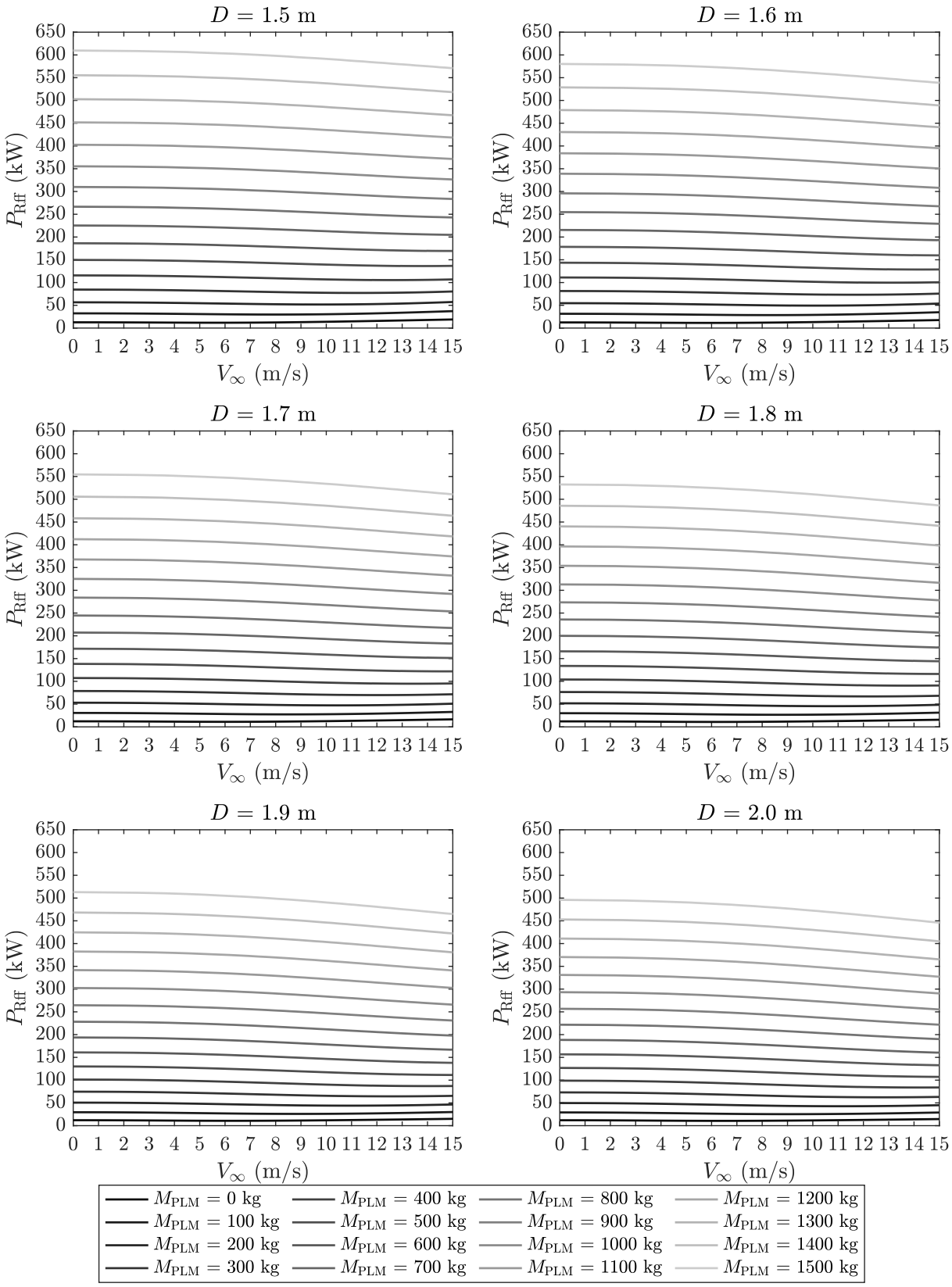

Figure 5.95: Required power in forward horizontal flight $P_{\mathrm{Rff}}\,(\mathrm{kW})$ as a function of forward flight velocity $V_\infty\left(\frac{\mathrm{m}}{\mathrm{s}}\right)$ and payload mass $M_{\mathrm{PLM}}\,(\mathrm{kg})$ for various propeller diameter $D\,(\mathrm{m})$ at 3000 revolutions per minute $n\left(\frac{1}{\mathrm{min}}\right)$; detail on low velocities.

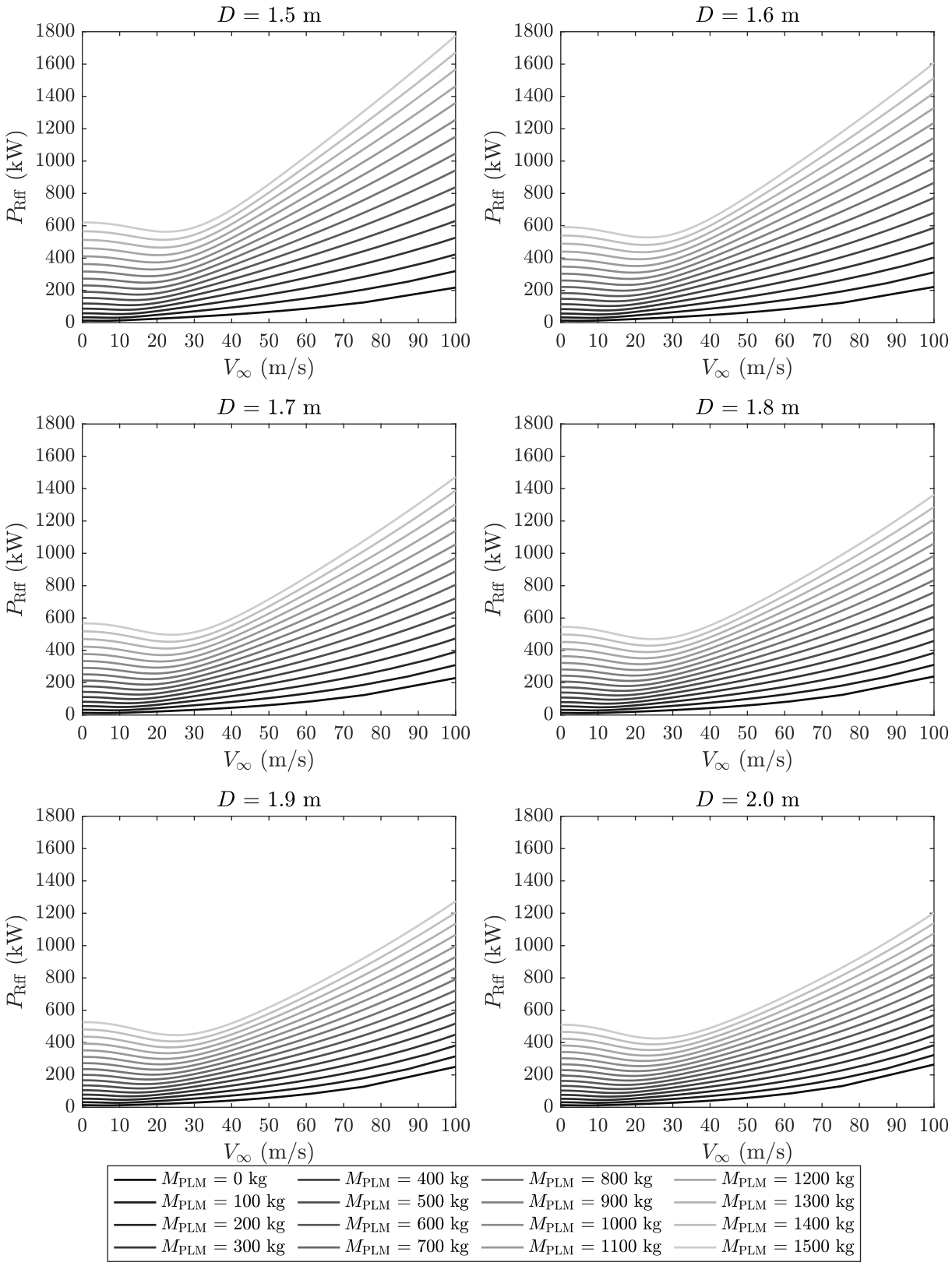

Figure 5.96: Required power in forward horizontal flight $P_{\mathrm{Rff}}\,(\mathrm{kW})$ as a function of forward flight velocity $V_\infty\left(\frac{\mathrm{m}}{\mathrm{s}}\right)$ and payload mass $M_{\mathrm{PLM}}\,(\mathrm{kg})$ for various propeller diameter $D\,(\mathrm{m})$ at 3500 revolutions per minute $n\left(\frac{1}{\mathrm{min}}\right)$.

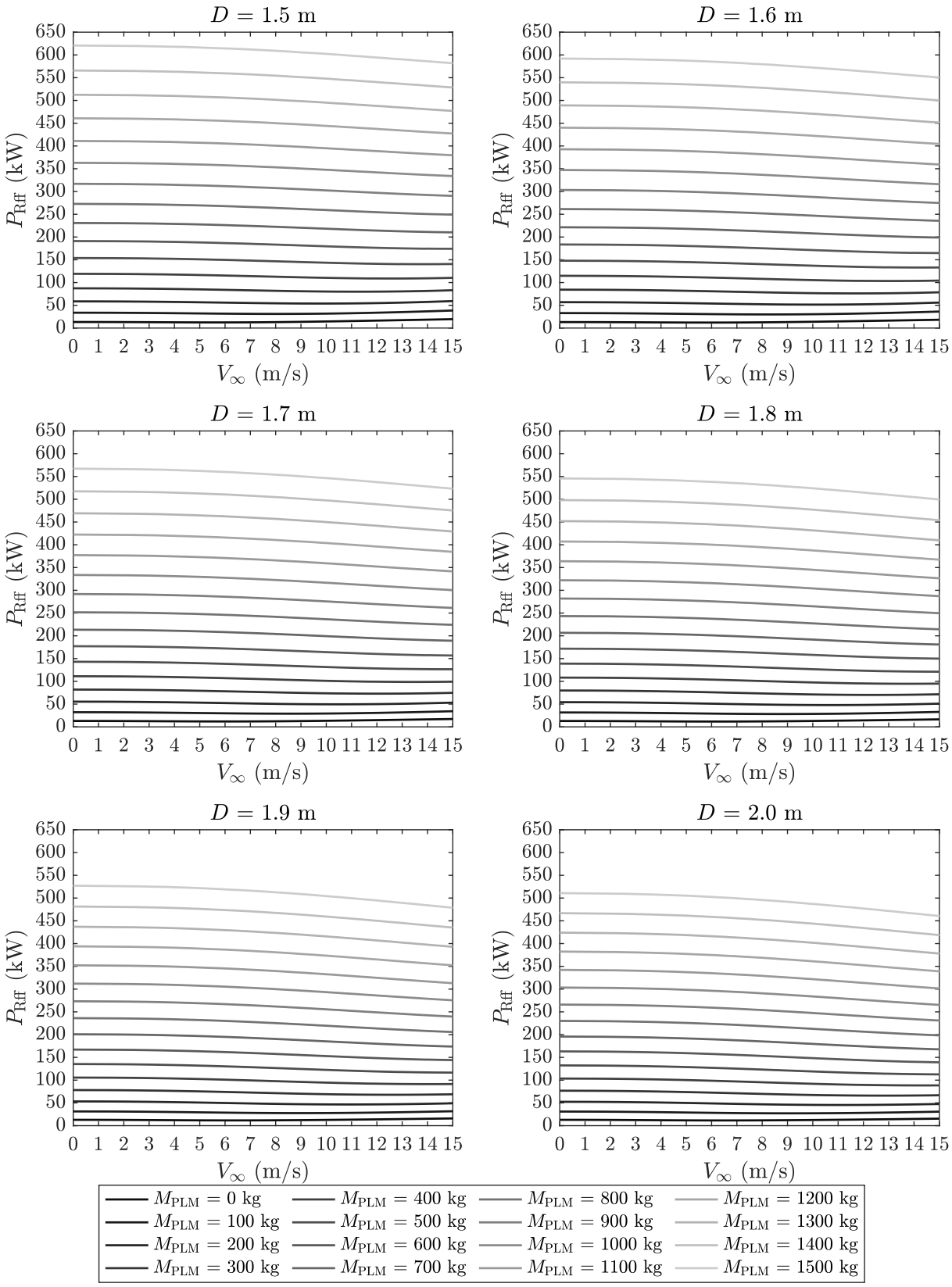

Figure 5.97: Required power in forward horizontal flight $P_{\mathrm{Rff}}\,(\mathrm{kW})$ as a function of forward flight velocity $V_\infty\left(\frac{\mathrm{m}}{\mathrm{s}}\right)$ and payload mass $M_{\mathrm{PLM}}\,(\mathrm{kg})$ for various propeller diameter $D\,(\mathrm{m})$ at 3500 revolutions per minute $n\left(\frac{1}{\mathrm{min}}\right)$; detail on low velocities.

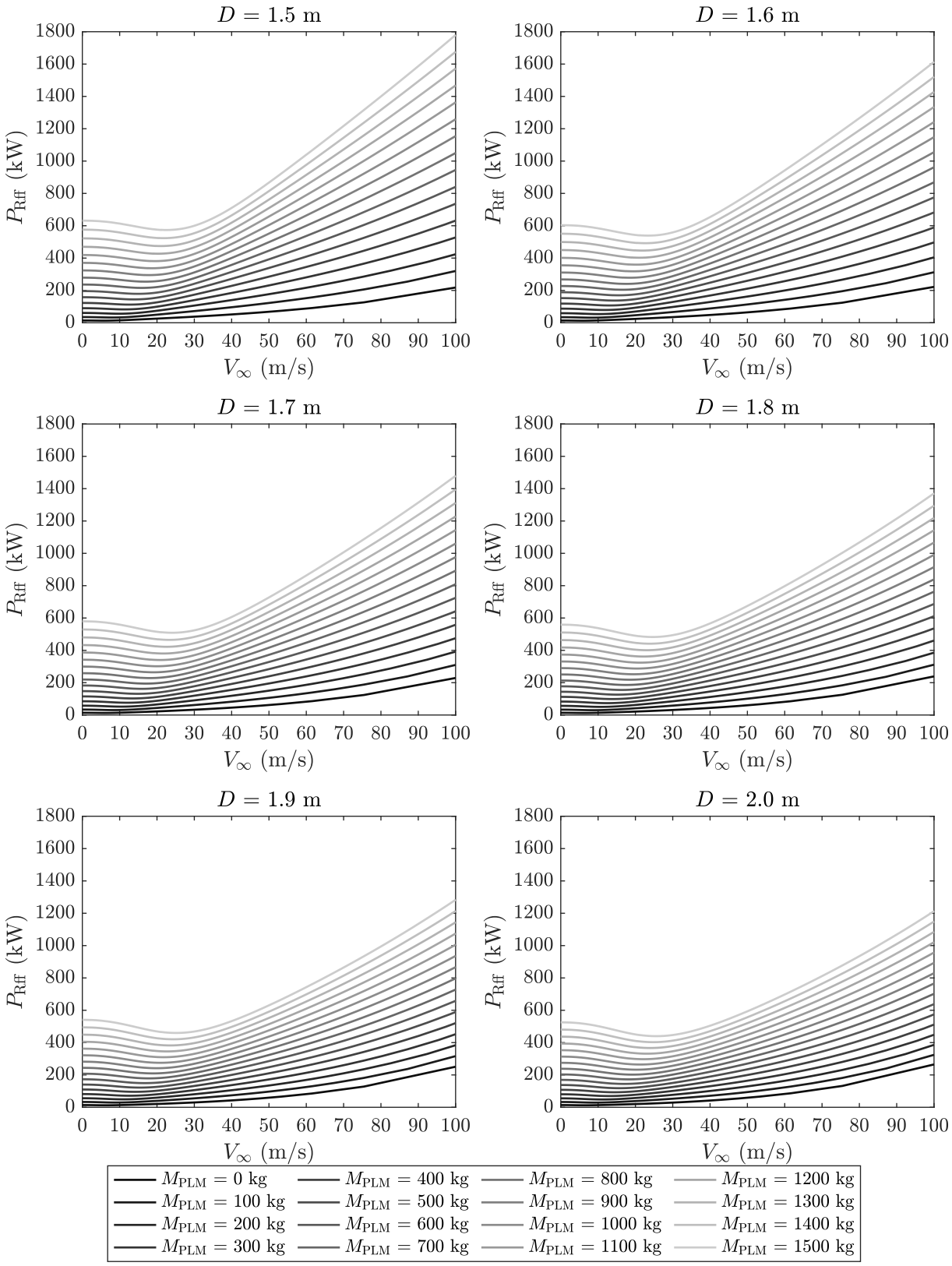

Figure 5.98: Required power in forward horizontal flight $P_{\mathrm{Rff}}\,(\mathrm{kW})$ as a function of forward flight velocity $V_\infty\left(\frac{\mathrm{m}}{\mathrm{s}}\right)$ and payload mass $M_{\mathrm{PLM}}\,(\mathrm{kg})$ for various propeller diameter $D\,(\mathrm{m})$ at 4000 revolutions per minute $n\left(\frac{1}{\mathrm{min}}\right)$.

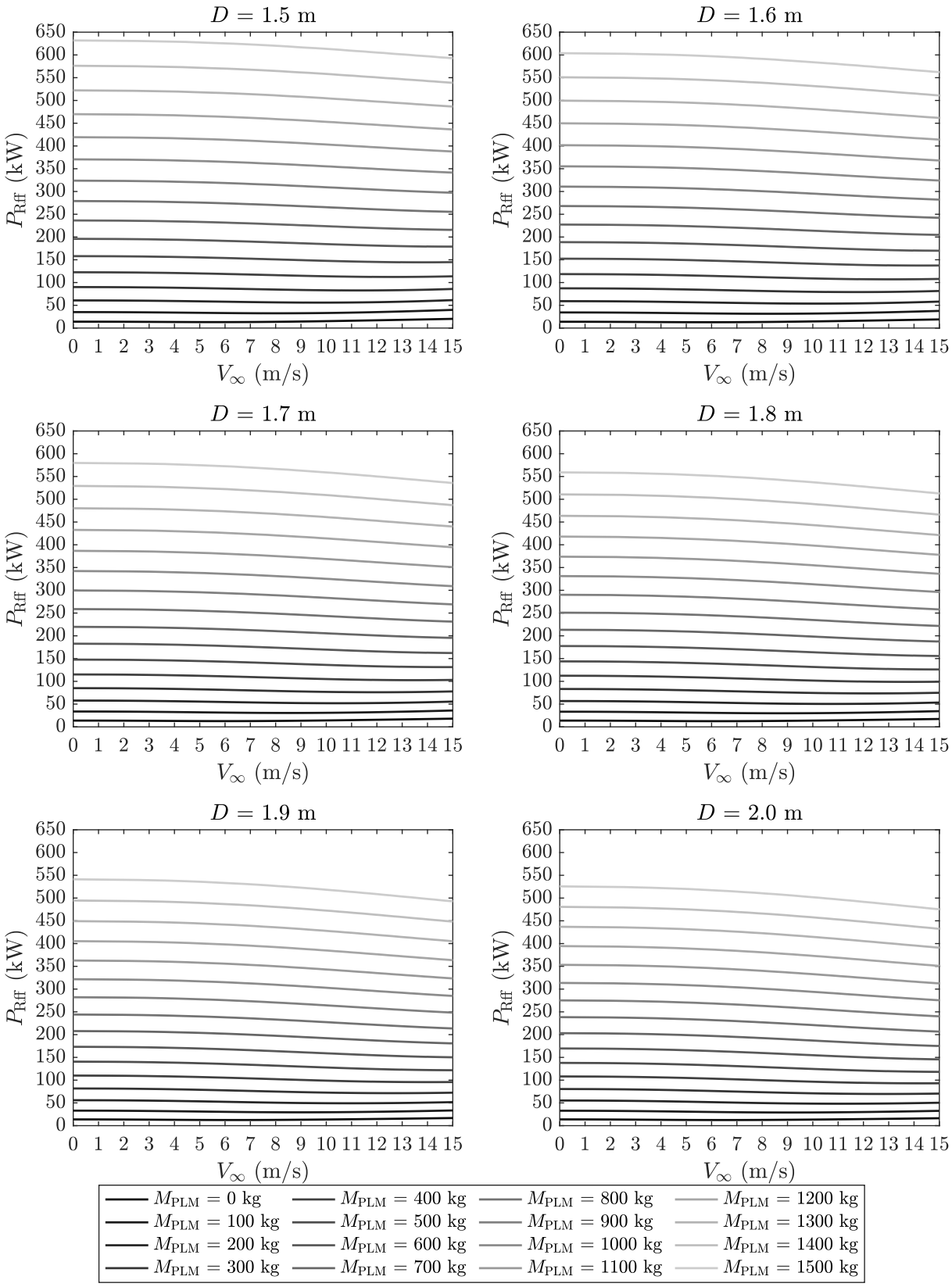

Figure 5.99: Required power in forward horizontal flight $P_{\mathrm{Rff}}\,(\mathrm{kW})$ as a function of forward flight velocity $V_\infty\left(\frac{\mathrm{m}}{\mathrm{s}}\right)$ and payload mass $M_{\mathrm{PLM}}\,(\mathrm{kg})$ for various propeller diameter $D\,(\mathrm{m})$ at 4000 revolutions per minute $n\left(\frac{1}{\mathrm{min}}\right)$; detail on low velocities.